Chem Soc Rev

REVIEW ARTICLE

View Article Online
View Journal | View Issue

Open Access Article. Published on 22 Junie 2020. Downloaded on 2026-02-11 12:42:38 nm.
This article is licensed under a Creative Commons Attribution-NonCommercial 3.0 Unported Licence.

Check for updates

Cite this: *Chem. Soc. Rev.*, 2020, **49**, 5225

Gas hydrates in sustainable chemistry

Aliakbar Hassanpouryouzband,*[abc] Edris Joonaki,†[ad] Mehrdad Vasheghani Farahani,†[a] Satoshi Takeya,[e] Carolyn Ruppel,[f] Jinhai Yang,*[a] Niall J. English,[g] Judith M. Schicks,[h] Katriona Edlmann,[b] Hadi Mehrabian,[c] Zachary M. Aman[i] and Bahman Tohidi[a]

Received 12th February 2020

DOI: 10.1039/c8cs00989a

rsc.li/chem-soc-rev

Gas hydrates have received considerable attention due to their important role in flow assurance for the oil and gas industry, their extensive natural occurrence on Earth and extraterrestrial planets, and their significant applications in sustainable technologies including but not limited to gas and energy storage, gas separation, and water desalination. Given not only their inherent structural flexibility depending on the type of guest gas molecules and formation conditions, but also the synthetic effects of a wide range of chemical additives on their properties, these variabilities could be exploited to optimise the role of gas hydrates. This includes increasing their industrial applications, understanding and utilising their role in Nature, identifying potential methods for safely extracting natural gases stored in naturally occurring hydrates within the Earth, and for developing green technologies. This review summarizes the different properties of gas hydrates as well as their formation and dissociation kinetics and then reviews the fast-growing literature reporting their role and applications in the aforementioned fields, mainly concentrating on advances during the last decade. Challenges, limitations, and future perspectives of each field are briefly discussed. The overall objective of this review is to provide readers with an extensive overview of gas hydrates that we hope will stimulate further work on this riveting field.

1. Introduction

Gas hydrates are ice-like solid compounds that naturally form (or can be formed) under certain conditions of pressure and temperature (*P*–*T*) within a gas/water mixture where water molecules hydrogen bond together forming a crystalline lattice and are known as hydrates or clathrates (terms are used interchangeably). Gas hydrates are at the centre of research within sustainable chemistry because of their innovative applications in a wide range of scientific and industrial contexts, such as permanently storing CO_2 present in flue gases by forming gas hydrates under oceans. The early era of gas hydrate-related research was primarily dominated by flow assurance, minimising hydrocarbon/gas pipeline blockage by hydrate formation. However, in recent years the upsurge of research in the field was stimulated by expanding the application of hydrates to energy recovery, CO_2 capture and storage, gas separation, water desalination, gas storage and transport, refrigeration, *etc.* More recently the potential for methane escaping from hydrate-bearing sediments and reaching the atmosphere has received significant attention due to the high greenhouse warming potential (GWP) of methane.

Recent experimental results backed by theoretical calculations reveal significant potential not only to continue to improve flow assurance but to dramatically increase the scope of gas hydrate-based applications, which requires enabling technologies and elucidation of a new master plan. This could not be achieved without concerted collaborative effort among researchers from different fields of chemistry, physics, geology, engineering, energy industry, humanities, *etc.*, standing as the key to unlocking the contribution hydrates can make to a cleaner atmosphere and support economic and sustainable development. This paper

[a] *Hydrates, Flow Assurance & Phase Equilibria Research Group, Institute of GeoEnergy Engineering, School of Energy, Geoscience, Infrastructure and Society, Heriot-Watt University, Riccarton, Edinburgh, EH14 4AS, UK. E-mail: Hssnpr@ed.ac.uk, Petjy@hw.ac.uk*
[b] *School of Geosciences, University of Edinburgh, Grant Institute, West Main Road, Edinburgh, EH9 3JW, UK*
[c] *Department of Chemical Engineering, Massachusetts Institute of Technology, Cambridge, Massachusetts 02139, USA*
[d] *TÜV SÜD National Engineering Laboratory, Scottish Enterprise Technology Park, East Kilbride, South Lanarkshire, G75 0QF, UK*
[e] *National Institute of Advanced Industrial Science and Technology (AIST), Central 5, 1-1-1 Higashi, Tsukuba 305-8565, Japan*
[f] *U.S. Geological Survey, Woods Hole, MA, USA*
[g] *School of Chemical and Bioprocess Engineering, University College Dublin, Belfield, Dublin 4, Ireland*
[h] *GFZ German Research Centre for Geosciences, Telegrafenberg, 14473 Potsdam, Germany*
[i] *Fluid Science & Resources, School of Engineering, University of Western Australia, 35 Stirling Highway, Perth, WA 6009, Australia*
† E. J. and M. V. F. have equally contributed to the review article.

Open Access Article. Published on 22 Junie 2020. Downloaded on 2026-02-11 12:42:38 nm..
This article is licensed under a Creative Commons Attribution-NonCommercial 3.0 Unported Licence.

aims to complete the missing links between recent experimental and theoretical efforts in chemistry, and highlight areas of research that will require multi-disciplinary research and collaboration. The idea of clathrate-based applications in a diverse range of sectors is of interest to all of the scientific community and the GWP is a concern to society as a whole. In particular, scientists studying low-carbon and unconventional energy have much to benefit from advances in gas hydrate technologies which can reduce costs and improve efficiencies within the multibillion-dollar oil industry either through the substitution of conventional fossil fuels or optimising extraction.

This paper reviews a substantial body of the theoretical, experimental, and industrial research, advances and lessons in the gas hydrate field, over the last decade. The review includes the current state of the art understanding and advances in technical developments, which are combined with expert perspectives and analyses. It is important to note that the purpose of this review is not to analyse in detail every contribution but to highlight the latest advancements, focus on the most pressing issues preventing further understanding of clathrate hydrates, and importantly realising the practical applications of hydrate-based technologies for sustainable chemistry. The review assembles the different gas hydrate-related subjects relevant to sustainable chemistry, appealing to an even broader community of readers. There are several excellent detailed reviews on different subsections of gas hydrates in the existing literature. Rather than duplicate these here, these reviews are cited here to provide the reader with guidance about critical information that is readily accessible elsewhere. Since the early pioneering reviews and books on the fundamentals of gas hydrates, the gas hydrate-community has driven significant developments and advances in novel hydrate-based technologies, seeking to improve their efficiencies and applicability. Building on these early studies, the evolving gas hydrate-based applications have led to many advances in various fields, allowing a wider range of scientific community to contribute in this area of science.

As outlined in Fig. 1, this review summarizes different properties of gas hydrates (Section 2) and their formation and dissociation kinetics (Section 3) from chemistry and physics perspectives. It then focuses on strategies for protection and removal of hydrocarbon pipelines from gas hydrates (Section 4), presence of natural gas hydrate reservoirs in the earth and potential strategies for their extraction, as well as extraterrestrial hydrates (Section 5). The role of gas hydrates in CO_2 capture and storage (Section 6) is discussed next, followed by a treatment of gas hydrates in sustainable development (Section 7). Throughout the review, each subsection covers the related challenges and directions for future investigations of hydrate-based technologies.

2. Gas hydrates' properties

The unique properties of gas hydrates under various conditions of temperature and pressure have numerous practical applications in science and technology, and they also influence the earth's natural cycles. One example of these natural cycles is the widespread escape of methane from natural reservoirs during certain climate warming events in Earth's history and the resulting changes in ocean chemistry that may have been related to these methane emission events.[1] The ability to control the properties of the clathrates using different methods and additives is of great importance to many industrial processes, particularly with regards to reducing the costs and controlling the kinetics of formation/dissociation to maximise the applicability of gas

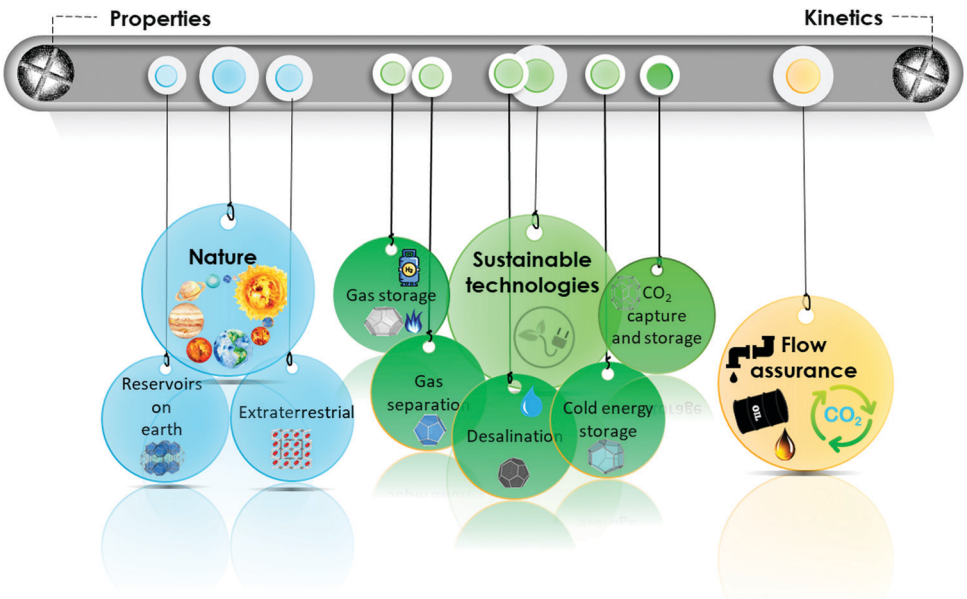

Fig. 1 Graphical contents of the review.

Open Access Article. Published on 22 Junie 2020. Downloaded on 2026-02-11 12:42:38 nm..
This article is licensed under a Creative Commons Attribution-NonCommercial 3.0 Unported Licence.

hydrate technologies. Even the multibillion-dollar international oil industry is affected by the properties of gas hydrates, which can form during hydrocarbon production and can plug production facilities and transport pipelines, imposing billions of dollars of financial loses every year. Finally, a fundamental understanding of the properties of gas hydrates is vital to developing hydrate-based technologies.

The properties for many types of gas hydrates are well-known within the gas hydrate community, as demonstrated by the many published review papers covering several aspects of this diverse field. This section of the review is focused almost exclusively on studies of gas hydrates properties from the last decade. This section is structured in seven parts, with each part introducing the important work that has provided insights into the different aspects of gas-hydrate properties.

2.1. Hydrate structures

The past few decades have witnessed an impressive body of experimental work devoted to gas hydrate structures and chemistry. For instance, thanks to *in situ* techniques such as X-ray diffraction (XRD),[2] Raman spectroscopy,[3] NMR,[4,5] and neutron diffraction[6] at very low temperatures and high pressures, we are now able to look in real-time into different structures of clathrates, identify cages occupancies, and their evolution over time, providing a deeper insight into the kinetic behaviour of these crystalline structures. The determination and understanding of gas hydrate properties are imperative for controlling their behaviour. For this purpose *in situ* techniques such as *in situ* Raman spectroscopy and *in situ* X-ray diffraction supplemented with calorimetry and/or NMR are helpful tools to determine hydrate formation and dissociation behaviour as well as roles of multiple molecules on structure and cage occupancy, especially for gas hydrates formed from gas mixtures, and as such determining the thermodynamic properties of the resulting hydrate phase. Despite the fact that structures modelled from a range of spectroscopy techniques have gained ground in the field, definitive structural solutions[7] by single-crystal XRD (SXRD) are needed mainly because atomic coordination and geometric parameters usually remain uncovered by other spectroscopy methods and complexity emerging from disorder framework is vague. However, the complexity of SXRD measurements requiring restricted size gas-hydrate single crystals mean that SXRD data for gas hydrates remain limited. This section of the review is focused on the discovered structures with particular emphasize on the structures that have not been discussed in previous reviews. Based on guest/host interactions, hydrates are classified into two main groups; (1) clathrate hydrates, crystals with encaged hydrophobic guest molecules in which the interaction between hydrogen-bonded network of water molecules and guest molecules is only by non-directional van der Waals forces. (2) Semi-clathrate hydrates: crystals in which active part of the guest particle molecule physically attach to the water framework and help stabilise hydrophobic guest molecules inside the hydrate lattice.

2.1.1. Clathrate hydrates

2.1.1.1. Natural gas hydrates. Natural gas hydrates are a common class of clathrate hydrates that have hitherto been identified in natural environments.[8] This class of well-known hydrates is classified into three main types: structure I (sI),[9] which usually forms by smaller guest molecules (0.4–0.55 nm) and is the most abundant gas hydrate structure on the Earth; structure II (sII),[10] which usually forms by larger guest molecules (0.6–0.7 nm) and structure H (sH)[8,11] (see Fig. 2), which usually requires both small and large guest molecules for formation. However, there are exceptions; for example, nitrogen, and hydrogen can form sII hydrates, and some intermediate size guest molecules could form both sI and sII depending on the *P–T* conditions. All three classes consist of a hydrogen-bonded water framework based primarily around a nearly spherical structure unit of pentagonal dodecahedra (small cage) with

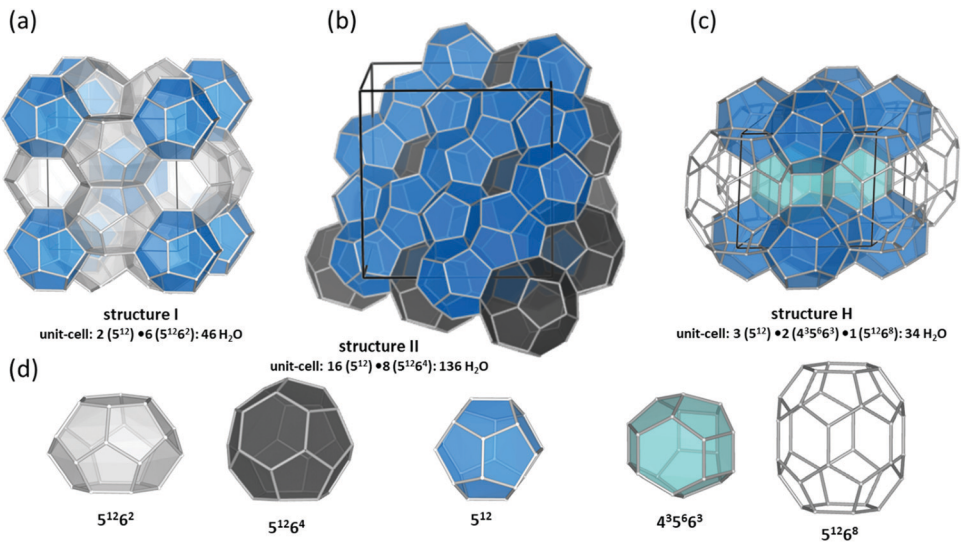

Fig. 2 Three natural gas hydrate structures. (a) Structure I, (b) structure II, and (c) structure H, and (d) five different host water cages. The solid lines represent the unit-cell of each hydrate. All the crystal structures through the review were drawn using a visualization software called "Vesta 3".[25]

Open Access Article. Published on 22 Junie 2020. Downloaded on 2026-02-11 12:42:38 nm..
This article is licensed under a Creative Commons Attribution-NonCommercial 3.0 Unported Licence.

12 planar pentagonal faces (5^{12}).[12] The difference between the structures arises from the way these small cages link; cubic sI unit cells comprise 46 water molecules forming two small cages and six, ellipsoidal-shaped, tetracaidecahedral (large sI cages) with 12 pentagonal and two hexagonal faces ($5^{12}6^2$) that formed by sharing vertices between 5^{12} blocks without direct face sharing; cubic sII unit cell comprises 136 water molecules located in 16 small cages and 8 hexakaidecahedral (large sII cages) with 12 pentagonal and four hexagonal faces ($5^{12}6^4$) that formed through sharing faces between small cavities;[13] sH unit cell with hexagonal symmetry comprises 34 water molecules arranged in 3 small cavities, two irregular dodecahedron $4^35^66^3$ (medium sH cavities), and one icosahedron $5^{12}6^8$ cage (large sH cavities) that is isostructural the hexagonal clathrasil dodecasil-lH.[14] The occupancy of each structure depends on the number of cages and each cage could accommodate one or more (such as nitrogen or hydrogen hydrates) guest molecules. The large cages in all structures are reported to commonly have around 100% occupancy,[15] but that is not a requirement for the stabilization of the crystals.[16] However, the occupancy of smaller cages strongly depends on the type of guest molecules and could be very low or zero in some cases. For example, in sI hydrates, the smaller guest molecules can fill either small or large cavities, whereas, larger guest molecules can only occupy large cages. The *P–T* of formation conditions strongly affect the occupancy, and as such a stable clathrate could have a range of nonstoichiometric compositions. It has also been reported that under suitable conditions transitions between structures are possible. For example, sI hydrate could transition to sII or sH, upon compression[17,18] or addition of appropriate guest molecules.[19] More details about the common structures can be found here.[12,13,20–24]

2.1.1.2. Other structures. The applications of gas hydrates in diverse fields motivate scientists to investigate different hydrate structures. One of the early examples is research by Udachin and Ripmeester,[26] which discovered 1.67 choline hydroxide·tetra-*n*-propylammonium fluoride·30.33H_2O, whose structure is characterized by stacks of sH and sII hydrate and which exhibits hydrophobic and hydrophilic (see Section 2.1.2) modes of hydration by guest molecules. Another example is the discovery of trigonal sT hydrate (with dimethyl ether as the guest gas), which lacks polyhedral (5^{12}) cages and instead consists of unit cells with 12 small cages ($4^25^86^1$) and three types of large cages with different ratios; $12(5^{12}6^3)$; $12(5^{12}6^2)$; $24(4^15^{10}6^3)$.[27]

Traditionally[28,29] it was believed that in the pressure range 1–2 GPa, methane liberates from the clathrates and could not be stable at extreme conditions. However, following studies on Titan, the giant moon of Saturn, Voyager 1[30] located a deep atmosphere made-up of nitrogen with considerable amounts of methane, which may be as high as 21% at the surface,[31] and requires a mechanism to keep methane intact over millennia against photochemical processes. Loveday *et al.*[32] was motivated by this finding to investigate methane hydrate above 2 GPa using X-ray and neutron diffraction. They reported methane can form a new hydrate phase (MH-III, known as filled ice[33] with an unusual combination of 4-, 6-, and 8-membered water molecules' rings) at higher pressures with a higher gas to water ratio and structural transition at about 1–2 GPa, remaining stable at least up to 10 GPa. Considering the reversibility of MH-I to MH-II and MH-II to MH-III, the authors suggested that the source of Titan's atmospheric methane is a layer of MH-I that is been formed because of gravitational differentiation from core methane in MH-III at the end of accretion and producing methane *via* convective processes. This discovery has prompted considerable research into clathrate hydrates at high pressure to investigate their existence in extraterrestrial settings.[33–43] Recently, it has been computationally supported that methane could form MH-IV (with 6-membered rings, similar to the ordinary ice (ice Ih))[41,44] at even higher pressures, which has been confirmed through experimental research[37] by Raman spectroscopy measurements using diamond anvil cells. The authors reported that MH-IV (methane to water ratio ∼ 0.5) forms beyond 40 GPa and is stable up to 150 GPa at room temperature. The behaviour of methane hydrate beyond 150 GPa and the effect of temperature at pressures over greater than 10 GPa needs to be investigated through future research (see Fig. 3).

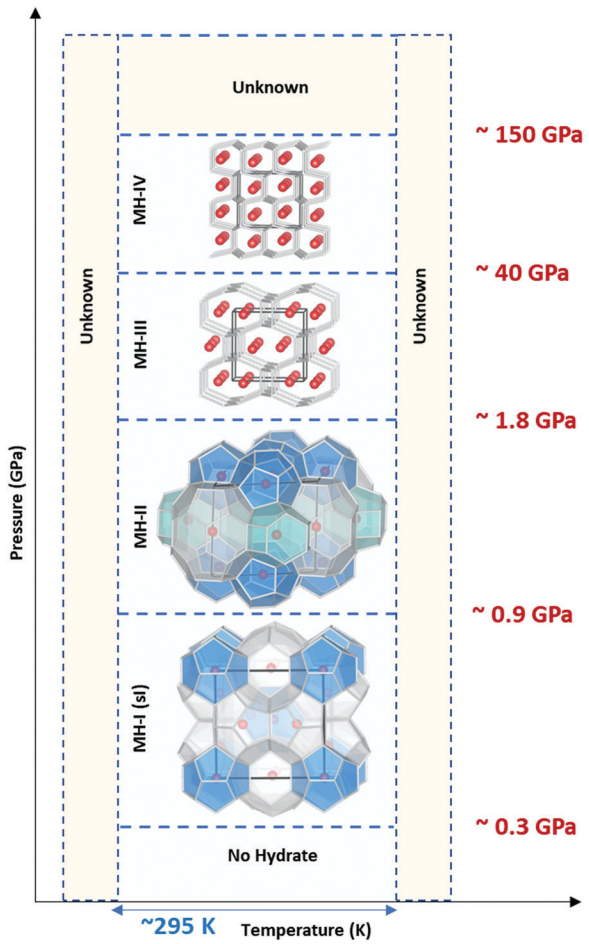

Fig. 3 Structural transition of methane hydrate upon compression up to 150 GPa at room temperature. MH-I is the known sI hydrate. MH-II is similar to sH hydrate and may be closely related to it. However, there are challenging reports about whether MH-II has sH structure or not.[17,32]

Open Access Article. Published on 22 Junie 2020. Downloaded on 2026-02-11 12:42:38 nm..
This article is licensed under a Creative Commons Attribution-NonCommercial 3.0 Unported Licence.

There are also studies that show that unusual clathrates of other gases could also form under specific conditions. It has been found that helium molecules could refill empty neon clathrates (ice XVI) and could enter into ice Ih and ice II structures.[45,46] Similarly, it has been shown that hydrogen also could fill ice by forming a structure similar to ice Ic.[47] Another study suggested that Ne and O_2 could fill ice XVII.[48] These findings suggest that, by choosing appropriate sized guest molecules and suitable *P–T* conditions, it is possible to fill open, low density phases of ice.[38] Still, significant further research will be required to characterize clathrates under extreme conditions for a wide range of compositions, temperatures, and pressures. Promising technologies for hydrate research could be advanced further using the developments from a variety of research fields that can contribute to investigating the existence of clathrates at unusual/extreme conditions.

2.1.2. Semi-clathrate hydrates

2.1.2.1. The quaternary ammonium salt hydrates. These class of lesser-known clathrate hydrates, namely the semi-clathrate hydrates of ammonium/phosphonium salts, received little attention after their initial description in 1940.[49] However, after examples of the separation[50] and storage[51] of various gases using these types of clathrates were presented, interest in semi-clathrate hydrates increased exponentially. One of the key features of these crystals compared to other classes of clathrate hydrates (sI, sII, and H) is their thermal stability at atmospheric pressure. For example, solutions of tetra-*n*-butylammonium fluoride under atmospheric conditions form hydrates with a melting point of 310 K.[49] The higher thermal stability of semi-clathrate compared to other hydrates is attributed to their structural variety, including, but not limited to, the ways in which the dodecahedra associate. This association can be either by sharing faces or by bonding among vertices to build a range of interstitial multifaceted polyhedrals for hosting guest gas molecules or the ion pairs without immensely disordering the hydrogen-bonding pattern of the water framework.[52]

In contrast to clathrate hydrates in which gas molecules are encaged with stability provided to cavities by van der Waals interactions, guest molecules in semi-clathrates are both physically attached to the water network by hydrogen bonding and occupy cages. The walls of some of these cages are partially removed or replaced with the active part of the guest particle.[53,54] In the case of tetra-*n*-butylammonium bromide (TBAB) (see Fig. 4) salt semi-clathrates, for example, negatively charged anions (Br^-) construct a cage structure with the water molecules. This behaviour makes this class of hydrates ionic rather than molecular inclusion compounds. Hydrophobic cations, however, takes a cage filling role by disordering water molecules and occupying the centre of four cages (namely two tetrakaidecahedra and two pentakaidecahedra)[55] without H-bonding with the neighbouring water molecules (*i.e.* hydrophobic inclusion). This, in turn, leads to shaping of a merged cavity composed of several simple cavities, each of which has a hydrocarbon radical that connects to others by water molecules missing from the vertices.[20] All the dodecahedral cages are empty and are potential vacancies to be occupied by another guest molecules. Non-volatility in case of exposure to gases such as H_2 and

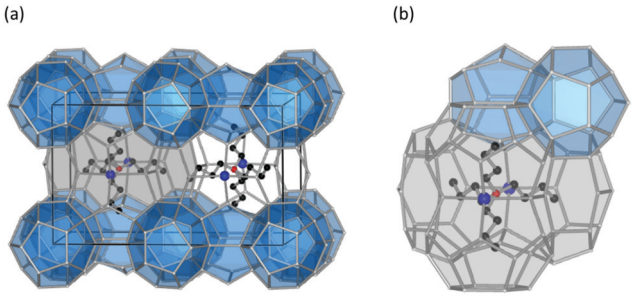

Fig. 4 (a) The structure of TBAB hydrate ($(C_4H_9)4N^+{\cdot}Br^-{\cdot}38H_2O$). The solid lines represent the unit-cell of each hydrate. (b) Magnification of TBAB hydrate structure near tetra-*n*-butylammonium cation. The blue shaded dodecahedral cages are empty, and as such are candidates for encaging small molecules.

CO_2, in addition to typical stability of these clathrates at ambient conditions, is a critical feature in the use of these salts in gas storage, as purity of gas phase is not affected after dissociation of semi-clathrate hydrates. Application of these hydrates in different sectors is reviewed below in relevant chapters.

2.1.2.2. The alkylamine hydrates. Amines are organic compounds consisting of a basic N atom with a lone pair of electrons in which one or more of the H atoms is replaced with an aryl or alkyl group, making it different from ammonia. Such amines and amine-related compounds are relevant in a variety of the broad range of anthropogenic uses, including industrial, pharmaceutical, scientific and commercial contexts.[56] Of particular importance are the associated risk for release of these compounds into the aquatic system[57,58] and potential for amine-based CO_2 capture.[59,60] Therefore, it is important to understand the processes related to amines in the aquatic environment and the formation of alkylamine hydrate in the presence of water and alkylamines is a key process.

The alkylamine hydrates are another class of little-known stoichiometric semi-clathrate hydrates, except for *tert*-butylamine,[53] which is a clathrate hydrate (see Section 2.1.1). In semi-clathrate alkylamine hydrates, the amine molecule is hydrogen-bonded to the water network, retaining the cage like structure. In contrast to clathrate hydrates, every amine has shown to create different and more complex water framework structures with greater distortions from equal edges and tetrahedral coordination at the vertices compared to that of clathrate hydrates. In the amine hydrate structures, similar to the quaternary ammonium salt hydrates, alkyl chains take the cage-filling role, while the functional group is hydrogen bonded with water latticework.[61]

Since the early studies of the existence of amine hydrates by Pickering were disclosed in 1893, several workers discovered different physical/chemical properties of these hydrates.[62] However, this class of hydrates sees little attention by scientists and there have been limited works on this topic in the last decade. In 2009, Ogata *et al.*[63] detailed the cage occupancy and phase equilibrium relations of mixed H_2-trimethylamine clathrates under varying conditions. Following this, several workers investigated various amine hydrate structure transitions when

Open Access Article. Published on 22 Junie 2020. Downloaded on 2026-02-11 12:42:38 nm..
This article is licensed under a Creative Commons Attribution-NonCommercial 3.0 Unported Licence.

exposed to pressurised CH_4[64–67] or H_2[68] providing significant information about guest–host interactions.

2.1.3. Molecular simulations. In recent decades, molecular simulation has contributed a great deal towards elucidating microscopic mechanisms of clathrate-hydrate behaviour, from equilibrium, structural and dynamical properties of the crystalline state, to time-dependent rate phenomena, such as nucleation, crystallisation and dissociation in heterogeneous environments (such as in marine silica). A comprehensive review on hydrate molecular simulation was presented recently by English & MacElroy,[69] building upon earlier work by Barnes & Sum.[70] The structures of various polymorphs of hydrate have been described earlier in the above sections. However, an important new development of insights into hydrate structure (and thermodynamics), to which molecular simulation has contributed over the years, lies in the nature of apparent long-term stability of the empty hydrate lattice. Counter to intuition, this lattice environment is a highly hydrophobic one: there are no available, or 'dangling', hydrogen bonds with which a guest molecule can form strong, sustained hydrogen bonds, meaning that weaker, transient bonds are formed, often between guest-molecule protons 'flitting' to lattice oxygen atoms with rotations. This phenomenon was modelled by English and Tse for H_2S hydrates with *ab initio* molecular-dynamics (AIMD) simulations.[71] In any event, Falenty *et al.* have determined experimentally that the empty neon hydrate lattice is stable;[72] very recently, Krishnan *et al.* have replicated this neon-release process using long MD simulations, also finding evidence of apparent empty-lattice stability.[73] This follows earlier MD studies of Tse *et al.*,[74] Wallqvist[75] and English and co-workers[76–78] suggesting stability over shorter (sub-nanosecond) simulation durations. For a more exhaustive examination of molecular-simulation studies in clathrates, the reader is referred to the existing comprehensive reviews on molecular simulations.[69,70,79]

An important, imaginative, and very recent new general trend in hydrate molecular simulation lies in assessing the effects of externally-applied magnetic fields on hydrates by non-equilibrium molecular dynamics (NEMD), including their kinetic properties – which may have profound geophysical implications.[80] English and Allen performed such NEMD simulation to show that magnetic fields, including their direction reversals, have important effects on gas-release dynamics from methane hydrates. For a field-polarity switch, there is a sudden increase in the gas release, from effects on rotating water molecules in the hydrate cages due to shifting Lorentz forces.[80] Intriguingly, and boldly, it was conjectured that these NEMD-based findings, especially involving switches in field direction, may have a causal link with superchron-related swaps in the Earth's magnetic-field polarity leading to increased methane release into the geosphere.[80]

2.2. Thermodynamics

As we learned from the previous chapter, gas hydrates are composed of two different kinds of molecules, the host molecules (water), forming the cavities and the guest molecules which are encased into the cavities and stabilize them.

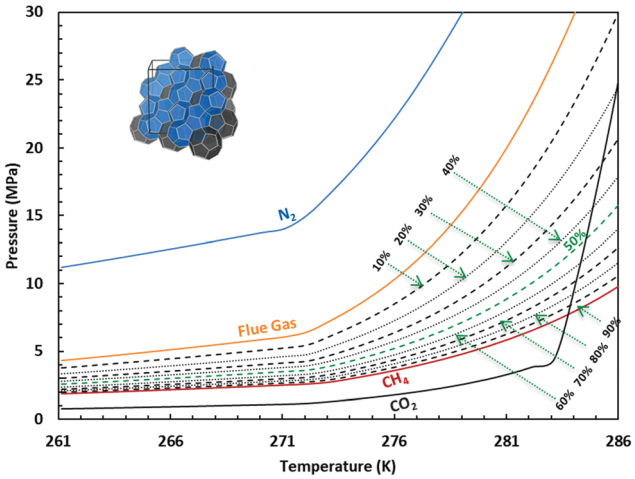

Fig. 5 Hydrate stability zones of CO_2, N_2, CH_4, flue gas (14.6% CO_2 and 85.4% N_2) and mixtures of flue gas with CH_4 (dotted lines) as a function of temperature. Increasing the pressure of the system above the predicated phase boundaries could initiate the hydrate formation. Adding gases with higher hydrate stability pressure zones to gases with lower hydrate stability pressure zones, shifts the system phase boundaries to the left (adapted with permission from Hassanpouryouzband *et al.*,[81] Copyright 2019 Springer Nature).

Depending on the *P–T* conditions (see Fig. 5), these components coexist in different phases at equilibrium state. Therefore, development of an efficient thermodynamic route is of significant importance for determining hydrate formation conditions and hydrate compositions of different systems and has a key role in contributing to the varied gas hydrate related industries. For instance, predicting the optimum amount of thermodynamic inhibitor that needs to be added to the gas production stream to stop pipeline blockage by hydrate formation would have been extremely costly without using thermodynamic models. Accordingly, scientific efforts in this area have led to significant advances in thermodynamic modelling.

2.2.1. Phase equilibria. To achieve an equilibrium state, pressure and temperature have to be the same throughout the complete system (*i.e.* liquid, gas, hydrate phases); in addition, the chemical potential of each component has to be the same in all coexisting phases. After initial correlations based on empirical results,[82,83] a first approach describing and predicting the phase behaviour of gas hydrates was presented by van der Waals and Platteeuw[84] in 1959, treating gas hydrates as dilute solid solutions with the water molecules as solvents and the guest molecules as solutes. This was based on van der Waals' previous work on clathrate structures.[85] They modelled hydrate formation as similar to localized adsorption in three-dimensions with the assumption that all processes are ideal (Langmuir model for gas adsorption). Although their proposed formulation was for a single encapsulated component in a hydrate lattice by applying ordinary partition functions, it is straightforward to extend this formulation to more complex systems. Their model is based on some prerequisites and assumptions, including the single occupancy of cavities, no guest–guest interactions, no arrangement of cavities in the water lattice and no lattice

Open Access Article. Published on 22 Junie 2020. Downloaded on 2026-02-11 12:42:38 nm..
This article is licensed under a Creative Commons Attribution-NonCommercial 3.0 Unported Licence.

distortions due to guest molecules. In reality, these conditions are often not fulfilled and may cause errors[86] in the predicted results. With regard to the assessment of the interactions between the host and guest molecules and their potential energy, the authors used the theory of Lennard-Jones and Devonshire.[87] Since this approach did not consider some effects of the size and shape of the guest molecule, *e.g.* the distortion of the cavity as a result of the encasement of large, linear molecules such as ethane or CO_2, McKoy and Sinanoglu[88] suggested the Kihara potential as a potentially better alternative. In 1972, Parish *et al.*[89] extended the van der Waals and Platteeuw model to complex gas systems using Kihara cell parameters. They tuned their parameters using empirical results in the presence of ice and hydrate and validated their iterative scheme based model by comparing the simulation results with the experimental results of other researchers such as HafeMann and Miller[90] for both sI and sII of cyclopropane. Following this, additional attempts have been made to further modify[91] van der Waals and Platteeuw and measure[92] Kihara cell parameters for different compositions.

In 1988, Englezos and Bishnoi[93] proposed the use of Gibbs minimization of closed system methods to calculate the hydrate fraction and composition in the same way Michelsen[94] had done for multiphase flash for liquids and vapour systems. They used the van der Waals and Platteeuw model to calculate the chemical potential of water in hydrate in a similar way to the previously mentioned model. This model was then extended[95,96] to multi-hydrate former systems and computationally strengthened. Ballard and Sloan[97] proposed another adaptation of general hydrate flash based on Gibbs minimization considering non-ideality about effect of gas adsorption on lattice size. The Gibbs-minimization method has been further improved by such modifications as increasing the speed and robustness of calculations,[98–100] implementing different equations of states and activity coefficient models for involving passes,[101–108] and *etc.*[86,109–111] to address further limitations of the method. As discussed in the previous section, the presence of ammonium/phosphonium salts also determines the thermodynamic behaviour of the resulting hydrate phase. After the initial neural network approach,[112] the first theoretical approach for modelling phase behaviour of semi clathrates was introduced using the statistical associating fluid theory with variable range for electrolytes (SAFT-VRE)[113] equation of state for the thermodynamic properties of the liquid phase and (vdW-P) theory combined with the new model for salt hydrates and applied the Gibbs-minimization method under stoichiometric constraints. Following this approach, many workers adjusted tuning parameters of SAFT-VRE for various semi clathrate compositions.[114–116] Other approaches such as electrolyte non-random two-liquid (e-NRTL),[117] modified Patel–Teja (MPT) EOS[118] and electrolyte Cubic-Plus-Association (e-CPA)[119] were also later applied for predicting semi clathrates phase equilibria.

In addition to the Gibbs minimization model based on modified van der Waals and Platteeuw (VDW-P), Chen and Guo followed a different approach to predict hydrate dissociation conditions that consists of a new two-step model; (1) quasi-chemical reaction for formation of basic hydrate and (2) adsorption of guest molecules. They considered local stability as well as kinetic mechanisms, which is absent in VDW-P theory.[120] In addition to their achievement in extended testing, they obtained more accurate results than VDW-P model in some cases for temperature between 259 & 304 K. However, this model lacks required accuracy over a wide range of pressure, temperature and compositions due to several factors: firstly the authors assumed that all large cavities were completely occupied, which is not in agreement with empirical data and secondly, they tuned the model parameters with the Antoine equation based fugacity functions that proved inaccurate for vapour pressures outside of tuned conditions.[121] To address these problems, Klauda and Sandler[122] in 2000, applied Quantum mechanical calculations to reduce the number of fitted parameters and remove the assumption of a constant crystal lattice for various guests inside a structure. They also used the quasi-polynomial, QL1[123] instead of the Antoine equation for calculation of Langmuir constants, which is accurate beyond the tuned temperature range. Subsequently, they applied their method to single and multi-hydrate former gas mixtures.[124] Similar to Gibbs minimization method, there were further modifications on the Chen and Guo method to increase the accuracy and remove the limitations.[125–127] Alongside the aforementioned approaches, various neural network algorithms have been reported for phase equilibria of gas hydrates.[128–130]

In summary, there have been significant advances in predicting hydrate phase equilibria modelling, and there enable us to predict hydrate stability zones, hydrate fractions and compositions plus other derived thermodynamic properties. Despite the major progress in experimental and simulation studies, a series of challenges remain unresolved which offer the opportunity to explore new directions from a thermodynamic modelling perspective. Firstly, current thermodynamic models work reasonably well for those hydrate systems with no or low concentrations of inhibitor; however, when high concentrations of inhibitors were used the errors in prediction increase significantly. Secondly, there are significant errors when calculating hydrate equilibria at high pressures or with very small guest molecules. Thirdly, for systems containing CO_2 or H_2S in the presence of second guest molecules, uncertainties increase significantly.[86]

2.2.2. Molecular simulations. Building upon this finding of stability of the empty hydrate lattice (see Section 2.1.3), in contrast to other thermodynamic models, such as that of van der Waals and Platteuw, there have been recent advances in the thermodynamic understanding of guest–guest interactions in hydrates, led by molecular simulation. Nowhere is this more apparent than in the field of hydrogen hydrates, where hydrogen molecules are capable of multiple cage occupancies and hopping between cages. As a case in point, Burnham *et al.*[131,132] and Cendagorta *et al.*[133] have carried out very detailed analyses of inter-cage hopping of hydrogen molecules in hydrogen-bearing hydrates, using path-integral sampling to estimate cage-hopping free-energy barriers and taking into account the critical nuclear quantum effects. In addition, Burnham *et al.* have fitted a bespoke force-field from force-matching of *ab initio* MD of hydrogen

Open Access Article. Published on 22 Junie 2020. Downloaded on 2026-02-11 12:42:38 nm..
This article is licensed under a Creative Commons Attribution-NonCommercial 3.0 Unported Licence.

hydrates with high-quality functionals,[134] finding that such potentials are important in being able to characterize more sensitively and accurately guest–guest and guest–water interactions and capture inter-cage hopping free-energy barriers more accurately.

More broadly, in terms of recent sophisticated thermodynamics modelling of cage occupancies, which depends strongly on modelling the subtleties of guest–guest and guest–lattice interactions, Brumby *et al.* have made impressive progress with Monte Carlo simulations of hydrogen hydrates in the isothermal–isobaric Gibbs ensemble, performing a detailed analysis of cage-occupation distributions.[135] In accordance with previous experimental and theoretical studies, they found evidence of very limited double occupancy of small cages, where approximately 0.1% of small cages were doubly occupied at 300 MPa between 225 and 250 K.[135]

Outside of hydrogen hydrates, where nuclear quantum effects can often be very important, as just discussed, molecular simulation has of course expanded our insights into thermodynamics for other guests. Here, the work of Kvamme *et al.*[136] is important in highlighting how residual thermodynamics and chemical potentials of a variety of guests (with particular focus on methane and CO_2, motivated by gas production in marine-hydrate-sediment contexts) and the water-lattice framework can be evaluated from (biased) molecular simulation. This offers the possibility of using molecular simulation as an important prototyping tool for evaluating thermodynamic hydrate-formation and dissociation propensities in a variety of marine-sediment and pipeline settings.

2.3. Thermal properties

A detailed understanding of the underlying mechanisms governing the thermal behaviour of clathrate hydrates, together with accessibility to accurate and reliable thermal property data, makes it possible to enhance simulation scenarios designed to achieve long-term resource recovery and determine the impact of hydrates on climate change.[137] The response of clathrate hydrates to a changing thermal environment is governed by the thermal conductivity, thermal diffusivity, specific heat, and enthalpy of formation/dissociation.[138]

2.3.1. Thermal properties of pure clathrate hydrates

2.3.1.1. Thermal conductivity. Distinguished from other molecular crystals, clathrate hydrates generally exhibit an anomalous thermal behaviour in natural systems with a glass-like temperature dependence (positive slope) resembling amorphous solids.[139–142] Hydrates have been observed to show a glass-like temperature dependence in thermal conductivity above the Debye temperature, similar to some clathrate-like compounds,[143–145] and a crystal-like behaviour below.[146,147] This intriguing behaviour is attributed to the interactions between localized low-frequency vibrations of the guest molecules with the acoustic phonons of the host lattice.[148–156] Pressure dependence of the thermal conductivity has also been studied by researchers, suggesting a weak direct proportionality.[157–162] Despite similarities on the molecular level and the other physical properties, thermal conductivity of clathrates hydrates has been found to be markedly lower than ice Ih.[23,163–165] Such behaviour arises also from larger anharmonicities in the intermolecular interactions when compared with ice.[148] Thermal conductivity measurements recently conducted on some semi-clathrate hydrates, however, revealed a weak negative temperature dependence, demonstrating the crystal heat transmission characteristics in semi-clathrate hydrates.[166,167]

Transient hot-wire[140,158,159,161,166,168,169] and transient plane source[162,164,167,170–174] techniques are the most widely used methods for measurement of the thermal conductivity of clathrate hydrates. Some other techniques, such as the steady-state potentiometric method[141,146,147,175] and guarded hot-plate method,[163,176] are also sometimes used to measure the thermal conductivity of hydrates. The main challenge associated with the laboratory measurement of the gas hydrates thermal conductivity is that the gas hydrate samples are usually porous and have free water/ice and gas which could impact the quality of the experimental data as the measured thermal conductivity includes the thermal contact resistance (TCR) due to the unavoidable imperfect contact.[146,147,164] Recently, however, an experimental system was introduced using the modified freestanding 3ω method which is able to reconstruct the intrinsic thermal properties (thermal conductivity and diffusivity) of clathrate hydrates.[177]

2.3.1.2. Thermal diffusivity. While thermal conductivity is a measure of the ability of a material to conduct heat thermal diffusivity is the thermal inertia of the material.[161] A new experimental configuration based on the approximation solution of the Navier–Stokes heat equation was first developed by Turner *et al.* in order to measure the thermal diffusivity of clathrate hydrates.[178,179] Waite *et al.* used the infinite line source formulation of Carslaw and Jaeger for simultaneous determination of thermal conductivity and thermal diffusivity using the transient hot-wire method.[161,168] Transient place source technique has also used to measure the thermal diffusivity of methane hydrate.[162,173]

2.3.1.3. Calorimetric studies. The heat stored in or extracted from a material due to a temperature change can be quantified by the heat capacity.[138] Clathrate hydrates heat capacity data can provide some information about the motion of encaged guest molecules or reordering of the guest and host.[180] Enthalpy data is also necessary as a key thermal property for a realistic evaluation of the recovery schemes proposed for exploitation of natural gas hydrate-bearing sediments.[181] Several experimental studies have been conducted to measure the heat capacity[142,180–189] and enthalpies of formation/dissociation[180,181,183,184,186,188,190–198] of clathrate hydrates, the majority of which use the heat-flow calorimeter[180,181,183,184,186,191,192,194] and differential-scanning calorimeter.[188,190,193,195,197–199]

Experimental measurement of gas hydrate heat capacity is always associated with two major challenges: (1) due to strong dependence of the vapour pressure of gas hydrates on the temperature, increasing the system temperature results in dissociation of the hydrates and consequently renders the apparent heat capacity much higher than the actual value; (2) the presence

Open Access Article. Published on 22 Junie 2020. Downloaded on 2026-02-11 12:42:38 nm..
This article is licensed under a Creative Commons Attribution-NonCommercial 3.0 Unported Licence.

of free hydrate former species (especially free water) could greatly influence the measured heat capacity of the hydrate.[188] Enthalpies of formation/dissociation are also determined indirectly by using the *P–T* diagram of the system and Clapeyron equation or its Calussius–Clapeyron approximation.[198,200] However, this method has limited application when used for semi-clathrate hydrates.[199,201] A detailed overview of the calculation of the dissociation enthalpy of methane hydrates can be found elsewhere.[202]

2.3.1.4. Perspectives on molecular modelling. Underlying mechanisms of the heat conduction in clathrate hydrates can now be explored *via* molecular simulation thanks to recent advances in computational power. In molecular simulation, thermal conductivity can be estimated by both equilibrium and non-equilibrium Molecular Dynamics (MD)[69] (see Fig. 6). A review on the contribution of molecular simulations to our detailed theoretical understanding of mechanisms of thermal conduction in clathrate hydrates can be found elsewhere.[69,137] Recently, MD was employed to further investigate the thermal behaviour of the clathrate hydrates,[203–206] particularly to evaluate the influence of guest occupancy ratios on the thermal performance of gas hydrates, suggesting an improved thermal conduction by the inclusion of more guest molecules in the cage.[207–209] The MD approach was also utilised to study the calorimetric properties of clathrate hydrates including the heat capacity[210] and endothermic dissociation process of clathrate hydrates.[202,211–213] However, the dependence of the experimental results on the samples' nature and quality together with the quality of the potential models used in molecular simulation and the system size and electrostatics render difficult a direct and quantitative comparison of theoretical and experimental values.[69] This clearly makes it necessary to seek novel and more suitable macroscopic experimental techniques to minimize the effect of the external/internal factors (confining pressure, temperature, residual water, gas or ice, presence of micropores,...) to obtain a well-defined sample whose thermal properties reflect those of pure hydrates.[214] Apart from challenges encountered in macroscale studies, there are still a number of technical issues that need to be addressed associated with the molecular modelling required to identify key microscopic mechanisms controlling the thermal properties. This would lead to improved reproducibility of the thermal properties already measured precisely in the laboratory. Integrating the experimental and theoretical studies would enable us to elucidate the thermal behaviour of hydrates at different conditions, especially those difficult or even impossible to achieve experimentally such as extremely low temperature or high pressure conditions. Such integration can be of particular interest when investigating the evolution of the thermal properties of hydrates during various processes such as formation and dissociation.[215] The importance of the thermal properties in various hydrate-based applications such as CCS, hydrogen storage, desalination and gas separation, and the key role of the molecular-level mechanisms in controlling the thermal conductivity of hydrates necessitate further experimental studies integrated with molecular simulations to shed light on the thermal behaviour of hydrates.

2.3.2. Thermal properties of hydrate-bearing sediments (HBS). Thermal properties of hydrate-bearing sediments (HBS) provide necessary inputs for evaluating gas production from natural gas hydrate reservoirs, seafloor stability of oceanic sediments, global climate change, and submarine slide formation.[217,218] Reliable thermal properties are necessary when assessing the response of HBS to exploitation operations and environmental changes.[219–221] Several experimental studies have been conducted to measure the thermal properties of HBS, particularly their effective thermal conductivity. Accurate measurement/prediction of the

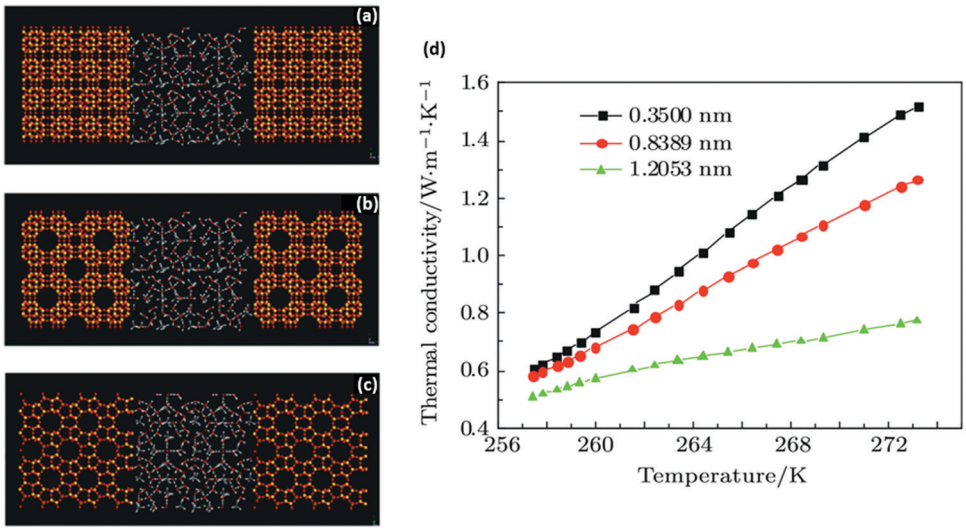

Fig. 6 Molecular-dynamics simulation of thermal conduction in methane hydrate–SiO_2 porous media: (a–c) snapshot of the final structure of hydrate + porous media simulation system with different pore sizes (a – 0.35, b – 0.8389, c – 1.2053 nm); (d) simulated thermal conductivity values *vs.* temperature. As observed, the thermal conductivity of the system increases with temperature increase. At a certain temperature, the thermal conductivity further increases as the pore size reduces due to improvement of the SiO_2 surface (with higher thermal conductivity) and the micro-energy transfer associated with hydrate–SiO_2 at lower pore sizes (adapted with permission from Guo *et al.*,[216] Copyright 2017 Institute of Physics).

Open Access Article. Published on 22 Junie 2020. Downloaded on 2026-02-11 12:42:38 nm..
This article is licensed under a Creative Commons Attribution-NonCommercial 3.0 Unported Licence.

effective thermal conductivity, however, is not straightforward due to the co-existence of gas hydrate, free water/ice, free gas and solid sediment grains, and, more importantly, their spatial distribution throughout the system.[222] Experimental studies have revealed a complex interplay among porosity, effective stress, particle size, and fluid-*versus*-hydrate filled pore spaces.[220,223,224] For HBS, the effective thermal conductivity strongly depends upon involving particle-level heat transport processes including (1) conduction along the mineral, (2) particle-to-particle conduction across contacts, (3) particle–fluid/hydrate–particle conduction near contacts, and (4) conduction/convection along the pore fluid within the pore space,[219] influenced by presence of free gas and water/ice, and hydrate growth pattern.[138] Detailed reviews on the effect of hydrate formation on the effective thermal conductivity of sediments can be found elsewhere.[138,225]

Laboratory measurements of the effective thermal conductivity of hydrate-bearing sediments are usually conducted using transient hot-wire[169,219,226,227] and transient plane source[172,174,220,228–232] techniques. Transient hot-wire technique, however, is not easily adapted for *in situ* measurement where sample penetration is difficult. This makes the transient plane source technique more conducive towards adaptation for field use.[137] Recently, a thermistor-based method combined with Micro-CT observations was employed to further investigate the effect of saturation and spatial distribution of co-existing phases on the effective thermal conductivity of HBS.[233–236]

Development of accurate predictive models for the effective thermal conductivity of composite materials such as HBS comprises an important portion of the literature about heat transfer in porous media. However, a unified model or prediction procedure with universal applicability has not been found yet.[237] Based on their principles, the existing predictive models can be categorized into Mixing Models, Empirical Models, Mathematical Models, Volume Fraction Models, Packing Structure Models, and Pressure-dependent Models. A detailed review of the existing models can be found elsewhere.[238]

There are few published data on the effective thermal diffusivity of gas hydrate-sand/sediment mixtures.[161,178,228] Gas hydrate-bearing sediments can change temperature more rapidly than hydrate-free sediments as the thermal diffusivity of methane hydrate is more than twice that of water.[138] Hydrate should therefore be accounted for in transient heat flow applications such as safety assessments for drilling into or through hydrate-bearing sediments.

Unlike the effective thermal diffusivity and conductivity, the heat capacity of HBS depends only on the mass fractions of sediment, hydrate, and pore fluids rather than on their pore-scale distribution and interfacial effects.[138] Therefore, hydrate formation can significantly lower the specific heat of sediments.

2.4. Electromagnetic properties

The electromagnetic characteristics of a material including the steady state charge migration under an electric field, polarization and magnetization can be quantitatively expressed by the Electrical conductivity (σ), magnetic permittivity (κ^*) and magnetic permeability (μ^*).[138] Electrical measurements have been widely used as a primary method to detect the spatial distribution of hydrate in natural sediments.[239–245] They can also be employed to monitor the formation/dissociation of clathrate hydrates or even to evaluate the performance of hydrate inhibitors.[240,246,247] When transformed from an aqueous phase system to pure hydrate, electrical conductivity decreases, meaning that this property can be used to detect hydrate formation/dissociation.[247,248] The ionic concentration in solution has a primary effect on resistivity and a second-order effect on magnetic permittivity, hence permittivity can be used as a more reliable parameter to estimate water saturation and extract volumetric hydrate saturation in a multiphase hydrate bearing system as well. For instance, the electrical resistivity logs acquired from natural gas hydrate bearing sediments confirm the presence of less conductive hydrate bearing zones relative to the water saturated regions.[249–255] The magnetic permeability, however, is usually considered to be unity for pure hydrates and hydrate bearing sediments as these materials are generally non-ferromagnetic.[138] In addition to the electromagnetic properties, dielectric measurements have also been employed to quantify gas hydrate saturation in both laboratory and field studies.[256–258]

2.4.1. Pure clathrate hydrates. Knowledge of the electrical conductivity of pure hydrates is essential for the quantitative investigation of hydrate distributions in porous media. Generally, clathrate hydrates exhibit a lower electrical conductivity compared with water and even ice. So far, there are a few studies reporting the electrical properties of pure clathrate hydrates.[259–261] Measurement of the electromagnetic properties of clathrate hydrates in the laboratory can be carried out *via* the Impedance Spectroscopy method, whereby the electrical behaviour, conduction mechanisms and other internal charges can be revealed *via* changing current frequencies.[262] Similar to the other physical properties of clathrate hydrates such as mechanical strength and thermal conductivity, the quality of the electromagnetic properties obtained experimentally is markedly affected by the specimen preparation technique, particularly for gas hydrate samples where the gas solubility in the water is limited and the hydrate formation usually starts from the gas–water interface.[263] Hydrate formation in brines results in increasing electrical conductivity for the bulk solution because hydrate formation excludes salts.[246,264] Conducting several heating/cooling cycles has been recently shown to be an appropriate method to obtain reliable electrical conductivity data for unmixed, polycrystalline methane hydrate samples.[260]

2.4.2. Hydrate-bearing sediments. Sediment components can be characterized in terms of their volume fraction and spatial distribution by evaluating the bulk electrical and electromagnetic properties.[265] The electrical conductivity of HBS is primarily controlled by the movement of hydrated ions in the pore water and in electrical double layers around mineral surfaces, particularly for the sediments with high specific surface area.[138] Electromagnetic remote sensing techniques such as controlled-source electromagnetic (CSEM) surveying methods, complement seismic studies for determination of the gas hydrates saturation and distribution in natural settings as they

Open Access Article. Published on 22 Junie 2020. Downloaded on 2026-02-11 12:42:38 nm..
This article is licensed under a Creative Commons Attribution-NonCommercial 3.0 Unported Licence.

are sensitive enough to distinguish less conductive hydrates from pore fluids in sediments.[250,266–275] Archie-type equations with empirical adjustment parameters can then be used to establish the connection between electrical properties and hydrate content in order to approximate the gas hydrate saturation.[276–278] However, such estimates are subject to error primarily due to the semi empirical nature of Archie's equations and the lack of reliable laboratory and field calibration studies.[279] In fact, when predicting the effective electrical conductivity of a given hydrate bearing specimen, it is essential to account for the pore-scale distribution of the co-existing compounds including the mineral grains, water/ice, hydrates and free gas.[280,281] A detailed review regarding the electrical conductivity models can be found elsewhere.[282]

Several fields and laboratory studies have been conducted to measure the electrical conductivity of hydrate bearing sediments.[283–290] Given that various factors such as the ionic concentration of the aqueous solution, gas exchange and fluid-filling porosity of the pores affect the electromagnetic properties of gas hydrate bearing sediments,[291] the electrical conductivity of porous polycrystalline methane hydrates in mixtures with brine and sand was recently studied *via in situ* impedance measurement to gain insights regarding the petrophysical relations between methane hydrates, brine salinity and the host sediment.[292,293] Several possible conduction mechanisms were also determined to correlate resistivity data with methane hydrate saturations, information that can be used to improve the reliability of existing and new electrical models. The models available in the literature have been mainly developed according to the rock-physics models.[294–296] As such models cannot sufficiently account for the spatial arrangement of hydrates, effort focuses on addressing this shortcoming using the finite-element method in order to simulate the electrical characteristics of hydrate bearing specimens reconstructed by different methods such as the diffusion limited aggregation (DLA) model.[297–299] In addition, electrical resistivity tomography (ERT) has been shown as promising in characterizing electrical properties of hydrate bearing sediments.[300,301]

The magnetic permittivity is expressed as a complex number to account for its magnitude as well as its phase relative to the excitation. In hydrate studies, however, the real component of the permittivity is mainly investigated given the typical small contribution due to polarization losses (represented by the imaginary component) in the operating frequencies ranging between Hz and kHz.[138] As discussed earlier, the magnetic permittivity is influenced by geometric and spatial effects. Some models proposed for estimation of the effective magnetic permittivity of hydrate bearing sediments include the volumetric linear and quadratic methods.

2.5. Mechanical properties

Understanding of the mechanical behaviour of clathrate hydrates and the internal mechanisms of their deformation as well as their interaction with the host sediment is essential in gas production from natural gas-hydrate-bearing sediments, environmental and climate impact studies, hydrogen storage and hydrate technology applications. Similar to the thermal properties, it has been revealed that the mechanical properties of clathrate hydrates are different from those of ice Ih.[302,303]

2.5.1. Mechanical properties of pure clathrate hydrates. Experimental determination of the mechanical properties of clathrate hydrates is usually conducted using an apparatus consisting of a hydrate former unit and a mechanical measurement unit. Upon completion of the hydrate formation process at a desired condition, the mechanical properties of the specimen can be measured *via* direct or indirect methods.[214] The quality of the experimental results is undoubtedly affected by the measurement technique, system temperature, pressure and hydrate sample compaction.[303] It is difficult to make pure non-porous gas hydrate samples using existing techniques, and the presence of residual water/ice and free gas in the system due to incomplete hydrate formation process can adversely influence the measurements.[302] Experimental studies of laboratory-formed methane hydrate specimens containing ice confirm the strong dependence of their mechanical characteristics on the ice content.[304,305] Efforts have been made to reduce the uncertainties associated with hydrate formation technique by growing aggregates of gas hydrate under static conditions *via* combining cold and pressurized gas with granulated ice and/or within custom-built pressure vessels where the specimen can be compacted to porosities lower than 2.0%;[306–308] however, the mechanical behaviour is still influenced by the presence of micropores.[309–311]

2.5.1.1. Indirect determination of the mechanical properties. Indirect methods such as acoustic measurements were initially used to infer the mechanical properties of pure clathrate hydrates. For these studies, elastic wave (compressional and shear wave) velocities were measured using different techniques such as the ultrasonic pulse transmission method[302,303,308,312–316] and Brillouin spectroscopy method;[317–321] the results were then used to calculate the parameters related to elasticity mechanics such as elastic moduli (bulk, shear and Young's moduli) and Poisson's ratio.[214] X-ray diffraction, neutron diffraction and Raman spectroscopy techniques are also utilised to calculate the isothermal bulk modulus by measuring the unit cell volume as a function of pressure.[322–329]

Experimental studies suggest that the elastic properties of pure clathrate hydrates depend upon the hydrate composition and structure, the guest molecule, and cage occupancy.[214,312,318] Increasing the system temperature results in a reduced bulk modulus and Poisson's ratio for clathrate hydrates and consequently, a lower compressional wave velocity, similar to observations for ice Ih. However, the Young's and shear moduli were observed to vary depending on the guest molecule and even show anomalous behaviour.[214,217,302,303,313,319,330] For different pressures, bulk modulus and Poisson's ratio of clathrate hydrates increase with an increase in the pressure while the Young's, and shear moduli variations strongly depend on the guest molecule.[214,302,323,330,331]

2.5.1.2. Direct determination of the mechanical properties. Influenced by the aforementioned sources of uncertainty, the

Open Access Article. Published on 22 Junie 2020. Downloaded on 2026-02-11 12:42:38 nm..
This article is licensed under a Creative Commons Attribution-NonCommercial 3.0 Unported Licence.

strength of pure clathrate hydrates was initially believed to be similar to ice Ih.[214,332] However, laboratory constant-strain-rate experiments conducted on poly-crystalline methane hydrate specimens suggested a different stress–strain behaviour with an extraordinary strength (20 to 40-fold higher) compared with ice, which could be attributed to dislocation movement and molecular diffusion.[214,306,333–335] Unlike ice Ih which typically displays an ultimate yield strength followed by relaxation to steady-state behaviour, methane hydrate exhibits an extensive strain hardening followed by strain softening during compression.[306,335,336] In fact, the methane hydrate stress–strain curve can be divided into two stages: (i) the rapid structural damage stage and (ii) the complete structural damage stage.[337] Interestingly, methane hydrates undergo partial decomposition during deformation due to a solid state disproportionation or exsolution process, even well within the stability zone.[307,334] Studies of the creep behaviour of methane hydrates suggest direct proportionality of axial and creep strains with external load.[335,338]

The mechanical strength of pure clathrate hydrates was experimentally shown to be influenced by the system temperature, confining pressure, strain rate and density.[214] More specifically, the compressive and shear strength of methane hydrates increase with increasing confining pressure, strain rate and density.[339–342] The deviatoric stress increases with an increase in the strain rate at confining pressures less than 10 MPa, while at higher values there is no obvious change in the deviatoric stress.[343] Methane hydrate strength was also observed to be very sensitive to temperature, with lower temperatures leading to higher the strength.[341,342] When well within the stability zone, the compressive strength of hydrates is higher than that of ice Ih; however, the strengths become closer in value when hydrate is less supercooled (relative to the hydrate phase boundary).[340,341] The essential mechanisms causing the difference in the mechanical properties of clathrate hydrates and ice is underpinned by the special hydrate lattice structure and the host, guest and host–guest interactions.[214] In the small strain regions ($<1.5\%$), the stress–strain behaviour is generally not influenced by the confining pressure and temperature; however, within at the whole strain region, the mechanical behaviour is markedly influenced by the strain rate.[344]

2.5.1.3. Theoretical studies. The stringent high pressure–low temperature conditions required for hydrate formation and stability make the direct measurement of the mechanical properties and deformation mechanisms of pure hydrates difficult using common experimental techniques. This in turn, results in poor accuracy for values for the mechanical properties, and the extrapolation of these values can be controversial controversial.[214] The rapid progress of modern computer technology together with the unavoidable uncertainties associated with the experimental studies means models are the most promising alternative for providing insights into the mechanical behaviour of pure clathrate hydrates.[214]

Theoretical approaches such as Density-Functional Theory (DFT),[345–352] Molecular Dynamics (MD)[336,353–363] and Lattice Dynamics (LD) simulations[364–367] have been used to probe the mechanical behaviour of clathrate hydrates, with links to macroscopic phenomena. They have also been employed to deliver insights into problems not well understood by experiments and to validate the experimental results. These models also help elucidate the underlying mechanisms controlling the mechanical properties of clathrate hydrates and to explore why the mechanical behaviour of the clathrate hydrates differ from ice Ih.[358]

Recently, DFT was successfully employed to investigate the ideal strength of methane hydrates under uniaxial, triaxial, and shear deformation modes and to compare its mechanical behaviour with that of ice Ih.[366] The effect of guest molecule size on the mechanical properties of a number of hydrates was also investigated using DFT, suggesting a close relationship between the shear modulus, wave velocity and the level of anisotropy in the hydrate lattice, which itself is a function of guest size.[346,347,368] More recently, a DFT study compared the mechanical and vibrational properties of tetrahydrofuran (THF) hydrates with natural gas hydrates, providing significant insights into the accuracy of using THF hydrates as an analogue for natural gas hydrates.[349]

MD simulations have assisted with the construction of theoretical stress–strain curves for pure clathrate hydrates for different structures and at different pressures and temperatures and led to the determination of such mechanical properties as Poisson's ratio, elastic moduli and strength and identification of fracture initiation process.[353,354,357,359,361] The origin of strain hardening in methane hydrates under compressive deformation was also investigated using MD simulations. The simulation results highlight the role of the guest molecules as non-deformable units preventing the failure of hydrate structures and thus leading to the strain-hardening phenomenon.[336] MD simulations also revealed that the temperature dependence of the elastic moduli of pure hydrates is dominated by the guest molecule, a phenomenon of particular importance in hydrate-based applications such as carbon capture and storage where CH_4 is replaced by CO_2.[354] The role of guest molecules on the mechanical properties of hydrates was further explored with the aid of tension MD simulations.[363] The results indicated that the tensile strength and Young's modulus of hydrates are influenced not only by the type, size and shape of guest molecules but also on its polarity. Of particular interest, MD simulations helped with shedding light on the mechanical instability of monocrystalline and polycrystalline methane hydrates, providing molecular insights regarding destabilising mechanisms of gas hydrates under mechanical loading and their grain-boundary structures[353] (see Fig. 7). Moreover, it was shown that polycrystalline hydrates under compression and tension exhibit grain size strengthening at low grain sizes and grain size weakening at larger grain sizes. The intrinsic differences in the mechanical properties of monocrystalline methane hydrate monocrystalline ice Ih were also explored using MD simulations. The simulation results suggest these differences could be due to the host–guest molecule interactions and relative angles which tetrahedral hydrogen bonds make to the loading direction.[358]

Open Access Article. Published on 22 Junie 2020. Downloaded on 2026-02-11 12:42:38 nm..
This article is licensed under a Creative Commons Attribution-NonCommercial 3.0 Unported Licence.

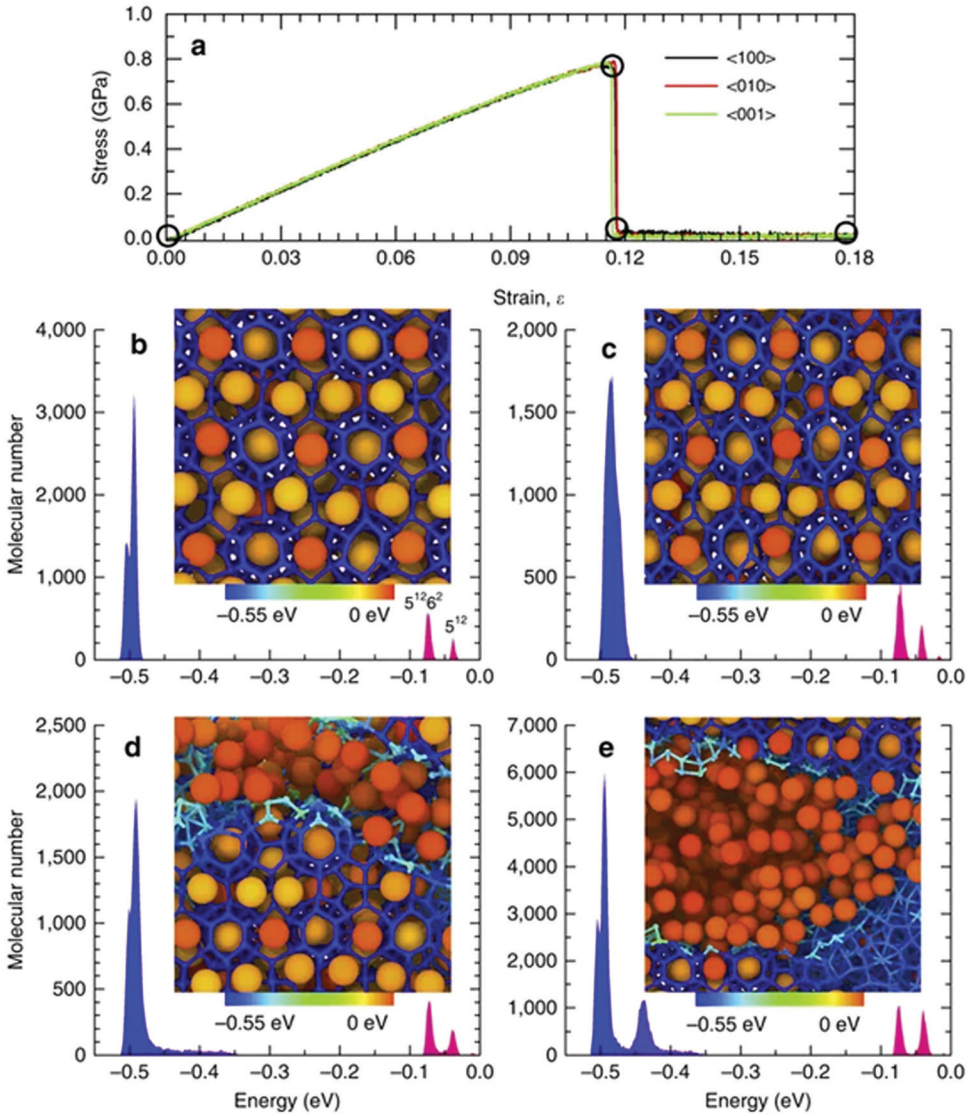

Fig. 7 (a) Stress–strain relationships for single-crystal methane hydrate. The molecular cohesive energy distributions and corresponding localized molecular structures (b) initially, (c) at the onset of fracture, (d) immediately after initial fracture and (e) at a strain of 0.18 (reprinted with permission from Wu *et al.*,[353] Copyright 2015 Springer Nature).

Microscopic insights offered by the molecular modelling efforts could establish the fundamental understanding of the mechanical responses of naturally occurring and artificial synthetic gas hydrates. However, there is a gap in the knowledge as most of the studies have focused on qualitative behaviours and mechanisms and are yet to fit these findings to laws to achieve upscaling.

2.5.2. Mechanical properties of gas hydrate-bearing sediments. The presence of gas hydrates within a formation controls the mechanical stability of gas hydrate-bearing sediments.[369] Hence, mechanical instability and degradation associated with gas hydrate dissociation in gas hydrate-bearing sediments due to natural processes[370] and human intervention (such as gas production,[371,372] CO_2 sequestration,[373] drilling operations[374–378]) may play a role in submarine slope failures, seabed subsidence, and failure of the foundations of seafloor installations.[379–384] It is thus imperative that the geophysical and geomechanical properties of gas hydrate-bearing sediments are well investigated to understand their occurrence and stress–strain and permeation characteristics. Laboratory testing of retrieved undisturbed field samples[385,386] and simulated gas hydrate-bearing sediments[387–391] can be employed to study the effect of the various parameters such as pressure, temperature and hydrate saturation on the geomechanical behaviour of gas hydrate-bearing sediments. According to the experimental studies, the mechanical properties of gas hydrate bearing sediments such as the elastic moduli decisively depend on the gas hydrate saturation and pore-scale distribution.[138,381,392–394] Depending on the sediment grain size, stress field, and the amount of water and natural gas available, gas hydrates formation may enhance the strength of the host sediment and reduce its permeability *via* displacing grains or interconnecting and cementing them.[394–397] On the other hand, gas hydrates dissociation is associated with the

Open Access Article. Published on 22 Junie 2020. Downloaded on 2026-02-11 12:42:38 nm..
This article is licensed under a Creative Commons Attribution-NonCommercial 3.0 Unported Licence.

release of the pore water and natural gas and migration of fine particles through porous sediments.[381,398,399]

The effects of hydrates on the mechanical properties of the host sediment properties strongly depend on where hydrates nucleate and grow in pore space. The pore-scale habit of hydrates is determined primarily by the state of effective stress and host sediment grain size (Fig. 8).[400] For coarse-grained natural HBS, when excess water presents in the system, the main pore-scale habit is preferred to be pore-filling,[401] whereby hydrates nucleate on the sediment grain boundaries and grow freely into the pore spaces without bridging two or more particles together. Moreover, since gas hydrate is suspended in pore fluid, it primarily alters the pore fluid bulk stiffness, fluid conduction properties and bulk density of the sediment.[402] At saturations generally more than 40%, pore-filling hydrates turn into load-bearing, where hydrates bridge neighbouring grains

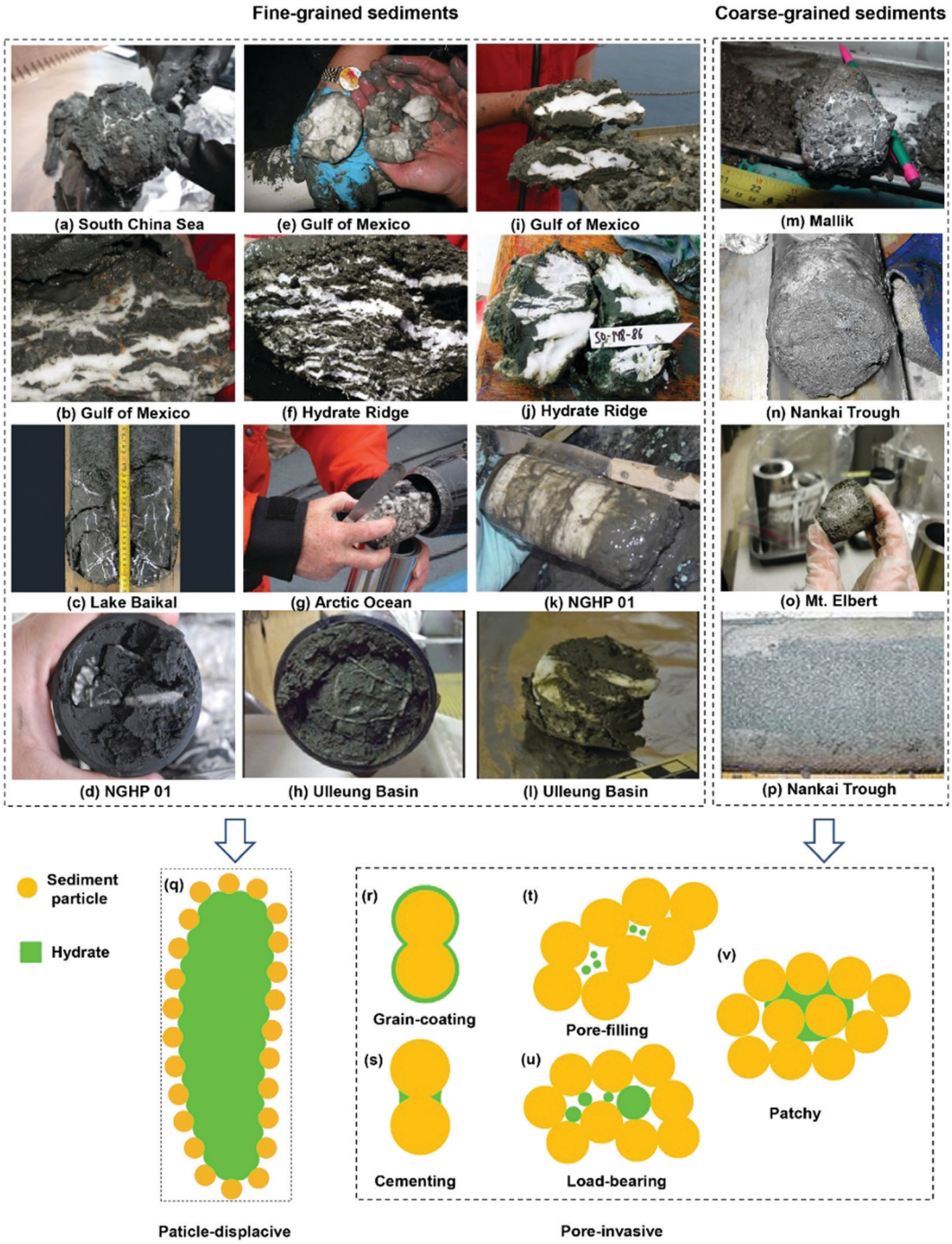

Fig. 8 Core-scale hydrate morphology in HBS samples and conceptual pore-scale habits for fine-grained and coarse-grained sediments (reprinted with permission from Ren *et al.*,[403] Copyright 2020 Elsevier Ltd).

Open Access Article. Published on 22 Junie 2020. Downloaded on 2026-02-11 12:42:38 nm..
This article is licensed under a Creative Commons Attribution-NonCommercial 3.0 Unported Licence.

and become a part of the skeleton and accordingly, contribute to the mechanical stability of the sediment. For these two pore-scale habits, there is always a water film remaining on the grain surface. When excess gas presents in the system, grain-coating habit is preferred by hydrates, whereby they form a coating around grains. When there is enough free gas in the system, the grain coatings can coalesce to cement intergranular contacts and even use up remaining water.[403] Pore-scale habit for fine-grained HBS is different from coarse-grained sediments, mainly due to smaller pore-size and higher specific surface. While capillarity acts as a hindrance for hydrate nucleation, hydrate growth can displace sediment grains, leading to particle-displacive segregated morphology, *e.g.* lenses, nodules, chunks and veins.[369] A comprehensive discussion regarding the pore-scale habit of HBS can be found elsewhere (Fig. 8).[403]

It must be noted that laboratory-formed HBS samples are more often used to study properties of HBS;[404] however, they are not necessarily representative of naturally occurring HBS samples, particularly in pore-scale habits and physical properties. In recent years, the advancement of pressure core acquisition and analysis technology has enabled scholars to image and interrogate pressure cores to study hydrate habits of nearly intact naturally occurring HBS preserved at their *in situ* pore pressures.[405,406] Post-recovery analytical capabilities for pressure core samples have also allowed for reliable and systematic measurement of physical properties.[407]

2.5.2.1. Fluid flow and permeability characteristics. Permeability is a measure of the ability of a porous medium to allow fluids to pass through it, and the relationship between fluid flow and permeability controls both fluid-flow pathways and the accumulation, distribution and saturation of gas hydrates.[138] This is particularly important for gas transport, production or migration into the oceanic environment.[408] Apart from the mineralogy, shape and packing arrangement of the grains and the size (specific surface area) and interconnectivity (tortuosity) of the pores, the presence of gas hydrates adds additional complexities because the spatial distribution of hydrates can alter the pore size, shape and interconnectivity and accordingly the permeability of sediments.[138] To date, numerous macro- and micro-scale experimental studies have been conducted to investigate fluid flow through hydrate bearing porous sediments and explore the link between the permeability evolution and hydrodynamics of gas-hydrate systems.[401,409–424] A review regarding the experimental techniques for investigating the permeability properties of hydrate-bearing sediments can be found elsewhere.[425]

Furthermore, several numerical simulation studies have been conducted to elucidate the geological processes associated with hydrate formation and dissociation in porous media under a wide range of conditions.[426–441] Studies also to predict the behaviour of gas hydrate bearing sediments during gas production,[442–449] a process for which the absolute and relative permeability values and relationships are crucial given their influence on gas and water production rates. A review regarding recently developed relative permeability models can be found elsewhere.[381] *In situ* observations of pore structures using X-ray microCT and Nuclear Magnetic Resonance Imaging (MRI) can significantly improve our pore-scale understanding of the permeability characteristics of gas hydrate bearing sediments as a function of hydrate saturation.[406,450–458] A review regarding the analytical and empirical correlations used for determination of permeability of hydrate bearing sediments has been published by Joseph *et al.*[459]

Fines, which commonly coexist with sediments that host natural gas hydrates, can be readily mobilized by water and/or gas flow during gas production.[460] Fines migration inherently involves the permeability impairment associated with the generation, movement, and retention of sub 100 μm solid particles in porous media.[461] Several experimental and numerical studies have recently been conducted to further understanding of the contribution to permeability evolution due to fines that are mobilized during gas production.[460,462–467]

To date, an accountable number of studies have been undertaken to characterize fluid flow in sediments containing hydrates given their vital role in exploration and exploitation of natural gas hydrate as well as assessment of the impacts due to the hydrate dissociation on submarine instabilities, marine ecosystem and global climate change. However, there exist several challenges mainly due to the difference between the simulated HBS samples, core samples and natural ones, leading to the discrepancies between the measured/estimated permeability and the real values.[403] The main challenges in lab-scale studies include difficulties associated with the HBS sample size and methods followed to form hydrates within the host sediment and maintain the equilibrium conditions during the test process (to avoid hydrate formation or dissociation).[401,462,468] On the other hand, the flow test method (Steady State/Unsteady State) adds more uncertainties since these methods are usually time-consuming and inherently rely on assumptions far from the real conditions governing HBS occurrences.[469] This makes it essential to address the lab challenges in accordance with the flow test methods. Of particular importance is the pore-sale habit of hydrates in artificial samples which is predominantly controlled by the hydrate formation method. The pore-scale habit in conjunction with the pore-structure, anisotropy and heterogeneity influence the permeability characteristics of HBS,[470] which makes it challenging to synthesize artificial samples imitating natural ones. Thus, to bridge the gap of measured permeability between laboratory samples and natural sediments, it is of utmost priority to upgrade the existing methods and apparatuses or even develop new measurement methods. Challenges encountered in theoretical analysis and numerical simulations are mainly due to several simplifications such as assuming homogeneous and isotropic reservoir/porous medium where hydrates are uniformly distributed with a predetermined pore-scale habit. Insights provided by the lab scale studies are required to be considered in numerical simulations to be able to make reliable permeability predictions. Further discussion in this regard can be found elsewhere.[403]

2.5.2.2. Geophysical properties. Geophysical studies are essential in assessing natural gas hydrate bearing sediments

Open Access Article. Published on 22 Junie 2020. Downloaded on 2026-02-11 12:42:38 nm..
This article is licensed under a Creative Commons Attribution-NonCommercial 3.0 Unported Licence.

and are extensively used for detection, mapping and characterization of gas hydrates occurrence[471] and tracking their formation/dissociation process within sediments[472] given that hydrates have much higher elastic moduli than the pore fluids and alter the stiffness of the pore fluid and host sediment.[473] Hydrate formation has an impact on the skeletal stiffness of host sediment, enlarging contacts between grains, which in turn, results in the reinforcement of the bulk and shear moduli. Accordingly, hydrate bearing sediments show elevated elastic wave velocities depending on the saturation and pore-scale habit of the hydrates within the sediment framework.[265] However, the strong dependence of the elastic moduli of hydrate bearing sediments on the pore-scale habit of the hydrates may cause ambiguity when inferring the hydrate saturations from measured velocities.[474,475] A review in this regard can be found elsewhere.[138]

A tremendous number of field-scale geophysical studies have been undertaken in North America,[476–482] Asia,[245,250,254,483–490] Europe,[491,492] Africa[493–496] and Oceania[497–502] in order to understand the natural occurrences of gas hydrates and quantify the extent and distribution of gas hydrates within the sediments for exploration purposes. Seismic techniques are the most commonly used methods for detecting gas hydrate occurrences, particularly in the marine environment, where they are employed to identify Bottom-Simulating Reflections (BSR).[503] BSRs can be observed at a depths of up to several hundred meters below the seafloor in continental margin sedimentary sections and are a seismic reflection likely to be caused by the elastic velocity contrast between the overlying gas hydrate-bearing sediments and the underlying gas saturated sediments.[504] The BSR is the main identifier for the presence of gas hydrates, corresponding to the deepest level at which natural gas hydrates are stable. BSRs can be either continuous, discontinuous, or plumbing.[505,506] However, sediments can contain gas hydrates without having a BSR, particularly if hydrate is not present near the phase boundary due to the nature of the sediments there or insufficient methane for hydrate to form directly above the free gas phase.[507] Elastic wave velocities combined with amplitude variation with offset (AVO) and amplitude variation with angle (AVA) data from BSRs have been used to estimate associated gas hydrate and free-gas concentrations as well as infer the distribution of natural gas hydrate bearing sediments.[508–516] Vertical seismic profiling surveys (VSP) are also used along with downhole log data to evaluate the effect of gas hydrates on the elastic velocity of hydrate bearing sediments.[517–519]

Laboratory analyses of natural or artificial gas hydrate bearing specimens have been conducted to study the impact of hydrates on the elastic wave velocities of different types of sediments. Laboratory studies confirm the significant impact of hydrates where increasing gas hydrates within the host sediments result in elevation of the elastic wave velocities.[284,520–528] However, the method of synthesizing gas hydrates in sediment substantially affects the pore-scale habit of hydrates.[138,284,529] Given the recent interest in permanent hydrate-based storage of CO_2 in geological formations, seismic survey methods could be used to remotely monitor the CH_4–CO_2 replacement process and evaluate the stability of the host sediment.[530–532]

Several models have also been developed to establish a relationship between the elastic moduli and the gas hydrate saturation in order to quantify the amount of gas hydrates accumulated in the sediments and predict HBS physical properties.[533] These models consider the elastic properties of sediments, pore fluid(s) and gas hydrates[534] and generally can be categorized into Time-average equations, Weighted-average equations, Cementation theory-based models, and Effective Medium Theory (EMT) models. Detailed reviews of these can be found elsewhere.[402,535–537] A number of theoretical and numerical approaches have also been developed to detect and quantify gas hydrates in submarine and permafrost regions to give more insights into elastic wave attenuation mechanisms.[538–540]

2.5.2.3. Geomechanical characteristics. The strength of a hydrate bearing sediment subjected to a principal effective stresses (axial (σ_1') and confining stress (σ_3')) at a specific pore *P–T* is expressed by the cohesive resistance (c) and frictional resistance and described by the friction angle (φ). These properties can be obtained by applying the Coulomb failure criterion which relates the shear stress at failure (τ_f) to the normal effective stress acting on the failure plane (σ_n') in the Mohr–Coulomb failure diagram.[138] The strength parameters together with the other geomechanical properties such as Young's modulus (E), Poisson's ratio (ν) and dilatancy angle (ψ) are measured using the triaxial compression tests.[381] Recently, numerous triaxial experiments have been carried out to determine the geomechanical properties of natural and synthetic gas hydrate bearing sediment samples at high pressure and low temperature conditions.[386,389,391,541–558] Shear strength of specimens at specific pore pressures and temperatures with a given hydrate saturation could be tested under undrained (CU) or drained (CD) modes after consolidation, a detailed discussion of this can be found elsewhere.[138] Given the fact that the geomechanical properties of sediment predominantly depends upon the grain type, shape, packing, fines content and degree of consolidation,[559,560] the presence of hydrates within sediment generally results in bridging/binding of sediment grains and consequently a higher stiffness, pre-failure dilation, and strength whereas the friction angle has been interestingly observed to remain constant with increasing the hydrate saturation.[381]

The pore-scale habit of hydrates can markedly affect the strength evolution of the host sediment, particularly at lower saturations ($<30.0\%$).[561] According to recent experimental studies, there is a critical saturation at which the local growth of hydrates and/or their extension across adjacent grains result in creating hydrate networks or frame structures throughout the specimens and accordingly substantial enhancement of the cohesive resistance, normalized stiffness and volumetric dilation as well as switchover of the stress–strain response from strain-hardening to strain-softening.[387,393,542,562–564] This critical saturation ranging from 15.0 to 50.0% is essentially affected by the spatial distribution of hydrates in the sediment matrix and requires to be taken into consideration to avoid the formation of geomechanical instabilities associated with the hydrate dissociation when predicting the response of gas

Open Access Article. Published on 22 Junie 2020. Downloaded on 2026-02-11 12:42:38 nm..
This article is licensed under a Creative Commons Attribution-NonCommercial 3.0 Unported Licence.

hydrate bearing sediments to different external stimuli such as mechanical loading and *P–T* variations during exploitation. At higher saturations (> 80.0%), however, the sediment grains will be cemented by hydrates exhibiting a monolithic system with minimal host sediment characteristics.[381] The presence of occluded pores within the sediment makes the measurement of the pore pressure difficult, hence interpretations at these saturations are usually based on the total stress, not the effective stress. Further details of this have been provided elsewhere.[381]

Confining stress (σ_3) and system temperature also affect the geomechanical behaviour of hydrate bearing sediments. At a given hydrate saturation, higher confining stresses result in higher interlocking and crushing of grains and accordingly overall increase in shear strength and stiffness, reduction in Poisson's ratio and dilatancy angle and switchover of the stress–strain response from strain-hardening to strain-softening.[565–567] Temperature reduction results in higher stability of hydrates within the host sediment and a higher shear strength. Several experimental studies have been conducted recently to explore the stress–strain response of hydrate bearing sediments as a function of hydrate dissociation. This process is associated with significant changes in the matrix of gas hydrate bearing sediments such as an increase in pore pressure under undrained condition or fluid flow under drained condition, secondary hydrate/ice formation and loosening of grains.[568–577] Creep tests have recently been conducted on hydrate bearing specimens which are particularly relevant given the importance of predicting the long-term stability of gas hydrate bearing sediments in Arctic and permafrost regions.[578–580] More recently, the geomechanical characteristics of gas hydrate bearing frozen sediments have been experimentally studied to investigate the influence of gas hydrates and ice coexistence on the geomechanical strength of the sediment.[581–583]

The geomechanical behaviour of gas hydrate bearing sediments has also been simulated mainly *via* applying the Mohr–Coulomb, Cam-clay, Duncan–Chang and critical-state models. These geomechanical models available in the literature have been employed to capture the effect of hydrate saturation and spatial distribution on the sediment strength, stiffness and dilation characteristics.[584–590] The geomechanical models are also increasingly included in numerical reservoir simulators to investigate the coupled geomechanical response of hydrate reservoirs to different external stimuli.[382,575,591–597] Additionally, the Discrete Element Method (DEM) has been extensively utilised for the simulation of the mechanical behaviour of hydrate bearing sediments under triaxial compression.[598–609] More recently, some micromechanical models have been proposed for hydrate bearing sediments whereby the hydrates are represented as solid particles positioned between sand particles and contributing to the skeleton response even for small strains.[610,611]

2.6. Rheological properties of hydrate slurries

Rheology studies on hydrates have provided insights into the rheological properties of hydrate-laden suspensions, which may be found in oil and gas transportation pipeline networks[612,613] during and after hydrate formation, in order to improve hydrate flow assurance strategies.[614,615] Investigation of the viscosity alteration of gas hydrate slurries due to presence of hydrate particles and aggregates in pipelines is essential in flow assurance studies. This enables the development of a reliable model capable of describing hydrate-laden flow characteristics in pipelines to reliably determine the extent to which hydrates may cause flow hindrance.[616,617] Recently there has been a paradigm shift in flow assurance from "complete hydrate avoidance" – where large quantities of hydrate inhibitors are injected into flowlines to prevent gas hydrate formation – to "hydrate management" – where gas hydrates are allowed to form in the flowline, but the hydrate slurry properties are controlled. This shift renders it imperative to gain knowledge of the rheological behaviour of the gas hydrate slurries in order to find the key factors influencing the transportability of gas hydrates in flowlines.[618] Clathrate hydrate slurries also have applications in refrigeration where hydrate slurries are used as a two-phase (solid–liquid) secondary refrigerant (TPSR)[619–623] to provide chilling.

To date, several efforts, including large-scale flow loop-based[619,620,624–637] and small-scale benchtop rheometer-based[638–653] studies, have been undertaken to obtain experimental evidence on the rheological properties of hydrates and investigate the effect of hydrate agglomeration and deposition on hydrate slurry viscosity. However, it has always been difficult to reproducibly control the hydrate formation under high pressures for hydrate slurry characterisation.[614,640] In flow loop-based studies, the turbulent behaviour of industrial pipelines is approximated, and the apparent slurry viscosity estimated from measured pressure drops by applying the Hagen–Poiseuille and Rabinowitsh–Mooney equations under a number of assumptions.[654] Flow loop experiments provide a practical way to study the effects of flow regimes and patterns on hydrate slurry rheological behaviour.[635] In benchtop rheometer-based studies, the shear rate, shear stress and accordingly the viscosity of a hydrate slurry sample are directly measured using high-pressure rheometers and/or autoclaves.[639,655,656] These studies allow for an intuitive approach when studying the effect of different factors such as water fraction, hydrate volume fraction and shear rate on the rheological behaviour of hydrate slurries.[635] However, since each measurement technique has its own limitations, comparison of different types of experimental studies is not straightforward. Moreover, most studies have been conducted under different conditions (temperature, pressure, composition) causing complexities when attempting to compare the experimental data with model predictions.[657]

To predict hydrate blockage in multiphase flowlines, the experimental studies are incorporated into the development of an appropriate formation/agglomeration model and coupled with transport and kinetic models. To date, a number of empirical and physical models have been developed to predict the rheological properties (viscosity and yield stress) of hydrate slurries formed from water-in-oil emulsions.[626,658,659] The rheological models currently available in the literature have been reviewed elsewhere.[657]

Further experimental and modelling studies are necessary to achieve reliable relative viscosity for a given hydrate slurry as a

Open Access Article. Published on 22 Junie 2020. Downloaded on 2026-02-11 12:42:38 nm..
This article is licensed under a Creative Commons Attribution-NonCommercial 3.0 Unported Licence.

function of the hydrate volume fraction. In addition, as initial work on understanding the viscosity of gas hydrate slurries focused on understanding the behaviour of ice slurries, comparing the rheological properties of ice slurries to those of a gas hydrate slurries could help with understanding the influence of particle agglomeration on viscosity and yield stress. An advanced knowledge of the rheological properties of gas hydrate slurries is also necessary for the other hydrate-based applications such as desalination, gas separation and energy storage, where hydrate-laden slurry flows in purpose-built flowlines with configurations different from oil and gas transportation pipeline networks. Literature survey shows that the experimental and modelling studies on rheology properties of gas hydrate slurries have been mainly concerned with energy applications. This makes it necessary to extend rheological studies in both experimental and modelling aspects in compliance with the other hydrate-based applications given the transportability of the hydrates in flowlines is controlled by the relative viscosity of hydrate slurry.

2.7 Interfacial phenomena

Interfacial systems consisting of fluids and surface-active materials play a critical role in gas hydrate nucleation and growth phenomena (Fig. 9). Thermodynamics of interfacial areas containing the alterations to the chemical potential, interfacial tension (IFT), entropy, and Gibbs free energy throughout the gas hydrate formation process are of enormous interest and require a fundamental understanding of the gas hydrates interfacial characteristics.[660] Due to the significant surface district created in the hydrate system, IFT can directly influence the total free energy.[661,662] The potential molecular interactions at the particle–particle and particle–surface interfaces will change based on the IFT, contact angle, and Gibbs free energy alterations,[663] when hydrate crystals exist in their various continuous phases including gaseous, oleic, and aqueous phases.

The interface free energy can be explained using an IFT per unit area, to exchange the pressure term in the Gibbs–Duhem equation as follows:[660,664]

$$\mathrm{d}G^{\sigma} = \sum_{j} n_j^{\sigma}\mathrm{d}\mu_j + A\mathrm{d}\gamma^{\sigma} + S^{\sigma}\mathrm{d}T$$

where G^{σ} is the free energy, n_j^{σ} is the number of molecules at the interface, μ_j is the chemical potential of moieties j. Moreover, A, γ^{σ}, S^{σ}, and T are assigned to the interface district, IFT, entropy, and the temperature of the system, respectively. It is worth mentioning that in the free energy definition for interfaces, the differential volume and pressure terms have been substituted with a differential interfacial region and the IFT; this explanation can describe the important physical role of IFT in 2D systems. In the systems without surface active species, the chemical potential effect could be ignored following Gibbs' formalism of the 2D partitioned surface with no volume. Although this hypothesis is helpful for streamlining the calculations, it does not illustrate the difference in continuous phase characteristics (*e.g.* density) when approaching the interface.[660] This density variation from the interface into the continuous phase leads to an equilibrium super-saturation of each moiety in the interface district. This demonstrates the physical drivers behind the hydrate nucleation phenomenon at the interface[665] (*e.g.* methane–water interface) through raising the possibility[666,667] of stabilising the preliminary hydrate cages.[668,669] Interfacial super-saturation is important to establish the feasible applications of hydrate inhibitors in the pipelines, since the injection of polar hydrate thermodynamic hydrate inhibitors (THIs) such as methanol (MeOH)[670] and salts[671] could augment the equilibrium solubility of small oleic species in the water phase.[672] On the other hand, some refrigerants are low-pressure hydrate crystals with increased solubility in the water phase.[673] The preliminary hydrate crystal growth at the aqueous–oleic interface is limited by this area of super-saturation with a related film thickness of 5 to 100 mm for the methane hydrate.[674,675] In the presence of limited water in oil micro-emulsions, some research have noted that the interfacial metastability needs a significant driving force for the nucleation of hydrate crystals.[676] Then, the formed hydrate crystals could exhibit an aqueous quasi-liquid layer (QLL)[677] at the solid hydrate–oleic phase interface. The thickness of the stratum can range from nm[678] to mm,[679] and can reduce the system global free energy.[680] As the temperature reduces down to beneath the hydrate melting point, the thickness of the liquid-like stratum would be suppressed and eventually vanished.[678] Typically, the interfacial forces mainly consist of electrostatic interactions

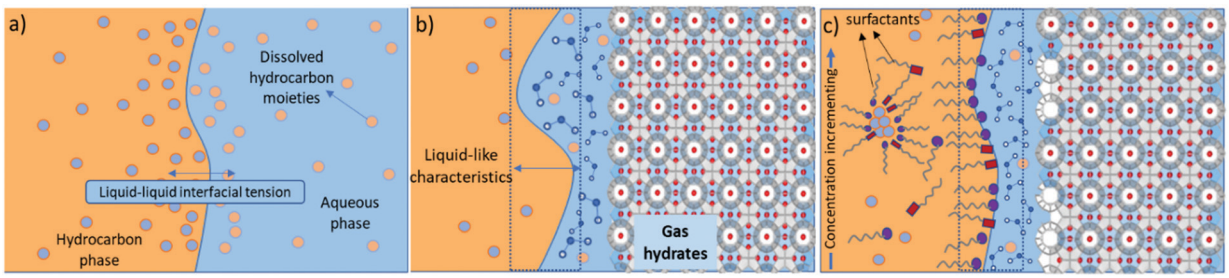

Fig. 9 The various solid hydrate and fluid–fluid interactions which play crucial roles in hydrates crystals formation and inhibitions phenomena; (a) formation of water in oleic phase and hydrocarbon in aqueous phase emulsions; (b) hydrate crystals (solid phase) formation, growth, and their interaction with peripheral water and hydrocarbon molecules at interface; (c) hydrate crystals-water-hydrocarbon molecular interactions in the presence of different surface-active chemical species.

Open Access Article. Published on 22 Junie 2020. Downloaded on 2026-02-11 12:42:38 nm..
This article is licensed under a Creative Commons Attribution-NonCommercial 3.0 Unported Licence.

(*e.g.*, electric double layer forces), van der Waals (vdW) interactions, hydration forces, capillary forces, intermolecular interactions, and hydrogen-bonding.[663,681] Therefore, interfacial forces implicating hydrate surfaces play significant roles in controlling the hydrate surfaces stability and the corresponding interactions with minerals in geological formations and inhibitors in flow lines.

Surface active chemicals or surfactants could affect the clathrates crystallization rate through various roles.[682,683] Surfactants could facilitate the hydrate nucleation phenomenon by reducing the clathrate–aqueous phase surface free energy, since they adsorb onto that interface.[684] Additionally, they could boost the mass transfer process by increasing the blending of water and methane which results in the acceleration of hydrate crystal growth. Surfactant adsorption onto the interface surface, however, could abate the hydrate crystals growth rate.[685] Various adsorption drivers have been suggested for surfactants at the hydrate crystals surfaces in contact with the aqueous phase.[682,686–691] Realisation of the drivers of the amphiphilic molecular interaction with the clathrate surface is critical for their utilisation and optimization for suppressing the hydrate crystallisation rate. In this regard, sodium dodecyl sulfate (SDS) was recognised as one of the most effectual surface active species to boost the nucleation and growth of gas hydrates crystals.[682,687,692]

By conducting zeta potential measurements,[686] it has been shown that SDS adsorbs to the hydrate surface through hydrogen bonding of the anionic head group of SDS to the water molecules on the hydrate surface, leading to an arrangement of the active moieties at the interface where the hydrocarbon tail stays in the aqueous phase.[686] Lo *et al.*[690] realised that SDS adsorbs to a cyclopentane hydrate through the Langmuir isotherm and noted that the first saturation point related to the generation of a monolayer surfactant *via* anionic hydrogen bonding to the hydrate surface. The second saturation point related to the creation of a bilayer with the ionic functional groups of the second surfactant stratum adjusted towards the water phase.

The influence of surfactants on the cyclopentane clathrate hydrate crystallization have been investigated.[693] At low surfactant volumes, reduced interfacial tension owing to the shrinking district of the water–cyclopentane interface was reported, resulting in formation of a planar clathrate hydrate crystal. At higher surfactant volumes, the interfacial tension fluctuated during the crystallisation phenomenon, which led to crystal morphology alteration towards the conical shape. The interfacial tension fluctuation behaviour is due to the growth and liberation of the hydrate crystals from the droplet surface. The prevalent interfacial behaviour presents a microscopic point of view, which can be employed to realise the cold flow operating strategy for hydrate slurries,[694] where the probable capillary-aggregation phenomenon between hydrate crystals is profoundly underrated within the gas hydrate stability region.

3. Kinetics of gas-hydrates formation and dissociation

Developing further potential applications of hydrates are primarily hindered by the problems associated with hydrate formation and dissociation. Understanding the kinetic process of clathrate hydrate remains a challenging aspect of hydrate-related problems. For instance, increasing the rate of gas hydrate formation is critical in gas storage and gas separation operations that utilise hydrates. Whereas depressing the rate of hydrate formation and rapid dissociation is important for hydrate risk management in the area of flow assurance. Controlling the rate of hydrate dissociation is important for natural gas storage and environmental issues. In this section, we review growth and dissociation kinetics of clathrate hydrates.

3.1. Crystallization

Crystallization occurs in two major steps (see Fig. 10). The first step is known as nucleation, which is the appearance of a crystalline phase from disordered or liquid-state molecules. The second step is known as crystal growth, which is the subsequent increase in the size of particles and leads to a crystalline form. Three canonical hydrate structures (sI, sII, and sH) are known and guest–host interactions play a crucial role as hydrates are thermodynamically stable only when a minimum number of cages are filled with the guest molecules. It has been found that the number ratio of cages filled with guest molecules (cage occupancy) of the largest cage is almost 100% and that the cage occupancy of smaller cages depends on the formation conditions. Thus, the stoichiometry of a hydrate depends on the formation conditions, such as pressure and temperature, and the type of guest molecule. Also, the kinetics of hydrates depend on temperatures above and below the melting point of ice (273 K) due to the phase change of water (solid, liquid, or vapour).

3.1.1. Nucleation. Nucleation is the initial step of the process of forming a new structure *via* self-organization.[695] There are two types of nucleation processes: homogeneous nucleation and heterogeneous nucleation. They differ according to the location at which a nucleus form. The homogenous nucleation occurs at the nucleus of the hydrate phase emerging directly from the parent phase, while heterogeneous nucleation

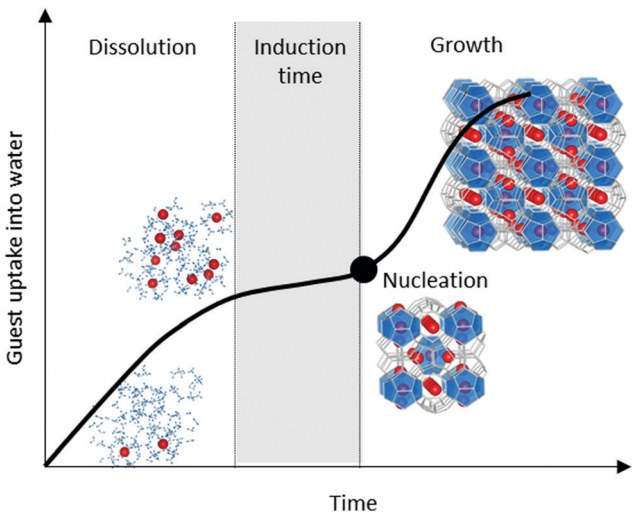

Fig. 10 Typical time dependence of the hydrate crystallization process.

Open Access Article. Published on 22 Junie 2020. Downloaded on 2026-02-11 12:42:38 nm..
This article is licensed under a Creative Commons Attribution-NonCommercial 3.0 Unported Licence.

occurs at nucleation sites on alien surfaces or particles. Nucleation is a stochastic event where nucleation will occur at different times even in identical systems. Since hydrates consist of water and guest molecules, the nucleation process starts with dissolution/adsorption of guest molecules into the water phase. The hydrate nucleation can be detected through a rapid decrease in pressure during the encapsulation of guest molecules within the crystalline hydrate structure, or a rapid rise in temperature as a result of the exothermic reaction of the hydrate.

The period between the times when the system temperature is lowered, or pressure is increased, to the equilibrium *P–T* condition at the time of hydrate nucleation is called the induction time. The induction time has been confirmed experimentally in various studies and the period basically depends on the driving force.[696] The induction time data for hydrates fits the probability function to the theoretical probability distribution function describing the behaviour of stochastic processes[697–702] based on classical nucleation theory (CNT). Crystalline hydrate growth occurs only after nuclei larger than critical radius, which is the minimum size that must be formed before crystalline hydrate growth, is attained. A molecular-level hypothesis of the induction time in homogeneous nucleation of hydrate is that cage-like water clusters surrounding guests combine to form the initial amorphous hydrate like structures.[703] This is called labile-cluster hypothesis (see Fig. 11), and several other mechanisms for homogeneous nucleation have been proposed by recent molecular dynamic simulations: local-structuring hypothesis,[704] blob hypothesis,[705] and cage-absorption hypothesis.[706] The reader is referred further to Section 3.1.3 of the present work. From experimental studies, Raman spectroscopic measurements of methane hydrates suggest that water clusters, which are similar to small cages of structure I hydrate, are readily formed and the formation of large cages of structure I hydrate from liquid water may be rate-determining during the hydrate formation.[707] However, no significant difference between the structure of water before methane hydrate formation and that after the hydrate dissociation was observed by neutron diffraction method.[708] Also, no significant difference between that of the liquid mixture of THF at room temperature and supercooled temperature was observed by X-ray Raman scattering measurements.[709]

A significant effect on shortening induction time of hydrate nucleation has been observed by using dissociated hydrate water or ice melted water.[710] This phenomenon is called a memory effect. The occurrence of residual structure is suggested by the difference in water viscosity between that before hydrate formation and that after hydrate dissociation.[711] The higher viscosity of water after the hydrate dissociation returns only after heating to a temperature well above hydrate equilibrium. The stochastic nature of these waters has been confirmed by statistical methods.[697,712,713] However, no significant structural difference of water after hydrate dissociation was found in different thermal histories by neutron diffraction.[714] Recently, the formation of submicron-sized bubbles, so called nanobubbles, due to hydrate dissociation was reported.[715,716] A significant number of nanobubbles remain dispersed in the dissociated water for more than 1 day, and the water has memory effect. MD simulations of methane hydrate dissociation also suggest the formation of methane nanobubbles in water.[717] The guest–water interfaces of these nanobubbles may act as nucleation sites for heterogeneous nucleation of hydrate without the need for residual structures. Detection and measurements of the sudden nucleation event may be difficult because the nucleation sites are themselves a stochastic process forming the crystalline hydrate phase at a certain point suddenly. Although previous investigations have not thoroughly examined the stochastic hydrate nucleation process, these hypotheses listed above as well as CNT may give insights into fully understanding the complex mechanism.

3.1.2. Growth. Understanding of geometric configuration of hydrate crystals such as their sizes or shapes (morphology) and factors that control the hydrate morphology is important for the development of hydrate-based technologies. Here, some of the key aspects of kinetic process at guest–water interface are considered. The mechanical stirring of water and guest components promote hydrate growth. The key is how to increase the surface area for guest–water mass transfer for recovering direct contact of guest and water phase.

(i) Guest–water system. At guest–water interfaces, hydrate films (layers) grow laterally along the interface after the nucleation. Investigations of hydrate crystals grown from the guest–water interface are important for the overall understanding of the kinetics of hydrate formation. Experimental studies on hydrate growth at the guest–water interface have been conducted.[718–720] The important considerations for modelling the lateral growth kinetics are mass or/and heat transfer at the growing front of hydrate film.[721,722] After the growth of hydrate film to around 10 μm in thickness,[723] the guest and water phases are separated, and further hydrate formation is suppressed. Polycrystalline film

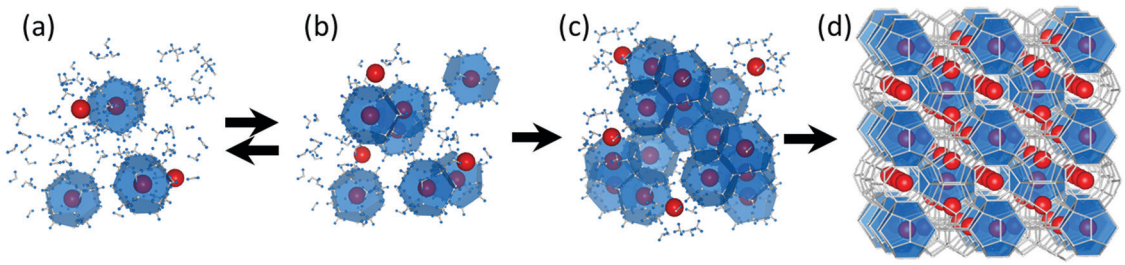

Fig. 11 Labile-cluster model of hydrate nucleation: (a) labile-clusters, (b) agglomeration of clusters, (c) primary nucleolus, and (d) hydrate crystal.

Open Access Article. Published on 22 Junie 2020. Downloaded on 2026-02-11 12:42:38 nm..
This article is licensed under a Creative Commons Attribution-NonCommercial 3.0 Unported Licence.

covering the interface and the morphologies of hydrate crystals have a significant dependence on subcooling and gas composition. With large subcooling, the shapes of hydrate crystals are generally sword-like or triangular, with the shape changing to a polygon and a large polygon when the subcooling is smaller.[724–727] Hydrate films grow in thickness though the films formed at guest–water interfaces by subsequent mass-transfer resulting in further hydrate formation. A detailed review of the hydrate growth models have been reported,[22] but it is still debated how to diffuse molecules through hydrate films to grow the thickness of hydrate film.[728]

(ii) Guest–ice system. At guest–ice interface, hydrate also grows although their formation rate may be smaller than that of liquid water. In the initial step of xenon hydrate formation, hydrate film with thickness less than 0.1 μm is formed before the reaction becomes too slow. The number ratio of small and large cage is about 1 during the early part of the reaction, and the ratio changes to its equilibrium value of 3–4 when nucleation processes were finished, and rapid growth commenced.[729] Moreover, the formation of transient hydrate structures has been observed in the initial step for pure methane,[730] carbon dioxide,[310] or carbon monoxide[731] hydrates. These experiments suggest that a precursor phase or initial structure are different from the equilibrium hydrate structure. MD simulations support the occurrence of transient structures.[732,733]

A shrinking-core model accounts for the growth of hydrate film in thickness.[310,734–737] In this model, the reaction consisted of three steps: (a) the initial reaction of guest with ice; (b) the growth of hydrate film and growth in thickness; (c) the mass diffusion of water/guest through the hydrate film. The activation energy of the processes was obtained from the kinetic rate constant as a function of temperature using the Arrhenius equation. Transport of guest molecules by a series of jumps between neighbouring hydrate cages was demonstrated and the rate-determining process may change in different temperature ranges.[738,739] Other mathematical diffusion models have been proposed,[740–742] and other factors affecting the growth of hydrates may need to be considered.[743] For a careful examination of the kinetic process proposed by the model, further comparative researches between experiment and theoretical simulations are required.

3.1.3. Molecular simulation. There has been much progress in recent years in molecular simulation, offering important insights into hydrate nucleation, and, more generally, into hydrate formation. Briefly, several main mechanisms have been proposed for hydrate nucleation:

(i) Labile-cluster hypothesis (LCH):[703] where unstable entities featuring a guest surrounded by water molecules in their first coordination shells diffuse in the liquid phase as a single entity, and the clusters of varying sizes combine to form larger stable clusters which grow into the hydrate crystal.[704,744]

(ii) Local-structuring hypothesis (LSH):[745] where well-solvated guests meet, forming a cluster with the guests in a configuration consistent with the clathrate crystal, the water molecules rearrange to form a hydrate framework.

(iii) Blob Hypothesis (BH):[705] a modified form of LSH, where stochastic local-density fluctuations of guests in water favour 'blob' formation as amorphous clusters of solvent-separated guests at high solvated-guest concentrations close to that in the hydrate.[746]

(iv) Cage-adsorption hypothesis (CAH):[706] where guest molecules increase their local concentration to induce hydrate formation by spontaneous cage formation, followed by guest "adsorption" to cages and stabilisation thereof.[704,706,747–749]

Although not at guest–water interfaces, homogeneous methane-hydrate nucleation studies have observed formation of methane–water clusters which combine to form a critical nucleus,[750–752] supporting the concept that locales with high guest concentration, although not highly structured (arising perhaps from either local-density fluctuations and/or cage adsorption), can result in hydrate nucleation.

Recent molecular-simulation studies have indicated typical hydrate-nucleation timescales of the order of microseconds,[665,705,706,745,746,750–753] and this is discussed further in Lauricella *et al.*[752] Often, a hydrate nucleates initially into phases inconsistent with common bulk crystal structures, but containing a variety of structural units,[665,750–753] as well as 'amorphous' units.[753,754] In relation to the Blob Hypothesis, English *et al.* studied the size of the water–methane interface at realistic solvated-methane concentrations, finding not-dissimilar early-stage nucleation mechanisms.[69] In addition, solvated-methane-concentration effect on nucleation rate have been assessed,[752,755] with innate challenges in MD simulation for methane-hydrate nucleation being discussed with some acuity[756] while Hall *et al.* have placed hydrate nucleation within the wider context of the funnel model, in view of the panoply of competing amenable pathways.[757,758] Recently, biased-simulation methods have offered much microscopic insight: Lauricella *et al.* have examined free-energy landscapes for hydrate nucleation from metadynamics,[747,759] and restrained MD.[752] Małolepsza *et al.* have developed an enhanced-sampling technique and applied to hydrate nucleation.[760] Bi *et al.* applied the Forward-Flux Sampling method to methane-hydrate nucleation,[761] computing nucleation-pathway free-energy landscapes.[762]

Since the pioneering gas-hydrate molecular simulations of Tse *et al.* over 35 years ago,[74] simulation has led to a great number of microscopic insights into hydrate behaviour and properties, from thermal-conduction mechanisms to hydrogen storage and carbon capture. In this brief foray into some very recent advances in molecular simulation since the review by English *et al.*,[69] it has been understandably impossible to be truly exhaustive in these 'cataloguing' exercises, such has been the recent surge in this specific research activity; rather, some important contemporary trends have been highlighted. One area not highlighted so far has been to remark on the (relative lack of) research 'crossover' between the clathrate-hydrate and inorganic-clathrates (*e.g.*, clathrasils) communities, which has been a feature to a lesser extent than, say, between the clathrate-hydrate and semi-clathrate arena. In the area of inorganic clathrates, important insights into cage and lattice behaviour, thermodynamics and dynamical properties (*e.g.*, thermal conductivity[763])

Open Access Article. Published on 22 Junie 2020. Downloaded on 2026-02-11 12:42:38 nm..
This article is licensed under a Creative Commons Attribution-NonCommercial 3.0 Unported Licence.

are being made, with important parallels to current and previous work in clathrate hydrates. Clearly, the power of molecular simulation to 'leverage' and transfer this body of experience and insight into transformational work in inorganic clathrates is an important contemporary trend in clathrate modelling; in this regard, the important contributions of Li, Stroebel and co-workers are to be welcomed.[764]

In the realm of clathrate hydrates, in terms of outlook for achieving greater levels of quantitative agreement relative to experiment for physical properties, the 'acid test' of spectroscopy (*e.g.*, Raman data) remains a formidable challenge. For instance, Futera *et al.*[765] discusses measures to potentially increase further the fidelity of H_2-water potential tailored for hydrogen hydrates. The use of force-matching to high-quality *ab initio* MD simulation[134] to achieve better-accuracy potentials, beyond the pairwise approximation for classic empirical potentials, is a future important area, and it is to be hoped that neural-network-tuned potentials will offer important progress here in the decades ahead, especially in hydrate-nucleation and formation simulations, with a large variety and heterogeneity in local environments – where model parameterisation in one phase alone will be less likely to succeed.

3.1.4. Control of the morphology. The morphology of hydrate crystals growing in liquid water saturated with and in contact with guest also depend on the concentration of the guest species and mass transfer in water.[766–768] Generally, the morphology of hydrate crystals growing in a liquid water changed from polygonal to dendrite with increasing fugacity. Hydrate inhibitors and hydrate promoters affect the growth rate of hydrates by changing the morphology of hydrate crystal.[769,770] Experiments of the inhibitor using hydrate single crystals showed a structural fit on the hydrate surface and strong bonding in specific configurations. The growth rate of hydrates in these systems may be adjustable by controlling hydrate morphology. The effect of these additives have also been investigated at the molecular level by using MD simulation.[771–773]

Since the effect of inhibitors and surfactants depend upon the guest species, the search for environmentally friendly and more effective materials have been conducted. For example, experimental results of methane + propane mixed gas hydrate suggest that porous hydrate film, but not an impermeable film, can be grown at the guest–water interface in the presence of SDS. The porous hydrate film then allows efficient water-to-gas contact for further crystallization.[683] The formation of smoke-like hydrate from gas bubbles, which are partially covered by hydrate film, in water with SDS is also suggested.[774] In the case of methane hydrate, the amount of crystalized hydrate increased in the presence of the SDS as the hydrate crystals detached from the interface due to increased wettability. The size of individual hydrate crystals with SDS become smaller than those formed from pure water systems due to increased hydrate nucleation. With higher subcooling temperature, the hydrates grow upright crystal fibres because of large capillary forces due to smaller pores between hydrate crystals.[775] Based on these experimental results, the crystal growth and morphology in the system with surfactant can be controllable by changing concentration of surfactant. A detailed review of the hydrate promoters including surfactants coupled with other promoters has been reported.[776,777]

3.2. Dissociation

Hydrate dissociation is an endothermic process as with ice melting. Hydrates separate into water and guest molecules by breaking up hydrogen bonding networks of water molecules and the van der Waals interaction forces between guest and host water molecules. Dissociation occurs in two major steps; (a) the initial destruction of the hydrate crystal and (b) the release of water and guest molecules. Dissociation kinetics of hydrates also largely depend on the temperature above and below 273 K.

3.2.1. Intrinsic kinetics of hydrate dissociation. Experimental studies by NMR suggest that the small and large cage occupancy ratio of xenon or methane hydrates remained constant during the dissociation process.[729,778] This suggests that there is no preferential dissociation of hydrate cages and the whole cage structure decompose during dissociation. The simultaneous dissociation of small and large cages in hydrate structures contrasts with results observed during hydrate nucleation process. However, different dissociation rates of small and large cages were observed in methane/ethane mixed gas hydrate.[779–782] Because the dissociation rate measured by spectroscopic methods, such as NMR or Raman, depends on both the rate constant and the number of encapsulating cages, this result might be caused by phase transition between structure I and structure II hydrate during the dissociation process, which cause different number ratio of small/large cages. In addition to these experimental results, MD simulations suggest rapid dissociation of empty hydrate cages[783] or the dependency of dissociation rates on cage occupancies.[784–786] More careful experiments would be needed for improved understanding of guest dynamics during hydrate dissociation process.

3.2.2. Hydrate dissociation in solutions. The dissociation rate is proportional to the particle surface area of hydrates and to the difference in the fugacity. The proportionality constant showed an Arrhenius temperature dependence.[787] Hydrate dissociation separates water and guest molecules, which cause a supersaturation state of guest in the water. Because the concentration of guest in the hydrate structure is more than several hundred times higher than the amount in water, then gas bubbles are formed in the water. This concept is in good agreement with the results by MD simulation of methane hydrate dissociation in liquid water.[684]

The dissociation rate is controlled by three factors: the intrinsic dissociation reaction rate, the rate of guest flow produced from the crystalline hydrate, and the rate of heat transfer to the hydrate for endothermic reaction. The hydrate dissociation kinetic models presented so far are based on either one of these factors or multiple factors to couple these effects. The effect of multicomponent hydrate-forming gas,[788] additives in the water or type of surrounding solutions[789–791] and the form and size of hydrate samples[792] may change the rate-determining stage of hydrate dissociation. A detailed review of the hydrate dissociation models has been reported.[793]

Open Access Article. Published on 22 Junie 2020. Downloaded on 2026-02-11 12:42:38 nm..
This article is licensed under a Creative Commons Attribution-NonCommercial 3.0 Unported Licence.

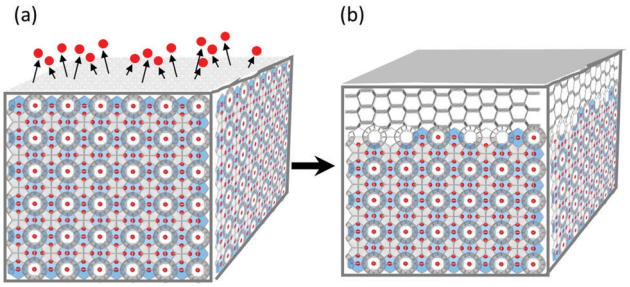

Fig. 12 Schematic model of the self-preservation or anomalous preservation of gas hydrate: (a) methane hydrate during dissociation and (b) the hydrate being covered by ice layer.

3.2.3. Self-preservation phenomena. When hydrate dissociates at temperatures below 273 K under atmospheric pressure conditions the dissociation rate of hydrate is much slower than that above 273 K.[183] This phenomenon is termed self-preservation.[794] Hydrate start to dissociate from its surface and water molecules released as the hydrate transform into ice. After the complete surface coverage by ice due to the hydrate dissociation, a shrinking-core model account for further hydrate dissociation and growth of ice film in thickness.[795] In this model, the dissociation reaction consisted of two steps: (a) the initial destruction of the hydrate surface and the growth of an ice layer, and (b) growth of the ice layer in thickness and the release of guest through the ice (see Fig. 12). This model reproduces experimental results of methane hydrate dissociation at temperatures below its equilibrium temperature at 0.1 MPa.[796] Theoretical simulation also accounts for the self-preservation phenomena based on ice-shielding, guest diffusion trough the ice, and heat transfer.[797–799]

Methane hydrate dissociation by rapid pressure drop under isothermal conditions is unexpectedly slow and occurs only for temperature ranges between 240 K and 270 K. The dissociation rates vary by several orders of magnitude with two minima at around 250 and 268 K. This phenomenon is termed as "anomalous preservation".[800] Experimental studies suggest that this anomalously slow dissociation is related to ice morphology or structures formed at the surface of the dissociating hydrate.[801–807] It has been revealed that the preserved methane hydrate is tightly covered by an ice layer with a thickness of about 100 μm or less.[808–810]

From a practical application perspective, hydrate pelletizing technology for natural gas storage and transportation have been proposed and evaluated.[811–813] To date, methane or natural gas have been successfully stored within hydrate pellets for more than three months at 253 K under atmospheric pressure.[814] Recently, the phenomena under more complex systems coexisting with other materials such as surfactant,[815] hydrophilic silica beads,[816] crude oil,[817] dry water,[818] and saline water[819–821] have been reported. The dissociation reactions largely depend on the type of guest species.[822,823]

3.3. Kinetics in sediments

The morphologies of naturally occurring hydrate are varied depending on hydrate kinetics as well as type of sediments: *e.g.* pore-filling hydrate in coarse sands or veined or nodule-type hydrate in fine sediments. Several hydrate habits in sediments have been known which were explained in Section 2.5.2. All these habits depend on hydrate nucleation and growth processes in the pore, where the physical properties of the hydrate sediments are affected by the hydrate formed in the pore space.[400,824] Accordingly, understanding of kinetics and microstructure of hydrate at the pore scale is important to advance our knowledge of hydrate sediments.

From experimental studies on hydrate sediments, mechanisms of hydrate formation and dissociation processes at the pore scale have been studied and incorporated into continuum scale simulations. Observations of hydrate nucleation, growth, and dissociation in 2D configuration glass micromodels were conducted by optical microscopy.[825–828] Morphology changes of hydrate mixed with fine glass beads inside of thin layer were observed as a function of growth rate.[829,830] Nondestructive imaging methods, such as MRI and X-ray Computed Tomography (CT), have been applied to study the distribution of hydrates in frozen sediments[831,832] and other attempts by means of microfocus X-ray CT contributed to continued studies of the sedimentary matrices at pore scale.[833,834] In the last decade, MRI and X-ray CT measurements have extended hydrate kinetic studies to 3D configurations of the microstructure of hydrate sediments. MRI measurements, which are suitable for detecting hydrate and water but suffer from insufficient spatial resolution for measurement at the pore scale, revealed multiple nucleation events at different times and locations within the sediment during hydrate formation processes.[835] X-ray CT with micro or higher spatial resolution has also been used for kinetic studies of hydrates in sediments with the aid of contrast agents or heavy guest substances such as Xe due to insufficient image contrast of X-ray CT for distinguishing hydrate and water or ice.[715,836–839] In the X-ray CT images of hydrate formation processes, nucleation starts at the water–gas interface from partially saturated water and that starts in the bulk of the liquid which is water saturated with guest substances. Occurrence of fluid phase films between hydrates and the sediment particles were also observed. In the hydrate dissociation images, the decomposition starts at the hydrate–gas interface with melt water accumulating at dissociating hydrate surfaces. Then inhomogeneous dissociation facilitates redistribution of water and local hydrate reformation in the pore space. From a basic science point of view, guest substances such as THF or CO_2 have been widely used as model samples for laboratory investigations. Because of the complete miscibility or high water solubility of these guests, growth rates of these hydrates from water are faster than methane. Also, to improve visibility of X-ray CT image, a contrast agent or Xe are used as a contrast medium even though they may change the hydrate kinetics. Ultimately, experiments using methane or natural gas with pure water or sea water are preferred for incorporating into the continuum scale simulations of geological systems. In addition to abovementioned imaging techniques, neutron scattering technique have also been employed[840] to investigate gas hydrate kinetics in the presence of solid surfaces. Cox *et al.*[840] utilised time-resolved

Open Access Article. Published on 22 Junie 2020. Downloaded on 2026-02-11 12:42:38 nm..
This article is licensed under a Creative Commons Attribution-NonCommercial 3.0 Unported Licence.

neutron scattering experiments and molecular dynamics simulations to identify that the methane hydrate formation is insensitive with respect to the presence of various clay and silica nanoparticle surfaces.

Recently, numerical models of pore-scale hydrate dissociation have been proposed to estimate the dissociation rate of methane hydrates. The numerical models suggest that the water layer prevents guest gas from escaping into the gas phase due to the mass-transfer-limitation, which ultimately affects the driving force of hydrate dissociation by depressurization.[841–843] A numerical model of methane hydrate formation was also proposed for determining the locations of the initial hydrate nucleation and for estimating the morphological distribution of methane hydrate in porous media using classical nucleation theory.[844]

Understanding the formation and dissociation kinetics of natural gas hydrates in sediment is important for the efficient and economic development of natural gas hydrates as unconventional natural gas resources in permafrost or marine sediments. On the other hand, dissociation of hydrates and subsequent outgassing could affect the atmosphere of solar planets[845,846] as well as the Earth.[1] The self-preservation phenomenon is also true in shallow permafrost locations. Gases releasing from the permafrost may contain natural gas produced by the dissociation of hydrates in the pore space of sediments, which can exist in permafrost due to self-preservation.[847,848] Accordingly, more detailed knowledge of the kinetic model of hydrates in complex system of sediments is needed.

3.4. Influence of additives

Gas hydrate formation is very susceptible to contamination owing to the presence of any foreign additives other than water and the guest gas moieties, which can result in critical influences on the thermodynamics and kinetics of gas hydrate formation. The foreign species, such as salts, bio-surfactants, alcohols, *etc.*, may be deliberately augmented to water–gas systems to influence the kinetics of hydrate formation. Additionally, gas hydrate nucleation and growth are strongly related to the hydrophobicity of gaseous species and chemical additives (*e.g.* nanoparticles) which can either be hydrophilic or hydrophobic and when in the aqueous phase might boost gas hydrate formation,[849,850] however, they could also prevent hydrate growth if they engaged at the aqueous–oleic phase interface.[851] While some results illustrated that nanoparticles might promote hydrate formation at lesser concentrations,[852,853] however, the authors did not denote whether the nanoparticles in their tests were hydrophilic or hydrophobic. A macroscopic experimental study conducted by Wang *et al.*[854] proposed that hydrophilic nanoparticles could influence a hydrate inhibition efficiency which could be used to decrease the hydrate reformation and aggregation throughout the gas hydrate or deep-water drilling if their contents could appropriately be controlled to avoid instability of the well borehole. Generally, some additives can introduce hydrophobicity influence[855] which results in organising the peripheral water molecules into a clathrate like hydrophobic hydration shell, creating an incremented local gas content surrounding the hydrophobe,[856,857] and increase the hydrate crystal formation rate accordingly. The creation of semiclathrate hydrates in the presence of partial hydrophobic additives (*e.g.* THF[858,859]) and pure hydrophobes (*e.g.* cyclopentane[860,861]) augments the hydrophobicity associated hydrates formation kinetics. Typically, the addition of surfactants which can be cationic (*e.g.* TBAB,[201,862–866] dodecyltrimethylammonium (DTAC),[862,867] dodecyl amine hydrochloride (DAH),[868] *N*-dodecylpropane-1,3-diamine hydrochloride, (DN2Cl)[868]), anionic (*e.g.* SDS,[682,867,869–871] sodium tetradecyl sulfate (STS),[871] sodium hexadecyl sulfate (SHS),[871] sodium oleate[871]), and nonionic (*e.g.* THF,[867,870,872,873] ethoxylated nonylphenol,[874] Tween 80,[875] cyclopentane[861,876]), at specific concentration could facilitate gas hydrate formation. Solid species can also have a hydrophobic effect and induced gas hydrate formation. Glass surfaces with various coatings including partial hydrophobic *N*,*N*-dimethyl-noctadecyl-3-aminopropyl trimethoxysilyl and hydrophobic octadecyltrichlorosilane[877] boosted hydrate crystallisation and incremented kinetics of hydrate formation.[878]

In the following subsections, the influences of typical additives, salts and alcohols, on gas hydrate formation have been reviewed and the existing hypothesis for their efficacies have been discussed.

3.4.1. Salts. As will be explained in Section 4.1.1, inorganic salts are recognised as thermodynamic hydrate inhibitors. Dong *et al.*[879,880] conducted an experimental investigation of the effects of salt and alkane hydrocarbon concentration on hydrate anti-agglomeration. They observed that salt elevates the hydrate anti-agglomeration phenomenon as well as normal alkanes. The adsorption of solute moieties on the hydrate surface is facilitated by NaCl ions in the aqueous phase[881] which means that the propensity of ions for water molecules and the aversion to hydrophobic species repel the surfactant molecules to the hydrate–aqueous phase interface. However, other recent research studies have observed the facilitated formation of CH_4 and CO_2 hydrates in low NaX (X = I^- and Br^-) concentration solutions along with inhibited systems in higher salts contents mixtures.[882–884] It has been denoted that the exotic influence of sodium halides on gas hydrate formation is because of ions charges and the size of the halide ions in the water structure.[882] Inorganic halide ions create their solvation shells in the aqueous phase which can be changed based on the size of the ion and the ion charge density, accordingly. Thus, as an example, the I^- electron shell, with largest radius and lowest charge density, interacts faintly with its nucleus and could be contorted by the nearby water dipoles.[885] Generally, smaller halide ions with higher charge density tend to have inhibition effects and potent interactions with water molecules, which result in breaking the inherent hydrogen bonded water molecule network.[885] Therefore, small F^-, as a hydrophilic halide ion, has a strong binding affinity to water molecules and opts to stay in the bulk aqueous phase compared to large hydrophobic I^- with cage-like solvation shell which prefers to remain at the solution surface as a hydrophobe.[886–888] These mentioned diverse effects of NaX on gas hydrate formation can be demonstrated by the explained hydrophobic effect hypothesis. At high NaX content, the

Open Access Article. Published on 22 Junie 2020. Downloaded on 2026-02-11 12:42:38 nm..
This article is licensed under a Creative Commons Attribution-NonCommercial 3.0 Unported Licence.

incremented rivalry among ions and gas species for water molecules leads to water deficiency for gas hydrate nucleation, and consequently formation inhibition. In the low salt dosage medium, however, the rivalry would not result in a significant influence on the water accessibility, yet the existence of cage-like hydration shells halide ions in the system are supposed to perform as kernel for gas hydrate nucleation. It has been observed that 3.0 wt% NaCl solution had a minimal influence on the phase equilibrium *P–T* conditions of mixed methane/THF hydrates.[889] Kumar *et al.*[890] identified that saline water/seawater, 1.1 mol% NaCl solution, is adequate for rapid methane storage through clathrate hydrate formation. Some other researchers,[891,892] however, contradictorily illustrated that the presence of salt ions in seawater hinder hydrate crystal growth by curbing the potent H-bonding network of water molecules and subsequent hydrate-associated water molecules interactions.

3.4.2. Alcohols. One of best types of thermodynamic hydrate inhibitors are alcoholic compounds (*e.g.*, MeOH, ethanol, ethylene glycol, *etc.*).[711,893,894] As will be explained in the next chapter of this review, it has been widely believed that THI's inhibit gas hydrate formation by suppressing the water activity. Alcohols are highly polar species which potently interact with water molecules through hydrogen bonding. This potent binding affinity results in enhanced racing with the hydrate creator for interaction with water which leads to lessened water availability for the gas hydrate formation.[895] The efficiency of an alcoholic functional material relies on its susceptibility to binding water.[893] For instance, although ethanol and ethylene glycol have similar molar volumes, ethylene glycol with two hydroxyl functional groups accessible for hydrogen bonding has more effectual hydrate inhibition performance compared to ethanol with only one hydroxyl group.[893] However, some of the alcohols might exhibit different behaviour and act as gas hydrate promoters when they are utilised at low dosage, where some tests have observed a boosted methane hydrate formation in solutions with lower alcohol contents.[895–897] Amtawong *et al.*[898] conducted a quantitative investigation into the rate of propane clathrate hydrate formation with varying MeOH contents in the aqueous phase. They realised that low dosages of MeOH could undeniably catalyse the hydrate formation reaction which highlights the potential suitability of small amounts of MeOH for enhancing gas storage onto the gas hydrate cages. The principle mechanisms behind the facilitated hydrate formation in the low alcoholic concentration solutions might be elucidated by the hydrophobic effect hypothesis as explained in the previous section.

3.5. Growth acceleration

Many researchers have employed non-surfactant-based methodologies to accelerate gas hydrate formation including sand packs, nanoparticles, hydrogels, and porous compounds such as activated carbon and porous nano-silica to enlarge the solid–liquid interface.[899–906] Nano-metal particles have been utilised to boost gas hydrate formation, which include nano-Cu,[907] synthesized silver nanoparticles,[908,909] spherical nano-copper oxide,[853,910] nano-Al_2O_3,[911] and nano-ZnO,[911,912] plus the use of advanced nanofluids consisting of carbon nanotubes[913–916] to improve heat and mass transfer phenomena throughout the gas hydrate formation process.[917] In the subsections below, we detail the effect of different techniques for facilitating the formation of gas hydrates and their corresponding kinetics.

3.5.1. Physical. Different techniques have been utilised to boost gas hydration formation phenomenon including fine spraying of water jet in gas atmosphere,[918] vibratory and various physical fields such as electromagnetic waves,[919,920] acoustic wave fields,[692,921–923] electric fields,[924,925] *etc.* Chernov *et al.*[926] proposed a new shock-wave technique for hydrate formation. They illustrated that the dominant driving process is gas bubbles segmentation in the shock wave which causes enhancement of heat and mass transfer processes and hydrate formation rates to increase accordingly. The hydrate formation phenomenon due to an applied temperate shock wave in the bubbles containing aqueous phase was examined and its kinetic model was developed when the heat influences are negligible.[927,928] Based on the bubbly liquid model distinguished with heeding to potential hydrate formation process, the dynamics of plain one-dimensional shock waves in such bubbly water medium was demonstrated.[929] The test design for heeding to the gas bubbles segmentation in the wave was proposed. Shock wave transmutation in water with carbon dioxide bubbles and its effects on bubble fragmentation, dissolution and hydrate formation were thoroughly investigated by conducting tests under various primary static pressures and moderate temperatures.[930–932] It was demonstrated that an increment in primary static pressure in the system suppresses respective wave amplitude which would result in gas bubble fragmentation. On the other hand, the generation of nanobubbles,[933] which can be promulgated by both hydrophilic and hydrophobic surfaces in various gas hydrate systems can accelerate the nucleation and growth of gas hydrates in the heterogeneous environment, which is more hydrate friendly when compared to the homogenous one.

A theoretical model of incorporated hydrate dissolution and formation when applying the shock wave along with diffusion in gas bubbles containing aqueous phase and consideration of heat influences throughout the process, was developed.[932] Integrated carbon dioxide hydrate formation and dissociation owing to the presence of the shock wave front in carbon dioxide + nitrogen mixture bubbles containing water in presence of a surfactant at various preliminary static pressures and moderate was illustrated experimentally and theoretically by Chernov and Dontsov.[934] They have developed a theoretical model of the studied multi-component gas mixture system taking into consideration heat influences, which is not considered in the generalised model.[932] They have observed that gas bubbles fragment into the tinier inclusions in the wave front which results in facilitation of hydrate formation owing to the increment increase of the water–gas interface area in addition to the movement of gas bubbles with a higher velocity in respect to the aqueous phase which leads to strengthening the heat and mass transfer phenomenon. It can be implied that the hydrate formation happens due to the hydrate film sorption progression

Open Access Article. Published on 22 Junie 2020. Downloaded on 2026-02-11 12:42:38 nm..
This article is licensed under a Creative Commons Attribution-NonCommercial 3.0 Unported Licence.

on the surface of small gas inclusions, and the acceleration of this phenomenon is attained by utilising the kinetic parameters in addition to the consideration of heat and mass transfer processes at the aqueous–gas phase interface, which are significant. The usual time of the gas hydration process in the presence of the shock wave is multiple orders lower when compared to the duration of hydrate formation process using the existing methods of hydration. Higher shock wave amplitudes cause higher rates of gas hydrate formation and dissociation, and the presence of surfactants seem to have no notable influence on the hydration and dissociation phenomena in a system facing shock waves.[934] While applying the physical fields has a promoting influence on gas hydrate formation and decomposition, it is typically assumed that physical fields demonstrate their positive effects within a particular span of frequency, and they have no influence on the kinetics of hydrate formation beyond that domain.

3.5.2. Mechanical. In addition to the physical methods discussed above, various additional methodologies have been employed to facilitate hydrate formation kinetics for gas storage purposes[692] including the addition of surface-active compounds in pure water[935,936] and utilising the sand filled fixed bed column.[937] It has been shown that continuous stirring in an isochoric cell can lead to suppression of mass and heat transfer resistances, which results in a more homogenous system which is desired for hydrate nucleation and formation.[938,939] Furthermore, the increase of aqueous phase–gas interfacial surface area owing to the stirring process[692] can cause an increase in the rate of hydrate formation. Generally, any parameter which can enhance the water–gas interface region such as stirring rate, might significantly increase the rate of hydrate formation.[940] Some researchers identified that increased stirring speeds lead to more hydrate presence within the system, through decreasing the metastable crystal formation time[941] and buffering bulk phase temperature and composition variations through heat and mass transfer improvement.[942] Turner *et al.*[938] recognised an increase in the rate of hydrate formation due to raising the impeller speed during a range of tests, with an upper threshold limit identified above which there was no effect on the kinetics of hydrates formation and some potential counter influences[943] could be seen within the system. It has been illustrated that all hydrate formation tests thoroughly rely on the studied system characteristics.[940] Catastrophic hydrate growth (CHG) and deployment of hydrate crystals have been observed in different research studies[865,944,945] and there is an interval after preliminary hydrate formation or induction time,[945] in which rapid hydrate formation happens within the system. Some other researchers have claimed that CHG is an interval when an involuntary hydrate formation occurs,[939] and when it begins a pointed pressure decline could be perceived within the system and this results in the formation of large hydrate clusters. Through determination of the optimum stirring speed and CHG interval recognition, the most appropriate operating conditions for the hydrates production plants could be identified. By employing a high-pressure autoclave cell (HPC) containing a mixture of gas and deionized water, Qureshi *et al.*[946] determined that the CHG in the studied system happened during the first hour after the hydrate induction time and this first hour was denoted as the interval of CHG. The optimised stirring speed and the test facility dimensions were utilised for the system up-scaling up required for the reliable evaluation of the worthiness of hydrate cages for gas storage and transportation. The spraying and gas bubbling are other conventional mechanical techniques for increasing the rate of gas hydrate formation. The spraying technique[947,948] atomises water or a solution into a gas-filled reaction vessel through a nozzle and notably increases the aqueous–vapour phase interfacial area which leads to an increase in the hydrate formation kinetics. Fig. 13 a shows the schematic diagram of this phenomenon.

The bubbling technique[949] where gas is injected at high pressure into the aqueous phase *via* a distributor at the underneath of the reactor results in movement of the gas bubbles in the aqueous phase due to the buoyancy forces, increasing the vapour–aqueous phase disturbance and kinetics of

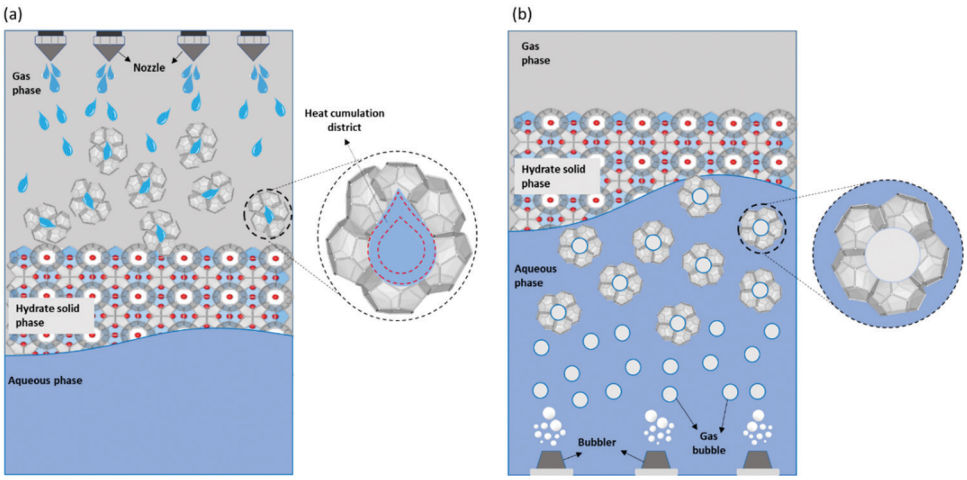

Fig. 13 (a) Formation of gas hydrate using the spraying technique (b) schematic diagram of hydrate formation as gas bubbles rise through the continuous aqueous phase.

Open Access Article. Published on 22 Junie 2020. Downloaded on 2026-02-11 12:42:38 nm..
This article is licensed under a Creative Commons Attribution-NonCommercial 3.0 Unported Licence.

hydrate formation at the periphery of the bubbles accordingly (see Fig. 13b).

3.5.3. Dry water. Dry water (DW), a type of vast dispersible functional compound, is prepared by nanoscale hydrophobic species (*e.g.* silica particles) enfolded in water and has an enormous liquid storage capacity and flowability.[950,951] DW material as a water in-air inverse foam creates a stable free-flowing powder which could be easily controlled at ambient conditions and hamper water droplet coagulation[950] owing to presence of the hydrophobic modified silica coating at the aqueous–vapour phase interface. Since DW moieties have a greater surface-to-volume ratio compared to bulk water, the tiny dispersed water droplets result in significantly raised clathration rate in the vapour phase which in turn leads to an increase in methane hydrate formation kinetics compared to the bulk aqueous phase.[936,952] Although the application of DW for improving methodologies for gas mixtures separation purposes has not yet been fully understood, it has been realised that the DW can augment the natural gas hydrates capability for gas storage inclusion[935] in a static system. Thus, DW can be employed as the bearer for gas separation in lieu of the conventional liquid medium in order to enhance the heat transfer phenomenon and thermal stability throughout the gas hydrate separation process. The influences of DW on gas hydrate separation and methane recovery kinetics have been investigated by Zhang *et al.*[953] by utilising chromatography data, it was observed under a range of stirring conditions, the augmentation of DW and THF/SDS solutions can improve the separation yields of gas hydrates compared to that of the pure aqueous phase system. It was concluded that the methane content after purification using DW was larger compared to its average content after purification in two other systems with stirring and in presence of THF + SDS solutions.[953] Additionally, the preparation methodology is much easier and scalable compared to the grinding and size-selective sifting of ice specks.[954] It was also determined that the inclusion of a hydrocolloid gelling agent drastically improves the system recyclability,[953] and this "dry gel" method could be employed in other disciplines where the effectual contiguity of gas species and aqueous phase would be needed.

4. Chemistry in flow assurance

The challenging hydrate nucleation and growth phenomena can occur at high pressure and low temperature conditions[895] as a result of unpremeditated shut-ins,[955] poor performance of chemicals injection pumps,[956] and incremental increase of aqueous phase in the stream,[957] which could result in occluded pipes and halted flow. Gas hydrate associated flow assurance challenges can occur not only in hydrocarbon pipeline systems but also within CO_2 and hydrogen transportation pipelines where trace amounts of water impurities could exist in the stream. Flow assurance problems need to be addressed using a wide range of adequate methodologies, otherwise they could also negatively affect the determination of quantities of valuable cargo fluids in custody transfer and allocation systems. In the last two decades, gas hydrate associated flow assurance research studies have been undertaken directed towards identifying optimised mitigation strategies to attain more appropriate management of gas hydrate blockages which can happen in pipeline systems. This section aims to summarise the current state of the art progress of the understanding of gas hydrate associated flow assurance challenges in the oil & gas, and carbon capture & storage (CCS) sectors and to provide an assessment of the current designs of gas hydrate inhibitors for remediation purposes. It also challenges the gas hydrate community to develop new experimental facilities, methodologies and mathematical models for improving the early diagnosis and treatment of complex gas hydrate induced pipeline blockage in a cost effective and influential manner. Some review articles[127,955,958–960] on gas hydrate associated flow assurance challenges and induced hydrate risks demonstrate different aspects of this important issue in the oil & gas industry. Fig. 14 shows that in harsh conditions, hydrate growth could lead to thorough transportation pipeline blockage through a mainly three-step process after the water in hydrocarbon emulsification phenomenon: (i) hydrate nucleation; (ii) hydrate-crystal growth and agglomeration; (iii) hydrate-plug formation from aggregates and blocking the flow line.

4.1. Inhibition methods

Different mitigation and remediation strategies are utilised to handle hydrate blockage within pipes such as depressurization,[616,961] chemical,[962] mechanical,[963] and thermal[961,964] methodologies. Owing to the risks associated with some of the aforementioned methods such as hydrate plug movements,[965] intensive research efforts have focused on potential applications of three types of chemistries (see Fig. 15) namely thermodynamic[966–968] and

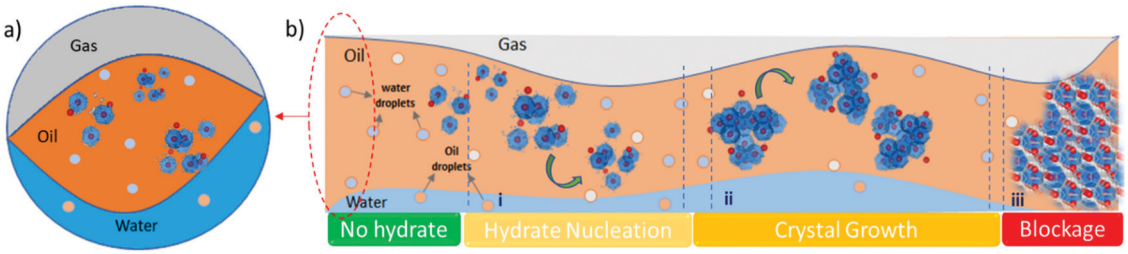

Fig. 14 (a) Schematic model of multiphase flow in pipeline, where hydrate crystal aggregates could flow in gaseous, oleic, and aqueous phases, and/or could deposit onto the pipe solid surface; (b) schematic diagram of the drivers of hydrate crystals formation and aggregation in hydrocarbon transportation pipelines and three-step process of (i) hydrate nucleation, (ii) crystal growth, and (iii) blockage.

Open Access Article. Published on 22 Junie 2020. Downloaded on 2026-02-11 12:42:38 nm..
This article is licensed under a Creative Commons Attribution-NonCommercial 3.0 Unported Licence.

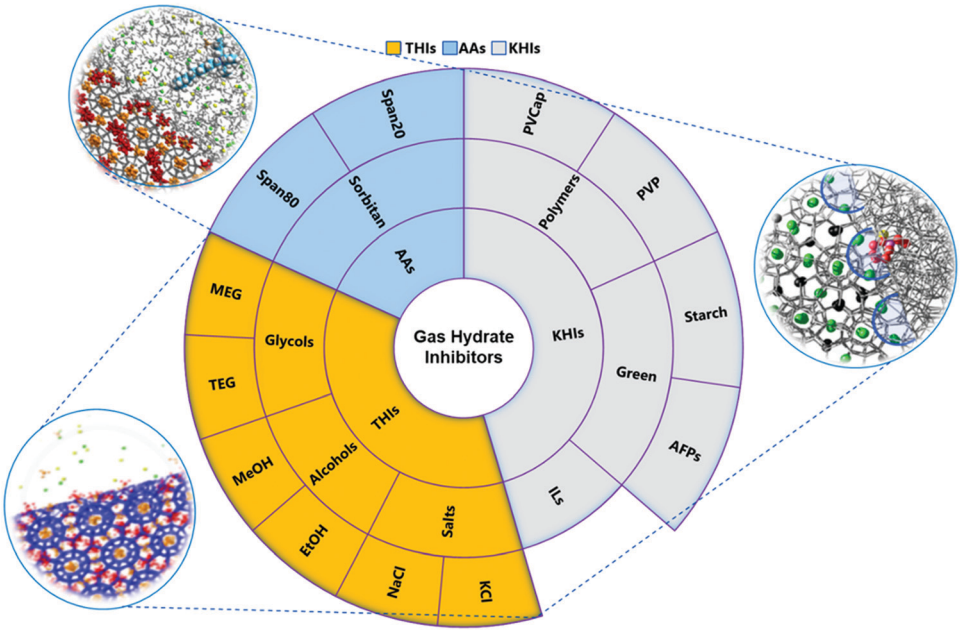

Fig. 15 Schematic examples of various types of gas hydrate inhibitors: THIs, KHIs, and AAs, and corresponding molecular interactions with clathrate hydrates.

kinetic hydrate inhibitors, THIs and KHIs respectively, and anti-agglomerates (AAs) to manage these risks. This section is structured in three subsections in which the detailed discussion of each class of hydrate inhibitors and their respective inhibition drivers have been addressed. Various reviews[660,957,969–971] regarding the fundamentals of chemical inhibition, interfacial and physiochemical phenomena of gas hydrates for hydrate risk management cover most of the significant research works on chemical injection scenarios. In the following subsections, we present the most recent findings out of research studies on chemical-hydrate inhibition.

4.1.1. Thermodynamic hydrate inhibitors (THIs). It is widely known that the dissociation temperature of gas hydrates can be changed through the chemical potential deduction of water molecules in the aqueous phase[972] by utilising chemistries named thermodynamic hydrate inhibitors (THIs) which include glycols (*e.g.* mono-ethylene glycol (MEG)), alcohols (*e.g.* MeOH),[895,973] and salts (*e.g.* NaCl, KCl, *etc.*).[974–977] Typically, the solid dissociation rate is prevailed by the discrepancy in the free energy among the initial and final states.[978] THIs suppress the free energy of the final state; however, it is not fully established if they also suppress the intermediate state free energy. If the intermediate state free energy were to be destabilised by a THI, the dissociation rate would be lowered in addition to the THI reducing the dissociation temperature.[684] The configuration of a supersaturated solution with gas species can happen by dissociation of the hydrates from which nano-bubbles are created. Hence, the quickly formed nano-bubbles can absorb dissolved gas moieties from the surrounding liquid, which results in incremental changes in hydrate dissociation rate. The influence of THIs dissolved in the surrounding liquid on hydrate dissociation phenomenon was investigated.[972,979] Yagasaki *et al.*[972,979] noted that THIs including sodium chloride (NaCl) and MeOH assist the creation of nano-bubbles, facilitating further hydrate dissociation. Sujith and Ramachandran[980] conducted a quantitative illustration of the influence of THIs concentration on the formation and stability of the nano-bubbles. Their simulation results observed that an increment in the concentration of THIs lowers the CH_4 molecule exchange amongst the bubble and the surrounding aqueous phase that reduces the dynamic of the nano-bubbles and boosts the creation of methane bubbles from the hydrate melt. They also showed that owing to the reposition of CO_2 molecules at the bubble–liquid interface, the nano-bubble nucleation process is enhanced. Kim *et al.*[981] studied the effect of THIs including MeOH, MEG, and NaCl on the morphology of methane hydrate crystals. Their experimental results showed that due to the fomentation influence of NaCl in mixtures containing MeOH, higher hydrate crystal growth was observed in both bulk solution and along the wall of the test cell compared to the MeOH only solution at the same sub-cooling condition. Additionally, they elucidated that the injection of MEG in NaCl solution resulted in a synergistic inhibition influence in additional hydrate growth by suppressing both upward and downward orientations along the gas–liquid interface. Generally, various mixtures of chloride salts of alkali and alkaline-earth metals with organic THIs[982–1004] results in synergistic influences of thermodynamic inhibitors through variety kinds of molecular interactions in those solution, *i.e.* a greater change to the equilibrium curve has been noted in THI mixtures with chloride salts when compared to the sole THI mixture. Aqueous mixtures of zwitterion amino acids containing amino and carboxylic functional groups[1005] have recently received attention as superior thermodynamic hydrate inhibitors for CH_4,[1006–1008] CO_2,[1009–1011] and natural gas[1012]

Open Access Article. Published on 22 Junie 2020. Downloaded on 2026-02-11 12:42:38 nm..
This article is licensed under a Creative Commons Attribution-NonCommercial 3.0 Unported Licence.

hydrates owing to their capability to potently interact with water molecules[1013] through H-bonding, as well as their non-toxic and environmentally friendly characteristics. When considering the environmental and economic aspects of THI's, the use of vast amounts of THIs along with the additional facilities required to handle undesired gas hydrate formations, the utilisation of THIs, particularly in the offshore environment becoming cumbersome.[21,1014]

4.1.2. Kinetic hydrate inhibitors (KHIs). As discussed in the previous subsection, THIs are most effective when using abundant amount, which results in high usage expenses and increased environmental risks. Therefore, as an alternative solution, two kinds of low dosage hydrate inhibitors (LDHIs), kinetic hydrate inhibitors (KHIs) and anti-agglomerants (AAs)[1015,1016] are injected to prevent and control gas hydrate formation in the pipeline networks.[1017,1018] The KHIs are typically low molecular weight water-soluble polymers containing hydrophilic amide and hydrophobic functional groups which bind to the clathrate hydrate and liquid water interface[971,1016] and cause a delay in hydrate formation.[1019,1020] The prevalent KHI structures are poly(vinylpyrrolidone) (PVP)[954,1021–1023] and polyvinylcaprolactam (PVCap)[773,954,1024–1029] which can be adsorbed onto the hydrate surface, following a Langmuir isotherm and the BET-type,[1030] through H-bonding between amide groups oxygen atoms and water molecules[1016,1031,1032] and retard hydrate crystal nucleation and growth. Various effectual KHI polymers with amide functional groups are based on *N*-alkyl-*N*-vinyl amides and *N*-alkyl-substituted acrylamides including poly(*N*-isopropylacrylamide),[1033] poly(*N*-isoproylmethacrylamide),[1034–1036] poly(acryloyl-pyrrolidine),[1037,1038] and *N*-methyl-*N*-vinylacetamide (VIMA) copolymers.[1039] Bertolazzo *et al.*[1040] and Yagasaki *et al.*[1031] realised that the KHI (*e.g.* PVCap) binding to the hydrate–water interface is not occurring because of amide H-bonds, instead it is dominated by the entropic affinity among the clathrate hydrate surface cavities and the KHI hydrophobic moieties (*e.g.* alkyl chains) due to larger hydrate surface cavities compared to those in the bulk liquid aqueous phase.[856,1041] Anderson *et al.*[772] determined the binding free energies of various KHIs on hydrate surfaces in the aqueous phase and the resulted order of the attained binding free energies concurred with that of the KHIs effectiveness. The monomers of KHIs demonstrate limited inhibition influence and the efficiency of KHIs increases significantly with increasing polymer size, due to stronger steric repulsion, which suppresses gently at constant concentrations of inhibitor.[1042–1044] It has been noted that mixtures of high and low molecular weight KHI polymers are more effective compared to the inhibitor with a unimodal molecular weight distribution,[971,1045] thus, low/high molecular weight PVCap mixtures are commercially utilised. Recently, the inhibition efficiency of a newly synthesised hydroxy-terminated PVCap (PVCap-OH)[1046] was investigated, and it demonstrated a better performance as a KHI compared to a common PVCap owing to the attachment of a hydroxyl group to the end of PVCap backbone chain. Commercial KHIs show lower critical mixture temperatures or a cloud point that is sometimes low but not much lower than the hydrate formation temperature at equilibrium condition. Several research studies noted that a low cloud point is a critical parameter, but not the most crucial one, which needs to be assumed in particular types of polymers with low molecular weights, pendant hydrophobic functional groups of an optimum size near to the polymer backbone, and authentic hydrophilic groups, that all lead to attaining appropriate hydrate formation inhibition yields.[1033,1047–1051] Along with water-soluble polymers, recently several research studies have been conducted to evaluate ionic liquids (ILs)[1052] as kinetic hydrate inhibitors. Different ILs chemistries belonging to the imidazolium, pyrrolidinium, and morpholinium families at various concentrations have been utilised to investigate their effects on the formation kinetics of methane[1053–1056] and CO_2[1057–1059] hydrates. ILs are also known as dual functional gas hydrate inhibitors,[1054] and at higher concentrations of ILs in the aqueous phase, more significant shifts of the equilibrium conditions toward lesser temperatures have been observed which lead them to be effectual thermodynamic inhibitors.[1060,1061] Shorter alkyl chain of the ILs cations as well as the existence of adequate H-bond-forming surface active functional groups (*e.g.*, OH, NH_2, NHCO, SO_3H) in an IL molecular structure could increase its gas hydrate formation inhibition efficiency. However, additional investigations would be required to realise the influences of varieties of ILs cations and anions on the rate of hydrate crystals formation and growth. Due to the high-expense and inadequate biodegradability of some commercial KHIs such as PVCap, different researchers have been conducting research on the development of green inhibitors like pyroglutamate polyester, Antifreeze proteins (AFPs)[967,1062] and some natural polymers including tapioca starch[1063–1066] (mixture of amylopectin and a linear polymer amylase), dextran[1067,1068] (polymer of anhydroglucose) chitosan[1069–1071] (a polysaccharide composed of *N*-acetyl-D-glucosamine and type β-(1-4)-linked D-glucosamine). Fig. 16 shows illustrative structures of some KHIs including some widely used polymers, ionic liquids, and green inhibitors.

The AFPs biomolecules or ice structuring proteins, which are found in specific cold-adapted organisms,[1072] could bind to germinal hydrate crystals and inhibit their growth within a given temperature range. Xu *et al.*[1073] found that pectin, which contains linear regions of 1,4-linked-α-D-galacturonosyl units and methyl esters with hydroxyl functional groups, could form H-bonds with water molecules and rupture water structures, hence, significantly lessen the hydrate crystal growth rate and hinder hydrate formation. In addition to aforementioned biochemistries of KHIs, the hydrophilic waterborne polyurea/urethanes (WPUUs)[1074–1076] with hydroxyl functional groups have recently gained interest from researchers as one of the greenest inhibitors owing to their eco-friendly/non-toxic nature.[1077–1079] Different researchers have investigated the compatibility of KHIs with other flow assurance chemicals such as corrosion inhibitors to measure potential suppressed KHIs efficiency. Recent studies[1080,1081] suggest newly designed KHIs for simultaneous inhibition of gas-hydrate formation and steel pipelines' corrosion.

4.1.3. Anti-agglomerants (AAs). Generally, gas-hydrate agglomeration is a three-step phenomenon of hydrate nucleation, hydrate crystal growth, and association of hydrate agglomerates,[1082]

Open Access Article. Published on 22 Junie 2020. Downloaded on 2026-02-11 12:42:38 nm..
This article is licensed under a Creative Commons Attribution-NonCommercial 3.0 Unported Licence.

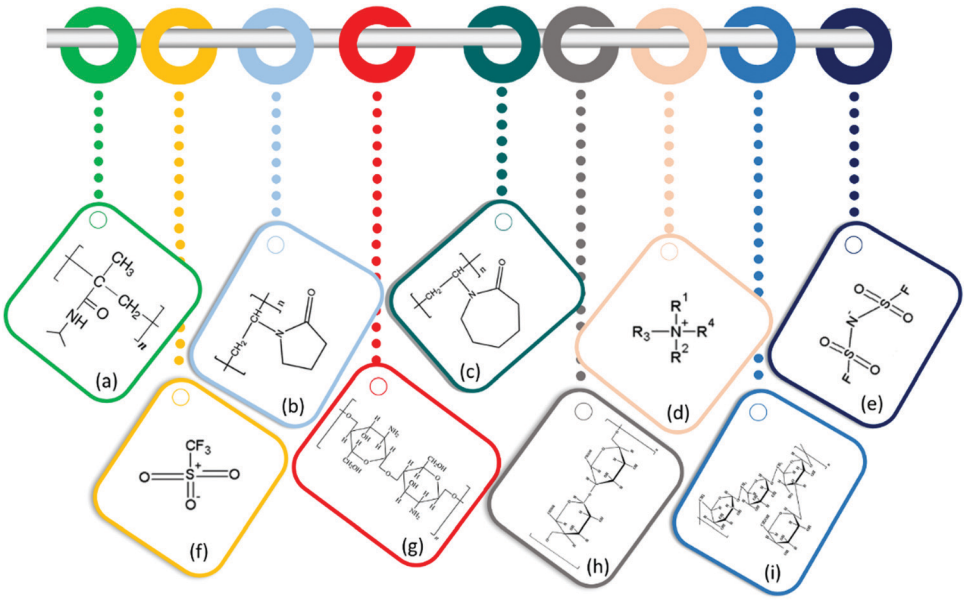

Fig. 16 (a) Molecular structure of poly(*N*-isopropylmethacrylamide); typical poly(*N*-vinyllactam) polymers with incrementing lactam ring sizes: (b) PVP (five-ring); (c) PVCap (seven-ring); some fundamental structures of ionic liquids (ILs) utilised as kinetic hydrate inhibitors in the literature. Cations: (d) tetraalkylammonium [$N_{n1,n2,n3,n4}$]; anions: (e) bis(fluorosulfonyl)imide [f_2N]; (f) triflate [OTf]; the chemical structures of green inhibitors: (g) chitosan; (h) tapioca starch; and (i) dextran.

which results in the formation of larger aggregates which can result in pipeline blockages.[958] In order to manage this undesirable process, the molecular interactions between hydrate aggregates and water molecules, which play a critical role in the agglomeration phenomenon,[1083,1084] need to be disrupted. Indeed, the gas saturated water droplets facilitate clathrate growth through their attachment to the crystals which leads to further crystallisation of water droplets[754] and the subsequent formation of larger aggregates. Anti-agglomerants (AAs), as a category of low dosage hydrate inhibitors (LDHIs), are typically amphiphilic surface-active compounds with intricate hydrophobic tails and hydrophilic headgroups[1085] which adsorb onto the gas hydrate aggregates surface[1086,1087] at the aqueous–oleic phase and/or hydrate–oil interfaces[1088] to maintain fluid flow in the hydrocarbon transportation pipeline systems[1089] operating at extreme subcooling environments where the KHIs cannot perform efficaciously.[1087] AAs can disperse the small hydrate aggregates in the oleic phase that can create a stabilised slurry flow through the pipelines.[1090,1091]

A widely utilised type of AAs contains quaternary ammonium surfactants[1092] which are usually bonded to *n*-butyl or *n*-pentyl functional groups along with long alkyl chains and form a well-structured AA hindrance thin layer at the clathrate–oleic phase interface.[1085] It has been illustrated that the AA thin film could hinder further hydrate aggregation and crystal growth processes through the formation of an obstacle for methane transfer to the hydrate surface.[694,1085] The creation of a thin interfacial layer of AAs at the clathrate–oleic phase interface could be crucial for minimising the agglomeration of hydrate aggregates[1087,1093] which consist of a combination of surfactants and alkanes from the oleic phase, as interfacial tests depict that linear alkanes would incorporate with the surface active species to create an ordered interfacial monolayer at the aqueous–oleic phase and/or the hydrate–oil interfaces.[1094,1095] Due to adequate adsorption of AAs onto the gas hydrate aggregates surface through head binding, tail binding, and head & tail binding, the contact angle of the hydrate surface would be incremented resulting in the wettability transition from water wet to oil wet,[1082,1084] reducing adhesion force between hydrate aggregates,[1096] and prevention of agglomeration phenomenon accordingly. Sometimes Sorbitan type surfactants, such as Span20 to Span80,[1086] are employed as AAs to inhibit hydrate particle agglomeration instead of ionic chemicals.[1097] It has been shown that AAs can augment the inhibition efficiency of alcoholic thermodynamic inhibitors including MeOH,[1098] and in presence of salts in the aqueous phase.[1099] Different research studies reported that the inhibition yield of ionic AAs are increased due to the salinity increment of the aqueous phase[1100,1101] which leads to higher stability of the emulsion,[1102] separating of the AA moieties away from the aqueous phase,[1014] and hindering of hydrate aggregates agglomeration processes. Recently, Mehrabian *et al.*[1103] developed a fundamental understanding of the influence of salt on quaternary ammonium cationic AA adsorption phenomenon onto the sII methane–propane hydrate surface in aqueous environment providing insights into the hydrate–salt and AA–salt molecular interactions on an energetic level. Their molecular dynamic simulation results noted that the AA molecule first adsorbs onto the hydrate surface through interactions with either its head or tail (Fig. 17a and b) and then, the other section of the molecule interacts as the second step, forming the head and tail binding configuration at the same time (Fig. 17c).

The salt-content augmentation in the aqueous phase can facilitate these interactions through AA solubility reduction in the aqueous phase and strong interactions of AA cationic head

Open Access Article. Published on 22 Junie 2020. Downloaded on 2026-02-11 12:42:38 nm..
This article is licensed under a Creative Commons Attribution-NonCommercial 3.0 Unported Licence.

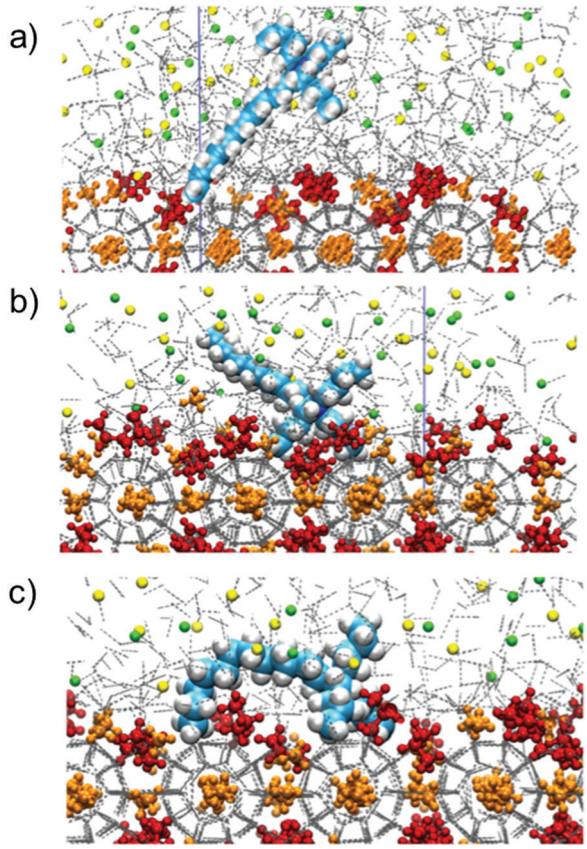

Fig. 17 Snapshots of molecular-dynamics simulation of AA molecule adsorption phenomenon onto the gas hydrate surface for three different kinds of molecular interactions with surface active species at the interface: (a) solely the long hydrocarbon tail of the AA molecule interacts with the hydrate surface, (b) solely the ionic head of the AA molecule has binding affinity to the hydrate surface, and (c) the AA molecule interacts with hydrate surface through simultaneously head and tail bindings to the surface (adapted with permission from Mehrabian *et al.*[1103] Copyright 2018 American Chemical Society).

groups with chloride anions at the interface which result in an AA efficiency increase. In some cases, AAs boost the formation of gas hydrates[1104] which can catalyse hydrate growth which facilitates novel applications in areas such as the storage of natural gas[7,1105,1106] and the desalination of water[1107,1108] amongst others.[1109,1110] Further research studies would be required through affiliating molecular level data using micromechanical force measurements, new molecular dynamic simulations[665,745,747,1111–1114] and macroscopic experiments including rocking cell to lead to the establishment of an appropriate synergism between modelling and tests results at all relative length and timescales that is required to handle the gas hydrate associated flow assurance challenges within the pipelines.

Moreover, some experimental studies using sum frequency generation or other spectroscopic techniques would also be needed to probe the molecular structure of AAs at different interfaces to build a fundamental understanding on how a variety of AAs perform in different systems. Such experimental data could assist scientists to realise whether the attained data from numerous simulation investigations are reliable or not in addition to determining potential applications of the studied systems in CO_2 hydrate-based CCS processes (see to Section 6.1.2.2).

4.2. Experimental test methods

Over the past decade, researchers have spent an enormous deal of effort on the development and application of various experimental facilities which have created new trajectories for hydrate mitigation and control in intricate pipeline systems.

Different flow loops with a variety of dimensions and operating conditions have been widely utilised to investigate the character of hydrate/ice plugging, deposition mechanisms and induced flow patterns under a series of flow rates and water cuts[1115–1117] for water dissolved in a liquid condensate system[1118] and multiphase systems (*e.g.* natural gas + diesel oil + water[1116]) with/out inhibitors,[1119] w/o emulsion systems.[1120] A high-pressure visual cell[1121] and stainless-steel hydrate equilibrium cell[1122,1123] were utilised to determine the kinetics of hydrate formation and methane hydrate film growth within a cold tube. Douïeb *et al.*[1124] illustrated the hydrate induction time using a stress/strain-controlled rheometer. They performed the tests at various flow shear rates and realised that higher shear rates could result in shorter hydrate formation induction times probably owing to the greater mixing severity.

A newly designed 1.5 m long cylindrical windowed experimental rig[965] was also employed to visually investigate the efficiency of some thermodynamic hydrate inhibitors[1125] and combinations of them, with different densities at removing hydrate blockage in vertical pipes. Although the accuracy and quantitative ranking capability of an automated lag-time apparatus (ALTA)[667,699] has been validated for hydrate nucleation and KHI chemical development, rocking cells[1126] have been widely utilised for the development and validation of KHIs as well. The high-pressure differential scanning calorimetry (DSC)[1053,1102,1127] is another experimental facility which has been employed to investigate the effects of AAs, KHIs and NaCl salt and their mixtures on water-in-oil emulsions and gas hydrate formation characteristics. In the last decade, various state of the art analytical techniques have been utilised to identify gas hydrate structures and respective noncovalent interactions at aqueous–vapour phase interface. Raman spectroscopy and synchrotron powder X-ray diffraction (PXRD)[1012] have been used for the characterisation of methane and natural gas hydrate crystal structures and corresponding hydrate cage occupation characteristics. In order to optimise gas hydrate inhibitor injection rate, numerous different analytical techniques have been used to determine the concentration of THIs, KHIs, and salt in the aqueous phase. Some experiments were conducted with an acoustic multisensory for determination of the MeOH and ethanol concentration in aqueous solutions without the presence of salts. A combination of near-infrared (NIR) and chemometric methods were applied to measure alcohol contents in gasoline[1128,1129] and ppm level concentration of dissolved chloride salts of a variety of alkali and earth alkaline cations in water.[1130] Additionally, tests using an ultraviolet

Open Access Article. Published on 22 Junie 2020. Downloaded on 2026-02-11 12:42:38 nm..
This article is licensed under a Creative Commons Attribution-NonCommercial 3.0 Unported Licence.

(UV)-visible spectrometer was performed to monitor the concentration of PVCAp[1131] and different types of polymers[1132] in water. Recently, Haghi *et al.*[1133] developed a novel methodology by combining the UV and NIR spectra associated with the partial least-squares (PLS) method to estimate the concentration of MEG, MeOH, and PVCap with/out presence of NaCl in water samples mainly for inhibitor injection rate optimisation purposes. A sealed pipe on a rocking surface called a rock-flow cell[1134] is a newly developed testing flow assurance tool to understand the formation and deposition of solids particles including gas hydrates under suitable field conditions including transient conditions, appropriate shear stress and involved flow regimes. Additionally, a new unidirectional growth technique[1021] has been employed to understand the interfacial phenomenon of tetrahydrofuran (THF) clathrate hydrate crystal growth from PVP containing an aqueous phase to study the influence of KHIs on hydrate crystal growth inhibition. For more rapid and accurate evaluation of KHIs, a new crystal-growth inhibition (CGI) based technique[1135,1136] has been developed with principles similar to the semi-industrial hydrate flow loop. Fig. 18 depicts the experimental CGI regions identified for 0.5 wt% PVCap with methane in both the autoclave setup and the rocking cell which exhibit that all the determined CGI regions are identical in both experimental facilities with minimal discrepancy within the ±0.5 °C experimental error.

Generally, it is well understood that gas hydrates are formed either in the bulk aqueous phase or the interspersed liquid phase. Most of the techniques which have been employed to form gas hydrates in the interspersed aqueous phase in which the vapour–aqueous phase interface area and mass transfer between phases are increased accordingly.

Numerous research studies on the effects of nanoparticles on gas hydrate formation have been conducted in an agitated vessel[902,915] instead of a packed bed[849] in the attendance of different chemical compounds including hydrogels,[1137] porous polymers,[1138] and foams.[1044] The utilisation of nanoparticles in solution has a positive influence on the enhancement of hydrate formation kinetics. Through the same drivers of surfactants' effectiveness, the affirmative influence of nanoparticles can be lessened as their concentration increases, which is occurred due to the extreme heat generation and a raise in the viscosity of the mixture.[899] Detailed discussion in this regard are presented in the growth acceleration section (Section 3.5).

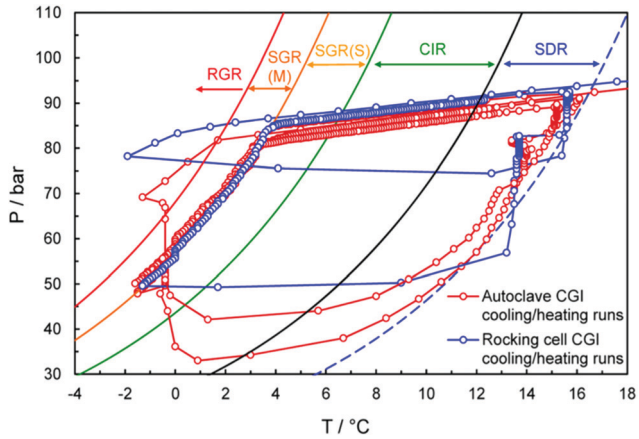

Fig. 18 Experimentally identified crystal growth inhibition (CGI) regions for 0.5 wt% PVCap in aqueous phase + methane; SDR: slow dissociation region, CIR: complete inhibition region, SGR(S), slow growth region (slow), SGR(M), slow growth region (medium), and RGR: rapid growth region. CGI cooling and heating tests for 0.5 wt% PVCap in aqueous phase + methane in the rocking cell and standard autoclave setups (adapted with permission from Mozaffar *et al.*,[1135] Copyright 2016 American Chemical Society).

4.3. Advancement

4.3.1. Early warning and monitoring techniques. Costly gas hydrate build-up induced pipeline blockage can occur due to accumulative hydrate formation which are not identified and treated during the initial stages of formation. The past decade has witnessed new technologies for providing the required information for the field operators to understand how close the gas hydrate system is thermodynamically to hydrate formation conditions and detect early signs of hydrate creation, termed gas hydrate early warning and monitoring systems. It is well known that owing to the formation of structure I (sI) and structure II (sII) hydrates and the corresponding gas trapping in the hydrate cages, concentrations of gaseous species (*e.g.* CH_4 for sI and C_3 & iC_4 for sII) in the hydrocarbon phase are suppressed. Thus, an experimental technique has been developed to identify early signs of hydrate crystals formation through the determination of gas composition in the pipelines or separators and/or gas content measurement released from the first stage water degasser.[1139] Furthermore, this methodology can be utilised for the systems where less than 5 barrels/mmscf water could be transformed into gas hydrates with the further assumption of the presence of hydrate crystals transfer due to gas phase quick motion. Yang *et al.*[1140] designed and developed a robust, reliable and fast technique for measuring the concentration of salts, thermodynamic and kinetic hydrate inhibitors in the aqueous phase based on integrated electrical conductivity and acoustic velocity data acquisition which fed into an Artificial Neural Network (ANN) system for prediction of aqueous phase chemical composition that leads to determination of hydrocarbon fluid composition and hydrate stability zone recognition accordingly. When there is no access to aqueous phase, Tohidi *et al.*[1139] proposed another methodology for the determination of hydrate stability zone and hydrate safety margin based on water content measurement in the gas phase, which is related to the water activity in the system. Additionally, Tohidi *et al.*[1141] proposed some techniques as hydrate monitoring and warning systems, which are based on freezing point and dielectric properties measurements. They employed a freezing point decrease of the aqueous phase to estimate the hydrate reduction temperatures of reservoir fluids in the presence of salts and inhibitors using a simple equation. It has been shown that dielectric properties at microwave frequencies[1141] could be utilised as a downstream analysis for identifying the preliminary hydrate formation stage and/or recognition of hydrate particles in the water structure transition owing to hydrate crystals constitution.

Open Access Article. Published on 22 Junie 2020. Downloaded on 2026-02-11 12:42:38 nm..
This article is licensed under a Creative Commons Attribution-NonCommercial 3.0 Unported Licence.

Focused beam reflectance measurements (FBRM)[1142] are often utilised to investigate the dispersed hydrate particle size. The FBRM probe determines both the number and size of chord lengths at a specific location in space, which result in the creation of a chord length distribution (CLD). The FBRM experiments have been successfully conducted for emulsions characterisation and droplet size distributions in oil,[1143,1144] illustration of hydrate nucleation and growth behaviour,[1145] evaluation of anti-agglomerate additives performance[1146,1147] and estimation of hydrate formation and dissociation rate in gas–water solutions.[1148] Moreover, the FBRM experimental data has been combined with resistance-to-flow determinations[1142] to unravel the connection between hydrate particle distribution and bed formation and determine the onset of hydrate bed formation.

4.3.2. Regeneration of MEG. As discussed in Section 4.1.1, there are some water-soluble thermodynamic hydrate inhibitors, including MeOH and MEG, which suppress the water activity, and correspondingly alter the hydrate phase boundary to higher pressure and/or lower temperature conditions. However, due to their required high dosage rates they could cause significant increases in CAPEX and OPEX, particularly at high water cut streams, in addition to the inevitable logistical and environmental issues. MEG is preferable when compared to other THIs due to its chemical stability and better efficiency, higher regeneration yield, reduced environmental impact, and lower solubility in the final gas phase.[1149] However, a vast amount of MEG is required in order to reach an influential hydrate mitigation strategy and even with a lower environmental impact than other THIs a discharge of MEG into the environment would have an impact, in addition to the financial cost of continuously refilling the MEG supply. The prevalent methodology is to recycle consumed MEG. Regeneration and reclamation are two main processes of MEG recycling. The high MEG content mixture, which could have undesirable impurities including oilfield chemicals (*e.g.* scale and/or corrosion inhibitors) and produced water, is re-concentrated through separating the produced water from the solution using distillation units that is called regeneration process. Then the regenerated MEG is then injected into the reclamation unit, where the solution is thermally exposed under vacuum conditions to the vaporisation temperature of MEG. This enables the MEG and water recovery through removing impurities as redundant yield.[1150] Regeneration of MEG is an inexpensive methodology, and its design and processes have been the subject of various research studies. The inhibition effectiveness of MEG after passing numerous regeneration/reclamation cycles has also been studied in the literature which allow users to take the required steps to ensure the lowest loss by appropriately identifying the optimum MEG injection rates. Khalid Alef *et al.*[1151] recognised a hydrate phase boundary shift due to presence of MEG which resulted in an incitement to hydrate formation as the MEG regeneration cycles continued. A new methodology based on gas hydrate crystal growth monitoring has been developed to address the challenges associated with produced water reinjection and MEG regeneration[1136] in presence of KHI in the aqueous phase which could precipitate out of the solution and deposit onto the solid surfaces.

4.3.3. Recycle of polymers. As explained in previous section, THIs when used in large quantities can be recovered and reused due to well established recovery processes, while low quantities of KHIs can be simply evacuated. However, the methods of KHI recovery are less efficient and could lead to produced water fouling. In order to suppress the pollution caused by KHI discharge, it became critical to separate KHI polymers from produced water prior to the usual methods of disposal. The primary active moieties in KHI formulations are the polymers, which are the most prohibitive components in KHIs. Thus, various field recycling techniques can be applied to recover and reinject these KHI polymers. In this regard, different methodologies were employed to remove up to 70% KHI from, where polymer oxidation is currently the most promising technique.[1152] Improved KHI removal can increase the interest in using KHI as an inhibition possibility in addition to thermodynamic inhibitors (THIs) or to decrease the amount of THI needed through a mixture of KHI + THI[1153] which is an attractive inhibition strategy, however this is limited by the KHI handling concerns. In this regard, various research studies have been conducted to develop techniques for the determination of low polymers contents in the aqueous phase and extract them from produced waters. An appropriate method in some circumstances is solvent extraction through the addition of particular high molecular weight solvents such as carboxylic acids with a carbon number of five or more[1131] (*e.g.* pentanoic acid and above) at the processing facilities and applying thermal treatment to attain the desired temperature for optimisation of mass transfer phenomenon. An approach of produced water fouling inhibition was proposed which was based on downhole KHIs injection incorporating a water-immiscible solvent with a high polarity index. A high molecular weight polymeric flocculant was also demonstrated to be able to remove KHIs from aqueous solutions.[1154] Membranes, which can trap and concentrate the KHI mixtures, and advanced oxidation process could also be cooperatively utilised[1152] to decrease the KHI content in the waste water streams. An international patent has shown a decrease in the KHIs content in the aqueous phase by employing an optimised treatment methodology chosen from different techniques including solvent extraction, chemical adsorption, chemical and electrochemical coagulations, and integrating them. Once the KHI has been recovered to varying extents, the effluent fluid might require to be evacuated based on the offshore or on-land disposal regulations using an adequate facility such as a heated centrifugal separator.[1155]

5. Gas hydrates in nature

5.1. Energy recovery

Naturally occurring gas hydrates that have accumulated in submarine continental margins (>97%), and permafrost regions (3%>) over millennia with methane as the predominant guest molecule, are considered as a low-carbon energy source and a CO_2 sink. The uncertainty in estimating total hydrate resources introduces considerable variability into the resulting projections

Open Access Article. Published on 22 Junie 2020. Downloaded on 2026-02-11 12:42:38 nm..
This article is licensed under a Creative Commons Attribution-NonCommercial 3.0 Unported Licence.

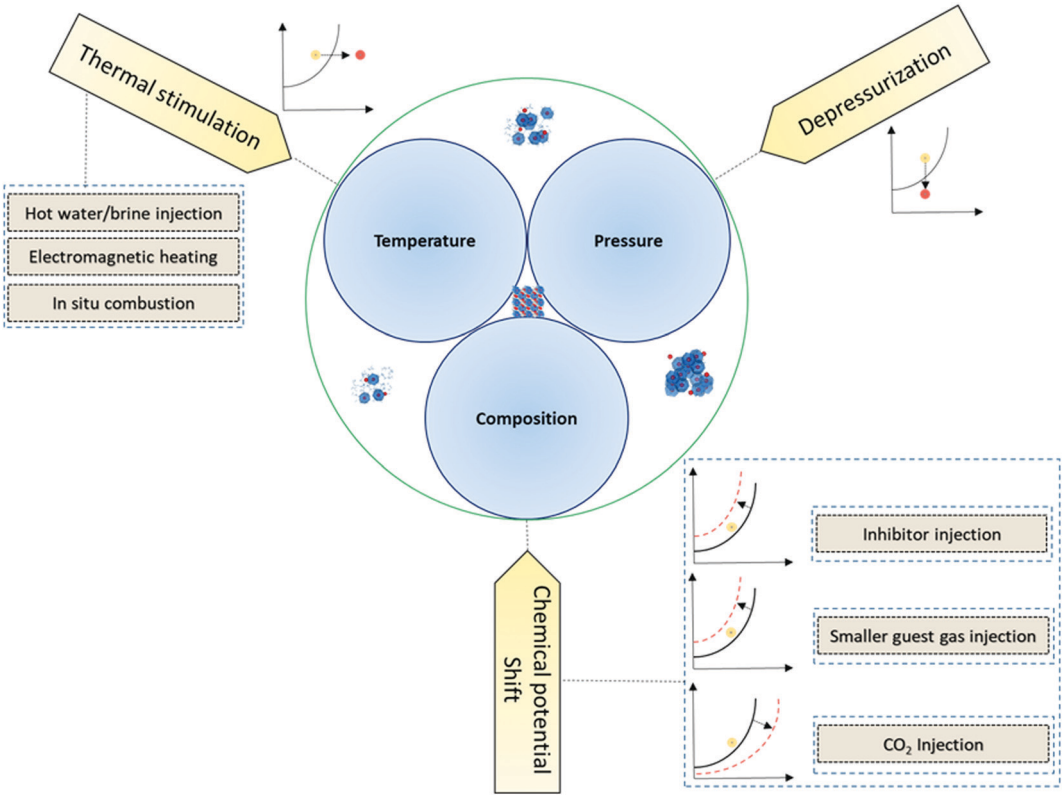

Fig. 19 Potential methods for extracting gas from hydrate reservoirs: (1) thermal stimulation: raising temperature of the reservoir by various techniques (yellow dot) to move the system condition outside of the Hydrate Stability Zone (HSZ) (red dot). (2) Depressurization: reducing the pressures of the reservoir by removing part of the gas phase to move the system outside of HSZ stimulates the hydrate dissociation. (3) Chemical potential shift – (i) inhibitor injection and (ii) smaller guest gas injection: shifting the HSZ above reservoir condition triggering the dissociation of hydrates. (iii) CO_2 replacement: destabilizing the existing gas in the hydrate phase by injection of more favourable guest molecules.

of the potential contribution of these reserves. However, estimation of the amount of energy stored in the hydrate reservoirs consistently outweighs that of the other conventional energy sources combined. For a more exhaustive examination of studies into gas hydrate reservoirs, the reader is referred to available reviews.[1156–1161] The purpose of this part of the review is to offer a brief overview of gas hydrates in nature and present the most recent advancement in strategies that have considered the potential options for energy recovery from hydrate reservoirs. A graphical summary of this section is provided in Fig. 19.

5.1.1. Thermal stimulation. The temperature of the gas hydrate reservoir controls the pressure of the system, because raising the temperature to outside the hydrate stability zone increases the pressure and pushing the encaged gases out of the water framework which results in a return of the system to equilibrium conditions. This in turn, makes more gases available for production. To increase the reservoir temperature, different methods are implemented including: hot water/brine[1162,1163] injection, steam-assisted gravity drainage, electromagnetic heating,[1164] and *in situ* combustion.[1165,1166] Results of typical hydrate dissociation experiments conducted by increasing the bath temperature are also appropriate. According to recent studies, an optimal reservoir gas permeability,[1167] reasonable thermal conductivity, information about the initial spatial distributions of the various phase saturations,[1168] and a suitable temperature rise to overcome self-preservation phenomena[821] as well as to provide the heat for the endothermic process are the requirements for efficient gas production from hydrate reservoirs by thermal stimulation.

Although thermal-stimulation methods have been considered as a promising candidate for fulfilling the gas-hydrate production goals from hydrate reservoirs, it is not an economically viable solution unless the hydrate layers exhibit sufficient thickness and saturation. To conquer this drawback, some strategies have attempted to combine thermal stimulation with other methods that are discussed in following sections.

5.1.2. Depressurization. Depressurization as the least energy intensive method of providing the driving force for destabilizing the clathrates and releasing encaged gases. To this end a variety of laboratory experiments, numerical simulations,[1169–1171] and real field trials[1172] have been conducted to investigate the effects of the relevant parameters. Researchers have explored the effects of pressure,[1173] temperature,[1174,1175] dissociation rate, initial hydrate/water/gas saturation and mineralogy of the reservoir (*i.e.* different classes of hydrate deposits)[1176,1177] along with different production scenarios,[1178–1180] wellbore type,[1181–1183] and *etc.*[1161,1184–1187] to optimize the efficiency of this method, resulting in more economical production.

As the gas is produced following the depressurization, the reservoirs can exhibit improved permeability when compared to its initial status. Thus, the availability of methane gas near

Open Access Article. Published on 22 Junie 2020. Downloaded on 2026-02-11 12:42:38 nm..
This article is licensed under a Creative Commons Attribution-NonCommercial 3.0 Unported Licence.

the wellbore is expected to improve in long-term operations, resulting in higher production rates. This factor plays the main role in the majority of the numerical simulations. However, there are still economic barriers regarding the challenging access to gas hydrate reserves, uncertainty on predicting the recoverable amounts,[1169] and more importantly, significant environmental hazards associated with the stability of the geological structures after gas production, all of which are the subject of ongoing discussions. The endothermic dissociation of gas hydrates,[1188] which would require an external energy source to transfer heat to the reservoirs, poses additional challenges and stands as the main challenge in the experimental modelling. It has also been reported that depressurization, apart from being a slow method, also has the possibility of ice formation[1189] when rapidly done, thereby causing a reduction or complete blockage of permeability which in turn affects the volume of gas produced. Accordingly, it is been widely suggested in the literature to combine the depressurisation technique with others to remove the aforementioned barriers. While thermal stimulation or inhibitor injection are expensive methods, depressurization usually requires the addition of heat to ensure that the heat consumed by decomposition of the gas hydrate will not reduce the production rate.[1190,1191]

5.1.3. Chemical potential shift

5.1.3.1. Inhibitor injection. Inhibitor injection is an established subject initiated decades ago[1192] and mostly applied to flow assurance related topics. However, we found only a limited number of studies dealing with application of this methodology in hydrate bearing sediments. Research interest has decreased in recent years, mostly driven by increasing concerns of the effect of injected inhibitors on the environment and the high cost of the method when considering amount of inhibitor that is required to be injected into the reservoir. Inhibitor injection is another strategy to shift the chemical potential of the hydrates by depressing the activity of water in coexisting phases to overcome the hydrogen bonding of water framework. The freezing-point depression of water by thermodynamic inhibitors is analogous to this method. The main inhibitors used in this method are salts and alcohols, the effect of which are reviewed in previous chapter. The conventional workflow in the preparation of methane recovery strategies with inhibitor injection begins with the selection and injection of inhibitors, which can be heated before injection, followed by depressurization. In the most recent studies, two groups of workers investigated the efficiency of methane production under MeOH[1193] and polyethylene glycol (PEG) polymer[1194] injection with various concentration and rates, and defined the optimum rate and concentration for inhibitor injection. Beside inhibitor injection concentration and rate, reservoir temperature, pressure and hydrate surface area in contact with inhibitor are important parameters for improving the efficiency.[1192] The possibility of combining this method with other methods will be discussed in following sections.

5.1.3.2. Heavier guest gas injection. The key approach here to produce methane is to use the higher stability of CO_2 in hydrates (causing the chemical disequilibrium) for replacement with methane, storing CO_2 and producing methane. A similar approach can be used to separate CO_2 from different gases streams. A notable research in the development of this method has been conducted over the past 10 years.[1195,1196] Hence, more detailed review about the application of gas hydrate related technology in CO_2 research is provided in Section 6.

5.1.3.3. Smaller guest gas injection. One of the established methods of gas exploitation from gas hydrate reserves is injecting smaller guest gases with a higher pressure hydrate stability zone (HSZ), releasing gases from the cages owing to chemical potential instability. This could address the safety concerns regarding the high-pressure gas pockets trapped between isolated regions and allow production of methane hydrate at higher pressures within the methane HSZ. Several gas mixtures candidates have been suggested in the past decade, mainly N_2 mixed gases. Injection of N_2, in this context, changes the fugacity of gas phases, making it easier for the CH_4 molecules encaged in water framework to be released, which may also be used as an alternative way for flow assurance.[1197] In a recent study, Okwananke *et al.*[1198] experimentally investigated the kinetics of methane recovery by N_2 and compressed air injection followed by step-wise depressurization over range of temperature and concluded that pure N_2 is a more efficient agent for methane recovery. Zhang *et al.*[1199] focused on N_2 injection methods by using a MRI system in order to characterize the phenomena and found that initial fast dissociation of CH_4 is followed by the slower rate limited N_2 diffusion. Both the mentioned studies suggest that this method is more useful for the dispersed hydrates with higher contact areas to increase the rate of dissociation. The rest of the studies combined with CO_2 mixed gases which will be reviewed in Section 6.

5.1.4. Field trials/case studies.

Field-scale and industrial demonstration projects for methane recovery from gas hydrate reservoirs are crucial for verifying observations and theories from laboratory and simulation studies and to prove the commercial viability of the production technology. Based on increased knowledge from laboratory and simulation studies, a number of onshore[1200] and offshore[1201] field production trials have been conducted. To date several methods including depressurization,[1200] chemical potential shift,[1202] thermal stimulation,[1203] or combination of these have been applied to field sites over a limited time scale. Nevertheless, as methane recovery approaches the commercial demonstration stage of development, some technical uncertainties remain, such as those related to continuous production of the gas, monitoring systems, proper forecasting system, reservoir heterogeneity, sand production, and heat flow. However, the demonstration projects will provide the practical information and experience needed to push forward this energy recovery technology to the commercialization scale, which is not expected to occur before 2025.[1204]

5.2. Environmental aspects

5.2.1. Gas hydrate–climate interactions.

Researchers have long considered whether gas hydrates could have a synergistic relationship with climate change processes.[1205–1207] The most

Open Access Article. Published on 22 Junie 2020. Downloaded on 2026-02-11 12:42:38 nm..
This article is licensed under a Creative Commons Attribution-NonCommercial 3.0 Unported Licence.

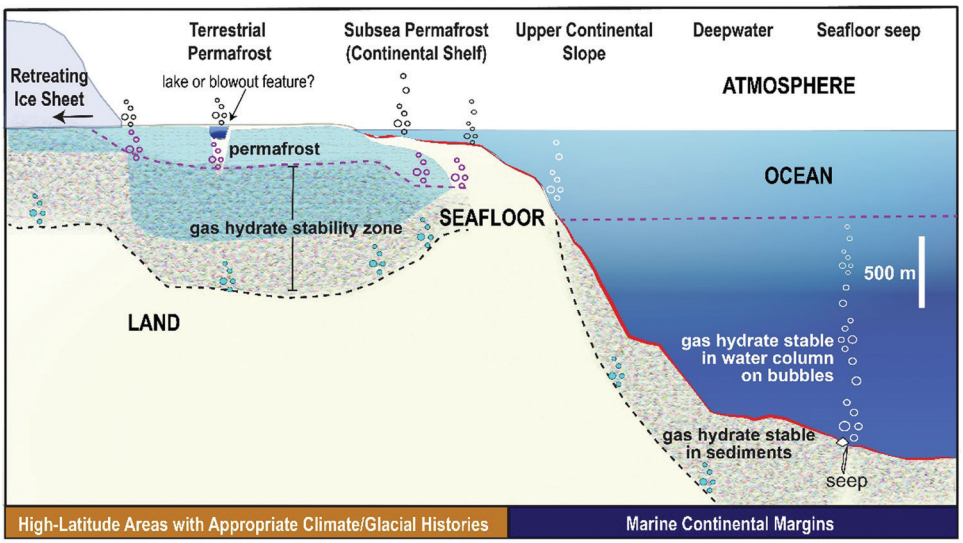

Fig. 20 Schematic shows various terrestrial and marine settings for gas hydrate occurrences and the impact of warming climate on gas hydrates. The base and top of the gas hydrate stability zone are denoted by dashed black and dashed violet curves, respectively. Note that the top of the gas hydrate stability zone in the ocean is within the water column, meaning that the seafloor lies well within the stability zone at depths greater than the upper continental slope. Permafrost is denoted as blue shading beneath the ice sheet (cold-based glacier) on the far left and beneath the land (terrestrial permafrost) and high-latitude continental shelf (subsea permafrost). Bubbles are shown to indicate possible gas emissions associated with hydrate breakdown and are color-coded depending on their fate. White bubbles are emitted as methane at the seafloor, but the methane is rapidly stripped from the bubbles so that no methane remains by the time these bubbles reach the sea surface. Methane that persists through the near-seafloor zone of anaerobic methane oxidation (shown in red) is usually oxidized aerobically once it reaches ocean waters. Blue bubbles are produced by gas hydrate degradation at the base of the stability zone, which will be the first locus of dissociation in the deep marine environment in response to ocean warming. In permafrost areas, gas hydrate can simultaneously dissociate at the top (purple bubbles) and bottom (blue bubbles) of the stability zone. The blue bubbles indicate gas that might re-form as new gas hydrate as the gas migrates upward to the stability zone after release. Purple bubbles have a better chance of migrating through the sediments towards the surface if they are not stopped by low permeability ice-bearing permafrost. This methane may be oxidized by microbes within sediments or remain as methane and continue migrating upward if pathways exist. Bubbles within no colour and outlined in black are those that may emit methane to the atmosphere. Locations experiencing deglaciation or subsea permafrost thaw since the last glacial maximum are the most prone to releasing gas hydrate methane that can reach the atmosphere. Upper continental slopes on many marine continental margins are likely experiencing net hydrate dissociation now, but this methane is not reaching the atmosphere based on the studies completed to date (adapted with permission from Ruppel and Kessler,[1] Copyright 2017 John Wiley and Sons).

frequently investigated scenario posits that a warming climate could trigger the breakdown of gas hydrate deposits, and that the liberated methane might then reach the atmosphere and exacerbate greenhouse warming, which in turn could drive more hydrate dissociation. For the case of extreme warming, some publications have described catastrophic scenarios and runaway hydrate dissociation.[1208–1211]

Gas hydrate dynamics (see Fig. 20) and past climate events have been linked in the literature for decades, and researchers have investigated the possible synergies especially for the Paleocene-Eocene Thermal Maximum hyperthermal event[1212–1214] and the Late Quaternary "clathrate gun hypothesis" of Kennett *et al.*,[1215,1216] which was re-examined by Cannariato and Stott.[1217] Recent findings about hydrate dynamics during these time periods are summarized by Ruppel and Kessler.[1] For the contemporary Earth, gas hydrates in certain geological settings could already be breaking down due to warming ocean waters[1205] and the residual effects of deglaciation since the Last Glacial Maximum,[1218] which are mostly relevant at high northern latitudes. The feedback component, which requires methane formerly bound in hydrates to reach the atmosphere, is not operating over the largest (deep-water marine) component of global reservoirs[1219–1221] or the shallow-water setting linked to degrading subsea permafrost.[1222] Elevated sea-air methane fluxes observed at other high-latitude sites[1223,1224] cannot presently be linked to methane released by gas hydrate degradation.

There are several characteristics of gas hydrates that motivate interest in possible synergies between gas hydrate dynamics and climate change. Firstly, 15% of global methane, corresponding to ~1500 Gt carbon, is estimated to be trapped in methane hydrate deposits,[1160] and methane is a greenhouse gas that is 25 times more potent (over a century) and 84 times more potent (over two decades) than CO_2 on a unit mass basis.[1225] Secondly, most gas hydrates exist at shallow depths (up to a few hundreds of meters) beneath the seafloor, even shallower depths in deglaciated terrains, and deeper depths, but still closer to the surface than conventional reservoirs, in permafrost areas. The proximity of these deposits to the surface/seafloor means that migration pathways are relatively short compared to those for gas migration from conventional reservoirs. Thirdly, because gas hydrates are stable only in a specific *P–T* range, climate change and sea level perturbations can perturb hydrate stability. For plausible changes in sea level and temperature over the next few centuries, the effect of rising temperatures on the gas hydrate reservoir will likely outstrip the stabilizing effect of sea level rise nearly everywhere in the oceans.[1]

Open Access Article. Published on 22 Junie 2020. Downloaded on 2026-02-11 12:42:38 nm..
This article is licensed under a Creative Commons Attribution-NonCommercial 3.0 Unported Licence.

An exhaustive review by Ruppel and Kessler[1] provides deep background on climate–hydrate interactions. They discuss the major geologic settings for gas hydrates and possible synergies with contemporary climate change; assess how the Intergovernmental Panel on Climate Change (IPCC) reports have incorporated hydrate sources;[1225] and detail the challenges for accurately tracking methane released from gas hydrate through the geosphere, ocean, or atmosphere. A review by James *et al.*[1226] provides additional information focused on the Arctic Ocean.

For the contemporary Earth, research mostly focuses on the response of gas hydrate reservoirs to warming ocean waters or atmospheric temperatures.[1,1227] Such perturbations can drive hydrate dissolution in pore waters within the stability zone and cause hydrate dissociation where gas hydrates are close to the stability boundary, which is a relatively narrow zone within the formation. For most marine hydrates, warming-induced dissociation would occur only at the base of the reservoir, while permafrost-associated and deglacial hydrates can experience dissociation simultaneously at both the top and base of the hydrate zone.[1228]

Dissociation of gas hydrate releases methane into the formation, where the methane mostly remains trapped. If the gas migrates to shallower depths, it often encounters the hydrate stability zone, where the gas may re-form hydrate with available free water, or the permafrost zone, where water ice may block flow conduits and prevent methane from reaching the surface. Methane released by hydrate dissociation in marine environments also encounters a biochemical barrier to reaching the seafloor since more than 90% of methane may be consumed by AOM processes within the sulfate reduction zone (SRZ) in the shallowest part of the seafloor.[1229]

If methane survives transport through the SRZ[1230] and reaches the seafloor, emitted bubbles usually do not retain their methane for long as they ascend in the water column due to dissolution into the seawater.[1231] Nominally, gas bubbles emitted at water depths greater than 100 m (the shallowest deepwater marine hydrate zone is ~350 m in high-latitude waters) will be stripped of their methane before the bubbles reach the sea surface.[1231] Bubbles emitted at seafloor that lies within the hydrate stability may form hydrate rinds as they ascend through the water column,[1232,1233] but the methane still escapes from the bubble,[1234] especially after the hydrate shell disappears. Methane dissolved in the oceans is rapidly consumed by bacterial aerobic oxidation, producing CO_2 as a byproduct.[1235,1236] This process can acidify deep waters[1237] but does prevent methane from reaching the atmosphere. An increasingly number of studies demonstrate that, even over seafloor seeps, sea-air methane flux in deep ocean environments is very low, partially because of the consumption of methane in the water column. Some studies also show that methane dissolved in near surface waters is dominated by young methane produced by planktonic processes, not the fossil methane typically trapped in hydrates.[1221,1222] The details of methane release for hydrate settings other than the deepwater marine environment are provided later in this section.

Where are contemporary gas hydrates most susceptible to climate change processes? At water depths greater than ~1000 m, seafloor conditions are supercooled relative to the hydrate stability, and bottom water temperature is expected to remain within the stability zone for hundreds to thousands of years into the future.[1,1227] The bulk of the global gas hydrate reservoir is therefore unlikely to be noticeably perturbed by warming climate over these time scales. Many studies of climate-driven gas hydrate degradation focus on upper continental slopes at the landward or "feather" edge[1227,1238] of gas hydrate stability,[1,431,1239–1242] which corresponds to 450 to 700 m water depth in temperate regions. Ruppel[1204] estimated that ~3.5% of the gas hydrate reservoirs could be within this depth range although several factors could contribute to gas hydrates being rarer in these locations than elsewhere in deepwater reservoirs. At upper continental slope water depths, seafloor *P–T* are close to the stability boundary. Ocean warming on seasonal, decadal, or longer time scales could lead to dissociation and release of methane, which does not need to migrate far through the sediments to reach the seafloor. The discovery of upper continental slope methane seeps[1243–1246] on numerous continental margins in the past few years has led to speculation that some of these features are sourced from gas hydrate dissociation. The connection is difficult to prove, particularly where the leaking gas does not have a special composition that can be linked to that of local gas-hydrate deposits.[1247]

A special case of climate-induced hydrate dissociation applies to high-latitude regions, where onshore permafrost has been thawing rapidly, even in the past decade. Intrapermafrost gas hydrate (Dallimore *et al.*, 2015), which is thought to be relatively rare, could be experiencing dissociation due to such thawing. Permafrost that developed sub-aerially (*i.e.*, not below ice sheets) is unlikely to host methane hydrates shallower than ~200 m deep, and contemporary methane releases in permafrost areas are probably attributable almost exclusively to non-hydrate sources.[1]

Subsea permafrost was formerly subaerial permafrost before it was inundated during deglacial sea level rise.[1248–1255] Degradation of subsea permafrost and any associated hydrates has been rapid since the Last glacial Maximum (LGM). However, water column methane does not carry a strong fossil methane signature, as would be expected if the methane were derived from gas hydrate degradation.[1222]

Formerly subglacial hydrates are a special case since hydrate can form at shallow depths in the ground beneath thick ice sheets (*e.g.*, Fig. 11 of Ruppel and Kessler[1]). Deglaciation raises the temperature and releases the pressure on these deposits, which then dissociate. Some of the gas released from the seafloor into shallow seas that cover such areas may reach the atmosphere[1256–1259] although more research is required to link methane releases directly to gas hydrate dissociation. Deglaciation could also be a factor in future methane releases from gas hydrates currently beneath ice sheets in Antarctica[1260] and Greenland.[1261]

5.2.2. Marine biology. Marine sediments as one of the most extensive microbial habitats, house more than two-thirds of the Earth's surface.[1262] Principally, there is a logarithmical decrease in microbial cell counts in subsurface sediments with depth,

Open Access Article. Published on 22 Junie 2020. Downloaded on 2026-02-11 12:42:38 nm..
This article is licensed under a Creative Commons Attribution-NonCommercial 3.0 Unported Licence.

presumably due to declining organic carbon quality and availability in older layers. Hydrate bearing marine sediments, in particular, are dominated by specific microbial communities including archaeal, and various bacteria. According to diversity studies on subsurface hydrate-bearing sediments,[1263–1274] gas hydrate sediments located in different marine regions are shown to have distinct microbial cells and microbial activities. Biologically, these microbes are one of the major sources of methane gas production through anaerobic bacterial metabolism. This is alongside other abiological processes for methane production namely, thermal breakdown of organic matter, crustal, hydrothermal,[1275] and geochemical.[1276] Similarly, microbial production of ethane and propane have been proposed as a reason of exploring these gases in deep marine regions.[1277]

In fact, part of the released methane migrates upwards into the sulfate methane transition zone (SMTZ), where sulfate is diffusing from upper layers, causing anaerobic oxidation of methane (AOM) by syntrophic partnership between anaerobic meth-anotrophs (ANME) and sulfate-reducing bacteria.[1230,1278] Here, methane acts as a fuel for the growth of anaerobic microorganisms.[1279] This oceanic methane biogeochemistry process, serve as a major sink, causing considerable increase in dissolved inorganic carbon, alkalinity, and hydrogen sulphide. Promotion of the precipitation of authigenic carbonates and iron sulphide is another effect of this process. This in turn, influences the sea floor morphology, and landscape.[1229]

5.2.3. Seafloor stability. Seafloor destabilization refers to the development of submarine slope failures (landslides) on continental margins and to possible failure of the seafloor near production wells in gas hydrate provinces. These natural and anthropogenically-induced forms of seafloor failure are discussed separately here. Although this section focuses on research that examines seafloor instability through the prism of gas hydrate dynamics,[380,1280] seafloor failures have also been investigated in terms of sea level rise, groundwater discharge, sediment fluid flow, interaction with salt diapirs, and even mantle-plume activity.[1281–1285]

The spatial association between hydrate-related features (*e.g.*, BSRs, gas-charged sediments) and submarine slope failures has been well-established on the margins of the Atlantic Ocean, northern Gulf of Mexico, the western Beaufort Sea, South China Sea, and Norwegian part of the Arctic Ocean, as well as on the New Zealand and Cascadia margins.[380,1286–1291] Among the many slides investigated for their potential interaction with gas hydrates, two mega-slides, the Storegga Slide offshore Norway[379,1292,1293] and the Cape Fear slide offshore the Southeastern United States,[1281] have been the best studied and experienced some failure stages large enough to have triggered tsunami. Neither of these mega-slides are now interpreted to have been triggered by processes related to gas hydrate dynamics: Haflidison *et al.*[1294] show that the Storegga slide started at the toe, where gas hydrate would have been actively forming in deepwater. A recent interpretation of the Cape Fear Slide highlights the role of inherited structure, sediment loading, and fluid flow in the initiation of the seafloor failure.[1282]

Many seafloor landslides originate on upper continental slopes in the depth range where gas hydrates are relatively ubiquitous on marine continental margins, and thus the spatial association between slides and hydrate-related features is not surprising. While the evidence for a link between gas hydrate dynamics and some other seafloor destabilization features[1258,1295,1296] (*e.g.*, pingos, pockmarks) is strong, the connection between gas hydrates and submarine slides remains more tenuous. Controversy persists about whether the existence of gas hydrates and/or free gas in the sedimentary section pre-conditions slopes to fail when triggered externally (*e.g.*, by an earthquake) or whether the hydrate-related features directly provoke slope failures.

Addressing this controversy requires reconstructing conditions in the hydrate reservoir prior to slope failure, a task rendered difficult by the fact that seafloor deformation and mass transport accompanying landslide events destroy many of the pre-existing features. The mechanical state of the slope immediately before failure depends on a combination of factors unrelated to gas hydrate dynamics (*e.g.*, bulk lithology, sedimentary layering, rate of sedimentation/erosion, fluid advection rates, and pore pressure, which can also be modulated by hydrates and gas) and factors related to the hydrate system itself (*e.g.*, hydrate and gas saturation, whether hydrate forms in unconsolidated or already consolidated sediments[1297]). As noted in Section 2.5, gas hydrates are rheologically much stronger than saturated, unconsolidated marine sediments,[334] but hydrates only provide cohesion to sediments when its saturation exceeds $\sim$40% of pore volume.[138,1298] At lower saturations, gas hydrate accumulations are strong components set in a weaker matrix of saturated marine sediments. Even low saturations of gas hydrate can clog permeability and lead to increased pore pressure, which in turn enhances the likelihood of hydraulic fracturing, gas migration, formation of pipe structures, and seafloor failure[1285,1299–1301] even for relatively gas hydrate deposits well within the stability zone. Stronger, hydrate-bearing sediments[1302,1303] are also typically arrayed above rheologically weak, gas-charged sediments that are below BSRs. The contrast in mechanical properties between hydrate-bearing sediments above and gas-charged sediments below could produce an unstable condition that leaves slopes poised for failure when triggered by external (*e.g.*, earthquakes, tides) or internal (hydraulic fracturing) events.

Although some researchers have postulated that depressurization of upper continental slope gas hydrates during periods of lowered sea level triggered widespread slope failures,[1304,1305] slide timing does not correlate well with sea level low-stands. Hydrate dissociation caused by warming of intermediate-depth ocean waters impinging on upper continental slopes therefore receives more attention in contemporary studies.[1240,1241,1246,1306,1307] Unless the gas and water released by hydrate dissociation at the base of the stability zone are removed by advection, the pore pressure can increase, weakening slope sediments through liquefaction or fracturing. Whether these changes drive slopes to failure or merely condition slopes for later failure returns to the crux of the controversy surrounding the interplay of gas hydrate dynamics and seafloor instability.

To place hydrate dissociation in context, it is important to consider that hydrate saturations are probably less than a few

Open Access Article. Published on 22 Junie 2020. Downloaded on 2026-02-11 12:42:38 nm..
This article is licensed under a Creative Commons Attribution-NonCommercial 3.0 Unported Licence.

percent of pore space in most marine sediments; that hydrate dissociation is endothermic and therefore self-limiting, meaning that runaway dissociation driven by only a single factor (*e.g.*, ocean warming) is unlikely;[1] and that hydrate dissociation in response to natural driving forces is a relatively slow process and already occurs continuously at the base of the stability zone in response to sedimentation. The best-studied submarine slide events occurred over several stages and thousands of years,[1282,1294] and it is possible that none, only one, or a few of the stages of these complex slope failures were preceded by hydrate-related processes, including dissociation.

Studies have attempted to link the timing of submarine slope failures to climate warming events such as Late Quaternary Dansgaard/Oeschger (D/O) cycles.[1308] However, within the limitations of available age data, large-scale slope failures in the North Atlantic coincide more closely with Heinrich events,[1309,1310] which are characterized by episodes of ice rafting and injection of cold meltwaters.

As noted by Maslin *et al.*,[380] much better dating of submarine slide events will be required before the temporal correlation between seafloor destabilization episodes and climate perturbations can be unraveled. Maslin *et al.*[380] also posit that future submarine slide events may be connected not to warming-induced dissociation in gas hydrate reservoirs, but rather depressurization-induced dissociation caused by melting of ice sheets in Greenland and Antarctica. Deglacial episodes since the Last Glacial Maximum are already implicated in some smaller-scale seafloor destabilizations like crater, pockmark, and marine pingo development.[1258,1311,1312]

Anthropogenic activities that affect hydrate-bearing sediments may also induce seafloor failure. For example, extraction of deep, warm fluids through a conductor that crosses hydrate-bearing layers could drive dissociation near a borehole, weaken seafloor sediments, and possibly threaten seafloor infrastructure.[1313,1314] In a case documented by Hadley *et al.*,[1315] the oil production strategy was altered to avoid the hazards associated with attendant hydrate dissociation in the reservoir. Seafloor stability is also a consideration in deepwater marine production testing that is conducted to analyze the efficiency of methane extraction during controlled gas hydrate dissociation.[1316,1317] Depending on the depth and lithology of the target hydrate reservoir and its hydrate saturation, the rate of dissociation and gas extraction, and the pre-existing shear stress in the sediments, seafloor collapse could be a potential hazard.

5.2.4. Extraterrestrial clathrates. Both clathrate hydrates (ice cages that typically enclose non-polar gas molecules) and non-clathrate hydrates have been inferred for extraterrestrial settings.[1318–1321] This section focuses on clathrate hydrates and does not review other extraterrestrial hydrates, such as sulfuric acid hydrate found on the surface of Europa[1322] or perchlorate hydrates that may be present on the Martian surface[1323] (see Fig. 21).

As recognized by Mille[1324] more than 50 years ago, *P–T* conditions on the surface of or within the interiors of some planets, moons, and comets and within some planetary atmospheres

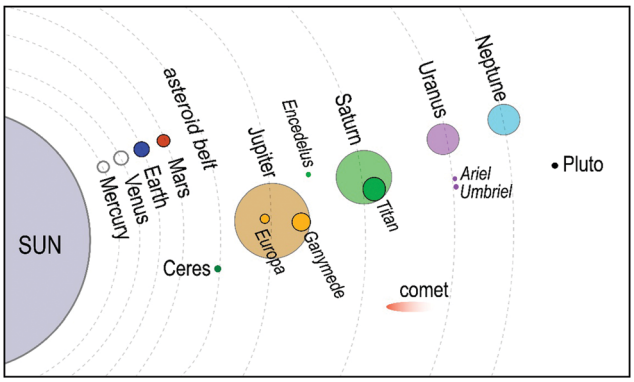

Fig. 21 The schematic depiction of the solar system shows the planets and other celestial bodies at their approximate orbital positions relative to the sun. The sizes of Pluto, Ceres, the moons of some gaseous planets, and the comet have been increased to make them visible. Bodies portrayed in colour are known or postulated to have clathrates at the surface, in their interiors, or in their atmospheres. For Jupiter, Saturn, and Uranus, only the moons with possible clathrates are shown. Comets move through the solar system, and one is portrayed here schematically to highlight that clathrates likely occur in some of these icy bodies.

are suitable for the formation and long-term stability of clathrates, including complex, multi-gas hydrates or hydrate structures that would be considered exotic on Earth.[34,323,1320,1325] Water, the critical building block for clathrate cages, is confirmed or inferred to exist in liquid or frozen form on Mars, Europa and Ganymede (moons of Jupiter), Titan and Enceladus (moons of Saturn), Pluto, and the dwarf planet Ceres, and water ice is a common constituent of comets.[1326]

On the surface or within the interiors of Mars, Saturn, Uranus, Neptune, and Pluto and on moons of Jupiter, Saturn, and Uranus, methane, ethane, CO_2, ammonia, and/or other gases coexist with water phases in varying amounts and are abundant enough to form clathrate. CO_2 and methane hydrate could form at or near the surface of Mars, particularly at the polar ice caps.[846,1327–1330] Methane and ethane hydrates are postulated to comprise the outer icy shell of Titan,[1320,1321,1331,1332] and methane hydrate may contribute to the strength of Ceres' outer crust.[1333] On Pluto, methane hydrate is postulated to form an insulating layer that protects the near-surface water ice from the deeper and warmer liquid-water layer.[1334] On Enceladus, the dynamics of water plumes detected at the surface may be affected by the presence of ammonia hydrate.[1335]

Clathrates also occur in comets,[1336,1337] which has led to the inference that hydrates may form within the interstellar medium,[1338] a view challenged by some laboratory experiments.[1339] The existence of clathrates on highly mobile comets implies that these objects could be important in delivering compounds like methane to other extraterrestrial bodies.[1340,1341]

The recognition of extraterrestrial clathrates containing gases sometimes produced on Earth by biological processes (*e.g.*, methane, ethane) has provoked substantial interest among astrobiologists. Outstanding questions include the source of the hydrocarbon compounds trapped in some extraterrestrial hydrates and the potential for other bodies in the solar system

Open Access Article. Published on 22 Junie 2020. Downloaded on 2026-02-11 12:42:38 nm.. This article is licensed under a Creative Commons Attribution-NonCommercial 3.0 Unported Licence.

to host the type of hydrate-associated microbial communities found beneath the ocean floor on Earth.[1326,1342,1343]

6. Gas hydrate-based CO_2 capture, transport and storage

The IPCC Special Report on the impacts of global warming of 1.5 °C above pre-industrial levels suggests that, to limit the possible impacts and risks on the people, economies and ecosystems to moderate levels, net global emissions of anthropogenic CO_2 must be reduced by about 45% by 2030 and to zero by 2050 compared to the 2010 levels.[1344] In addition to the use of low-carbon energy and improvements to energy efficiency, CCS has also been considered as one of the most effective approaches to meet the stringent reduction target for CO_2 emissions.[1345] CCS operation is a chain of CO_2 capture or separation from flue gas, transport of the captured CO_2 to a storage site and finally, storage of the CO_2 in a desired geological formation. The current CO_2 capture technologies such as physical adsorption, chemical absorption, cryogenic separation, and membranes are technically applicable but not economically viable for large-scale applications in the short to medium term.[1346,1347] Gas hydrate-based CCS technologies have been extensively studied in the past decades as a route towards significant improvements to the economic feasibility of large-scale CCS operations.[1348]

6.1. CO_2 capture

6.1.1. Mechanism. CO_2 molecules are small and nonpolar and can form sI hydrates in a formula of $CO_2{\cdot}nH_2O$. One unit cell of the structure I hydrate consists of 2 small cages (5^{12}, pentagonal dodecahedron) and 6 large cages ($5^{12}6^2$, tetrakaidecahedron).[1349] *n* represents the hydration number, depending on the occupancy of the cages (primarily the large cages) because CO_2 molecules favour the occupation of the large cages due to its molecular size. CO_2 molecules can also enter the large cages ($5^{12}6^4$, hexakaidecahedron) of sII hydrate in the presence of sII hydrate formers such as propane, cyclopentane (CP) and THF, or the small cages (5^{12}) of semi-clathrate hydrates of TBAB, tetra-*n*-butyl ammonium fluoride (TBAF), and tetra-*n*-butyl ammonium nitrate.

CO_2, N_2 (nitrogen) and O_2 (oxygen); H_2 (hydrogen) and CO_2; and CH_4 (methane) and CO_2 are the major gas components for a flue gas, fuel gas, and biogas, respectively. All these gases can form hydrates at certain thermodynamic conditions. Experimental data and thermodynamic prediction of gas hydrate phase equilibria show that, for temperatures from 273 to 283 K, the phase equilibrium pressure of CO_2 hydrate is more than 10 MPa lower than those of N_2 hydrate and O_2 hydrate, and more than 200 MPa lower than that of H_2 hydrate. The significantly lower formation pressure of CO_2 hydrate leads to a higher affinity to occupancy of the suitable cages in hydrate crystals compared to the other gases, which is the fundamental basis of a hydrate-based gas separation process (HBSP). Chazallon and Pirim quantitatively found that the flue gas containing 2 to 70 mol% CO_2 will form structure I hydrate, while structure II hydrate was thermodynamically stable for the flue gas with 1 mol% CO_2.[1350] Hassanpouryouzband *et al.* observed formation of sII hydrates in the presence of CO_2 + N_2 at higher pressures with up to 14.6 mol% CO_2 in the system.[1351] Furthermore, it was found that statically constant *P*–*T* conditions are not signs of thermodynamic equilibrium for the CO_2–N_2 mixtures and a significant fraction of CO_2 captured in the hydrate phase could occur at the final constant pressure.[1352] In short, flue gas or fuel gas can form CO_2 hydrate or CO_2-mixed hydrates in which CO_2 occupies the majority of the guest molecules at certain temperature and pressure conditions; decomposition of the hydrates can produce CO_2-rich gas; the CO_2-rich gas could be further processed through a series of HBSP cycles to achieve the desired purity of CO_2 gas.

6.1.2. Promotion of hydrate formation

6.1.2.1. Thermodynamic promoters. Thermodynamic promoters are chemical additives that are added to the system to reduce the hydrate formation pressure.[1060,1353–1357] These additives themselves can form hydrates in which some cages are left to accommodate small molecules such CO_2, N_2, CH_4 and H_2. The most-studied thermodynamic promoters include tetrahydrofuran (THF), cyclopentane (CP), propane (C_3H_8) and tetra-*n*-butyl quaternary ammonium along with phosphonium salts such as TBAB, tetra-*n*-butyl ammonium chloride (TBAC), TBAF, tetra-*n*-butyl ammonium nitrate ($TBANO_3$), tetra-*n*-butyl phosphonium bromide (TBPB), and tetra-*n*-butyl phosphonium chloride (TBPC),[54,1348,1358–1360] some of which are discussed in Section 2.1.2.

The THF, CP and C_3H_8 are structure II hydrate formers. Given that their molecules will occupy some of the large cavities of the structure II hydrate, CO_2 molecules can only fill the rest of the large cavities or some of the small cavities and the occupancy depends on the gas composition and thermodynamic conditions.[1361–1363] The tetra-*n*-butyl ammonium and phosphonium salts form semiclathrate hydrates.[54,1364,1365] X-ray diffraction and Raman spectroscopic analyses indicated that there are different structures of the semiclathrate hydrates, such as tetragonal hydrate structure (TBAC), orthorhombic hydrate structure (TBPB and TBPC), and polymorphic phases with both orthorhombic and tetragonal hydrate structures (TBAB).[1366,1367] In such semiclathrate hydrate structures, water molecules incorporated with the cations form cage-like structures through hydrogen-bonds, whilst tetra-*n*-butyl ammonium (TBA) cations and tetra-*n*-butyl phosphonium (TBP) cations (*i.e.*, the butyl chains) occupy the large cages. The small pentagonal dodecahedral cages (5^{12}) are usually left empty for small gas molecules such as CO_2, N_2, CH_4 and O_2. Fig. 4 illustrates the structure of TBAB hydrate with a hydration number of 38 ($(C_4H_9)_4N^+{\cdot}Br^-{\cdot}38H_2O$).[1366] Br^- anions and water molecules build the clathrate cages indicated in solid lines, two TBA cations fill four large cages, six dodecahedra are empty, the dashed lines indicate the broken part of the cage structure (H atoms are not indicated for simplicity).

The presence of low concentrations of the thermodynamic promoters leads to a large shift of the hydrate phase equilibrium conditions towards lower pressure or higher temperature, which is crucial to reduce the energy penalty of the gas

Open Access Article. Published on 22 Junie 2020. Downloaded on 2026-02-11 12:42:38 nm..
This article is licensed under a Creative Commons Attribution-NonCommercial 3.0 Unported Licence.

hydrate-based CO_2 capture process. The shift in the hydrate formation pressures and temperatures is related to both the concentration of the promoter and the composition of the gas mixture. In general, the reduction in the hydrate formation pressure is relatively smaller for the structure II hydrate promoters than for the semiclathrate hydrate promoters. Among the aforementioned semiclathrate hydrate promoters TBAF has the lowest formation pressure, hence the highest formation temperature.[1365] Two parameters, namely split fraction and separation factor, are introduced for a quantitative assessment of HBSP:[1368] split fraction is defined as the ratio of the amount of CO_2 in the hydrate phase and the feed gas mixture, indicating the capability of CO_2 capture with hydrate formation; the separation factor is defined as a ratio of the relative amount of CO_2 and the second gas component in the hydrate phase and gas phase after hydrate formation, indicating the capability of separating CO_2 from the other gas component. Furthermore, low formation pressures and high formation rates are essential to facilitate a HBSP for CO_2 capture at industrial scales.

Kim *et al.* investigated the effect of three typical types of thermodynamic hydrate promoters on CO_2 capture from a simulated flue gas that was composed of 20 mol% CO_2 and 80 mol% N_2, including THF (soluble in water, sII clathrate former), CP (insoluble in water, sII clathrate former), and TBAC (water-soluble, semiclathrate former).[1362] They set the experiments at the same pressure (3.1 MPa) and the same degree of subcooling (5.0 K) in the presence of the same volume of the aqueous phase. For 1.0 mol% of each promoter, the TBAC hydrate had the highest CO_2 concentration in the hydrate phase and the highest CO_2 split fraction. This is attributed to the fact that THF molecules and CP molecules will form structure II hydrates and occupy a certain portion of the large cages ($5^{12}6^4$) while CO_2 molecules also prefer the large cages. This competition considerably reduces the availability of the large cages for CO_2 molecules.[1369] Hashimoto *et al.* reported dependence of CO_2 selectivity on semiclathrate hydrate structures of TBAB, TBAC, TBPB and TBPC for a gas mixture of 15 mol% CO_2 and 85 mol% N_2. Their results showed that as the initial pressure increases, the gas uptake in the hydrate phase linearly increases and the mole fraction of CO_2 in the hydrate phase does not change much for TBAC, TBPB and TBPC. The CO_2 fraction irregularly responds to the increase in the initial pressure at 1 MPa. Given that, the TBAC has the lowest gas uptake and the highest CO_2 fraction in its hydrate phase, which was also reported for CO_2–CH_4 gas mixtures (*i.e.* fuel gas),[1370] it is a plausible explanation that the orthorhombic structure of the TBPB and TBPC hydrates has the largest gas capacity,[54] the tetragonal structure of the TBAC hydrates has the highest selectivity for CO_2, and the TBAB hydrates with both orthorhombic and tetragonal hydrate structures show the highest gas capacity and high selectivity for CO_2 capture. Rodriguez *et al.* recently reported that the separation factor of TBAB hydrates depends slightly on the cooling rate and strongly on the types of TBAB hydrates.[1371]

The CO_2 split fraction and separation factor are relative to a number of parameters such as the composition of feed gases, the concentration of the chemical additive, and the driving force (*i.e.*, the difference in the temperature and pressure between the experimental conditions and the hydrate equilibrium conditions). The CO_2 split fraction also strongly depends on the ratio of the feed gas to the aqueous solution. As a typical example, both CO_2 split fraction and separation factor are much higher for a fuel gas containing 40 mol% CO_2 and 60 mol% H_2 than for a flue gas containing 15 mol% CO_2 and 85 mol% N_2. This can be understood given that there is a much higher CO_2 content in the fuel gas and H_2 molecules require a significantly higher pressure to stay in the hydrate cages compared to N_2 molecules in the flue gas.[1360] Moreover, the presence of thermodynamic promotion additives usually reduces the separation factor and split fraction for fuel gases but not for flue gases.[1348]

6.1.2.2. Kinetic promoters. Some surfactants in the aqueous phase can act as kinetic promoters to shorten the induction time and promote hydrate growth,[776] while some other surfactants are used to prevent gas hydrate agglomeration for flow assurance (Section 4.1.3) and control of hydrate morphology (Section 3.1.4). There are three types of surfactants including anionic, cationic, and non-ionic surfactant. Experimental studies showed that anionic surfactants such as SDS, sodium tetradecyl sulfate (STS) and sodium hexadecyl sulfate (SHS)[871] are the most effective kinetic promoters[692,1372] when compared to non-ionic and cationic surfactants such as Tween-40, Twenn-80, DTACl[875] and amino acids.[1373,1374] The molecules of such a surfactant have a hydrophilic head and a lipophilic (hydrophobic) end that are amphiphilic to both polar and nonpolar substances. At a concentration above the critical micellar concentration,[686,1375] the molecules of a hydrate former form some kind of molecular clusters with the surfactant molecules through the hydrophobic interactions. Raman spectra indicate that these molecular clusters may have a structure similar to the hydrate cages.[1376] The presence of surfactants also enhances dissolution of hydrate forming gases in water, supplying gas molecules for fast hydrate growth. These enable hydrate structures to form more easily and faster and thus reduce the induction time. Furthermore, surfactants reduce the interfacial tension between the surfaces of hydrate crystals and water, resulting in a significant influence on the hydrate morphology. Lo *et al.* investigated the adsorption of SDS on CP hydrates and THF hydrates by measurement of zeta potential and pyrene fluorescence. As schematically illustrated in Fig. 22, the dissociated DS^- anions adsorb on the CP hydrate surface and then the electrostatic repulsion forces push the hydrate particles apart from each other.[686,1375] As a result, the SDS adsorption leads to the formation of small hydrate particles and hence good contact between gas and water, promoting the kinetics of gas hydrate formation.

Zhang *et al.*[1377] studied the effect of SDS on the kinetics of hydrate formation for CO_2–CH_4 mixtures simulating biogas in a glass bead pack at 274.2 K and 6 MPa with 288 ppm of SDS in water. Their results showed that 288 ppm of SDS in water promoted hydrate formation for CO_2–CH_4 mixtures and the presence of CO_2 deteriorated the promotion performance of SDS because of the competing adsorption of the HCO_3^- and SD^- at the surface of the hydrate crystals. It was reported that,

Open Access Article. Published on 22 Junie 2020. Downloaded on 2026-02-11 12:42:38 nm..
This article is licensed under a Creative Commons Attribution-NonCommercial 3.0 Unported Licence.

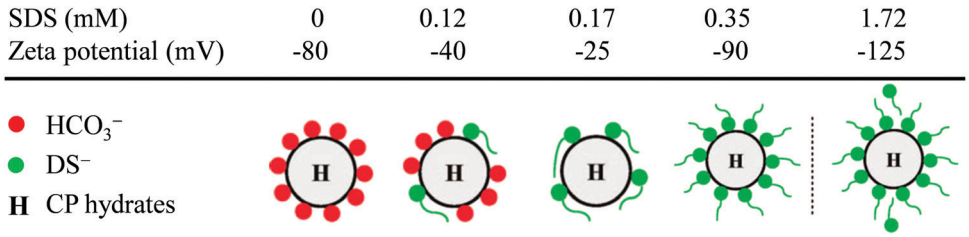

Fig. 22 SDS adsorption at the interface between CP hydrates and water. It was assumed that the bicarbonate anions (HCO_3^-) came from dissolved CO_2 from air. A monolayer of DS^- is completed at 0.17 mM of SDS, at which the induction time sharply decreased (adapted with permission from Lo *et al.*,[1375] Copyright 2008 American Chemical Society).

for a biogas with 40% CO_2 and 60% CH_4, the presence of SDS reduces the separation factor and the addition of some ligin derivatives improves the CO_2 separation.[1378,1379] It was recently found that for ternary gas mixtures of CO_2, CH_4 and N_2, SDS provided a much stronger promotion of CO_2 hydrate formation, compared to CH_4 and N_2.[1377] Ricaurte *et al.* also found that mixing 3000 ppm of SDS with 4.0 wt% of THF significantly improved both the split separation and separation factor for a gas mixture of 75 mol% CO_2 and 25 mol% CH_4 at a target temperature of 275 K and a load pressure of 4.0 MP.[1380]

The kinetics of hydrate formation can also be improved in some physical materials by increasing the hydrate forming gas–water contact area and enhancing the heat transfer process during hydrate formation,[899] more details of which can be found in Section 3.5. The materials that were investigated for CO_2 capture include silica sand,[1108,1381] silica gels,[1382,1383] foams,[1384] nanoparticles,[1385,1386] and hydroquinone hydrate-bearing porous particles.[1387] Additionally materials were experimentally tested for storage of methane and hydrogen as clathrate hydrates, such as nano-hollow silica,[1388] metal foams,[1389] emulsions,[1138] hydrogel,[1390] dry water,[951,1391] and porous carbon in nanotubes.[854,1392] Li *et al.* found that the addition of nano-Al_2O_3 particles in TBAB significantly improved the hydrate formation process for a syngas with 39.8 mol% CO_2 and 60.2 mol% H_2.[1393] A graphene–SO_3^-–Ag nanoparticle material was also found to be a few times more efficient than SDS to promote CO_2 hydrate formation.[1394] A comparison of silica sand, polyurethane foam, silica gel, and stirred reactors indicated that silica sand leads to the highest hydrate conversion rate in 120 minutes at 274.2 K and 6.0 MPa for a gas mixture with 38.1 mol% CO_2, 59.4 mol% hydrogen, and 2.5 mol% propane.[1348]

6.1.3. Effect of impurities in CO_2 streams. CO_2 captured from combustion at power plants always contains impurities such as N_2, O_2, CH_4, Ar (argon), H_2, SO_2 (sulfur dioxide), H_2S (hydrogen sulfide), NO_x (nitrogen oxides), *etc.* in addition to H_2O (water vapour) depending on the capture technologies as well as the types of fuel.[1395] In terms of gas hydrate-based CO_2 capture the presence of these impurities in the captured CO_2 may shift the thermodynamic equilibrium conditions of CO_2 hydrate formation, alter some thermodynamic properties of the CO_2 stream, and reduce the storage capacity of CO_2.

Thermodynamic modelling and molecular dynamic simulation show that, among these impure components, SO_2 and H_2S are stronger hydrate formers and more stable in clathrate structures than CO_2.[1396–1398] Experimental results using conventional autoclaves[1399–1401] and Raman spectroscopy[1402] confirmed the model prediction of the hydrate phase equilibrium. For the other impure components that are less stable in clathrate structures, the presence of these impurities leads to a shift of the phase boundary of CO_2 hydrate toward higher pressure and lower temperature before the appearance of liquid CO_2, as shown in Fig. 23.[1403,1404] Equilibrium and non-equilibrium thermodynamic modelling suggests that H_2S not only shifts CO_2 hydrate formation conditions but also improves the kinetics

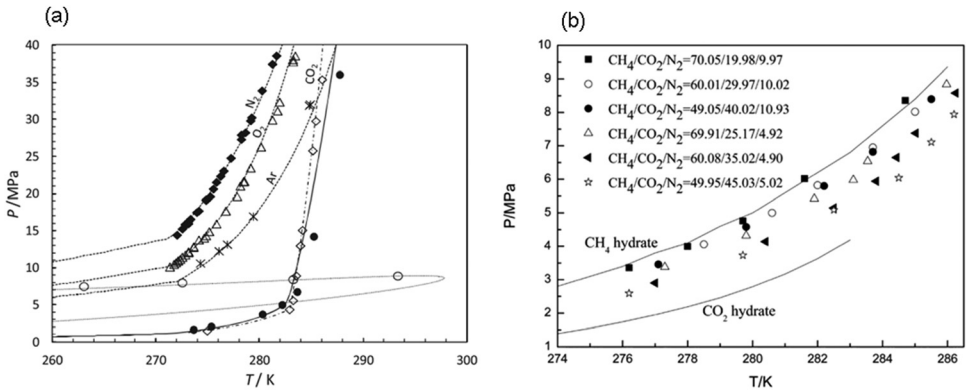

Fig. 23 Effect of common impurities on the phase equilibrium of CO_2 hydrate. (a) ● (○ phase envelope) CO_2 with 5.05 mol% O_2, 2.05 mol% Ar and 3.07 mol% N_2; ◊ pure CO_2; ♦ pure N_2; △ pure O_2; * pure Ar; ○ (adapted with permission from Chapoy *et al.*,[1403] Copyright 2013 Elsevier Ltd). (b) CH_4–CO_2–N_2 mixtures (adapted with permission from Zang *et al.*,[1404] Copyright 2018 American Chemical Society).

Open Access Article. Published on 22 Junie 2020. Downloaded on 2026-02-11 12:42:38 nm..
This article is licensed under a Creative Commons Attribution-NonCommercial 3.0 Unported Licence.

of CO_2 hydrate growth due to its high solubility in water, while CH_4, Ar and N_2 that are not very soluble in water do not measurably affect the kinetics of CO_2 hydrate formation.[1405] Similar experimental results were reported for a synthetic flue gas with 1 mol% of SO_2.[1399]

Chapoy *et al.* experimentally investigated the effect of thermodynamic properties of CO_2-rich systems containing impurities such as O_2, N_2 and Ar. Their results showed that the presence of 5.05 mol% O_2, 2.05 mol% Ar and 3.07 mol% N_2 in the CO_2-rich system results in a water content 10–30% less and a density 35% lower compared to that of pure CO_2.[1403] Lang and Servio measured the solubility of CO_2–N_2 gas mixtures under hydrate–liquid–vapour equilibrium and found that CO_2 solubility decreases and N_2 solubility increases when the system pressure increases at a constant temperature.[1406] More recently, Hassanpouryouzband *et al.* measured solubility parameters for various molar combinations of CO_2–N_2 mixtures over wide range of pressures, temperatures, and water salinities. The authors then used the measured data to calibrate available thermodynamic models.[1407]

Burnol *et al.* conducted a sensitivity analysis of the capacity of CO_2 storage in the deep saline aquifers of the Paris Basin.[1408] Their results indicated that a few molar percent of N_2 or/and CH_4 in the simulated CO_2 streams leads to one order of magnitude reduction in the storage capacity of CO_2, which was attributed to the effect of N_2 and CH_4 on the negative buoyancy zone and the gas hydrate stability zone. The negative change in the Gibbs free energy calculated from molecular dynamics suggested that SO_2 molecules have higher tendency to occupy the large cages in structure I hydrate that are preferred by CO_2 molecules, while H_2S molecules will compete with CO_2 molecules for the small cages,[1397] which was observed using Raman spectroscopy.[1402] As a result, a high concentration of these impure components present in the CO_2 stream will also reduce the amount of CO_2 in the hydrate phase and in turn the storage capacity of CO_2 as gas hydrates.

6.2. CO_2 storage

6.2.1. Hydrate storage of CO_2. Geological storage of CO_2 has been considered as one of the most feasible options to reduce the greenhouse gas emission into atmosphere.[1409–1412] Potential candidates for geological storage include deep saline aquifers, depleted oil and gas reservoirs, and coalbeds.[1409] If the temperature and pressure in a geologic formation is suitable, the injected CO_2 can be converted into gas hydrate.[1413,1414] CO_2 hydrate as a solid has a much lower mobility than gas, liquid, or supercritical CO_2, and one cubic meter of CO_2 hydrate can store up to 162 m^3 of CO_2 gas at standard conditions. However, the formation of CO_2 hydrate will significantly reduce the permeability of the geologic formation by filling the pore space or clogging the pore throats of the sediments,[441,525,1415–1417] but, the presence of CO_2 hydrate can also enhance the mechanical strength of the sediments.[1418,1419]

Hydrate storage of CO_2 has been studied through theoretical simulations and laboratory experiments, mainly focused on the feasibility of CO_2 storage as hydrate in depleted oil and gas reservoirs. This is because their geological characteristics are well known, the desired seal integrity is proven, and the necessary infrastructures are already in place. Reservoir simulations show that a number of depleted gas reservoirs in Northern Alberta (Canada) are suitable for CO_2 hydrate formation and that the storage capacity will be influenced by the initial reservoir conditions including pressure, temperature and porosity, the residual hydrocarbon gas, temperature rise due to heat release from the exothermic reaction of CO_2 hydrate formation, and the operational conditions of CO_2 injection such as injection rate and pressure.[1420,1421] Experimental measurements of the interfacial tension between CO_2 hydrate and water is 18 times smaller than that between ice and water.[1422] The low interfacial tension allows porous media and other foreign particles to help the adsorption of CO_2 molecules on hydrate crystals, and thus to promote CO_2 hydrate nucleation and formation kinetics,[904,1423–1425] which is also in agreement with the outcome of molecular dynamic simulations.[1426] The presence of salts in pore water enhances CO_2 hydrate nucleation but leads to less CO_2 hydrate formation.[904,1424,1425,1427] Englezos and his colleagues carried out a series of experiments using different injection methods to simulate *in situ* process of CO_2 injection into depleted gas and oil reservoirs in Northern Alberta (Canada), such as vertical injection,[1428] horizontal injection,[1429] and two spiral tubes at both top and bottom of the simulated sediments.[1430] They concluded that the storage of CO_2 as gas hydrate in depleted oil or gas reservoirs is feasible in terms of both hydrate formation kinetics and the storage capacity.[1431] More recently, the formation of flue gas hydrate (CO_2 + N_2) in permafrost regions and marine sediments is been suggested as an option for CO_2 storage and secondary sealing of hydrate reservoirs.[1351] It was found that more than 92% of the CO_2 present in the injection gas could be stored at certain conditions. In addition, the presence of N_2 in the injection phase increases the safety of storage in case of a temperature rise, as N_2 releases first with continued retention of CO_2 in the hydrate phase.[1351]

6.2.2. CO_2 capture and storage in methane hydrate reservoirs. Experimental measurement of hydrate phase equilibria and theoretical calculation of Gibbs free energy showed that CO_2 molecules have a relatively high tendency to replace the methane molecules from the methane hydrate cages.[1432–1435] This provides a promising option for CO_2 storage as solid hydrates in sediments and simultaneous methane recovery from gas hydrate reservoirs, potentially making geological storage of CO_2 and methane recovery from gas hydrate economically viable. Additionally, the formation of CO_2 hydrate or CO_2 mixed hydrates through the displacement process can avoid damage to the geomechanical stability of the formation of methane hydrate reservoirs during methane recovery.[1418,1419] In principle, the process of CO_2 displacement could be fast and efficient at suitable heat and mass transfer conditions. For example, it was observed using magnetic resonance imaging that nearly all methane in a methane hydrate was replaced by CO_2 in two half cylindrical sand-stone cores separated with a purpose-made spacer.[1436,1437] How much methane originally in

Open Access Article. Published on 22 Junie 2020. Downloaded on 2026-02-11 12:42:38 nm..
This article is licensed under a Creative Commons Attribution-NonCommercial 3.0 Unported Licence.

the methane hydrate can be replaced by CO_2 depends on the experimental conditions such as temperature and pressure, CO_2 gas or liquid CO_2, and the porous media used.[1438–1440] Raman spectroscopy analysis showed that CO_2 molecules prefer to replace the methane molecules in the large cages ($5^{12}6^2$), leading to faster decomposition of the large cages compared to the small cages (5^{12}).[1441,1442] Molecular simulations confirmed the characteristics of hydrate cavity occupancy.[747,1443] Monte Carlo simulation suggested that the CO_2 occupancy of the large cages reduces and the methane occupancy of the small cages increases as the methane concentration in the gas phase increases, while very limited CO_2 gets into the small cages.[1444] Experimental work was also conducted for structures II and H hydrates, confirming occurrence of CO_2 replacement leading to hydrate structure transition.[1445–1447] It was also observed, that the exchange of CH_4 or other hydrocarbons with CO_2 is a reversible process.[1448]

In sediments the CO_2 replacement process is constrained by heat and mass transfer due to fine pores and secondary hydrate formation. Experimental studies showed that the presence of excess water and clays resulted in slow CO_2–CH_4 exchange rate[1449] and that formation of CO_2 hydrate crusts wrapping on the methane hydrate crystals can act as a barrier to prevent CO_2 molecule from diffusing into the methane hydrate crystals.[1440,1450,1451] Thermal stimulation can destabilize methane hydrates and thus enhance the process of CO_2 replacement reaction.[1452–1454] It was reported that the injection of CO_2–N_2 mixtures, compressed air, or flue gas can enhance methane recovery from methane hydrate because the N_2 molecules help to move some of the methane molecules out of the small cages, while CO_2 molecules replace the methane molecules in the large cages,[1455–1457] and was confirmed by thermodynamic modelling.[1458] Cha *et al.* measured the composition of the methane hydrate by ^{13}C nuclear magnetic resonance analysis and found that the methane composition formula changed from (1.6S)·(6.0L)·46H_2O and (1.0S)·(4.1L)·46H_2O before and after contact with a gas mixture of 20 mol% CO_2 and 80 mol% N_2 at 273 K and 10 MPa, respectively.[4] The first field trial of the CO_2 replacement technique was successfully completed in the North Slope of Alaska.[1459] 77% N_2 was added to the CO_2 stream to prevent secondary hydrate formation and promote CO_2–CH_4 replacement. After about 6 weeks of gas production, about 54% of the injected CO_2 was stored underground and more than 50% of the produced methane was retained in the hydrate reservoir until the well pressure was further reduced below the methane hydrate dissociation pressure.

Direct injection of flue gas into methane hydrate-bearing sediments was experimentally investigated to reduce the cost of CO_2 capture.[81,1407,1460,1461] The nitrogen present in the injected flue gas shifted the hydrate equilibrium conditions, leading to decomposition of a large portion of the methane hydrate. The CO_2 can the form CO_2 hydrate or CO_2–CH_4 or CO_2–CH_4–N_2 hydrates from the dissociated methane hydrate or by CO_2 replacement in the methane hydrate-bearing sediments.[1462,1463] It was further reported that 81.9% CO_2 present in the injected flue gas was captured and stored in methane hydrate-bearing frozen sediments at 261.2 K.[81] Fig. 24 illustrates the principal mechanism of the flue gas injection method.

There is not a clear picture how CO_2 molecules replace the methane molecules that are entrapped in the methane hydrate. Early molecular dynamic simulations indicated that methane hydrate dissociates first after contacting with CO_2 and then reform CO_2 hydrate or CO_2-mixed hydrates,[1443,1464] while some simulation work suggested that direct swapping of methane and CO_2 molecules or a transient co-occupation of one hydrate cage could occur in the outer lay next to the hydrate surface, which is buffered by the fluctuation of water molecules.[1465] The recent molecular dynamic simulation by Wu *et al.* suggested that adsorption of CO_2 molecules on methane hydrate surfaces can help to stabilize the methane hydrate and that both direct swapping and co-growth of CO_2-mixed hydrates could occur

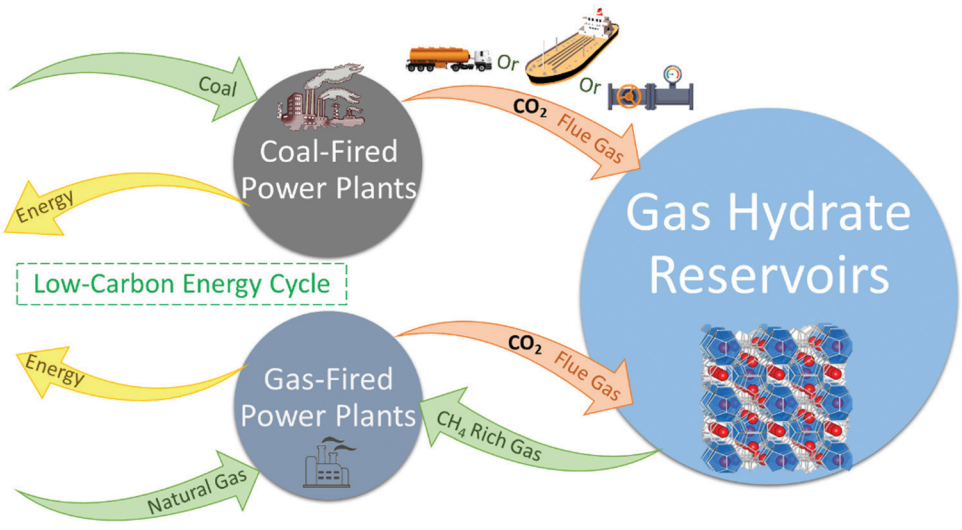

Fig. 24 Illustration of the principal mechanism of the direct injection of flue gas for methane recovery from gas hydrate reservoirs and CO_2 capture and storage simultaneously (adapted with permission from Hassanpouryouzband *et al.*,[81] Copyright 2019 Springer Nature).

Open Access Article. Published on 22 Junie 2020. Downloaded on 2026-02-11 12:42:38 nm..
This article is licensed under a Creative Commons Attribution-NonCommercial 3.0 Unported Licence.

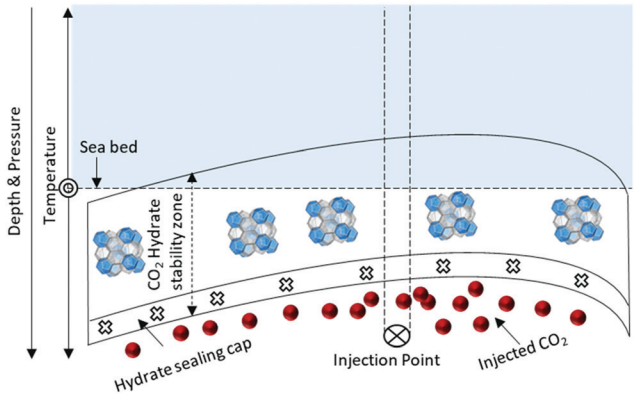

Fig. 25 Schematic diagram of the CO_2 self-sealing mechanism.

during a CO_2 replacement process.[1466] However, most of the experiments showed that methane hydrate dissociation was not observed using a range of different methods including magnetic resonance imaging,[1436,1437] differential scanning calorimeter,[1467] electrical resistance.[1451] In contrast, observations using *in situ* Raman spectroscopy found that free water phase appeared during CO_2 replacement.[1450] The physical models of CO_2–CH_4 molecular exchange were developed based on an assumption of a solid-to-solid transition process.[1468,1469]

6.2.3. Self-sealing of CO_2 hydrate. Caprock integrity is essential to retain CO_2 safely over hundreds or thousands of years for geologic storage of CO_2.[1470,1471] Based on the fact that CO_2 hydrate formation can fill or block the pores in sediments, a self-sealing mechanism was proposed to improve the integrity of the cap layer of a storage formation,[1472] as shown in Fig. 25. A geological review indicated that storage of CO_2 in cool sedimentary formations could offer certain advantages in terms of physical, chemical and mineralogical processes to avoid or reduce CO_2 escape.[1473] Geological mapping showed the worldwide distribution and thickness of self-sealing marine sedimentary strata that are capable of storing between 1260–28 500 gigatonnes of CO_2, or about 40–1000 years of total global CO_2 emissions, depending on the *in situ* density of CO_2, sediment porosity, and sweep efficiency.[1474,1475] Tohidi *et al.* conducted several time-lasting experiments demonstrating that the upward migrating CO_2 tends to form hydrates at the base of the hydrate stability zone and that the CO_2 hydrate formation process and the formed CO_2 hydrate layer slowed down the CO_2 diffusion rate by several times to 3 orders of magnitude.[1476] In addition to CO_2 hydrate formation, molecular dynamic simulations suggested that intercalation of CO_2 within smectite minerals in brine aquifers can induce clay swelling to restrict CO_2 migration.[1477] The recent experimental results from The University of Bergen showed that a self-sealing layer could form in hours with injection of CO_2 into cool aquifers and that the formation of the CO_2 hydrate seal strongly depends on the rock properties.[1416,1478]

6.3. Transport of CO_2

Gas hydrate slurries (*i.e.*, mixtures of CO_2 hydrate and water) were initially proposed as an alternative to liquefied natural gas to reduce the cost of natural gas transport for long distances.[1479,1480] It was further developed and investigated as a cold flow technology to prevent hydrate blockage in hydrocarbon transport pipelines.[626,1481,1482] Further developments in the cold flow technology are reviewed in Section 7.2. The feasibility of CO_2 hydrate slurries for CO_2 transport was investigated recently.[1483,1484] The main advantage of this concept is that it is expected to reduce the energy required for compression or liquefaction because the CO_2 hydrate can be produced through the gas hydrate-based separation process. Similar to the transport of natural gas as solid hydrates,[1485] CO_2 hydrate can be made into pellets and transported using trucks or ships.[332] The self-preservation and stability at relatively low pressures of CO_2 hydrates make it feasible to carry the CO_2 hydrate pellets for long distance using existing cargo ships that can provide chilled tanks at 1.5–2 MPa and around 243 K.[814,1486] However, it should be noted that the transport of CO_2 as hydrate forms is still a new concept in its early development stage.

6.4. Further development toward large-scale deployments

In the past decades extensive experimental studies have successfully led to significant reductions in the hydrate formation temperature and pressure for CO_2 separation from flue gas, syngas and fuel gas. Meanwhile, a variety of thermodynamic models, molecular dynamic models, and other physical models have been developed to describe the separation phenomena and processes. The results of lab-based research have demonstrated that gas hydrate-based CO_2 capture technology is an energy efficient, environmentally friendly, and simple process compared to the other conventional technologies.[1346,1359,1487] So far no industrial usage of gas hydrate-based CO_2 capture technology has been reported. Therefore, further development is expected to be directed toward trials and implementation of large-scale deployments, such as the study of suitability and performance of combined thermodynamic and kinetic promoters and the design and optimisation of continuous separation processes,[1487,1488] hybrid processes,[1489] and integration with renewable energy (*e.g.*, solar energy).[1490] For transport of CO_2 in the form of CO_2 hydrate, there is still lack of fundamental understanding of the characteristics and rheological properties of CO_2 hydrate slurries. For geological storage of CO_2 as hydrates, systematic investigation is needed to provide a better understanding of the effect of CO_2 hydrate formation on the integrity of CO_2 injection wells, and the geomechanical, geophysical and geothermal properties of the storage formations.[1491–1493] After the first field trial of the CO_2 replacement method in the North Slope of Alaska,[1459] more scientific test trials are ultimately demanded to undertake *in situ* evaluations of the different approaches that have proved feasible in lab experiments, for example, the CO_2 replacement method and flue gas injection method. Moreover, comprehensive economic assessments of an entire chain of the hydrate-based CO_2 capture and storage process are needed to provide the policymakers and the CCS industry with sufficient confidence for large-scale deployments of hydrate-based CCS technologies.

Open Access Article. Published on 22 Junie 2020. Downloaded on 2026-02-11 12:42:38 nm..
This article is licensed under a Creative Commons Attribution-NonCommercial 3.0 Unported Licence.

7. Other industries

7.1. Gas storage

7.1.1. Hydrogen. To overcome the limitations of intermittent clean and renewable energies (*e.g.*, wind, solar, tidal, geothermal, and *etc.*) influenced by weather, uneven distribution, and mismatch in output and demand; energy storage technologies emerged.[1494] In this regards, hydrogen has been considered as an energy carrier as it can be produced by renewable sources (*e.g.*, gasification of biomass and electrolysis of water using solar energy and wind energy) as well as stream forming of natural gas[1495] and can be used across all the energy vectors. Various approaches for hydrogen storage are being considered, including compression, liquefaction, physical adsorption, chemical absorption and carbon nanotubes, and underground gas storage.[1496] An overview of the various hydrogen storage methods with their pros and cons can be found in other reviews.[1497–1503] Of particular interest is hydrogen storage in molecular clathrates (see Fig. 26) which are cost-effective, safe, and environmentally friendly. During the past decades, hydrate-based hydrogen storage has undergone substantial advances in development and attracted significant interest due to their favourable chemical and physical features and promising applications in the energy sectors. To date, several reviews[1497,1504–1508] have discussed the details of these approaches. Here, we cover the most recent advancements and summarize the challenges in moving forward for hydrate-based hydrogen storage.

Considering the molecular diameter of hydrogen, in the past it was considered too small to stabilize the water framework either as a single guest or in a gas mixture. However, after several successive reports about H_2 hydrate formation,[47,1318] and H_2–THF hydrate formation[1509] at extreme *P*–*T* conditions, interest in the potential of this field increased. Since then, numerous studies[1510,1511] have characterized binary H_2 hydrates at different condition as sII clathrates, having a maximum reported[1512] storage capacity of 11.2 wt% at 500 MPa and 77 K. These forms of storage are not suitable for widespread commercial application as there are significant energy costs in storing and transporting sII hydrogen clathrates. The research developed to add THF[859] to form hydrogen-THF clathrates at low pressures with around 1 wt% H_2. Following that, a study[1513] claimed that it is possible to store hydrogen up to around 4 wt% at low pressures by "tuning THF contents". In response, several studies[1514,1515] challenged the capacities reported in the previous study, claiming the maximum storage of hydrogen couldn't be more than 1 wt% in the investigated conditions. Although the maximum hydrogen capacity is a matter of conflict, the success of the tuning effect for mixed guest hydrates was developed and reported in later studies.[1516,1517] THF is a volatile organic compound and contamination of hydrogen after dissociation with these compounds would be harmful to fuel cells or turbines. To circumvent this problem, it is been suggested to store hydrogen in semi-clathrates of quaternary ammonium compounds with a maximum reported storage capacity of

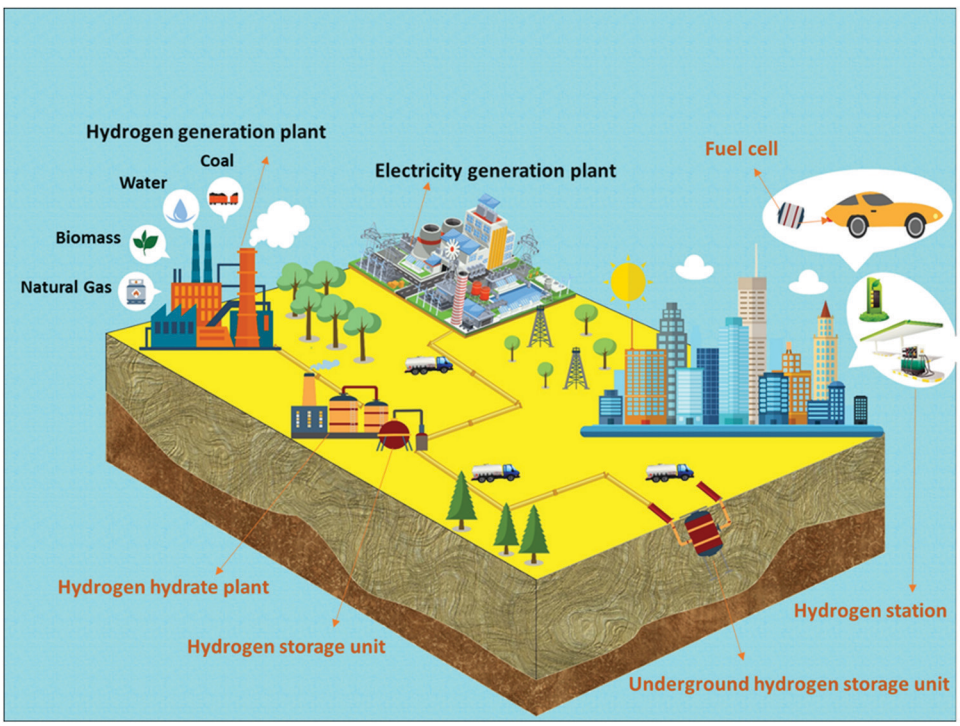

Fig. 26 A graphical illustration of an entire clathrate hydrate-based hydrogen storage system that consists of three parts: hydrate synthetic plant, storage unit, and release unit in addition to transportation facilities. Hydrogen gas from a hydrogen production plant is converted into hydrogen hydrate at a hydrate plant. The hydrogen hydrate can be in a form of transportable slurries through pipelines. The hydrate slurries are then transported to a storage unit such as storage tanks or underground silos.

 This journal is © The Royal Society of Chemistry 2020

Open Access Article. Published on 22 Junie 2020. Downloaded on 2026-02-11 12:42:38 nm..
This article is licensed under a Creative Commons Attribution-NonCommercial 3.0 Unported Licence.

about 1 wt% H_2.[51] In addition to the different studies on THF-mixed[1518–1520] hydrates, quaternary ammonium-mixed hydrates,[866,1521,1522] or other sII promoters-mixed (*e.g.* cyclopentane,[1523] cyclohexanone,[1524] furan and tetrahydrothiophene[1525]) hydrates, attempts been made to use other promoters for storing hydrogen in different structures such as sH,[1526] alkylamine hydrates,[63] and *etc.*[1505,1508] However, all of the above-mentioned promoters suffer from lower hydrogen storage capacity when compared to pure hydrogen hydrates, as the promoters occupy major[1527] fractions of the large cavities, reducing the hydrogen occupancy in the hydrate phase.

The kinetics of hydrogen hydrate formation and dissociation is another parameter that plays a crucial role in the commercialization potential of clathrate based hydrogen storage. The time required for the formation of hydrogen hydrate could be in the order of a day, resulting in an extreme energy penalty for keeping the system at low temperatures and high pressures for that duration. Therefore, methods for increasing the rate of hydrogen hydrate formation have been widely studied and include formation of hydrate from reactive forms of ice[1528] or quenching the seeds of clathrates in the system.[1529] More recently, it is been suggested to mix hydrogen with natural gas components, mainly, methane,[1530–1533] and propane[1534,1535] to enhance the formation kinetics. Here methane and propane could serve a dual purpose, *i.e.* as they will be used as a promoter to form hydrogen hydrate at lower pressures and also, they could be burnt to produce energy, increasing the energy density of the clathrates.

The research into the application of clathrate hydrates in hydrogen storage has experienced a remarkable growth in the last few years. Several milestones have been achieved: the storage of hydrogen at low pressures, the increase of hydrogen hydrate formation rate, and strategies to improve the capacity of hydrogen storage. Important efforts are also being driven toward improving the understanding of the physical properties of hydrogen inside clathrates.[1536–1538] These advances envisage a promising future for hydrate-based hydrogen storage, yet important limitations must be addressed. The capacity of hydrogen storage needs to be further increased under moderate conditions to ensure progress. The kinetics of hydrate formation and dissociation required to be further improved to make the hydrate-based technologies competitive with other energy storage sectors. Reaching a few seconds time-scale for formation could be the next milestone for kinetics improvement. Full chain economic analysis for this method is also missing in the literature. The future of the field will not only depend on how the scientists circumvent the mentioned and forthcoming problems but also on how they tackle the technical challenges experienced in the other hydrogen storage methods.

7.1.2. Solidified natural gas. Another substitute for petroleum as the world's dominant fuel is natural gas, which has the highest[1539,1540] H to C ratio among fossil fuels and lower sulphur and nitrogen contents, resulting in less carbon, SO_x and NO_x emissions.[1541] Accordingly, development of different methods for natural gas storage and transportation has gained significant momentum in recent years. Various methods have been identified as potential ways to store natural gas including but not limited to, compressed natural gas (CNG), liquefied natural gas (LNG), adsorbed natural gas (ANG),[1542] and *etc.*[1543] Among the additional natural gas storage methods, gas-hydrate based storage or "solidified natural gas (SNG)" is one of the most comprehensively studied methods. This approach offers several advantages over other approaches including lower energy requirements (in most cases), reduced environmental hazards, up to near 100% recovery, and higher safety.[1544,1545] Nevertheless, the volumetric energy density of SNG is far less than LNG (being known as the most applied approach) but it is competitive with other methods. However, the high cost of the requirement for cryogenic cooling and handling a cryogenic fuel for LNG has paved the way for the development of other methods.[1546] Hydrate-based technologies have the potential to reduce cost and match or surpass the typical capacities of physical storage systems.[1485,1547]

After proposing the possibility of natural gas storage in hydrates,[1548] similar to that of hydrogen storage, development of natural gas storage in hydrates has followed the same pathways. Numerous works have been done on characterizing methane (as the major component of natural gas) hydrates,[767,1549–1551] followed by attempts for moderating the formation *P–T* conditions and increasing the storage capacity of clathrates such as using Ice powder,[1552,1553] THF,[1554–1556] semi clathrates,[1557,1558] and *etc.*[1559] Various methods[890,1560–1566] have also been applied to increase the kinetics of natural gas/methane hydrate formation. The formation pressure of methane hydrate in comparison with hydrogen is significantly lower at similar temperatures, and even lower when mixed with other heavier natural gas components that is the main reason for further development of clathrate based natural gas storage. During the last decade, global research activity into natural gas storage in hydrates has increased to the point where several demonstration phase projects have been undertaken, such as the natural gas hydrates pellet reactor[814,1567] which didn't encounter any fundamental technical barriers and has led to several commercialization analysis report[812,1568] being published. A more detailed review and list of the patents in the commercialization pathway of this technology can be found in another review paper.[1485] As gas hydrate based natural gas storage approaches the commercial stages of development, some technical uncertainties remain, such as those related to gas capacity and the kinetics of hydrate formation and dissociation/energy recovery mainly due to limited heat transfer and self-preservation effect; however success of the demonstration projects provided experiences and practical data to push the technology forward to commercial stage.

7.1.3. Ozone. Ozone with the chemical formula of O_3, exists naturally in the stratosphere and protects the earth from ultraviolet light. Presence of Ozone at the ground level, however, is toxic and poses a hazard to living organisms.[1569] This allotrope of oxygen, is an effective oxidant[1570] and is applied widely throughout various industries including water and wastewater treatment,[1571] air purification,[1572] perishables,[1573] paper and pulp processing, and *etc.*[1574] Owing to the high reactivity or very short half-time of ozone molecules, they are now being generated at point of use, which is cost and energy intensive.[1575]

Open Access Article. Published on 22 Junie 2020. Downloaded on 2026-02-11 12:42:38 nm..
This article is licensed under a Creative Commons Attribution-NonCommercial 3.0 Unported Licence.

To solve this problem, Mcturk and Waller[1576] reported a method for continuous storage of O_3 in the form of molecular clathrates to isolate them, preserving the O_3 for a longer time. To reduce the hydrate formation pressure, they used carbon tetrachloride (CCl_4) as the ozone solvent and help guest due to its stability to Ozone. Nevertheless, they were unable to store O_3 in more than 30% of the small cages and the remaining small cages were left free. Hence, they suggested the use of ozone clathrates at higher pressures for a higher storage capacity. Following this, Vysokikh *et al.*,[1577] experimentally investigated the possibility of hydrate formation under the Earth's stratosphere conditions by forming hydrate with O_3-ice and O_3-hydrogen chloride. Subsequently Muromachi *et al.*,[1578] investigated the formation of O_3–O_2, and O_3–CCl_4 hydrates. The authors found that O_3 could be preserved for more than 20 days after hydrate formation under atmospheric pressure. These hydrates have three orders of magnitude more O_3 than a typical "ozonated water" and has been used for disinfection. Nakajima *et al.*[1579] investigated the formation hydrate from mixtures of $O_3 + O_2 + CO_2$ and concluded that the ozone could be preserved at atmospheric pressure for more than four weeks by forming clathrates of the mentioned mixture. These findings have sparked considerable interest in clathrate hydrates as potential ozone storage materials and many workers have assessed the formation of O_3 mixed hydrates,[1580–1585] in an attempt to increase the capacity of O_3 in the clathrates formed from the $O_3 + O_2 + CO_2$ mixture.[1586,1587] In 2018, Subbotin *et al.*[1588] studied the storage capacity of O_3 in $O_3 + O_2 + N_2 + CO_2$ mixed gas hydrates. They found that the storage capacity of such hydrates could be several times higher than $O_3 + O_2 + CO_2$ mixed hydrates, providing more favourable thermobaric conditions for O_3 storage. More recently, Watanabe *et al.*[1589] conducted a more detailed study on the kinetics of continuous $O_3 + O_2 + CO_2$ mixed hydrate formation by detailing the effect various influencing parameters on the storage capacity, kinetics of O_3 mixed hydrate formation, and O_3 decomposition to O_2 in the gas phase.

7.2. Cold energy storage

The need for reducing hydrofluorocarbons in refrigeration according to the Kyoto Protocol and Montreal Protocol[1590] has directed considerable efforts toward the development of more environmentally friendly refrigerants[1591–1593] and the construction of more efficient refrigerant systems as well as the wider applications of cost-effective cold storage systems which have been proposed as another solution for storing intermittent renewable energies.[1594,1595] Among different working media for cold storage systems such as water, ice, and eutectic salt gas hydrates are attractive and versatile because of their high temperature zone, suitable latent heat of fusion (more than Ice in CO_2 hydrate), and better heat transfer efficiency has and have been described and compared in detail in several reviews.[920,1596–1600] The conventional workflow for hydrate cold storage begins with the reduction of the system temperature to hydrate formation point, followed by exothermic hydrate formation that is the main cold storage part. Finally, stored cold energy could be consumed through endothermic hydrate dissociation either through depressurization, receiving heat from the environment (see Fig. 27), or a combination of both. Based on this, many lab-scale hydrate-based cold storage systems[1601,1602] have been developed including direct contact type, and indirect contact type, also known as secondary refrigeration, where the primary circuit (cold generation place) and secondary system (the place to be cooled) are physically separated and the generated cold is transferred by the fluid/phase change material (PCM)[1603] between two places.[920,1596,1604,1605] The longstanding interest in investigating the hydrate phase equilibria and their formation/dissociation kinetics due to their importance in different sectors, removes the initial barriers. The potential of using different hydrate formers such as CO_2,[1604,1606,1607] CH_4 and various refrigerants[1608–1613] or their combinations[1614–1618] (*e.g.* CO_2–THF,[1619,1620] and a refrigerant + methane[1621]/CO_2[1622]) as guest molecules in hydrate-based cold storage is well-demonstrated. Among different candidates, CO_2 or CO_2-mixed (additives such as THF to reduce formation pressure) has received greater attention due to the higher solubility of CO_2, higher latent heat of fusion,[1623] availability, lower environmental impact (if captured from CO_2 production industry) and moderate formation conditions. However, CO_2 is a corrosive gas and will cost extra for building and maintaining the CO_2-resistive cold storage systems.[1624] Therefore, choosing a suitable guest molecule/s for

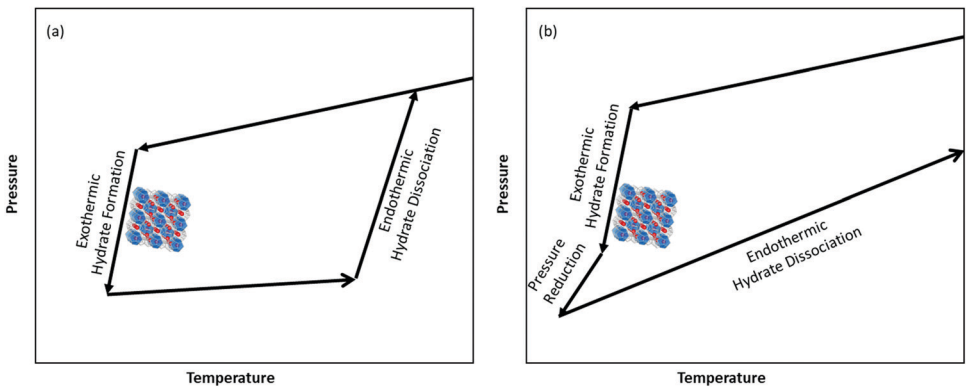

Fig. 27 Two modes of hydrate cold storage technology, namely heating (a) and (b) depressurising for cooling (based on Cheng *et al.*[920]).

Open Access Article. Published on 22 Junie 2020. Downloaded on 2026-02-11 12:42:38 nm..
This article is licensed under a Creative Commons Attribution-NonCommercial 3.0 Unported Licence.

hydrate-based cold storage is an ongoing topic. Following the choosing of a satisfactory guest molecule, characterizing hydrate formation/dissociation in the relevant environments[1151,1625,1626] and applying a suitable growth acceleration method, the principal understanding of hydrate slurries properties become important (see Section 2.6) and are the main step for all the hydrate-based applications. Since continued advancements in hydrate-based cold storage systems highly depend on the further improvement of the devices for efficient cold storage systems, concerns about the possibility of gas leakage and the energy penalty for gas compression could be significant. Another critical point we would like to highlight is that a detailed economic assessment for a large-scale hydrate-based cold storage method is required to reach the next milestone. It is expected that the research in this field will further develop by fusion of various fields such as process engineering and metallurgy. We hope that the remaining barriers for applying this technology will be removed in the near future.

7.3. Clathrate hydrate-based desalination

The escalating freshwater demand by the growing global population and industrial/agricultural activities is putting unprecedented pressure on the world's freshwater resources. The current pace of human population growth, industrialization, urbanization and the over-exploitation of the freshwater resources are contributing substantially to the global water scarcity.[1627,1628] To address the declining trend in global freshwater availability[1629] a radical rethink of the global water management strategies and policies is necessary to ensure human welfare,[1630] and ensure the long-term viability of the Earth's freshwater resources.[1631] Given the limited total usable freshwater supply, a variety of seawater desalination technologies have been developed over the last several decades to meet the rapid growth of the worldwide water demand and augment the supply of water, particularly in arid regions such as the Middle East.[1632] Desalination is the process of removing salt from seawater or brackish water to make it usable for drinking or irrigation.[1633] Traditional thermal-based, membrane-based and chemical-based desalination technologies, such as Multi-Stage Flashing (MSF), Multi-Effect Desalination (MED) and Reverse Osmosis (RO), are energy-intensive processes normally using fossil fuels, which in turn contribute to global warming.[1632,1634,1635] Given ice crystals are made up of essentially pure water, desalination technologies based on indirect and direct freezing were also introduced, yet are not widely applied commercially due to high costs.[1636] Thus, to make a real impact, innovative desalination technologies must be developed to secure safe sufficient clean water, while reducing the cost and energy use.[1637] The emerging desalination technologies for water treatment have been critically reviewed in the literature.[1633]

Clathrate hydrate-based desalination (see Fig. 28), classified as a freezing or crystallization approach, was proposed more than 70 years ago as a potential technology for the desalination of seawater.[1638] In this process, an electrolyte solution such as seawater or brackish water is contacted with a hydrate forming agent at a favourable P–T (which could be above the freezing point of water). The water molecules encage the hydrate former

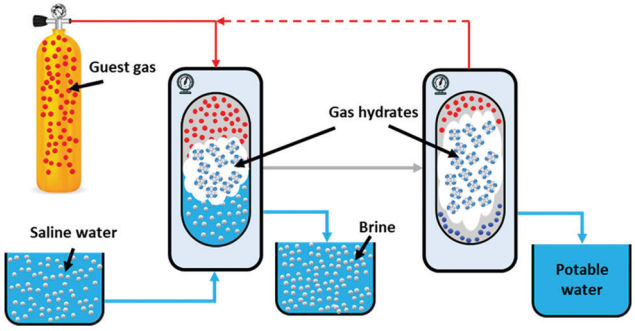

Fig. 28 Schematic diagram of the clathrate hydrate-based desalination process. Seawater is contacted with an appropriate hydrate former such as CO_2 at desired thermodynamic conditions to form clathrate hydrates while excluding salts from the crystalline structure. The hydrate crystal can then be removed from the brine and dissociated to drinking water and hydrate former which could be recycled.

molecules and form the clathrate hydrate, thereby salts and other impurities become excluded from the crystalline structure.[1639] The salt does not disturb the morphology of the hydrate crystal and acts as a thermodynamic inhibitor, shifting the hydrate phase equilibrium to a higher pressure at a given temperature and accordingly, reducing the driving force for the hydrate formation (see Sections 3.4.1 and 4.1.1). The hydrate crystal can then be mechanically separated and removed from the brine and decomposed to potable water and hydrate former which is then recovered and recycled.[1638] The volumetric efficiency of the process is represented by the water recovery, which is defined as the volume of freshwater recovered from the feed solution, and depends upon the kinetics of the hydrate formation and the volume of water converted to hydrates along with the recoverable amount of hydrate crystals at the separation step from brine.[1640] It must be noted that the eutectic composition of the feed solution constrains the maximum recoverable water. Another metric is salt rejection, which represents the efficiency of the salt removal in the process and is defined as the salt concentration evolution relative to its initial value.[1638]

The application of hydrates in the field of seawater desalination has been happening since the 1940s. Since then, a great deal of research has been carried out worldwide to find suitable hydrate formers considering the important factors of eco-friendliness, non-toxicity, stability, availability and economic viability.[1641] To date the application of a variety of hydrate forming agents such as propane (C_3H_8),[1642,1643] cyclopentane (C_5H_{10}),[1639,1644–1649] carbon dioxide (CO_2),[900,1107,1650,1651] refrigerant gases (HFC, HCFC and CFC)[1652–1655] and sulphur hexafluoride (SF_6)[1656] have been applied to the hydrate-based desalination process. Numerous studies and pilot plant scale tests have also been conducted to determine phase equilibrium[975,1657–1662] and evaluate/improve the kinetics or alleviate the temperature requirements for hydrate formation (*e.g.* by using secondary hydrate guest gases).[1663–1669] Given the main hindrance for the early commercialization of hydrate-based desalination was the challenges associated with the

Open Access Article. Published on 22 Junie 2020. Downloaded on 2026-02-11 12:42:38 nm..
This article is licensed under a Creative Commons Attribution-NonCommercial 3.0 Unported Licence.

separation of the hydrate phase out of the brine, studies have been conducted to investigate the salt removal efficiency and enhance it *via* secondary treatment processes after hydrate formation.[1670–1677] Moreover, there have been a number of inventions focused on crystal separation from the saline water, salt removal from the hydrate slurry and reduction in induction time, a detailed review of which can be found elsewhere.[1638]

The criteria for a suitable hydrate former together with other technical issues have made it challenging to propose a commercial hydrate-based desalination scheme. For instance, SF_6, CFC, HFC and HCFC have been found to be inappropriate as they have an adverse impact on ozone depletion even though they are atmospheric hydrate formers and alkanes and cycloalkanes are flammable fluids which pose safety issues at large-scale applications. Ethane and propane, however, have been proposed as favourable hydrate formers according to an integrated thermodynamic approach.[1641] Moreover, a comprehensive and systematic assessment conducted on cyclopentane revealed its viability as an atmospheric hydrate forming agent.[1649] Despite all the efforts and inventions developed attempting to commercialize the hydrate-based desalination process by addressing the technical challenges together with energy efficiency and environmental concerns, its application on a commercial scale has not yet been successful. Economic feasibility must be accounted for as the operation cost depends upon a variety of factors such as brine temperature, favourable thermodynamic conditions, salt content, mobility of salt and yield.[1678–1680] Therefore, there is still a need to develop eco-friendly and energy-efficient hydrate-based desalination methods that are viable to be deployed at the industrial scale.

Recently, an optimal design approach of the RO-hydrate hybrid system for seawater desalination was proposed.[1681] Moreover, a novel hydrate-based desalination process utilizing LNG waste cold energy as a heat sink has been modelled, simulated and its economic feasibility evaluated.[1682–1684] The results show that LNG appropriately replaces the external refrigeration cycle, hence the process is able to desalinate high concentration brines with low energy consumption, and hence this coupling could be economically favourable at higher plant capacity. A multifunctional desalination apparatus *via* gas hydrate with various operation modes and separation methods were also developed and its application was tested for a continuous desalination process with multi-time injection, separation and purging.[1685] The ultimate desalination efficiency was observed to be higher than 80% with a water recovery of above 30%. As a form of CO_2-hydrate, CO_2 can act with dual character extracting potable water from brine while being collected from gas stream. Therefore, it could be considered as a potential working medium for the developing technology of coupled CO_2 capture-clathrate hydrate-based desalination, whereby CO_2 is captured as CO_2-hydrate in the presence of seawater, then decomposed to CO_2 and desalinated water where both are desired.[1686] Although few investigations have been conducted in this regard so far,[1108,1687–1690] such capability undoubtedly could provide a huge potential opportunity for more active research in this field, particularly on the technical aspects such as the favourable formation pressure and rate along with cost minimization. Recent advances in both technical and economic aspects continue progress toward commercial and viable clathrate-hydrate based desalination technologies. However, further experimental studies are required to enhance the desalination efficiency *via* reducing the amount of salts trapped among hydrate crystals in each cycle as well as optimizing key operating parameters such as the working gas (hydrate formers), usage of different additives, and finally operating pressure and temperature. At molecular level, MD simulation could also be undertaken to provide fundamental insights regarding the role of crystal nucleation, growth and separation for applications in hydrate-based desalination.

7.4. Gas separation

Gas separation refers to an operation that is being used to either purify or separate certain component/s from the feed gas. Gas separation is necessary for different sectors including natural gas purification,[1691] hydrogen separation,[1692] CO_2 seperation,[1693] biogas separations,[1694] and *etc.*[1695] This technique is commonly implemented in multiphase system. Since, for separating a certain group of molecules in a homogeneous gas mixture, molecular recognition is mandatory. Here, each phase can be described as mechanically separable and a discrete homogenous part of the system. The three most common gas separation methods are solvent/sorbent based separation,[1696] cryogenic distillation,[1697] and membranes.[1698] Recently, hydrate-based gas separation has emerged as a potential technique. The applicability of this method lies in the strong affinity of some of gas molecules to the hydrate phase. In fact, the main challenge in the separation field is the variation in phase affinity of different molecules during phase change, increasing the difficulty of generalizing the separation method.

One remarkable property of gas hydrates is their various occupancies for different gases which can be used to capture and separate less desirable species from the feed gas by forming hydrates followed by dissociating of the formed hydrates after separating from the gas phase. In such a process, the composition of both remaining gas phase and dissociated gas phase will be significantly different from the feed gas. Variation in solubility of different gases (*e.g.* CO_2 and N_2[1407]) helps this process, since gases with higher solubility usually have higher cage occupancy at the hydrate phase. In some cases (*e.g.* $CO_2 + N_2$[1351]), the purity of the captured species could be more than 90% percent after the first attempt. Repeating this process will increase the purity of the separated gases to the desired value (see Fig. 29). Another attractive point of using gas hydrate for gas separation is the endothermic nature of hydrate formation which reduces the required energy for cooling the system during the process. In terms of temperature and pressure effect, the cage occupancy of gases depends on both of these factors, which in turn affects the selectivity of gases in the hydrate phase.

Although it looks quite simple to employ this separation process, in practice it demands complicated operations to separate the gas phase from the hydrate phase efficiently and keep the process continuous, as plugging different parts of the

Open Access Article. Published on 22 Junie 2020. Downloaded on 2026-02-11 12:42:38 nm..
This article is licensed under a Creative Commons Attribution-NonCommercial 3.0 Unported Licence.

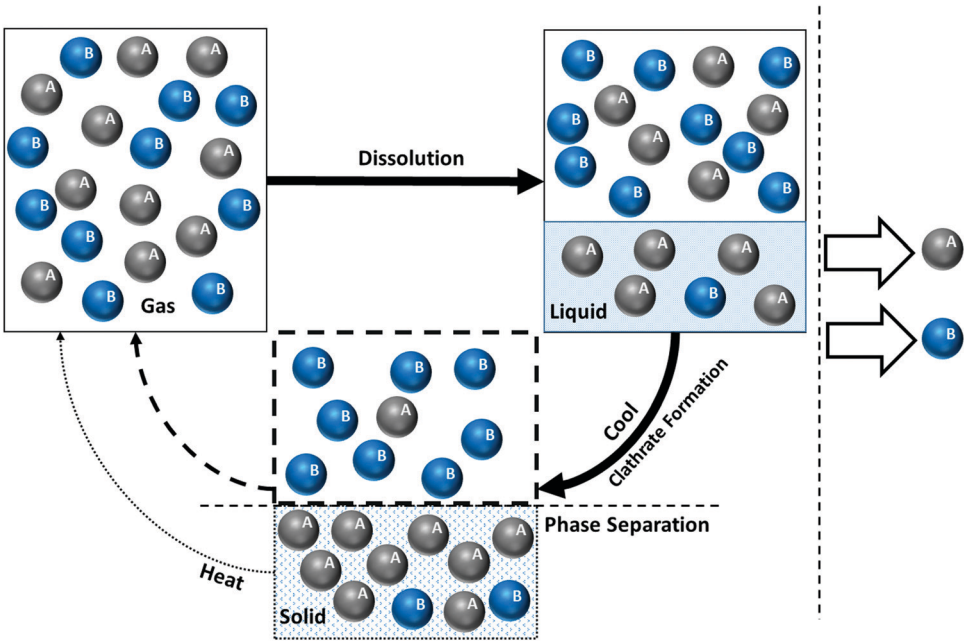

Fig. 29 Schematic diagram of hydrate-based gas separation.

separation apparatus by hydrate formation is a predictable problem.[1110,1360,1699–1702] Accordingly, different types of reactor configurations have been suggested, one of which is SIMTECHE, which has reached the commercial demonstration stage. Other reactors exist including but not limited to stirred reactors, unstirred reactors, fixed bed[1703] reactors, a detailed review of which can be found elsewhere.[1348] Despite the fact that this method is based on the differences in cage occupancies, the key limitation of this method is the cage occupancies of the gases, as it can't be used to separate gases with similar cage occupancies. Accordingly hydrate based separation is mostly associated with CO_2 capture and separation (see Section 6) that has considerably lower HSZ and consequently higher cage occupancies. However, it is also used to separate other gases such as N_2,[1352] H_2,[1704] H_2S,[1705] CH_4,[1706] SF_6,[1707–1710] N_2O,[1711] CHF_3,[1712] and other refrigerant gases.[1713–1715] In the majority of hydrate-based gas separation studies, the authors studied the equilibrium condition of mixed gases, the effect of additives for enhancing gas uptake rate or the neutralising separation *P*–*T* conditions that have already been reviewed in the relevant sections of this article. Recently, it is been suggested to combine this method with membranes[1716,1717] or chemical absorption[1489] to enhance the efficiency of gas separation. The results show that when combined with chemical absorption methods it has about 30% lower energy when compared with cryogenic separation only.[1489]

Although there has been substantial research into hydrate based gas separation since the introduction of the field and the advantages of this method over conventional techniques in terms of being the most environmentally benign approach, there are still numerous issues to be addressed to persuade industries and societies to accept the developed hydrate-based gas separation methods. The fact that establishing new separation plants is capital-intensive makes it harder to persuade the industry, especially when economic studies for most of the proposed method are missing, making it a very high-risk investment for the industry. It is however important and necessary to compare the efficiency of the method with existing separation methods in detail from both the scientific and commercial point of view. In the field of hydrate-based gas separation, the challenge is to design more efficient reactors beside other common challenges such as kinetics and neutralised *P*–*T* conditions. On the basis of the promising development of hydrate-based gas separation in recent years, and the considerable growth potential, hydrate-based gas separation is an excellent candidate technique to make a significant shift in gas separation processes in various industrial applications.

8. Final remarks

Over the past decade, significant progress has been achieved in characterising gas hydrates' behaviour, understanding their role in Nature, and developing gas hydrate-based applications for sustainable technologies. In this review, the main properties of gas hydrates and their kinetic behaviour have been summarized, including those related to pure hydrates and those that can exist in Nature within sediments. This was followed by reviewing the role of gas hydrates in conventional flow assurance that appears to have reached a satisfying level of maturity. However, there is always the need for further optimisation of the hydrate-inhibition process by reducing the costs associated with buying substances or services. The discovery of a vast number of natural gas hydrates reservoirs has enabled the establishment of a new and fruitful area within natural gas recovery, offering different methods for recovering the gas hydrates. The potential interaction of these reservoirs with the atmosphere, however, is of

Open Access Article. Published on 22 Junie 2020. Downloaded on 2026-02-11 12:42:38 nm..
This article is licensed under a Creative Commons Attribution-NonCommercial 3.0 Unported Licence.

increasing concern particularly with regards to their greenhouse warming potential and their potential role in marine stability. In addition, the stability of gas hydrates at extremely high pressures has gathered interest in the field from various branches of astronomy and planetary research. This review has summarized the different potential interactions of gas hydrates and their existence in nature as well as developing methods for extracting gas hydrates. The development of a broad range of applications for gas-hydrate-based technologies in sustainable development including CO_2 capture and storage, water desalination, energy storage, *etc.*, has also increased research attention in this field. Numerous diverse methods have been designed to demonstrate and enhance the capability of gas-hydrate-based technologies. The ongoing investigation in designing new apparatus, processes, or promotional compounds for increasing hydrates' capacity or enhancing their formation/dissociation rate has provided many successful approaches for the application of gas hydrates in sustainable development. This review also compiles the potential application of gas hydrates in sustainable industries, focusing on the general findings in these fields. Considering the extended coverage of the review article, when relevant, the related outlook was provided at the end of each subsection. Although the application of gas hydrates in sustainable industries is in its infancy, intensive research for characterising gas hydrates has already provided important advances, enhancing technologies at the conceptual level. Therefore, we anticipate that the emergence of new gas-hydrate-based applications in sustainable industries will be delivered in the near future, allowing the gas-hydrate community to continue to take an active role in the transition to a lower-carbon economy. Accordingly, we hope the current review will help to motivate scientists working in this exciting field to achieve this commendable goal.

Conflicts of interest

The authors declare no conflicts of interest.

Acknowledgements

A. H. and K. E. were partially supported by funding from UKRI-EPSRC (grant number EP/S027815/1). C. R. was partially supported by DOE-USGS Interagency agreement DE-FE0023495. C. R. thanks L. Stern and W. Waite for insights that improved her contributions. E. J. is partially supported by Flow Programme project sponsored by Department for Business, Energy and Industrial Strategy (BEIS), UK. Any use of trade, firm or product name is for descriptive purposes only and does not imply endorsement by the U.S. Government.

References

1 C. D. Ruppel and J. D. Kessler, *Rev. Geophys.*, 2017, **55**, 126–168.
2 M. T. Kirchner, R. Boese, W. E. Billups and L. R. Norman, *J. Am. Chem. Soc.*, 2004, **126**, 9407–9412.
3 C. Petuya, F. Damay, D. Talaga and A. Desmedt, *J. Phys. Chem. C*, 2017, **121**, 13798–13802.
4 M. Cha, K. Shin, H. Lee, I. L. Moudrakovski, J. A. Ripmeester and Y. Seo, *Environ. Sci. Technol.*, 2015, **49**, 1964–1971.
5 A. Haber, M. Akhfash, C. K. Loh, Z. M. Aman, E. O. Fridjonsson, E. F. May and M. L. Johns, *Langmuir*, 2015, **31**, 8786–8794.
6 A. Klapproth, R. O. Piltz, S. J. Kennedy and K. A. Kozielski, *J. Phys. Chem. C*, 2019, **123**, 2703–2715.
7 C. A. Koh, E. D. Sloan, A. K. Sum and D. T. Wu, *Annu. Rev. Chem. Biomol. Eng.*, 2011, **2**, 237–257.
8 H. Lu, Y. T. Seo, J. W. Lee, I. Moudrakovski, J. A. Ripmeester, N. R. Chapman, R. B. Coffin, G. Gardner and J. Pohlman, *Nature*, 2007, **445**, 303–306.
9 R. K. McMullan and G. A. Jeffrey, *J. Chem. Phys.*, 1965, **42**, 2725–2732.
10 T. C. W. Mak and R. K. McMullan, *J. Chem. Phys.*, 1965, **42**, 2732–2737.
11 J. A. Ripmeester, J. S. Tse, C. I. Ratcliffe and B. M. Powell, *Nature*, 1987, **325**, 135–136.
12 D. W. Davidson, *Water in crystalline hydrates aqueous solutions of simple nonelectrolytes*, Springer, 1973, pp. 115–234.
13 D. Hornby, *Hydrogen bonding in biological structures*, Springer Science & Business Media, 1993, vol. 323.
14 S. Alavi, J. A. Ripmeester and D. D. Klug, *J. Chem. Phys.*, 2006, **125**, 104501.
15 Y. A. Dyadin and K. A. Udachin, *J. Struct. Chem.*, 1987, **28**, 394–432.
16 J. A. Ripmeester and D. W. Davidson, *J. Mol. Struct.*, 1981, **75**, 67–72.
17 I. M. Chou, A. Sharma, R. C. Burruss, J. Shu, H. K. Mao, R. J. Hemley, A. F. Goncharov, L. A. Stern and S. H. Kirby, *Proc. Natl. Acad. Sci. U. S. A.*, 2000, **97**, 13484–13487.
18 L. Yang, C. A. Tulk, D. D. Klug, I. L. Moudrakovski, C. I. Ratcliffe, J. A. Ripmeester, B. C. Chakoumakos, L. Ehmd, C. D. Martin and J. B. Parise, *Proc. Natl. Acad. Sci. U. S. A.*, 2009, **106**, 6060–6064.
19 J. A. Ripmeester, C. I. Ratcliffe and J. S. Tse, *J. Chem. Soc., Faraday Trans. 1*, 1988, **84**, 3731–3745.
20 Y. A. Dyadin, I. V. Bondaryuk and L. S. Aladko, *J. Struct. Chem.*, 1995, **36**, 995–1045.
21 C. A. Koh, *Chem. Soc. Rev.*, 2002, **31**, 157–167.
22 E. D. Sloan Jr., C. A. Koh and C. A. Koh, *Clathrate Hydrates of Natural Gases*, CRC Press, 2007, vol. 20074156.
23 E. D. Sloan, *Nature*, 2003, **426**, 353–359.
24 S. Alavi, K. Udachin, C. I. Ratcliffe and J. A. Ripmeester, *Supramolecular Chemistry: From Molecules to Nanomaterials*, 2012.
25 K. Momma and F. Izumi, *J. Appl. Crystallogr.*, 2011, **44**, 1272–1276.
26 K. A. Udachin and J. A. Ripmeester, *Nature*, 1999, **397**, 420–423.
27 K. A. Udachin, C. I. Ratcliffe and J. A. Ripmeester, *Angew. Chem., Int. Ed.*, 2001, **40**, 1303–1305.
28 H. Hirai, T. Kondo, M. Hasegawa, T. Yagi, Y. Yamamoto, T. Komai, K. Nagashima, M. Sakashita, H. Fujihisa and K. Aoki, *J. Phys. Chem. B*, 2000, **104**, 1429–1433.

 This journal is © The Royal Society of Chemistry 2020

Open Access Article. Published on 22 Junie 2020. Downloaded on 2026-02-11 12:42:38 nm..
This article is licensed under a Creative Commons Attribution-NonCommercial 3.0 Unported Licence.

29 O. Grasset, C. Sotin and F. Deschamps, *Planet. Space Sci.*, 2000, **48**, 617–636.
30 O. B. Toon, C. P. McKay, R. Courtin and T. P. Ackerman, *Icarus*, 1988, **75**, 255–284.
31 E. Lellouch, A. Coustenis, D. Gautier, F. Raulin, N. Dubouloz and C. Frère, *Icarus*, 1989, **79**, 328–349.
32 J. S. Loveday, R. J. Nelmes, M. Guthrie, S. A. Belmonte, D. R. Allan, D. D. Klug, J. S. Tse and Y. P. Handa, *Nature*, 2001, **410**, 661–663.
33 A. Levi and R. E. Cohen, *Astrophys. J.*, 2019, **882**, 71.
34 J. S. Loveday and R. J. Nelmes, *Phys. Chem. Chem. Phys.*, 2008, **10**, 937–950.
35 H. Hirai, T. Tanaka, T. Kawamura, Y. Yamamoto and T. Yagi, *J. Phys. Chem. Solids*, 2004, **65**, 1555–1559.
36 L. E. Bove and U. Ranieri, *Philos. Trans. R. Soc., A*, 2019, **377**, 20180262.
37 S. Schaack, U. Ranieri, P. Depondt, R. Gaal, W. F. Kuhs, P. Gillet, F. Finocchi and L. E. Bove, *Proc. Natl. Acad. Sci. U. S. A.*, 2019, **116**, 16204–16209.
38 C. G. Salzmann, *Proc. Natl. Acad. Sci. U. S. A.*, 2019, **116**, 16164–16166.
39 H. Kadobayashi, H. Hirai, H. Ohfuji, M. Ohtake and Y. Yamamoto, *J. Chem. Phys.*, 2018, **148**, 164503.
40 T. Tanaka, H. Hirai, T. Matsuoka, Y. Ohishi, T. Yagi, M. Ohtake, Y. Yamamoto, S. Nakano and T. Irifune, *J. Chem. Phys.*, 2013, **139**, 104701.
41 X. Cao, Y. Huang, X. Jiang, Y. Su and J. Zhao, *Phys. Chem. Chem. Phys.*, 2017, **19**, 15996–16002.
42 J. E. Proctor, H. E. Maynard-Casely, M. A. Hakeem and D. Cantiah, *J. Raman Spectrosc.*, 2017, **48**, 1777–1782.
43 L. Bezacier, E. Le Menn, O. Grasset, O. Bollengier, A. Oancea, M. Mezouar and G. Tobie, *Phys. Earth Planet. Inter.*, 2014, **229**, 144–152.
44 Y. Huang, K. Li, X. Jiang, Y. Su, X. Cao and J. Zhao, *J. Phys. Chem. A*, 2018, **122**, 6007–6013.
45 D. Londono, W. F. Kuhs and J. L. Finney, *Nature*, 1988, **332**, 141.
46 W. F. Kuhs, T. C. Hansen and A. Falenty, *J. Phys. Chem. Lett.*, 2018, **9**, 3194–3198.
47 W. L. Vos, L. W. Finger, R. J. Hemley and H. K. Mao, *Phys. Rev. Lett.*, 1993, **71**, 3150–3153.
48 M. Catti, L. del Rosso, L. Ulivi, M. Celli, F. Grazzi and T. Hansen, *Phys. Chem. Chem. Phys.*, 2019, **21**, 14671–14677.
49 D. L. Fowler, W. V. Loebenstein, D. B. Pall and C. A. Kraus, *J. Am. Chem. Soc.*, 1940, **62**, 1140–1142.
50 Y. Kamata, H. Oyama, W. Shimada, T. Ebinuma, S. Takeya, T. Uchida, J. Nagao and H. Narita, *Jpn. J. Appl. Phys., Part 1*, 2004, **43**, 362–365.
51 A. Chapoy, R. Anderson and B. Tohidi, *J. Am. Chem. Soc.*, 2007, **129**, 746–747.
52 R. K. McMullan, M. Bonamico and G. A. Jeffrey, *J. Chem. Phys.*, 1963, **39**, 3295–3310.
53 D. W. Devidson, *Water Compr. Treatise*, 1973, 115–234.
54 G. A. Jeffrey, *J. Inclusion Phenom.*, 1984, **1**, 211–222.
55 W. Shimada, M. Shiro, H. Kondo, S. Takeya, H. Oyama, T. Ebinuma and H. Narita, *Acta Crystallogr., Sect. C: Cryst. Struct. Commun.*, 2005, **61**, o65–o66.
56 S. A. Lawrence, *Amines: synthesis, properties and applications*, Cambridge University Press, 2004.
57 F. Ma, Y. Wan, G. Yuan, L. Meng, Z. Dong and J. Hu, *Environ. Sci. Technol.*, 2012, **46**, 3236–3243.
58 X. Ge, A. S. Wexler and S. L. Clegg, *Atmos. Environ.*, 2011, **45**, 524–546.
59 O. G. Brakstad, L. Sørensen, K. Zahlsen, K. Bonaunet, A. Hyldbakk and A. M. Booth, *Int. J. Greenhouse Gas Control*, 2018, **70**, 157–163.
60 H. Guo, C. Li, X. Shi, H. Li and S. Shen, *Appl. Energy*, 2019, **239**, 725–734.
61 G. A. Jeffrey and R. K. M. Ullan, *Prog. Inorg. Chem.*, 2009, **16**, 43.
62 M. D. Gregory, *Hydration of Several Aliphatic Amines in Some Non-Polar Solvents*, The University of Oklahoma, 1968.
63 K. Ogata, T. Tsuda, S. Amano, S. Hashimoto, T. Sugahara and K. Ohgaki, *Chem. Eng. Sci.*, 2010, **65**, 1616–1620.
64 W. Shin, S. Park, J. W. Lee, Y. Seo, D. Y. Koh, J. Seol and H. Lee, *J. Phys. Chem. C*, 2012, **116**, 16352–16357.
65 S. Lee, Y. Lee, S. Park and Y. Seo, *J. Phys. Chem. B*, 2012, **116**, 13476–13480.
66 Y. Youn, J. Seol, M. Cha, Y. H. Ahn and H. Lee, *J. Chem. Eng. Data*, 2014, **59**, 2004–2012.
67 Y. Youn, M. Cha and H. Lee, *Fluid Phase Equilib.*, 2016, **413**, 123–128.
68 S. Park, H. Kang, K. Shin, Y. Seo and H. Lee, *Phys. Chem. Chem. Phys.*, 2015, **17**, 1949–1956.
69 N. J. English and J. M. D. MacElroy, *Chem. Eng. Sci.*, 2015, **121**, 133–156.
70 B. C. Barnes and A. K. Sum, *Curr. Opin. Chem. Eng.*, 2013, **2**, 184–190.
71 N. J. English and J. S. Tse, *J. Phys. Chem. A*, 2011, **115**, 6226–6232.
72 A. Falenty, T. C. Hansen and W. F. Kuhs, *Nature*, 2014, **516**, 231.
73 Y. Krishnan, M. R. Ghaani and N. J. English, *J. Phys. Chem. C*, 2019, **123**, 27554–27560.
74 J. S. Tse, M. L. Klein and I. R. McDonald, *J. Phys. Chem.*, 1983, **87**, 4198–4203.
75 A. Wallqvist, *J. Chem. Phys.*, 1992, **96**, 5377–5382.
76 N. J. English and G. M. Phelan, *J. Chem. Phys.*, 2009, **131**, 74704.
77 N. J. English and S. T. John, *Phys. Rev. Lett.*, 2009, **103**, 15901.
78 N. J. English, S. T. John and D. J. Carey, *Phys. Rev. B: Condens. Matter Mater. Phys.*, 2009, **80**, 134306.
79 P. Warrier, M. N. Khan, V. Srivastava, C. M. Maupin and C. A. Koh, *J. Chem. Phys.*, 2016, **145**, 211705.
80 N. J. English and C. C. R. Allen, *Sci. Total Environ*, 2019, **661**, 664–669.
81 A. Hassanpouryouzband, J. Yang, A. Okwananke, R. Burgass, B. Tohidi, E. Chuvilin, V. Istomin and B. Bukhanov, *Sci. Rep.*, 2019, **9**, 1–9.
82 T. E. Chnology, *J. Pet. Technol.*, 1941, **43**, 1–414.
83 D. L. Katz, *Trans. AIME*, 1945, **160**, 140–149.
84 J. H. van der Waals and J. C. Platteeuw, *Adv. Chem. Phys.*, 1958, 1–57.

Open Access Article. Published on 22 Junie 2020. Downloaded on 2026-02-11 12:42:38 nm..
This article is licensed under a Creative Commons Attribution-NonCommercial 3.0 Unported Licence.

85 J. H. van der Waals, *Trans. Faraday Soc.*, 1956, **52**, 184–193.
86 M. N. Khan, P. Warrier, C. J. Peters and C. A. Koh, *Fluid Phase Equilib.*, 2018, **463**, 48–61.
87 J. E. Lennard-Jones and A. F. Devonshire, *Proc. R. Soc. London, Ser. A*, 1937, **163**, 53–70.
88 V. McKoy and O. Sinanoğlu, *J. Chem. Phys.*, 1963, **38**, 2946–2956.
89 W. R. Parrish and J. M. Prausnitz, *Ind. Eng. Chem. Process Des. Dev.*, 1972, **11**, 26–35.
90 D. R. Hafemann and S. L. Miller, *J. Phys. Chem.*, 1969, **73**, 1392–1397.
91 H. J. Ng and D. B. Robinson, *Ind. Eng. Chem. Fundam.*, 1976, **15**, 293–298.
92 G. D. Holder, G. Corbin and K. D. Papadopoulos, *Ind. Eng. Chem. Fundam.*, 1980, **19**, 282–286.
93 P. Englezos and P. R. Bishnoi, *Fluid Phase Equilib.*, 1988, **42**, 129–140.
94 M. L. Michelsen, *Fluid Phase Equilib.*, 1982, **9**, 1–19.
95 P. R. Bishnoi, A. K. Gupta, P. Englezos and N. Kalogerakis, *Fluid Phase Equilib.*, 1989, **53**, 97–104.
96 A. K. Gupta, P. Raj Bishnoi and N. Kalogerakis, *Fluid Phase Equilib.*, 1991, **63**, 65–89.
97 A. L. Ballard and E. D. Sloan, *Fluid Phase Equilib.*, 2002, **194–197**, 371–383.
98 I. S. V. Segtovich, A. G. Barreto and F. W. Tavares, *Fluid Phase Equilib.*, 2016, **413**, 196–208.
99 T. H. Sirino, M. A. M. Neto, D. Bertoldi, R. E. M. Morales and A. K. Sum, *Fluid Phase Equilib.*, 2018, **475**, 45–63.
100 S. Hielscher, V. Vinš, A. Jäger, J. Hrubý, C. Breitkopf and R. Span, *Fluid Phase Equilib.*, 2018, **459**, 170–185.
101 M. A. Mahabadian, A. Chapoy, R. Burgass and B. Tohidi, *Fluid Phase Equilib.*, 2016, **414**, 117–132.
102 N. M. Alsaifi and P. Englezos, *Fluid Phase Equilib.*, 2011, **302**, 169–178.
103 H. Haghighi, A. Chapoy, R. Burgess and B. Tohidi, *Fluid Phase Equilib.*, 2009, **276**, 24–30.
104 L. Li, L. Zhu and J. Fan, *Fluid Phase Equilib.*, 2016, **409**, 291–300.
105 A. H. S. Dehaghani and M. H. Badizad, *Fluid Phase Equilib.*, 2016, **427**, 328–339.
106 J. Kondori, S. Zendehboudi and L. James, *Ind. Eng. Chem. Res.*, 2018, **57**, 13833–13855.
107 A. M. Palma, A. J. Queimada and J. A. P. Coutinho, *Ind. Eng. Chem. Res.*, 2019, **58**, 19239–19250.
108 M. S. Waseem and N. M. Alsaifi, *J. Chem. Thermodyn.*, 2018, **117**, 223–235.
109 M. N. Khan, P. Warrier, C. J. Peters and C. A. Koh, *J. Nat. Gas Sci. Eng.*, 2016, **35**, 1388–1404.
110 M. N. Khan, P. Warrier, C. J. Peters and C. A. Koh, *J. Nat. Gas Sci. Eng.*, 2016, **35**, 1355–1361.
111 M. Connolly, H. Pan and H. Tchelepi, *Ind. Eng. Chem. Res.*, 2019, **58**, 14954–14974.
112 A. H. Mohammadi, V. Belandria and D. Richon, *Chem. Eng. Sci.*, 2010, **65**, 4302–4305.
113 A. Galindo, A. Gil-Villegas, G. Jackson and A. N. Burgess, *J. Phys. Chem. B*, 1999, **103**, 10272–10281.
114 A. Fukumoto, L. P. S. Silva, P. Paricaud, D. Dalmazzone and W. Fürst, *Int. J. Hydrogen Energy*, 2015, **40**, 9254–9266.
115 P. Babu, P. Paricaud and P. Linga, *Fluid Phase Equilib.*, 2016, **413**, 80–85.
116 A. Fukumoto, P. Paricaud, D. Dalmazzone, W. Bouchafaa, T. T.-S. Ho and W. Fürst, *J. Chem. Eng. Data*, 2014, **59**, 3193–3204.
117 H. Najibi, K. Momeni, M. T. Sadeghi and A. H. Mohammadi, *J. Chem. Thermodyn.*, 2015, **87**, 122–128.
118 Q.-L. Ma, J.-L. Qi, G.-J. Chen and C.-Y. Sun, *Fluid Phase Equilib.*, 2016, **430**, 178–187.
119 L. Sun, X. Liang, N. Von Solms and G. M. Kontogeorgis, *Fluid Phase Equilib.*, 2019, **486**, 37–47.
120 G.-J. Chen and T.-M. Guo, *Fluid Phase Equilib.*, 2002, **122**, 43–65.
121 K. Růržička and V. Majer, *AIChE J.*, 2004, **42**, 1723–1740.
122 J. B. Klauda and S. I. Sandler, *Ind. Eng. Chem. Res.*, 2000, **39**, 3377–3386.
123 K. Růržička and V. Majer, *AIChE J.*, 1996, **42**, 1723–1740.
124 J. B. Klauda and S. I. Sandler, *Chem. Eng. Sci.*, 2003, **58**, 27–41.
125 A. Martin and C. J. Peters, *J. Phys. Chem. C*, 2008, **113**, 422–430.
126 H. Delavar and A. Haghtalab, *Fluid Phase Equilib.*, 2015, **394**, 101–117.
127 S. Shahnazar and N. Hasan, *Fluid Phase Equilib.*, 2014, **379**, 72–85.
128 E. Khamehchi, E. Shamohammadi and S. H. Yousefi, *Gas Process. J.*, 2013, **1**, 41–50.
129 A. Chapoy, A. H. Mohammadi and D. Richon, *Oil Gas Sci. Technol.*, 2007, **62**, 701–706.
130 A. A. Ibrahim, T. A. Lemma, M. L. Kean and M. G. Zewge, *Appl. Mech. Mater.*, 2016, **819**, 569–574.
131 C. J. Burnham and N. J. English, *J. Phys. Chem. C*, 2016, **120**, 16561–16567.
132 C. J. Burnham, Z. Futera and N. J. English, *Phys. Chem. Chem. Phys.*, 2017, **19**, 717–728.
133 M. Pérez-Rodríguez, J. Otero-Fernández, A. Comesaña, Á. M. Fernández-Fernández and M. M. Piñeiro, *ACS Omega*, 2018, **3**, 18771–18782.
134 C. J. Burnham, Z. Futera and N. J. English, *J. Chem. Phys.*, 2018, **148**, 102323, DOI: 10.1063/1.4999909.
135 P. E. Brumby, D. Yuhara, T. Hasegawa, D. T. Wu, A. K. Sum and K. Yasuoka, *J. Chem. Phys.*, 2019, **150**, 134503, DOI: 10.1063/1.5084785.
136 B. Kvamme, J. Zhao, N. Wei and N. Saeidi, *Energies*, 2020, **13**, 880.
137 N. J. English and J. S. Tse, *Energies*, 2010, 3.
138 W. F. Waite, J. C. Santamarina, D. D. Cortes, B. Dugan, D. N. Espinoza, J. Germaine, J. Jang, J. W. Jung, T. J. Kneafsey, H. Shin, K. Soga, W. J. Winters and T. Yun, *Rev. Geophys.*, 2009, **47**, 1–38.
139 R. G. Ross, P. Andersson and G. Bäckström, *Nature*, 1981, **290**, 322–323.
140 P. Andersson and R. G. Ross, *J. Phys. C: Solid State Phys.*, 1983, **16**, 1423–1432.

Open Access Article. Published on 22 Junie 2020. Downloaded on 2026-02-11 12:42:38 nm..
This article is licensed under a Creative Commons Attribution-NonCommercial 3.0 Unported Licence.

141 J. S. Tse and M. A. White, *J. Phys. Chem.*, 1988, **92**, 5006–5011.
142 R. G. Ross and P. Andersson, *Can. J. Chem.*, 1982, **60**, 881–892.
143 G. A. Slack, *MRS Proc.*, 1997, **478**, 47.
144 G. S. Nolas, D. T. Morelli and T. M. Tritt, *Annu. Rev. Mater. Sci.*, 1999, **29**, 89–116.
145 J. L. Cohn, G. S. Nolas, V. Fessatidis, T. H. Metcalf and G. A. Slack, *Phys. Rev. Lett.*, 1999, **82**, 779–782.
146 A. I. Krivchikov, B. Y. Gorodilov, O. A. Korolyuk, V. G. Manzhelii, H. Conrad and W. Press, *J. Low Temp. Phys.*, 2005, **139**, 693–702.
147 A. I. Krivchikov, B. Y. Gorodilov, O. A. Korolyuk, V. G. Manzhelii, O. O. Romantsova, H. Conrad, W. Press, J. S. Tse and D. D. Klug, *Phys. Rev. B: Condens. Matter Mater. Phys.*, 2006, **73**, 64203.
148 J. S. Tse, *J. Inclusion Phenom. Mol. Recognit. Chem.*, 1994, **17**, 259–266.
149 R. Inoue, H. Tanaka and K. Nakanishi, *J. Chem. Phys.*, 1996, **104**, 9569–9577.
150 J. S. Tse, V. P. Shpakov, V. V. Murashov and V. R. Belosludov, *J. Chem. Phys.*, 1997, **107**, 9271–9274.
151 J. S. Tse, C. I. Ratcliffe, B. M. Powell, V. F. Sears and Y. P. Handa, *J. Phys. Chem. A*, 1997, **101**, 4491–4495.
152 J. Baumert, C. Gutt, V. P. Shpakov, J. S. Tse, M. Krisch, M. Müller, H. Requardt, D. D. Klug, S. Janssen and W. Press, *Phys. Rev. B: Condens. Matter Mater. Phys.*, 2003, **68**, 174301.
153 A. I. Krivchikov, A. N. Yushchenko, O. A. Korolyuk, F. J. Bermejo, R. Fernandez-Perea, I. Bustinduy and M. A. González, *Phys. Rev. B: Condens. Matter Mater. Phys.*, 2008, **77**, 24202.
154 T. Takabatake, K. Suekuni, T. Nakayama and E. Kaneshita, *Rev. Mod. Phys.*, 2014, **86**, 669–716.
155 A. Desmedt, L. Bedouret, E. Pefoute, M. Pouvreau, S. Say-Liang-Fat and M. Alvarez, *Eur. Phys. J.-Spec. Top.*, 2012, **213**, 103–127.
156 R. P. Warzinski, I. K. Gamwo, E. J. Rosenbaum, E. M. Myshakin, H. Jiang, K. D. Jordan, N. J. English and D. W. Shaw, *Alternative Energy and Shale Gas Encyclopedia*, 2016, pp. 680–686.
157 M. M. Safarov and M. A. Zaripova, *Meas. Tech.*, 1993, **36**, 435–438.
158 O. Andersson and H. Suga, *J. Phys. Chem. Solids*, 1996, **57**, 125–132.
159 O. Andersson and G. P. Johari, *J. Chem. Phys.*, 2009, **131**, 114503.
160 N. J. English, J. S. Tse and R. Gallagher, *Phys. Rev. B: Condens. Matter Mater. Phys.*, 2010, **82**, 92201.
161 W. F. Waite, L. A. Stern, S. H. Kirby, W. J. Winters and D. H. Mason, *Geophys. J. Int.*, 2007, **169**, 767–774.
162 J. Zhao, S. Sun, C. Liu and Q. Meng, *Heat Mass Transfer*, 2018, **54**, 3287–3295.
163 J. G. Cook and D. G. Leaist, *Geophys. Res. Lett.*, 1983, **10**, 397–399.
164 D. Huang and S. Fan, *J. Chem. Eng. Data*, 2004, **49**, 1479–1482.
165 J. F. Gabitto and C. Tsouris, Physical properties of gas hydrates: A review, *J. Thermodyn.*, 2010, 271291, http://downloads.hindawi.com/journals/jtd/2010/271291.pdf.
166 K. Fujiura, Y. Nakamoto, Y. Taguchi, R. Ohmura and Y. Nagasaka, *Fluid Phase Equilib.*, 2016, **413**, 129–136.
167 D. Li, D. Liang, H. Peng and L. Wan, *J. Therm. Anal. Calorim.*, 2016, **123**, 1391–1397.
168 W. F. Waite, L. Y. Gilbert, W. J. Winters and D. H. Mason, *Rev. Sci. Instrum.*, 2006, **77**, 44904.
169 W. F. Waite, *Preliminary Laboratory Thermal Conductivity Measurements in Pure Methane Hydrate and Methane Hydrate-Sediment Mixtures: A Progress Report*, 2011.
170 D. Z. Huang, S. S. Fan, D. Q. Liang and Z. P. Feng, *Chin. J. Geophys.*, 2005, **48**, 1201–1207.
171 D. Li, J. Du, S. He, D. Liang, X. Zhao and X. Yang, *Sci. China: Chem.*, 2012, **55**, 373–379.
172 S. Sun, X. Jin, C. Liu, Q. Meng and Y. Zhang, *Int. J. Heat Mass Transfer*, 2018, **127**, 88–96.
173 E. J. Rosenbaum, N. J. English, J. K. Johnson, D. W. Shaw and R. P. Warzinski, *J. Phys. Chem. B*, 2007, **111**, 13194–13205.
174 S. Sun, J. Zhao, J. Zhao, Y. Hao and J. Yang, *J. Chem. Thermodyn.*, 2019, **132**, 423–431.
175 A. I. Krivchikov, V. G. Manzhelii, O. A. Korolyuk, B. Y. Gorodilov and O. O. Romantsova, *Phys. Chem. Chem. Phys.*, 2005, **7**, 728–730.
176 Y. Handa and J. G. Cook, *J. Phys. Chem.*, 1987, **91**, 6327–6328.
177 J. Li, Z.-L. Wang and G.-C. Yao, *Chin. Phys. Lett.*, 2018, **35**, 70502.
178 P. Kumar, D. Turner and E. D. Sloan, *J. Geophys. Res. Solid Earth*, 2004, **109**, B01207, DOI: 10.1029/2003JB002763.
179 D. J. Turner, P. Kumar and E. D. Sloan, *Int. J. Thermophys.*, 2005, **26**, 1681–1691.
180 Y. P. Handa, R. E. Hawkins and J. J. Murray, *J. Chem. Thermodyn.*, 1984, **16**, 623–632.
181 D. G. Leaist, J. J. Murray, M. L. Post and D. W. Davidson, *J. Phys. Chem.*, 1982, **86**, 4175–4178.
182 Y. P. Handa, *J. Chem. Thermodyn.*, 1985, **17**, 201–208.
183 Y. P. Handa, *J. Chem. Thermodyn.*, 1986, **18**, 891–902.
184 Y. P. Handa, *J. Chem. Thermodyn.*, 1986, **18**, 915–921.
185 O. Yamamuro, M. Oguni, T. Matsuo and H. Suga, *Solid State Commun.*, 1987, **62**, 289–292.
186 Y. Paul Handa, *Ind. Eng. Chem. Res.*, 1988, **27**, 872–874.
187 O. Yamamuro, M. Oguni, T. Matsuo and H. Suga, *J. Phys. Chem. Solids*, 1988, **49**, 425–434.
188 R. M. Rueff, E. Dendy Sloan and V. F. Yesavage, *AIChE J.*, 1988, **34**, 1468–1476.
189 E. Tombari, S. Presto, G. Salvetti and G. P. Johari, *J. Chem. Phys.*, 2006, **124**, 154507, DOI: 10.1063/1.2188944.
190 J. Gao and N. M. Kenneth, *Chin. J. Chem. Eng.*, 2003, **11**, 276–279.
191 J. S. Lievois, R. Perkins, R. J. Martin and R. Kobayashi, *Fluid Phase Equilib.*, 1990, **59**, 73–97.
192 S.-P. Kang, H. Lee and B.-J. Ryu, *J. Chem. Thermodyn.*, 2001, **33**, 513–521.

Open Access Article. Published on 22 Junie 2020. Downloaded on 2026-02-11 12:42:38 nm..
This article is licensed under a Creative Commons Attribution-NonCommercial 3.0 Unported Licence.

193 Y. Zhang, P. G. Debenedetti, R. K. PruD'Homme and B. A. Pethica, *J. Phys. Chem. B*, 2004, **108**, 16717–16722.
194 M. B. Rydzy, J. M. Schicks, R. Naumann and J. Erzinger, *J. Phys. Chem. B*, 2007, **111**, 9539–9545.
195 G. Li, D. Liu and Y. Xie, *J. Therm. Anal. Calorim.*, 2010, **102**, 819–826.
196 T.-H. Kwon, T. J. Kneafsey and E. V. L. Rees, *J. Phys. Chem. B*, 2011, **115**, 8169–8175.
197 Y. Lee, S. Lee, J. Lee and Y. Seo, *Chem. Eng. J.*, 2014, **246**, 20–26.
198 L. Mu and N. von Solms, *J. Chem. Thermodyn.*, 2018, **117**, 33–42.
199 J. Deschamps and D. Dalmazzone, *J. Therm. Anal. Calorim.*, 2009, **98**, 113.
200 S. Sun, J. Zhao and D. Yu, *Fluid Phase Equilib.*, 2018, **456**, 92–97.
201 W. Lin, A. Delahaye and L. Fournaison, *Fluid Phase Equilib.*, 2008, **264**, 220–227.
202 I. N. Tsimpanogiannis, V. K. Michalis and I. G. Economou, *Fluid Phase Equilib.*, 2019, **489**, 30–40.
203 Z.-L. Wang, K.-P. Yuan and D.-W. Tang, *Chin. Phys. Lett.*, 2015, **32**, 104401.
204 Q.-B. Li and C. Liu, *K. Cheng Je Wu Li Hsueh Pao/Journal Eng. Thermophys.*, 2015, 36, 714–719.
205 D. Yang, Y. Liu, Y. Xiu, H. Xu, K. Yuan and Z. Xu, *Zhongguo Shiyou Daxue Xuebao (Ziran Kexue Ban)/Journal China Univ. Pet. (Edition Nat. Sci.)*, 2016, **40**, 141–145.
206 H. Ghafari and H. Mohammadi-Manesh, *Mol. Simul.*, 2019, **45**, 614–622.
207 L. Wan, D. Liang, N. Wu and J. Guan, *Huagong Xuebao*, 2012, **63**, 382–386.
208 L. Wan, D. Liang, N. Wu and J. Guan, *Sci. China: Chem.*, 2012, **55**, 167–174.
209 L. H. Wan, D. Q. Liang and J. A. Guan, *Adv. Mater. Res.*, 2014, **1008–1009**, 861–872.
210 F. L. Ning, K. Glavatskiy, Z. Ji, S. Kjelstrup and T. J. H. Vlugt, *Phys. Chem. Chem. Phys.*, 2015, **17**, 2869–2883.
211 V. S. Baghel, R. Kumar and S. Roy, *J. Phys. Chem. C*, 2013, **117**, 12172–12182.
212 S. Alavi and R. Ohmura, *J. Chem. Phys.*, 2016, **145**, 154708, DOI: 10.1063/1.4964673.
213 Y. Hu, B. R. Lee and A. K. Sum, *Fluid Phase Equilib.*, 2017, **450**, 24–29.
214 F. Ning, Y. Yu, S. Kjelstrup, T. J. H. Vlugt and K. Glavatskiy, *Energy Environ. Sci.*, 2012, **5**, 6779–6795.
215 J. Kondori, S. Zendehboudi and M. E. Hossain, *J. Pet. Sci. Eng.*, 2017, **159**, 754–772.
216 P. Guo, Y.-K. Pan, L.-L. Li and B. Tang, *Chin. Phys. B*, 2017, **26**, 73101.
217 C. Ruppel, Thermal State of the Gas Hydrate Reservoir, in *Natural Gas Hydrate*, ed. M. D. Max, Springer Netherlands, Dordrecht, 2000, pp. 29–42.
218 Q. Chen, S. Diao and Y. Ye, Thermophysical Properties of Gas Hydrate in Porous Media, in *Natural Gas Hydrates*, ed. Y. Ye and C. Liu, Springer Berlin Heidelberg, Berlin, Heidelberg, 2013, pp. 141–167.
219 D. D. Cortes, A. I. Martin, T. S. Yun, F. M. Francisca, J. C. Santamarina and C. Ruppel, *J. Geophys. Res. Solid Earth*, 2009, **114**, B11103, DOI: 10.1029/2008JB006235.
220 D. Huang and S. Fan, *J. Geophys. Res. Solid Earth*, 2005, **110**, B01311, DOI: 10.1029/2004JB003314.
221 J. Zhao, C. Cheng, Y. Song, W. Liu, Y. Liu, K. Xue, Z. Zhu, Z. Yang, D. Wang and M. Yang, *Energies*, 2012, 5.
222 S. Dangayach, D. N. Singh, P. Kumar, S. K. Dewri, B. Roy, C. Tandi and J. Singh, *Mar. Pet. Geol.*, 2015, **67**, 653–662.
223 Z. R. Chong, S. H. B. Yang, P. Babu, P. Linga and X.-S. Li, *Appl. Energy*, 2016, **162**, 1633–1652.
224 E. Chuvilin and B. Bukhanov, *Energy Fuels*, 2017, **31**, 5246–5254.
225 E. Chuvilin, Effect of Ice and Hydrate Formation on Thermal Conductivity of Sediments, in *Impact of Thermal Conductivity on Energy Technologies*, ed. B. Bukhanov, Intech Open, Rijeka, 2018, ch. 7.
226 R. D. Stoll and G. M. Bryan, *J. Geophys. Res.*, 1979, **84**, 1629–1634.
227 W. F. Waite, B. J. deMartin, S. H. Kirby, J. Pinkston and C. D. Ruppel, *Geophys. Res. Lett.*, 2002, **29**, 82–84.
228 M. Muraoka, M. Ohtake, N. Susuki, Y. Yamamoto, K. Suzuki and T. Tsuji, *J. Geophys. Res. Solid Earth*, 2014, **119**, 8021–8033.
229 S. Dai, J.-H. Cha, E. J. Rosenbaum, W. Zhang and Y. Seol, *Geophys. Res. Lett.*, 2015, **42**, 6295–6305.
230 M. Muraoka, N. Susuki, H. Yamaguchi, T. Tsuji and Y. Yamamoto, *Energy Fuels*, 2015, **29**, 1345–1351.
231 D. Li and D. Liang, *Int. J. Heat Mass Transfer*, 2016, **92**, 8–14.
232 L. Dongliang, P. Hao and L. Deqing, *Int. J. Heat Mass Transfer*, 2017, **104**, 566–573.
233 J. Zhao, B. Wang, L. Yang, C. Cheng and Y. Song, *Rev. Sci. Instrum.*, 2015, **86**, 85110.
234 L. Yang, J. Zhao, W. Liu, M. Yang and Y. Song, *Energy*, 2015, **79**, 203–211.
235 L. Yang, J. Zhao, B. Wang, W. Liu, M. Yang and Y. Song, *Fuel*, 2016, **179**, 87–96.
236 B. Wang, Z. Fan, P. Lv, J. Zhao and Y. Song, *Int. J. Heat Mass Transfer*, 2017, **110**, 142–150.
237 Y. Dong, J. S. McCartney and N. Lu, *Geotech. Geol. Eng.*, 2015, **33**, 207–221.
238 J. Mo and H. Ban, *Case Stud. Therm. Eng.*, 2017, **10**, 423–433.
239 R. D. Hyndman, T. Yuan and K. Moran, *Earth Planet. Sci. Lett.*, 1999, **172**, 167–177.
240 X. Zhou, S. Fan, D. Liang, D. Wang and N. Huang, *J. Nat. Gas Chem.*, 2007, **16**, 399–403.
241 A. E. Cook, B. I. Anderson, A. Malinverno, S. Mrozewski and D. S. Goldberg, *Geophysics*, 2010, **75**, F173–F185.
242 G. Y. Kim, B. Y. Yi, D. G. Yoo, B. J. Ryu and M. Riedel, *Mar. Pet. Geol.*, 2011, **28**, 1979–1985.
243 M. W. Lee and T. S. Collett, *Mar. Pet. Geol.*, 2011, **28**, 439–449.
244 A. E. Cook, B. I. Anderson, J. Rasmus, K. Sun, Q. Li, T. S. Collett and D. S. Goldberg, *Mar. Pet. Geol.*, 2012, **34**, 72–84.

 This journal is © The Royal Society of Chemistry 2020

Open Access Article. Published on 22 Junie 2020. Downloaded on 2026-02-11 12:42:38 nm..
This article is licensed under a Creative Commons Attribution-NonCommercial 3.0 Unported Licence.

245 M. W. Lee and T. S. Collett, *Mar. Pet. Geol.*, 2013, **47**, 195–203.
246 M. Priegnitz, J. Thaler, E. Spangenberg, C. Rücker and J. M. Schicks, *Rev. Sci. Instrum.*, 2013, **84**, 104502.
247 M. Karamoddin and F. Varaminian, *J. Ind. Eng. Chem.*, 2014, **20**, 3815–3820.
248 B. Tohidi, J. Yang, M. Salehabadi, R. Anderson and A. Chapoy, *Environ. Sci. Technol.*, 2010, **44**, 1509–1514.
249 K. Schwalenberg, E. Willoughby, R. Mir and R. N. Edwards, Marine Gas Hydrate Electromagnetic Signatures in Cascadia and Their Correlation with Seismic Blank Zones, *First Break*, 2005, **23**, 57–63.
250 U. Shankar and M. Riedel, *Mar. Pet. Geol.*, 2011, **28**, 1768–1778.
251 X. Wang, S. Wu, M. Lee, Y. Guo, S. Yang and J. Liang, *Mar. Pet. Geol.*, 2011, **28**, 1625–1633.
252 X. Wang, M. Lee, T. Collett, S. Yang, Y. Guo and S. Wu, *Mar. Pet. Geol.*, 2014, **51**, 298–306.
253 X. Wang, T. S. Collett, M. W. Lee, S. Yang, Y. Guo and S. Wu, *Mar. Geol.*, 2014, **357**, 272–292.
254 J. Liu, J. Zhang, F. Ma, M. Wang and Y. Sun, *Mar. Pet. Geol.*, 2017, **88**, 225–234.
255 J. Wei, Y. Fang, H. Lu, H. Lu, J. Lu, J. Liang and S. Yang, *Mar. Pet. Geol.*, 2018, **98**, 622–628.
256 J. R. Kliner and J. L. H. Grozic, *Can. Geotech. J.*, 2006, **43**, 551–562.
257 Y. F. Sun and D. Goldberg, *Geophys. Res. Lett.*, 2005, **32**, L04313, DOI: 10.1029/2004GL021976.
258 Y. Sun, D. Goldberg, T. Collett and R. Hunter, *Mar. Pet. Geol.*, 2011, **28**, 450–459.
259 R. E. Grimm, D. E. Stillman, S. F. Dec and M. A. Bullock, *J. Phys. Chem. B*, 2008, **112**, 15382–15390.
260 W. L. Du Frane, L. A. Stern, K. A. Weitemeyer, S. Constable, J. C. Pinkston and J. J. Roberts, *Geophys. Res. Lett.*, 2011, **38**, L09313, DOI: 10.1029/2011GL047243.
261 W. L. Du Frane, L. A. Stern, K. A. Weitemeyer, S. Constable, J. C. Pinkston and J. J. Roberts, *Electrical conductivity of laboratory-synthesized methane hydrate*, Lawrence Livermore National Lab (LLNL), Livermore, CA, United States, 2011.
262 T. M. Nahir, *J. Am. Chem. Soc.*, 2005, **127**, 12431.
263 L. Stern, W. L. Du Frane, K. A. Weitemeyer, S. Constable and J. J. Roberts, *AGU Fall Meeting Abstracts*, 2012.
264 R. Lu, L. A. Stern, W. L. Du Frane, J. C. Pinkston, J. J. Roberts and S. Constable, *AGU Fall Meeting Abstracts*, 2018.
265 J. Lee, *Hydrate-Bearing Sediments: Formation and Geophysical Properties*, Georgia Institute of Technology, 2007.
266 K. A. Weitemeyer, S. C. Constable, K. W. Key and J. P. Behrens, *Geophys. Res. Lett.*, 2006, **33**, L03304, DOI: 10.1029/2005GL024896.
267 K. Schwalenberg, M. Haeckel, J. Poort and M. Jegen, *Mar. Geol.*, 2010, **272**, 79–88.
268 K. A. Weitemeyer, S. Constable and A. M. Tréhu, *Geophys. J. Int.*, 2011, **187**, 45–62.
269 S.-K. Hsu, C.-W. Chiang, R. L. Evans, C.-S. Chen, S.-D. Chiu, Y.-F. Ma, S.-C. Chen, C.-H. Tsai, S.-S. Lin and Y. Wang, *J. Asian Earth Sci.*, 2014, **92**, 224–232.
270 B. K. Goswami, K. A. Weitemeyer, T. A. Minshull, M. C. Sinha, G. K. Westbrook, A. Chabert, T. J. Henstock and S. Ker, *J. Geophys. Res. Solid Earth*, 2015, **120**, 6797–6822.
271 E. Attias, K. Weitemeyer, T. A. Minshull, A. I. Best, M. Sinha, M. Jegen-Kulcsar, S. Hölz and C. Berndt, *Geophys. J. Int.*, 2016, **206**, 1093–1110.
272 D. Lim, H. Ro, Y. J. Seo, J. Y. Lee, J. Lee, S. J. Kim, Y. Park and H. Lee, *Energy Fuels*, 2017, **31**, 708–713.
273 K. Schwalenberg, D. Rippe, S. Koch and C. Scholl, *J. Geophys. Res. Solid Earth*, 2017, **122**, 3334–3350.
274 J. Jing, K. Chen, M. Deng, Q. Zhao, X. Luo, G. Tu and M. Wang, *J. Asian Earth Sci.*, 2019, **171**, 201–212.
275 R. Tharimela, A. Augustin, M. Ketzer, J. Cupertino, D. Miller, A. Viana and K. Senger, *Interpretation*, 2019, **7**, SH111–SH131.
276 M. Riedel, T. S. Collett, H.-S. Kim, J.-J. Bahk, J.-H. Kim, B.-J. Ryu and G. Y. Kim, *Mar. Pet. Geol.*, 2013, **47**, 222–235.
277 U. Shankar and M. Riedel, *Mar. Pet. Geol.*, 2014, **58**, 265–277.
278 A. E. Cook and W. F. Waite, *J. Geophys. Res. Solid Earth*, 2018, **123**, 2069–2089.
279 E. Attias, K. Weitemeyer, S. Hölz, S. Naif, T. A. Minshull, A. I. Best, A. Haroon, M. Jegen-Kulcsar and C. Berndt, *Geophys. J. Int.*, 2018, **214**, 1701–1714.
280 Z. Weidong, L. Yongjun, R. Shaoran and W. Ruihe, *2011 International Conference on Materials for Renewable Energy & Environment*, IEEE, 2011, vol. 2, pp. 1954–1958.
281 Y. Chen, D. Li, D. Liang, X. Zhou and N. Wu, *Acta Pet. Sin.*, 2013, **34**, 507–512.
282 J. Cai, W. Wei, X. Hu and D. A. Wood, *Earth-Sci. Rev.*, 2017, **171**, 419–433.
283 J. C. Santamarina, F. Francisca, T. S. Yun, J. Y. Lee, A. I. Martin and C. Ruppel, AAPG Hedberg Conference: Gas hydrates: Energy resource potential and associated geological hazards. AAPG, Vancouver, BC, 2004.
284 J. Y. Lee, J. C. Santamarina and C. Ruppel, *J. Geophys. Res. Solid Earth*, 2010, **115**, B11104, DOI: 10.1029/2009JB006669.
285 J. C. Santamarina and C. Ruppel, *Geophys. Charact. Gas Hydrates, Geophys. Dev. Ser.*, 2010, **14**, 373–384.
286 E. Spangenberg and J. Kulenkampff, *Geophys. Res. Lett.*, 2006, **33**, L24315, DOI: 10.1029/2006GL028188.
287 S. R. Ren, Y. Liu, Y. Liu and W. Zhang, *J. Pet. Sci. Eng.*, 2010, **70**, 52–56.
288 Y. F. Chen, D. Q. Liang and N. Y. Wu, *Appl. Mech. Mater.*, 2013, **432**, 104–108.
289 M. E. Permyakov, N. A. Manchenko, A. D. Duchkov, A. Y. Manakov, A. N. Drobchik and A. K. Manshtein, *Russ. Geol. Geophys.*, 2017, **58**, 642–649.
290 M. Pohl, *Ultrasonic and Electrical Properties of Hydrate-Bearing Sediments*, Colorado School of Mine, Arthur Lakes Library, 2018.
291 F.-G. Li, C.-Y. Sun, S.-L. Li, G.-J. Chen, X.-Q. Guo, L.-Y. Yang, H. Pan, S. Li and K. Zhang, *Energy Fuels*, 2012, **26**, 6210–6217.
292 W. L. Du Frane, L. A. Stern, S. Constable, K. A. Weitemeyer, M. M. Smith and J. J. Roberts, *J. Geophys. Res. Solid Earth*, 2015, **120**, 4773–4783.

Open Access Article. Published on 22 Junie 2020. Downloaded on 2026-02-11 12:42:38 nm.. This article is licensed under a Creative Commons Attribution-NonCommercial 3.0 Unported Licence.

293 R. Lu, L. A. Stern, W. L. Du Frane, J. C. Pinkston, J. J. Roberts and S. Constable, *J. Geophys. Res. Solid Earth*, 2019, **124**, 10877–10892, DOI: 10.1029/2019JB018364.
294 X. Hu, C. Zou, Z. Lu, C. Yu, C. Peng, W. Li, Y. Tang, A. Liu and K. S. Kouamelan, *J. Geophys. Eng.*, 2019, **16**, 215–228.
295 H. Pan, H. Li, D. Grana, Y. Zhang, T. Liu and C. Geng, *Mar. Pet. Geol.*, 2019, **105**, 273–283.
296 T. Liu, X. Liu and T. Zhu, *Mar. Pet. Geol.*, 2019, 104036.
297 D. Huaimin, S. Jianmeng, C. Likai, S. Liyuan, Y. Weichao, L. Yafen, L. Zhenzhou and F. Hui, *J. Geophys. Eng.*, 2018, **15**, 1399–1406.
298 H. Dong, J. Sun, Z. Lin, H. Fang, Y. Li, L. Cui and W. Yan, *J. Geophys. Eng.*, 2018, **15**, 275–285.
299 H. Dong, J. Sun, J. Zhu, L. Liu, Z. Lin, N. Golsanami, L. Cui and W. Yan, *Fuel*, 2019, **248**, 27–37.
300 M. Priegnitz, J. Thaler, E. Spangenberg, J. M. Schicks, J. Schrötter and S. Abendroth, *Geophys. J. Int.*, 2015, **202**, 1599–1612.
301 T. Kremer, C. Vieira and A. Maineult, *J. Appl. Geophys.*, 2018, **158**, 11–28.
302 M. B. Helgerud, *Wave speeds in gas hydrate and sediments containing gas hydrate: A laboratory and modeling study*, Stanford University, Palo Alto, 2001.
303 M. B. Helgerud, W. F. Waite, S. H. Kirby and A. Nur, *J. Geophys. Res. Solid Earth*, 2009, **114**, B02212, DOI: 10.1029/2008JB006132.
304 Y. Li, Y. Song, W. Liu and F. Yu, *Energies*, 2012, 5.
305 L. Yanghui, Z. Honghua, Y. Feng, S. Yongchen, L. Weiguo, L. Qingping and Y. Haiyuan, *J. Cold Reg. Eng.*, 2012, **26**, 149–159.
306 L. A. Stern, S. H. Kirby and W. B. Durham, *Science*, 1996, **273**, 1843–1848.
307 L. A. Stern, S. H. Kirby and W. B. Durham, *Energy Fuels*, 1998, **12**, 201–211.
308 W. F. Waite, M. B. Helgerud, A. Nur, J. C. Pinkston, L. A. Stern, S. H. Kirby and W. B. Durham, *Ann. N. Y. Acad. Sci.*, 2000, **912**, 1003–1010.
309 W. F. Kuhs, A. Klapproth, F. Gotthardt, K. Techmer and T. Heinrichs, *Geophys. Res. Lett.*, 2000, **27**, 2929–2932.
310 D. K. Staykova, W. F. Kuhs, A. N. Salamatin and T. Hansen, *J. Phys. Chem. B*, 2003, **107**, 10299–10311.
311 W. F. Kuhs, G. Genov, E. Goreshnik, A. Zeller, K. S. Techmer and G. Bohrmann, *Int. J. Offshore Polar Eng.*, 2004, **14**, ISOPE-04-14-4-305.
312 B. I. Pandit and M. S. King, *Proceedings of the 4th Canadian Permafrost Conference*, 1982, pp. 335–342.
313 M. Bathe, S. Vagle, G. A. Saunders and E. F. Lambson, *J. Mater. Sci. Lett.*, 1984, **3**, 904–906.
314 L. I. Berge, K. A. Jacobsen and A. Solstad, *J. Geophys. Res. Solid Earth*, 1999, **104**, 15415–15424.
315 M. B. Helgerud, W. F. Waite, S. H. Kirby and A. Nur, *Can. J. Phys.*, 2003, **81**, 47–53.
316 M. Pohl, M. Prasad and M. L. Batzle, *Geophys. Prospect.*, 2018, **66**, 1349–1357.
317 B. L. Whiffen, H. Kiefte and M. J. Clouter, *Geophys. Res. Lett.*, 1982, **9**, 645–648.
318 H. Kiefte, M. J. Clouter and R. E. Gagnon, *J. Phys. Chem.*, 1985, **89**, 3103–3108.
319 H. Shimizu, T. Kumazaki, T. Kume and S. Sasaki, *Phys. Rev. B: Condens. Matter Mater. Phys.*, 2002, **65**, 212102.
320 S. Sasaki, T. Kumazaki, I. Suwa, T. Kume and H. Shimizu, *J. Phys.: Condens. Matter*, 2002, **14**, 10445.
321 J. Beam, J. Yang, J. Liu, C. Liu and J.-F. Lin, *J. Chem. Phys.*, 2016, **144**, 154501.
322 W. F. Kuhs, B. Chazallon, P. G. Radaelli and F. Pauer, *J. Inclusion Phenom. Mol. Recognit. Chem.*, 1997, **29**, 65–77.
323 J. S. Loveday, R. J. Nelmes, M. Guthrie, S. A. Belmonte, D. R. Allan, D. D. Klug, J. S. Tse and Y. P. Handa, *Nature*, 2001, **410**, 661–663.
324 B. Chazallon and W. F. Kuhs, *J. Chem. Phys.*, 2002, **117**, 308–320.
325 C. Sanloup, H. Mao and R. J. Hemley, *Proc. Natl. Acad. Sci. U. S. A.*, 2002, **99**, 25–28.
326 A. Klapproth, E. Goreshnik, D. Staykova, H. Klein and W. F. Kuhs, *Can. J. Phys.*, 2003, **81**, 503–518.
327 Z. M. Jendi, A. D. Rey and P. Servio, *Mol. Simul.*, 2015, **41**, 572–579.
328 J. Baumert, C. Gutt, M. Krisch, H. Requardt, M. Müller, J. S. Tse, D. D. Klug and W. Press, *Phys. Rev. B: Condens. Matter Mater. Phys.*, 2005, **72**, 54302.
329 A. Y. Manakov, A. Y. Likhacheva, V. A. Potemkin, A. G. Ogienko, A. V. Kurnosov and A. I. Ancharov, *ChemPhysChem*, 2011, **12**, 2476–2484.
330 D. Wang, D. Li, H. Zhang, S. Fan and H. Zhao, *Sci. China, Ser. G: Phys., Mech. Astron.*, 2008, **51**, 1905–1913.
331 H. Hirai, Y. Uchihara, H. Fujihisa, M. Sakashita, E. Katoh, K. Aoki, K. Nagashima, Y. Yamamoto and T. Yagi, *J. Chem. Phys.*, 2001, **115**, 7066–7070.
332 S. Tanaka, F. Maruyama, O. Takano, K. Uchida and N. Oya, *Int. Confer. Gas Hydrate, Trondheim, Norw*.
333 W. Zhang, Experimental Deformation of Methane Hydrate: New Results, *National Energy Technology Laboratory*, 1999.
334 W. B. Durham, S. H. Kirby, L. A. Stern and W. Zhang, *J. Geophys. Res. Solid Earth*, 2003, 108, DOI: 10.1029/2002JB001872.
335 W. B. Durham, L. A. Stern and S. H. Kirby, *Can. J. Phys.*, 2003, **81**, 373–380.
336 J. Jia, Y. Liang, T. Tsuji, S. Murata and T. Matsuoka, *Sci. Rep.*, 2016, **6**, 23548.
337 F. Yu, Y. Song, W. Liu, Y. Li and W. Lam, *J. Pet. Sci. Eng.*, 2011, **77**, 183–188.
338 Y. Li, W. Liu, Y. Song, M. Yang and J. Zhao, *J. Nat. Gas Sci. Eng.*, 2016, **33**, 347–354.
339 M. Hyodo, Y. Nakata, N. Yoshimoto, M. Fukunaga, K. Kubo, Y. Nanjo, T. Matsuo, A. F. L. Hyde and K. Nakamura, *The Twelfth International Offshore and Polar Engineering Conference*, International Society of Offshore and Polar Engineers, 2002.
340 Y. Nabeshima and T. T. Matsui, Static Shear Behaviors of Methane Hydrate and Ice, *Proc. ISOPE Ocean Min. Symp.*, 2003, 156–159.

 This journal is © The Royal Society of Chemistry 2020

Open Access Article. Published on 22 Junie 2020. Downloaded on 2026-02-11 12:42:38 nm..
This article is licensed under a Creative Commons Attribution-NonCommercial 3.0 Unported Licence.

341 Y. Nabeshima and T. Matsui, *Fifth ISOPE Ocean Min. Symp.*, 2003, 4.
342 Y. Nabeshima, Y. Takai and T. Komai, Sixth ISOPE Ocean Min. Symp., 2005, 4.
343 Y. Song, F. Yu, Y. Li, W. Liu and J. Zhao, *J. Nat. Gas Chem.*, 2010, **19**, 246–250.
344 F. Yu, Y. Song, W. Liu, Y. Li and J. Zhao, *Proc. Int. Conf. Offshore Mech. Arct. Eng.*, 2010, 705–710, DOI: 10.1115/OMAE2010-21174.
345 C. R. Miranda and T. Matsuoka, Proceedings of the 6th International Conference on Gas Hydrates, 2008.
346 T. M. Vlasic, P. D. Servio and A. D. Rey, *Cryst. Growth Des.*, 2017, **17**, 6407–6416.
347 X. Zong, G. Cheng, N. Qiu, Q. Huang, J. He, S. Du and Y. Li, *Chem. Lett.*, 2017, **46**, 1141–1144.
348 Z. M. Jendi, *Multiscale Modelling of Gas Hydrate Mechanical and Thermal Properties*, McGill University, 2015.
349 T. M. Vlasic, P. D. Servio and A. D. Rey, *Ind. Eng. Chem. Res.*, 2019, **58**, 16588–16596.
350 H. Huo, Y. Liu, Z. Zheng, J. Zhao, C. Jin and T. Lv, *J. Renewable Sustainable Energy*, 2011, **3**, 63110.
351 T. M. Vlasic, P. Servio and A. D. Rey, *AIP Adv.*, 2016, **6**, 85317.
352 Z. M. Jendi, P. Servio and A. D. Rey, *Phys. Chem. Chem. Phys.*, 2016, **18**, 10320–10328.
353 J. Wu, F. Ning, T. T. Trinh, S. Kjelstrup, T. J. H. Vlugt, J. He, B. H. Skallerud and Z. Zhang, *Nat. Commun.*, 2015, **6**, 8743.
354 J. Jia, Y. Liang, T. Tsuji, S. Murata and T. Matsuoka, *Sci. Rep.*, 2017, **7**, 1290.
355 F. Ning, K. Glavatskiy, T. Vlugt and S. Kjelstrup, *Prepr. Pap. – Am. Chem. Soc., Div. Fuel Chem.*, 2010, **55**, 1.
356 H. Jiang and K. D. Jordan, *J. Phys. Chem. C*, 2010, **114**, 5555–5564.
357 H. A. Sveinsson, *Molecular modeling of fracture in methane hydrates*, MS thesis, 2015.
358 P. Cao, J. Wu, Z. Zhang, B. Fang and F. Ning, *J. Phys. Chem. C*, 2018, **122**, 29081–29093.
359 H. A. Sveinsson and A. Malthe-Sørenssen, *Phys. Chem. Chem. Phys.*, 2019, **21**, 13539–13544.
360 S. V. Gudkovskikh and M. V. Kirov, *J. Mol. Model.*, 2019, **25**, 32.
361 S. Cai, Q. Tang, S. Tian, Y. Lu and X. Gao, *Int. J. Mol. Sci.*, 2019, 20.
362 J. Wu, B. Skallerud, J. He and Z. Zhang, *Procedia IUTAM*, 2017, **21**, 11–16.
363 Q. Shi, P. Cao, Z. Han, F. Ning, H. Gong, Y. Xin, Z. Zhang and J. Wu, *Cryst. Growth Des.*, 2018, **18**, 6729–6741.
364 V. P. Shpakov, J. S. Tse, C. A. Tulk, B. Kvamme and V. R. Belosludov, *Chem. Phys. Lett.*, 1998, **282**, 107–114.
365 V. R. Belosludov, V. P. Shpakov, J. S. Tse, R. V. Belosludov and Y. Kawazoe, *Ann. N. Y. Acad. Sci.*, 2000, **912**, 993–1002.
366 Z. M. Jendi, P. Servio and A. D. Rey, *Cryst. Growth Des.*, 2015, **15**, 5301–5309.
367 A. O. Akheramka, *Molecular Dynamics Simulations to Study the Effect of Fracturing on the Efficiency Of CH4–CO2 Replacement in Hydrates*, University of Alaska Fairbanks, 2018.
368 S. M. Daghash, P. Servio and A. D. Rey, *Mol. Simul.*, 2019, 1–14.
369 L. Lei and J. C. Santamarina, *Mar. Pet. Geol.*, 2019, **109**, 899–911.
370 S. Goto, O. Matsubayashi and S. Nagakubo, *J. Geophys. Res. Solid Earth*, 2016, **121**, 3200–3219.
371 J. Rutqvist, G. J. Moridis, T. Grover and T. Collett, *J. Pet. Sci. Eng.*, 2009, **67**, 1–12.
372 J. Yoneda, A. Masui, Y. Konno, Y. Jin, K. Egawa, M. Kida, T. Ito, J. Nagao and N. Tenma, *Mar. Pet. Geol.*, 2014, **66**, 471–486.
373 H. Lee, Y. Seo, Y. T. Seo, I. L. Moudrakovski and J. A. Ripmeester, *Angew. Chem., Int. Ed.*, 2003, **42**, 5048–5051.
374 T. S. Collett, Proc. 4th Int. Conf. Gas Hydrate, 2002, 2002.
375 J. Rutqvist and G. J. Moridis, *Offshore Technol. Conf.*, 2008, 17.
376 F. Ning, N. Wu, Y. Yu, K. Zhang, G. Jiang, L. Zhang, J. Sun and M. Zheng, *Geophys. J. Int.*, 2013, **193**, 1385–1398.
377 J. Sun, F. Ning, H. Lei, X. Gai, M. Sánchez, J. Lu, Y. Li, L. Liu, C. Liu, N. Wu, Y. He and M. Wu, *J. Pet. Sci. Eng.*, 2018, **170**, 345–367.
378 H. N. Wang, X. P. Chen, M. J. Jiang and Z. Y. Guo, *J. Nat. Gas Sci. Eng.*, 2019, **68**, 102885.
379 N. Sultan, P. Cochonat, J.-P. Foucher and J. Mienert, *Mar. Geol.*, 2004, **213**, 379–401.
380 M. Maslin, M. Owen, R. Betts, S. Day, T. D. Jones and A. Ridgwell, *Philos. Trans. R. Soc., A*, 2010, **368**, 2369–2393.
381 K. P. Lijith, B. R. C. Malagar and D. N. Singh, *Mar. Pet. Geol.*, 2019, **104**, 270–285.
382 B. Song, Y. Cheng, C. Yan, Y. Lyu, J. Wei, J. Ding and Y. Li, *J. Nat. Gas Sci. Eng.*, 2019, **65**, 197–211.
383 A. L. Handwerger, A. W. Rempel and R. M. Skarbek, *Geochem., Geophys., Geosyst.*, 2017, **18**, 2429–2445.
384 A. Li, R. J. Davies and J. Yang, *Mar. Geol.*, 2016, **380**, 264–271.
385 J. A. Priest, C. R. I. Clayton and E. V. L. Rees, *Mar. Pet. Geol.*, 2014, **58**, 187–198.
386 J. Yoneda, A. Masui, Y. Konno, Y. Jin, K. Egawa, M. Kida, T. Ito, J. Nagao and N. Tenma, *Mar. Pet. Geol.*, 2015, **66**, 451–459.
387 K. Miyazaki, A. Masui, Y. Sakamoto, K. Aoki, N. Tenma and T. Yamaguchi, *J. Geophys. Res. Solid Earth*, 2011, **116**, B06102, DOI: 10.1029/2010JB008049.
388 Y. Li, Y. Song, F. Yu, W. Liu and R. Wang, *Pet. Explor. Dev.*, 2011, **38**, 637–640.
389 M. Hyodo, Y. Li, J. Yoneda, Y. Nakata, N. Yoshimoto, A. Nishimura and Y. Song, *J. Geophys. Res. Solid Earth*, 2013, **118**, 5185–5194.
390 Z. Liu, H. Wei, L. Peng, C. Wei and F. Ning, *J. Pet. Sci. Eng.*, 2017, **149**, 56–64.
391 B. Wang, P. Huo, T. Luo, Z. Fan, F. Liu, B. Xiao, M. Yang, J. Zhao and Y. Song, *Energies*, 2017, **10**, 531.
392 T. S. Yun, F. M. Francisca, J. C. Santamarina and C. Ruppel, *Geophys. Res. Lett.*, 2005, **32**, L10609, DOI: 10.1029/2005GL022607.

Open Access Article. Published on 22 Junie 2020. Downloaded on 2026-02-11 12:42:38 nm..
This article is licensed under a Creative Commons Attribution-NonCommercial 3.0 Unported Licence.

393 T. S. Yun, J. C. Santamarina and C. Ruppel, *J. Geophys. Res. Solid Earth*, 2007, **112**, B04106, DOI: 10.1029/2006JB004484.
394 J. Jang and J. C. Santamarina, *Mar. Pet. Geol.*, 2016, **77**, 235–246.
395 M. Ben Clennell, M. Hovland, J. S. Booth, P. Henry and W. J. Winters, *J. Geophys. Res. Solid Earth*, 1999, **104**, 22985–23003.
396 C. R. I. Clayton, J. A. Priest and E. V. L. Rees, *Geotechnique*, 2010, **60**, 435.
397 L. Lei and J. C. Santamarina, *J. Geophys. Res. Solid Earth*, 2018, **123**, 2583–2596.
398 W. Lingyun and J. L. Grozic, *J. Geotech. Geoenviron. Eng.*, 2008, **134**, 547–550.
399 Y. Xu, Y. Seol, J. Jang and S. Dai, *Geotechnical Frontiers 2017*, 2017, pp. 766–772.
400 S. Dai, J. C. Santamarina, W. F. Waite and T. J. Kneafsey, *J. Geophys. Res. Solid Earth*, 2012, **117**, B11205, DOI: 10.1029/2012JB009667.
401 N. Mahabadi, S. Dai, Y. Seol and J. Jang, *J. Pet. Sci. Eng.*, 2019, **174**, 696–703.
402 W. F. Waite, J. C. Santamarina, D. D. Cortes, B. Dugan, D. N. Espinoza, J. Germaine, J. Jang, J. W. Jung, T. J. Kneafsey and H. Shin, *Rev. Geophys.*, 2009, **47**(4), DOI: 10.1029/2008RG000279.
403 X. Ren, Z. Guo, F. Ning and S. Ma, *Earth-Sci. Rev.*, 2020, 103100.
404 L. Lei, Z. Liu, Y. Seol, R. Boswell and S. Dai, *J. Geophys. Res. Solid Earth*, 2019, **124**, 3335–3349.
405 S. Dai, R. Boswell, W. F. Waite, J. Jang, J. Y. Lee and Y. Seol, *The 9th International Conference on Gas Hydrates*, 2017, pp. 25–30.
406 C. D. Ruppel, J. Y. Lee and I. Pecher, *J. Geophys. Res. Solid Earth*, 2019, **124**, 7525–7537.
407 J. Jang, S. Dai, J. Yoneda, W. F. Waite, L. A. Stern, L.-G. Boze, T. S. Collett and P. Kumar, *Mar. Pet. Geol.*, 2019, **108**, 537–550.
408 M. T. Reagan and G. J. Moridis, *Geophys. Res. Lett.*, 2007, **34**, L22709, DOI: 10.1029/2007GL031671.
409 H. Minagawa, R. Ohmura, Y. Kamata, T. Ebinuma, H. Narita and Y. Masuda, *Fifth International Conference on Gas Hydrates*, Tapir Acad. Trondheim, Norway, 2005, p. 1058.
410 A. Kumar, B. Maini, P. R. Bishnoi, M. Clarke, O. Zatsepina and S. Srinivasan, *J. Pet. Sci. Eng.*, 2010, **70**, 114–122.
411 H. Liang, Y. Song, Y. Chen and Y. Liu, *Pet. Sci. Technol.*, 2011, **29**, 79–87.
412 A. Johnson, S. Patil and A. Dandekar, *Mar. Pet. Geol.*, 2011, **28**, 419–426.
413 B. Li, X.-S. Li, G. Li, J.-L. Jia and J.-C. Feng, *Energies*, 2013, **6**, 3622–3636.
414 M. L. Delli and J. L. H. Grozic, *J. Pet. Sci. Eng.*, 2014, **120**, 1–9.
415 C.-H. Li, Q. Zhao, H.-J. Xu, K. Feng and X.-W. Liu, *Appl. Geophys.*, 2014, **11**, 207–214.
416 Y. Konno, J. Yoneda, K. Egawa, T. Ito, Y. Jin, M. Kida, K. Suzuki, T. Fujii and J. Nagao, *Mar. Pet. Geol.*, 2014, **66**, 487–495.
417 W. Liu, Z. Wu, Y. Li, Y. Song, Z. Ling, J. Zhao and Q. Lv, *J. Nat. Gas Sci. Eng.*, 2016, **36**, 378–384.
418 G. Li, D.-M. Wu, X.-S. Li, Q.-N. Lv, C. Li and Y. Zhang, *Appl. Energy*, 2017, **202**, 282–292.
419 Z. Wu, Y. Li, X. Sun, P. Wu and J. Zheng, *Appl. Energy*, 2018, **230**, 1304–1310.
420 S. Dai, J. Kim, Y. Xu, W. F. Waite, J. Jang, J. Yoneda, T. S. Collett and P. Kumar, *Mar. Pet. Geol.*, 2019, **108**, 705–713, DOI: 10.1016/j.marpetgeo.2018.08.016.
421 D. W. Meyer, P. B. Flemings, D. DiCarlo, K. You, S. C. Phillips and T. J. Kneafsey, *J. Geophys. Res. Solid Earth*, 2018, **123**, 5350–5371.
422 J. Yoneda, M. Oshima, M. Kida, A. Kato, Y. Konno, Y. Jin, J. Jang, W. F. Waite, P. Kumar and N. Tenma, *Mar. Pet. Geol.*, 2019, **108**, 524–536.
423 Z. Wu, Y. Li, X. Sun, M. Li and R. Jia, *Mar. Pet. Geol.*, 2018, **91**, 373–380.
424 A. Okwananke, A. Hassanpouryouzband, M. Vasheghani Farahani, J. Yang, B. Tohidi, E. Chuvilin, V. Istomin and B. Bukhanov, *J. Pet. Sci. Eng.*, 2019, **180**, 435–444.
425 J. Zhang, Y. Ye, G. Hu and S. Diao, Experimental Techniques for Permeability and Mechanical Properties of Hydrate-Bearing Sediments, in *Natural Gas Hydrates*, ed. Y. Ye and C. Liu, Springer Berlin Heidelberg, Berlin, Heidelberg, 2013, pp. 169–192.
426 S. K. Garg, J. W. Pritchett, A. Katoh, K. Baba and T. Fujii, *J. Geophys. Res. Solid Earth*, 2008, **113**, B01201, DOI: 10.1029/2006JB004768.
427 Q. Zhao, K.-J. Dunn and X.-W. Liu, *Appl. Geophys.*, 2011, **8**, 101–109.
428 M. L. Delli and J. L. H. Grozic, *SPE J.*, 2013, **18**, 274–284.
429 S. Chatterjee, G. Bhatnagar, B. Dugan, G. R. Dickens, W. G. Chapman and G. J. Hirasaki, *J. Geophys. Res. Solid Earth*, 2014, **119**, 6705–6732.
430 S. Dai and Y. Seol, *Geophys. Res. Lett.*, 2014, **41**, 4176–4184.
431 K. N. Darnell and P. B. Flemings, *Geophys. Res. Lett.*, 2015, **42**, 10–765.
432 D. H. Kang, T. S. Yun, K. Y. Kim and J. Jang, *Geophys. Res. Lett.*, 2016, **43**, 9018–9025.
433 H. Daigle, *J. Pet. Sci. Eng.*, 2016, **146**, 526–535.
434 J. Katagiri, Y. Konno, J. Yoneda and N. Tenma, *J. Nat. Gas Sci. Eng.*, 2017, **45**, 537–551.
435 J. Behseresht and S. L. Bryant, *J. Geophys. Res. Solid Earth*, 2017, **122**, 3585–3623.
436 K. You and P. B. Flemings, *J. Geophys. Res. Solid Earth*, 2018, **123**, 4582–4600.
437 P. Mohammadmoradi and A. Kantzas, *Mar. Pet. Geol.*, 2018, **89**, 786–798.
438 J. Liu, M. Haeckel, J. Rutqvist, S. Wang and W. Yan, *J. Geophys. Res. Solid Earth*, 2019, **124**, 4399–4427.
439 L. Wei, A. Cook, H. Daigle, A. Malinverno, M. Nole and K. You, *Geochem., Geophys., Geosyst.*, 2019, **20**, 3985–4000.
440 H. Singh, E. M. Myshakin and Y. Seol, *SPE J.*, 2019, **24**, 547–562.
441 J. Nimblett and C. Ruppel, *J. Geophys. Res. Solid Earth*, 2003, **108**(B9), DOI: 10.1029/2001jb001650.

 This journal is © The Royal Society of Chemistry 2020

Open Access Article. Published on 22 Junie 2020. Downloaded on 2026-02-11 12:42:38 nm..
This article is licensed under a Creative Commons Attribution-NonCommercial 3.0 Unported Licence.

442 M. Kurihara, K. Funatsu, H. Ouchi, Y. Masuda, M. Yasuda, K. Yamamoto, M. Numasawa, T. Fujii, H. Narita and S. R. Dallimore, *Proceedings of the 6th International Conference on Gas Hydrates (ICGH 2008)*, Vancouver, British Columbia, 2008.
443 E. M. Myshakin, B. J. Anderson, K. Rose and R. Boswell, *Energy Fuels*, 2011, **25**, 1077–1091.
444 E. M. Myshakin, M. Gaddipati, K. Rose and B. J. Anderson, *Mar. Pet. Geol.*, 2012, **34**, 169–185.
445 N. Mahabadi and J. Jang, *Geochem., Geophys., Geosyst.*, 2014, **15**, 2346–2353.
446 J. Sun, F. Ning, S. Li, K. Zhang, T. Liu, L. Zhang, G. Jiang and N. Wu, *J. Unconv. Oil Gas Resour.*, 2015, **12**, 23–33.
447 N. Mahabadi, S. Dai, Y. Seol, T. Sup Yun and J. Jang, *Geochem., Geophys., Geosyst.*, 2016, **17**, 3099–3110.
448 N. Mahabadi, X. Zheng and J. Jang, *Geophys. Res. Lett.*, 2016, **43**, 4279–4287.
449 B. P. VanderBeek and A. W. Rempel, *J. Geophys. Res. Solid Earth*, 2018, **123**, 5394–5411.
450 Y. Jin, J. Hayashi, J. Nagao, K. Suzuki, H. Minagawa, T. Ebinuma and H. Narita, *Jpn. J. Appl. Phys.*, 2007, **46**, 3159–3162.
451 Y. Seol and T. J. Kneafsey, *J. Geophys. Res. Solid Earth*, 2011, **116**, B08102.
452 T. J. Kneafsey, Y. Seol, A. Gupta and L. Tomutsa, *SPE J.*, 2011, **16**, 78–94.
453 Y. Konno, Y. Jin, T. Uchiumi and J. Nagao, *Rev. Sci. Instrum.*, 2013, **84**, 64501.
454 J.-Q. Wang, J.-F. Zhao, M.-J. Yang, Y.-H. Li, W.-G. Liu and Y.-C. Song, *Fuel*, 2015, **145**, 170–179.
455 X. Chen, R. Verma, D. N. Espinoza and M. Prodanović, *Water Resour. Res.*, 2018, **54**, 600–608.
456 E. Kossel, C. Deusner, N. Bigalke and M. Haeckel, *J. Geophys. Res. Solid Earth*, 2018, **123**, 1235–1251.
457 J. Wang, L. Zhang, J. Zhao, L. Ai and L. Yang, *J. Nat. Gas Sci. Eng.*, 2018, **51**, 141–146.
458 S. Chanda and R. P. Singh, *Therm. Sci. Eng. Prog.*, 2019, **11**, 380–391.
459 J. Joseph, D. N. Singh, P. Kumar, S. K. Dewri, C. Tandi and J. Singh, *Mar. Georesour. Geotechnol.*, 2016, **34**, 450–464.
460 S. C. Cao, J. Jang, J. Jung, W. F. Waite, T. S. Collett and P. Kumar, *Mar. Pet. Geol.*, 2019, **108**, 714–730, DOI: 10.1016/j.marpetgeo.2018.09.010.
461 M. Vasheghani Farahani, S. Foroughi, S. Norouzi and S. Jamshidi, *J. Energy Resour. Technol.*, 2019, **141**(12), DOI: 10.1115/1.4044976.
462 J. W. Jung, J. Jang, J. C. Santamarina, C. Tsouris, T. J. Phelps and C. J. Rawn, *Energy Fuels*, 2012, **26**, 480–487.
463 G. Han, T. Kwon, J. Y. Lee and T. J. Kneafsey, *J. Geophys. Res. Solid Earth*, 2018, **123**, 2539–2558.
464 Z. A. Jarrar, R. I. Al-Raoush, J. A. Hannun, K. A. Alshibli and J. Jung, *Geomech. Energy Environ.*, 2018, 100105.
465 G. Han, T.-H. Kwon, J. Y. Lee and J. Jung, *Geomech. Energy Environ.*, 2019, 100131.
466 C. Shuang, J. Jung and T. Kwon, *The Characteristics of Fines Migration and Clogging of Sediments Recovered from the Gas Hydrate Deposits from the Ulleng Basin, East Sea, Korea, Proceedings of the XVII ECSMGE*, 2019.
467 J. Jung, H. Kang, S. C. Cao, R. I. Al-Raoush, K. Alshibli and J. Y. Lee, *Geofluids*, 2019, DOI: 10.1155/2019/5061216.
468 G. Moridis, T. S. Collett, M. Pooladi-Darvish, S. H. Hancock, C. Santamarina, R. Boswell, T. J. Kneafsey, J. Rutqvist, M. B. Kowalsky, M. T. Reagan, E. D. Sloan, A. Sum and C. Koh, *SPE Reserv. Eval. Eng.*, 2011, **14**, 76–112.
469 W. M. Mahmud, S. Elmabrouk and H. K. Ben Mahmud, *Int. J. Pet. Petrochemical Eng. Vol.*, 2017, **3**, 54–64.
470 J. Choi, S. Dai, J. Cha and Y. Seol, *Geochem., Geophys., Geosyst.*, 2014, **15**, 1648–1656.
471 J. Wang, P. Jaiswal, S. S. Haines, P. E. Hart and S. Wu, *Geophysics*, 2018, **83**, B167–B181.
472 Q. T. Bu, G. W. Hu, Y. G. Ye, C. L. Liu, C. F. Li, A. I. Best and J. S. Wang, *J. Geophys. Eng.*, 2017, **14**, 555–569.
473 M. Riedel, E. C. Willoughby and S. Chopra, *Geophysical characterization of gas hydrates*, Society of Exploration Geophysicists, 2010.
474 A. I. Best, J. A. Priest, C. R. I. Clayton and E. V. L. Rees, *Earth Planet. Sci. Lett.*, 2013, **368**, 78–87.
475 Y. Luo, J. Peng, P. Li, J. He and L. Li, *J. Nat. Gas Sci. Eng.*, 2015, **22**, 90–97.
476 R. Ghosh, K. Sain and M. Ojha, *Mar. Geophys. Res.*, 2010, **31**, 29–37.
477 Z. Zhang, D. H. Han and Q. Yao, *Geophysics*, 2011, **76**, B139–B150.
478 R. Dash and G. Spence, *Geophys. J. Int.*, 2011, **187**, 1363–1377.
479 A. Schlesinger, J. Cullen, G. Spence, R. Hyndman, K. Louden and D. Mosher, *Mar. Pet. Geol.*, 2012, **35**, 105–115.
480 Z. Zhang, D. R. McConnell and D. H. Han, *Mar. Pet. Geol.*, 2012, **34**, 119–133.
481 J. I. T. Hillman, A. E. Cook, H. Daigle, M. Nole, A. Malinverno, K. Meazell and P. B. Flemings, *Mar. Pet. Geol.*, 2017, **86**, 1357–1373.
482 J. Wang, P. Jaiswal, S. S. Haines, Y. Yang, P. E. Hart and S. Wu, *Interpretation*, 2019, 1–56.
483 N. Satyavani and K. Sain, *Mar. Georesources Geotechnol.*, 2015, **33**, 191–201.
484 Y. Konno, Y. Jin, J. Yoneda, M. Kida, K. Egawa, T. Ito, K. Suzuki and J. Nagao, *Mar. Pet. Geol.*, 2014, **66**, 425–433.
485 R. Chatterjee, D. K. Singha, M. Ojha, M. K. Sen and K. Sain, *J. Nat. Gas Sci. Eng.*, 2016, **33**, 562–572.
486 J. Qian, X. Wang, T. S. Collett, D. Dong, Y. Guo, P. Su and J. Liang, *Interpretation*, 2017, **5**, SM33–SM48.
487 X. Wang, B. Liu, J. Qian, X. Zhang, Y. Guo, P. Su, J. Liang, J. Jin, Z. Luan, D. Chen, S. Xi and C. Li, *J. Asian Earth Sci.*, 2018, **168**, 27–37.
488 J. Guan and D. Liang, *Mar. Pet. Geol.*, 2018, **91**, 225–235.
489 S. Gullapalli, P. Dewangan, A. Kumar, G. Dakara and C. K. Mishra, *Mar. Pet. Geol.*, 2019, **110**, 695–705.
490 C. K. Mishra, P. Dewangan, G. Sriram, A. Kumar and G. Dakara, *Mar. Pet. Geol.*, 2019, 104037.
491 S. Singhroha, S. Chand and S. Bünz, *J. Geophys. Res. Solid Earth*, 2019, **124**, 4343–4364, DOI: 10.1029/2018JB016574.

Open Access Article. Published on 22 Junie 2020. Downloaded on 2026-02-11 12:42:38 nm..
This article is licensed under a Creative Commons Attribution-NonCommercial 3.0 Unported Licence.

492 T. A. Minshull, H. Marín-Moreno, P. Betlem, J. Bialas, S. Bünz, E. Burwicz, A. L. Cameselle, G. Cifci, M. Giustiniani, J. I. T. Hillman, S. Hölz, J. R. Hopper, G. Ion, R. León, V. Magalhaes, Y. Makovsky, M.-P. Mata, M. D. Max, T. Nielsen, S. Okay, I. Ostrovsky, N. O'Neill, L. M. Pinheiro, A. A. Plaza-Faverola, D. Rey, S. Roy, K. Schwalenberg, K. Senger, S. Vadakkepuliyambatta, A. Vasilev and J.-T. Vázquez, *Mar. Pet. Geol.*, 2020, **111**, 735–764.
493 M. Nyamapfumba and G. A. McMechan, *Geophysics*, 2012, **77**, O55–O63.
494 J. Wei, T. Pape, N. Sultan, J. L. Colliat, T. Himmler, L. Ruffine, A. de Prunelé, B. Dennielou, S. Garziglia, T. Marsset, C. A. Peters, A. Rabiu and G. Bohrmann, *Mar. Pet. Geol.*, 2015, **59**, 359–370.
495 A. N. Le, M. Huuse, J. Redfern, R. L. Gawthorpe and D. Irving, *Mar. Pet. Geol.*, 2015, **68**, 629–647.
496 O. T. Akinsanpe, A. A. Adepelumi, U. K. Benjamin and D. E. Falebita, *J. Ocean Univ. China*, 2017, **16**, 1027–1034.
497 G. J. Crutchley, D. R. A. Fraser, I. A. Pecher, A. R. Gorman, G. Maslen and S. A. Henrys, *J. Geophys. Res. Solid Earth*, 2015, **120**, 725–743.
498 G. J. Crutchley, G. Maslen, I. A. Pecher and J. J. Mountjoy, *Interpretation*, 2016, **4**, SA1–SA12.
499 D. R. A. Fraser, A. R. Gorman, I. A. Pecher, G. J. Crutchley and S. A. Henrys, *Mar. Pet. Geol.*, 2016, **77**, 399–408.
500 S. Koch, H. Schroeder, M. Haeckel, C. Berndt, J. Bialas, C. Papenberg, D. Klaeschen and A. Plaza-Faverola, *Geo-Mar. Lett.*, 2016, **36**, 187–196.
501 H. Wang, G. J. Crutchley and T. Stern, *Mar. Pet. Geol.*, 2017, **88**, 69–80.
502 A. R. Gorman, P. T. Fletcher, D. Baker, D. R. A. Fraser, G. J. Crutchley and S. A. Henrys, *ASEG Ext. Abstr.*, 2018, **2018**, 1–4.
503 U. Majumdar, A. E. Cook, W. Shedd and M. Frye, *Geophys. Res. Lett.*, 2016, **43**, 7044–7051.
504 J. A. Priest, A. I. Best and C. R. I. Clayton, *J. Geophys. Res. Solid Earth*, 2005, **110**, 1–13.
505 J. I. T. Hillman, A. E. Cook, D. E. Sawyer, H. M. Küçük and D. S. Goldberg, *Earth Planet. Sci. Lett.*, 2017, **459**, 157–169.
506 P. Aird, in *Deepwater Drilling*, ed. P. B. T.-D. D. Aird, Gulf Professional Publishing, 2019, pp. 17–68.
507 W. Xu and C. Ruppel, *J. Geophys. Res. Solid Earth*, 1999, **104**, 5081–5095.
508 C. Ecker, J. Dvorkin and A. Nur, *Geophysics*, 1998, **63**, 1659–1669.
509 D. C. Mosher, *Mar. Pet. Geol.*, 2011, **28**, 1540–1553.
510 W. Shedd, R. Boswell, M. Frye, P. Godfriaux and K. Kramer, *Mar. Pet. Geol.*, 2012, **34**, 31–40.
511 G. Sriram, P. Dewangan, T. Ramprasad and P. Rama Rao, *J. Geophys. Res. Solid Earth*, 2013, **118**, 2258–2274.
512 J. Qian, X.-J. Wang, S.-G. Wu, Z. Wang and S.-X. Yang, *Mar. Geophys. Res.*, 2014, **35**, 125–140.
513 B. Hosseini Shoar, A. Javaherian, N. Keshavarz Farajkhah and M. Seddigh Arabani, *Mar. Pet. Geol.*, 2014, **51**, 184–196.
514 R.-W. Zhang, H.-Q. Li, B.-J. Zhang, H.-D. Huang and P.-F. Wen, *Appl. Geophys.*, 2015, **12**, 453–464.
515 T. Liu and X. Liu, *Geophysics*, 2018, **83**, B143–B154.
516 K. P. Arun, K. Sain and J. Kumar, *J. Nat. Gas Sci. Eng.*, 2018, **50**, 90–100.
517 Y. Mi, A. Sakai, R. Walia, R. D. Hyndman and S. R. Dallimore, *CREWES Res. Rep*.
518 H. Tak, J. Byun, S. J. Seol and D. G. Yoo, *Mar. Pet. Geol.*, 2013, **47**, 204–213.
519 U. S. Yadav, K. M. Shukla, M. Ojha, P. Kumar and U. Shankar, *Mar. Pet. Geol.*, 2019, **108**, 551–561, DOI: 10.1016/j.marpetgeo.2019.02.001.
520 G. W. Hu, Y. G. Ye, J. Zhang, C. L. Liu, S. B. Diao and J. S. Wang, *J. Geophys. Res. Solid Earth*, 2010, **115**, B02102, DOI: 10.1029/2008JB006160.
521 Q. Zhang, F.-G. Li, C.-Y. Sun, Q.-P. Li, X.-Y. Wu, B. Liu and G.-J. Chen, *Am. Mineral.*, 2011, **96**, 1425–1432.
522 G. W. Hu, Y. G. Ye, J. Zhang, S. B. Diao and C. L. Liu, *Chin. J. Geophys.*, 2012, **55**, 635–647, DOI: 10.1002/cjg2.1758.
523 G. Hu, Y. Ye, J. Zhang, C. Liu and Q. Li, *Mar. Pet. Geol.*, 2014, **52**, 1–8.
524 M. Schindler, M. L. Batzle and M. Prasad, *Geophys. Prospect.*, 2017, **65**, 1025–1036.
525 D. Sadeq, K. Alef, S. Iglauer, M. Lebedev and A. Barifcani, *Int. J. Hydrogen Energy*, 2018, **43**, 23193–23200.
526 X. Li, Y. Liu, H. Zhang, B. Xiao, X. Lv, H. Yao, W. Pang, Q. Li, L. Yang, Y. Song and J. Zhao, *Energies*, 2019, **12**(10), 1997.
527 Z. Liu, J. Kim, L. Lei, F. Ning and S. Dai, *J. Geophys. Res. Solid Earth*, 2019, **124**, 3307–3319.
528 T. S. Yun, *Mechanical and Thermal Study of Hydrate Bearing Sediments*, Georgia Institute of Technology, 2005.
529 W. J. Winters, W. F. Waite, D. H. Mason, L. Y. Gilbert and I. A. Pecher, *J. Pet. Sci. Eng.*, 2007, **56**, 127–135.
530 D. N. Espinoza and J. C. Santamarina, *Int. J. Greenhouse Gas Control*, 2011, **5**, 1031–1038.
531 H.-S. Kim, G.-C. Cho and T.-H. Kwon, *Geochem., Geophys., Geosyst.*, 2013, **14**, 1787–1799.
532 X.-H. Wang, F.-G. Li, Y.-X. Xu, C.-Y. Sun, H. Pan, B. Liu, L.-Y. Yang, G.-J. Chen and Q.-P. Li, *Energy Convers. Manage.*, 2015, **99**, 274–281.
533 S. Chand, T. A. Minshull, D. Gei and J. M. Carcione, *Geophys. J. Int.*, 2004, **159**, 573–590.
534 X. Liu, X. Yin and X. Luan, *Sci. China: Earth Sci.*, 2018, **61**, 1261–1278.
535 D. Sava and B. Hardage, Rock-Physics Models for Gas-Hydrate Systems Associated with Unconsolidated Marine Sediments, in *Natural Gas Hydrates–Energy Resource Potential and Associated Geologic Hazards*, ed. T. Collett, A. Johnson, C. Knapp and R. Boswell, AAPG Memoir 89, 2009, pp. 505–524.
536 H. Pan, H. Li, J. Chen, Y. Zhang, X. Liu, S. Cai and C. Cao, *J. Pet. Sci. Eng.*, 2019, **182**, 106268.
537 G. A. Dugarov, A. A. Duchkov, A. D. Duchkov and A. N. Drobchik, *J. Nat. Gas Sci. Eng.*, 2019, **63**, 38–46.
538 S. Chand, T. A. Minshull, J. A. Priest, A. I. Best, C. R. I. Clayton and W. F. Waite, *Geophys. J. Int.*, 2006, **166**, 543–552.
539 F. I. Zyserman, P. M. Gauzellino and J. E. Santos, *J. Appl. Geophys.*, 2012, **86**, 98–108.

Open Access Article. Published on 22 Junie 2020. Downloaded on 2026-02-11 12:42:38 nm..
This article is licensed under a Creative Commons Attribution-NonCommercial 3.0 Unported Licence.

540 H. Marín-Moreno, S. K. Sahoo and A. I. Best, *J. Geophys. Res. Solid Earth*, 2017, **122**, 1835–1847.
541 W. Liu, J. Zhao, Y. Luo, Y. Song, Y. Li, M. Yang, Y. Zhang, Y. Liu and D. Wang, *Mar. Pet. Geol.*, 2013, **46**, 201–209.
542 Z. M. Sun, J. Zhang, C. L. Liu, S. J. Zhao and Y. G. Ye, *Appl. Mech. Mater.*, 2013, **275–277**, 326–331.
543 H. Ghiassian and J. L. H. Grozic, *Mar. Pet. Geol.*, 2013, **43**, 310–319.
544 S. Pinkert and J. L. H. Grozic, *J. Geophys. Res. Solid Earth*, 2016, **121**, 4147–4155.
545 W. Liu, T. Luo, Y. Li, Y. Song, Y. Zhu, Y. Liu, J. Zhao, Z. Wu and X. Xu, *J. Nat. Gas Sci. Eng.*, 2016, **32**, 20–27.
546 T. Luo, Y. Song, Y. Zhu, W. Liu, Y. Liu, Y. Li and Z. Wu, *Mar. Pet. Geol.*, 2016, **77**, 507–514.
547 S. Gupta, C. Deusner, M. Haeckel, R. Helmig and B. Wohlmuth, *Geochem., Geophys., Geosyst.*, 2017, **18**, 3419–3437.
548 S. Kajiyama, Y. Wu, M. Hyodo, Y. Nakata, K. Nakashima and N. Yoshimoto, *J. Nat. Gas Sci. Eng.*, 2017, **45**, 96–107.
549 T. Luo, Y. Li, W. Liu, X. Sun and S. Shen, *Energies*, 2017, 10.
550 Z. Liu, S. Dai, F. Ning, L. Peng, H. Wei and C. Wei, *Geophys. Res. Lett.*, 2018, **45**, 715–723.
551 T. Luo, Y. Li, X. Sun, S. Shen and P. Wu, *J. Pet. Sci. Eng.*, 2018, **171**, 302–314.
552 T. Hirose, W. Tanikawa, Y. Hamada, W. Lin, K. Hatakeda, O. Tadai, H. Y. Wu, S. Nomura, N. Abe, L. P. Gupta, T. Sugihara, Y. Masaki, M. Kinoshita and Y. Yamada, *Mar. Pet. Geol.*, 2019, **108**, 348–355, DOI: 10.1016/j.marpetgeo.2018.08.017.
553 Y. Kuang, L. Yang, Q. Li, X. Lv, Y. Li, B. Yu, S. Leng, Y. Song and J. Zhao, *J. Pet. Sci. Eng.*, 2019, **181**, 106173.
554 D. Li, Z. Wang, D. Liang and X. Wu, *Energies*, 2019, 12.
555 Y. Li, T. Luo, X. Sun, W. Liu, Q. Li, Y. Li and Y. Song, *Energies*, 2019, 12.
556 B. Gong, Y. Jiang and L. Chen, *J. Nat. Gas Sci. Eng.*, 2019, **69**, 102915.
557 Y. Li, P. Wu, W. Liu, X. Sun, Z. Cui and Y. Song, *Rev. Sci. Instrum.*, 2019, **90**, 55106.
558 L. Dong, Y. Li, H. Liao, C. Liu, Q. Chen, G. Hu, L. Liu and Q. Meng, *J. Pet. Sci. Eng.*, 2020, **184**, 106478.
559 M. Hyodo, Y. Wu, K. Nakashima, S. Kajiyama and Y. Nakata, *J. Geophys. Res. Solid Earth*, 2017, **122**, 7511–7524.
560 B. Loret, *Fluid Injection in Deformable Geological Formations*, Springer, 2019, pp. 305–367.
561 B. N. Madhusudhan, C. R. I. Clayton and J. A. Priest, *J. Geophys. Res. Solid Earth*, 2019, **124**, 65–75.
562 X. H. Zhang, X. B. Lu, Y. H. Shi and Z. Xia, *Mar. Pet. Geol.*, 2015, **67**, 72–80.
563 J.-H. Choi, S. Dai, J.-S. Lin and Y. Seol, *J. Geophys. Res. Solid Earth*, 2018, **123**, 3347–3357.
564 X. H. Zhang, D. S. Luo, X. B. Lu, L. L. Liu and C. L. Liu, *Acta Mech. Sin.*, 2018, **34**, 266–274.
565 K. Miyazaki, N. Tenma, K. Aoki and T. Yamaguchi, *Energies*, 2012, 5.
566 M. Hyodo, Y. Li, J. Yoneda, Y. Nakata, N. Yoshimoto and A. Nishimura, *Mar. Pet. Geol.*, 2014, **51**, 52–62.
567 C. Yan, Y. Cheng, M. Li, Z. Han, H. Zhang, Q. Li, F. Teng and J. Ding, *Int. J. Hydrogen Energy*, 2017, **42**, 19810–19818.
568 M. Hyodo, J. Yoneda, N. Yoshimoto and Y. Nakata, *Soils Found.*, 2013, **53**, 299–314.
569 Y. Song, Y. Zhu, W. Liu, J. Zhao, Y. Li, Y. Chen, Z. Shen, Y. Lu and C. Ji, *Mar. Pet. Geol.*, 2014, **51**, 70–78.
570 S. Uchida, A. Klar and K. Yamamoto, *Second EAGE Workshop on Geomechanics and Energy*, 2015.
571 M. Hyodo, Y. Nakata and N. Yoshimoto, *Japanese Geotech. Soc. Spec. Publ.*, 2016, **2**, 62–75.
572 H. Han, Y. Wang, X.-S. Li, J.-X. Yu, J.-C. Feng and Y. Zhang, *Fuel*, 2016, **182**, 446–453.
573 Y. Song, Y. Zhu, W. Liu, Y. Li, Y. Lu and Z. Shen, *J. Pet. Sci. Eng.*, 2016, **147**, 77–86.
574 H. Iwai, Y. Konishi, K. Saimyou, S. Kimoto and F. Oka, *Soils Found.*, 2018, **58**, 1113–1132.
575 M. Zhou, K. Soga, K. Yamamoto and H. Huang, *Geomech. Energy Environ.*, 2018, 100111.
576 B. Song, Y. Cheng, C. Yan, Z. Han and Q. Li, *53rd US Rock Mechanics/Geomechanics Symposium*, American Rock Mechanics Association, 2019.
577 Y. Song, T. Luo, B. N. Madhusudhan, X. Sun, Y. Liu, X. Kong and Y. Li, *J. Nat. Gas Sci. Eng.*, 2019, **72**, 103031.
578 R. Wang, W. Liu, Y. Li, F. Yu, X. Nie and Y. Song, *Proc. Int. Conf. Offshore Mech. Arct. Eng.*, 2012, 703–708, DOI: 10.1115/OMAE2012-84080.
579 K. Miyazaki, N. Tenma and T. Yamaguchi, *Energies*, 2017, 10.
580 Y. Li, P. Wu, X. Sun, W. Liu, Y. Song and J. Zhao, *Energies*, 2019, 12.
581 Y. Li, W. Liu, Y. Zhu, Y. Chen, Y. Song and Q. Li, *Appl. Energy*, 2016, **162**, 1627–1632.
582 E. M. Chuvilin, B. A. Bukhanov, S. I. Grebenkin, V. V. Doroshin and A. V. Iospa, *Cold Reg. Sci. Technol.*, 2018, **153**, 101–105.
583 J. Yang, A. Hassanpouryouzband, B. Tohidi, E. Chuvilin, B. Bukhanov, V. Istomin and A. Cheremisin, *J. Geophys. Res. Solid Earth*, 2019, **124**, 2551–2563.
584 S. Uchida, K. Soga and K. Yamamoto, *J. Geophys. Res. Solid Earth*, 2012, **117**, B03209, DOI: 10.1029/2011JB008661.
585 M. Jiang, F. Zhu, F. Liu and S. Utili, *Int. J. Numer. Anal. Methods Geomech.*, 2014, **38**, 1823–1854.
586 S. Uchida, X.-G. Xie and Y. F. Leung, *J. Geophys. Res. Solid Earth*, 2016, **121**, 5580–5595.
587 X. Gai and M. Sánchez, *Gas*, 2017, **1**, 2.
588 X. Zhang, J. Lin, X. Lu, L. Liu, C. Liu, M. Li and Y. Su, *Int. J. Numer. Anal. Methods Geomech.*, 2018, **42**, 931–942.
589 K. Li, R. Liu, L. Kong and X. Zhao, *Geotech. Geol. Eng.*, 2019, **37**, 2893–2902.
590 J. Liu and M. Jiang, *Environ. Geotech.*, 2019, 1–12.
591 S. Gupta, R. Helmig and B. Wohlmuth, *Comput. Geosci.*, 2015, **19**, 1063–1088.
592 X. Chen, X. Zhang, X. Lu, W. Wei and Y. Shi, *Acta Mech. Sin.*, 2016, **32**, 905–914.
593 Q. Li, Y. Cheng, H. Zhang, C. Yan and Y. Liu, *J. Ocean Univ. China*, 2018, **17**, 35–45.

Open Access Article. Published on 22 Junie 2020. Downloaded on 2026-02-11 12:42:38 nm..
This article is licensed under a Creative Commons Attribution-NonCommercial 3.0 Unported Licence.

594 G. Jin, H. Lei, T. Xu, X. Xin, Y. Yuan, Y. Xia and J. Juo, *Mar. Pet. Geol.*, 2018, **92**, 424–436.
595 M. Sánchez, C. Santamarina, M. Teymouri and X. Gai, *J. Geophys. Res. Solid Earth*, 2018, **123**, 10326–10348.
596 Y. Sohn, J. Y. Lee, K.-I. Song and T.-H. Kwon, *Offshore Technol. Conf.*, 2019, 17.
597 X. Sun, L. Wang, H. Luo, Y. Song and Y. Li, *J. Pet. Sci. Eng.*, 2019, **177**, 971–982.
598 J.-W. Jung, J. C. Santamarina and K. Soga, *J. Geophys. Res. Solid Earth*, 2012, **117**, B04202, DOI: 10.1029/2011JB009040.
599 M. Jiang, F. Zhu and S. Utili, *Comput. Geotech.*, 2015, **69**, 551–563.
600 Z. Shen and M. Jiang, *Comput. Geotech.*, 2016, **75**, 225–243.
601 M. Xu, E. Song, H. Jiang and J. Hong, *Granul. Matter*, 2016, **18**, 79.
602 J. Mingjing, H. Jie, W. Jianfeng, C. Bruno and Z. Fangyuan, *Int. J. Geomech.*, 2016, **16**, 4015087.
603 M. Jiang, J. He, J. Wang, Y. Zhou and F. Zhu, *C. R. Mec.*, 2017, **345**, 868–889.
604 M. Jiang, D. Peng and J. Y. Ooi, *Eng. Geol.*, 2017, **223**, 92–109.
605 M. Jiang, Z. Shen and D. Wu, *Landslides*, 2018, **15**, 2227–2241.
606 M. Jiang, Z. Shen, W. Zhou, M. Arroyo and W. Zhang, *Granul. Matter*, 2018, **20**, 63.
607 M. Jiang, J. Liu, C. Y. Kwok and Z. Shen, *C. R. Mec.*, 2018, **346**, 815–832.
608 M. Jiang, J. Liu and Z. Shen, *Eng. Geol.*, 2019, **261**, 105280.
609 Y. Jiang and B. Gong, *Mar. Georesources Geotechnol.*, 2019, 1–15.
610 E. Cohen and A. Klar, *Granul. Matter*, 2019, **21**, 36.
611 E. Cohen, A. Klar and K. Yamamoto, *Energies*, 2019, **12**, 2131.
612 A. Sinquin, T. Palermo and Y. Peysson, *Oil Gas Sci. Technol.*, 2004, **59**, 41–57.
613 A. Fidel-Dufour, F. Gruy and J.-M. Herri, *Chem. Eng. Sci.*, 2006, **61**, 505–515.
614 A. K. Sum, C. A. Koh and E. D. Sloan, *Ind. Eng. Chem. Res.*, 2009, **48**, 7457–7465.
615 A. Ahuja, *Hydrate Forming Emulsion: Rheology and Morphology Analysis for Flow Assurance*, The City College of New York, 2015.
616 E. D. Sloan, *Natural gas hydrates in flow assurance*, Gulf Professional Publishing, 2010.
617 J. G. Delgado-Linares, A. A. A. Majid, E. D. Sloan, C. A. Koh and A. K. Sum, *Energy Fuels*, 2013, **27**, 4564–4573.
618 K.-L. Yan, K. Guo, C.-Y. Sun, S.-S. Niu, B. Liu, D.-J. Shen, J. Chen, R.-Q. Zhong, G.-J. Chen and Q.-P. Li, *Fluid Phase Equilib.*, 2014, **377**, 9–15.
619 M. Darbouret, M. Cournil and J.-M. Herri, *Int. J. Refrig.*, 2005, **28**, 663–671.
620 A. Delahaye, L. Fournaison, S. Marinhas and M. C. Martínez, *Chem. Eng. Sci.*, 2008, **63**, 3551–3559.
621 Y. Salehy, P. Clain, A. Boufares, V. Osswald, A. Delahaye and L. Fournaison, *Energetika*, 2017, **63**(3), DOI: 10.6001/energetika.v63i3.3561.
622 J. Oignet, A. Delahaye, J.-P. Torré, C. Dicharry, H. M. Hoang, P. Clain, V. Osswald, Z. Youssef and L. Fournaison, *Chem. Eng. Sci.*, 2017, **158**, 294–303.
623 N. Liu, J. Zhou, M. Gao and P. Cheng, *Int. Commun. Heat Mass Transfer*, 2019, **102**, 34–41.
624 S. Jerbi, A. Delahaye, L. Fournaison and P. Haberschill, *Int. J. Refrig.*, 2010, **33**, 1625–1631.
625 Z. W. Ma, P. Zhang, R. Z. Wang, S. Furui and G. N. Xi, *Int. J. Heat Mass Transfer*, 2010, **53**, 3745–3757.
626 A. Delahaye, L. Fournaison, S. Jerbi and N. Mayoufi, *Ind. Eng. Chem. Res.*, 2011, **50**, 8344–8353.
627 P. Clain, A. Delahaye, L. Fournaison, N. Mayoufi, D. Dalmazzone and W. Fürst, *Chem. Eng. J.*, 2012, **193–194**, 112–122.
628 B.-Z. Peng, J. Chen, C.-Y. Sun, A. Dandekar, S.-H. Guo, B. Liu, L. Mu, L.-Y. Yang, W.-Z. Li and G.-J. Chen, *Chem. Eng. Sci.*, 2012, **84**, 333–344.
629 X. Lv, B. Shi, Y. Wang and J. Gong, *Energy Fuels*, 2013, **27**, 7294–7302.
630 S. Jerbi, A. Delahaye, J. Oignet, L. Fournaison and P. Haberschill, *Int. J. Refrig.*, 2013, **36**, 1294–1301.
631 K.-L. Yan, C.-Y. Sun, J. Chen, L.-T. Chen, D.-J. Shen, B. Liu, M.-L. Jia, M. Niu, Y.-N. Lv, N. Li, Z.-Y. Song, S.-S. Niu and G.-J. Chen, *Chem. Eng. Sci.*, 2014, **106**, 99–108.
632 L. Ding, B. Shi, X. Lv, Y. Liu, H. Wu, W. Wang and J. Gong, *Chem. Eng. Sci.*, 2016, **146**, 199–206.
633 Z. Rehman, K. Seong, S. Lee and M. H. Song, *Chem. Eng. Commun.*, 2018, **205**, 822–832.
634 B.-H. Shi, L. Ding, W.-Q. Li, X.-F. Lv, Y. Liu, S.-F. Song, C.-Y. Ruan, H.-H. Wu, W. Wang and J. Gong, *Asia-Pac. J. Chem. Eng.*, 2018, **13**, e2193.
635 L. Ding, B. Shi, Y. Liu, S. Song, W. Wang, H. Wu and J. Gong, *Fuel*, 2019, **239**, 126–137.
636 X. Lv, J. Zuo, Y. Liu, S.-D. Zhou, D. Lu, B. Shi and H. Zhao, *RSC Adv.*, 2019, **9**, 32873–32888.
637 W. Fu, Z. Wang, J. Zhang, Y. Cao and B. Sun, *J. Pet. Sci. Eng.*, 2020, **184**, 106504.
638 J. Peixinho, P. U. Karanjkar, J. W. Lee and J. F. Morris, *Langmuir*, 2010, **26**, 11699–11704.
639 E. B. Webb, P. J. Rensing, C. A. Koh, E. Dendy Sloan, A. K. Sum and M. W. Liberatore, *Rev. Sci. Instrum.*, 2012, **83**, 15106.
640 E. B. Webb, P. J. Rensing, C. A. Koh, E. D. Sloan, A. K. Sum and M. W. Liberatore, *Energy Fuels*, 2012, **26**, 3504–3509.
641 E. B. Webb, C. A. Koh and M. W. Liberatore, *Langmuir*, 2013, **29**, 10997–11004.
642 G. Zylyftari, J. W. Lee and J. F. Morris, *Chem. Eng. Sci.*, 2013, **95**, 148–160.
643 E. B. Webb, C. A. Koh and M. W. Liberatore, *Ind. Eng. Chem. Res.*, 2014, **53**, 6998–7007.
644 A. Ahuja, G. Zylyftari and J. F. Morris, *J. Chem. Eng. Data*, 2015, **60**, 362–368.
645 A. Memon and H.-J. Ng, *J. Chem. Eng. Data*, 2015, **60**, 293–298.
646 A. Ahuja, G. Zylyftari and J. F. Morris, *J. Nonnewton. Fluid Mech.*, 2015, **220**, 116–125.

 This journal is © The Royal Society of Chemistry 2020

Open Access Article. Published on 22 Junie 2020. Downloaded on 2026-02-11 12:42:38 nm..
This article is licensed under a Creative Commons Attribution-NonCommercial 3.0 Unported Licence.

647 A. K. Yegya Raman, S. Koteeswaran, D. Venkataramani, P. Clark, S. Bhagwat and C. P. Aichele, *Fuel*, 2016, **179**, 141–149.
648 P. U. Karanjkar, A. Ahuja, G. Zylyftari, J. W. Lee and J. F. Morris, *Rheol. Acta*, 2016, **55**, 235–243.
649 A. A. A. Majid, D. T. Wu and C. A. Koh, *Langmuir*, 2017, **33**, 11436–11445.
650 B.-H. Shi, S. Chai, L. Ding, Y.-C. Chen, Y. Liu, S.-F. Song, H.-Y. Yao, H.-H. Wu, W. Wang and J. Gong, *AIChE J.*, 2018, **64**, 3502–3518.
651 G. A. B. Sandoval, E. J. Soares, R. L. Thompson, R. do Nascimento Siqueira, R. M. de Andrade, F. Campos and A. Teixeira, *Energy Fuels*, 2018, **32**, 2733–2741.
652 A. Ahuja, A. Iqbal, M. Iqbal, J. W. Lee and J. F. Morris, *Energy Fuels*, 2018, **32**, 5877–5884.
653 Y. Qin, P. F. Pickering, M. L. Johns, E. F. May and Z. M. Aman, *Energy Fuels*, 2020, DOI: 10.1021/acs.energyfuels.9b00395.
654 B.-H. Shi, S. Chai, L.-Y. Wang, X. Lv, H.-S. Liu, H.-H. Wu, W. Wang, D. Yu and J. Gong, *Fuel*, 2016, **185**, 323–338.
655 Y. Qin, Z. M. Aman, P. F. Pickering, M. L. Johns and E. F. May, *J. Nonnewton. Fluid Mech.*, 2017, **248**, 40–49.
656 Y. Hoon Sohn, J. Kim, K. Shin, D. Chang, Y. Seo, Z. M. Aman and E. F. May, *Chem. Eng. Sci.*, 2015, **126**, 711–718.
657 A. A. A. Majid, D. T. Wu and C. A. Koh, *Engineering*, 2018, **4**, 321–329.
658 R. Camargo and T. Palermo, *Proceedings of the 4th International Conference on Gas Hydrates*, 2002, vol. 1, pp. 880–885.
659 H. Moradpour, A. Chapoy and B. Tohidi, *Fuel*, 2011, **90**, 3343–3351.
660 Z. M. Aman and C. A. Koh, *Chem. Soc. Rev.*, 2016, **45**, 1678–1690.
661 R. H. Fowler, *Proc. R. Soc. London, Ser. A*, 1937, **159**, 229–246.
662 S. R. H. Fowler and E. A. Guggenheim, *Statistical Thermodynamics. A Version of Statistical Mechanics [by RH Fowler] for Students of Physics and Chemistry*, Cambridge, 1939.
663 J. N. Israelachvili, *Intermolecular and surface forces*, Academic Press, 2015.
664 E. B. Nauman, *Chemical reactor design, optimization, and scaleup*, John Wiley & Sons, 2008.
665 M. R. Walsh, C. A. Koh, E. D. Sloan, A. K. Sum and D. T. Wu, *Science*, 2009, **326**, 1095–1098.
666 E. F. May and R. Wu, *Chem. Eng. Sci.*, 2014, **107**, 1–12.
667 R. Wu, K. A. Kozielski, P. G. Hartley, E. F. May, J. Boxall and N. Maeda, *AIChE J.*, 2013, **59**, 2640–2646.
668 B. C. Barnes, G. T. Beckham, D. T. Wu and A. K. Sum, *J. Chem. Phys.*, 2014, **140**, 164506.
669 B. C. Barnes, B. C. Knott, G. T. Beckham, D. T. Wu and A. K. Sum, *J. Phys. Chem. B*, 2014, **118**, 13236–13243.
670 K. Kinnari, J. Hundseid, X. Li and K. M. Askvik, *J. Chem. Eng. Data*, 2015, **60**, 437–446.
671 M. Kharrat and D. Dalmazzone, *J. Chem. Thermodyn.*, 2003, **35**, 1489–1505.
672 L.-K. Wang, G.-J. Chen, G.-H. Han, X.-Q. Guo and T.-M. Guo, *Fluid Phase Equilib.*, 2003, **207**, 143–154.
673 D. Liang, K. Guo, R. Wang and S. Fan, *Fluid Phase Equilib.*, 2001, **187**, 61–70.
674 C. J. Taylor, K. T. Miller, C. A. Koh and E. D. Sloan Jr, *Chem. Eng. Sci.*, 2007, **62**, 6524–6533.
675 S. Li, C. Sun, B. Liu, X. Feng, F. Li, L. Chen and G. Chen, *AIChE J.*, 2013, **59**, 2145–2154.
676 J. Chen, C. Sun, B. Liu, B. Peng, X. Wang, G. Chen, J. Y. Zuo and H. Ng, *AIChE J.*, 2012, **58**, 2216–2225.
677 I. E. Dzyaloshinskii, E. M. Lifshitz and L. P. Pitaevskii, *Adv. Phys.*, 1961, **10**, 165–209.
678 M. Bienfait, *Surf. Sci.*, 1992, **272**, 1–9.
679 Z. M. Aman, E. P. Brown, E. D. Sloan, A. K. Sum and C. A. Koh, *Phys. Chem. Chem. Phys.*, 2011, **13**, 19796–19806.
680 D. Nenow and A. Trayanov, *J. Cryst. Growth*, 1986, **79**, 801–805.
681 H.-J. Butt and M. Kappl, *Surface and interfacial forces*, Wiley Online Library, 2010.
682 J. S. Zhang, S. Lee and J. W. Lee, *Ind. Eng. Chem. Res.*, 2007, **46**, 6353–6359.
683 J. Yoslim, P. Linga and P. Englezos, *J. Cryst. Growth*, 2010, **313**, 68–80.
684 T. Yagasaki, M. Matsumoto, Y. Andoh, S. Okazaki and H. Tanaka, *J. Phys. Chem. B*, 2014, **118**, 1900–1906.
685 P. M. Naullage, Y. Qiu and V. Molinero, *J. Phys. Chem. Lett.*, 2018, **9**, 1712–1720.
686 J. S. Zhang, C. Lo, P. Somasundaran, S. Lu, A. Couzis and J. W. Lee, *J. Phys. Chem. C*, 2008, **112**, 12381–12385.
687 J. Zhang and J. W. Lee, *Energy Fuels*, 2009, **23**, 3045–3047.
688 P. U. Karanjkar, J. W. Lee and J. F. Morris, *Cryst. Growth Des.*, 2012, **12**, 3817–3824.
689 O. Salako, C. Lo, A. Couzis, P. Somasundaran and J. W. Lee, *J. Colloid Interface Sci.*, 2013, **412**, 1–6.
690 C. Lo, J. S. Zhang, A. Couzis, P. Somasundaran and J. W. Lee, *J. Phys. Chem. C*, 2010, **114**, 13385–13389.
691 C. Lo, J. Zhang, P. Somasundaran and J. W. Lee, *J. Colloid Interface Sci.*, 2012, **376**, 173–176.
692 Y. Zhong and R. E. Rogers, *Chem. Eng. Sci.*, 2000, **55**, 4175–4187.
693 K. Dann and L. Rosenfeld, *Langmuir*, 2018, **34**, 6085–6094.
694 F. Sicard, T. Bui, D. Monteiro, Q. Lan, M. Ceglio, C. Burress and A. Striolo, *Langmuir*, 2018, **34**, 9701–9710.
695 M. Khurana, Z. Yin and P. Linga, *ACS Sustainable Chem. Eng.*, 2017, **5**, 11176–11203.
696 V. Natarajan, P. R. Bishnoi and N. Kalogerakis, *Chem. Eng. Sci.*, 1994, **49**, 2075–2087.
697 S. Takeya, A. Hori, T. Hondoh and T. Uchida, *J. Phys. Chem. B*, 2000, **104**, 4164–4168.
698 I. L. Moudrakovski, G. E. McLaurin, C. I. Ratcliffe and J. A. Ripmeester, *J. Phys. Chem. B*, 2004, **108**, 17591–17595.
699 N. Maeda, *Rev. Sci. Instrum.*, 2014, **85**, 65115.
700 T. M. Svartaas, W. Ke, S. Tantciura and A. U. Bratland, *Energy Fuels*, 2015, **29**, 8195–8207.
701 S. Sun, X. Peng, Y. Zhang, J. Zhao and Y. Kong, *J. Chem. Thermodyn.*, 2017, **107**, 141–152.
702 P. J. Metaxas, V. W. S. Lim, C. Booth, J. Zhen, P. L. Stanwix, M. L. Johns, Z. M. Aman, G. Haandrikman, D. Crosby and E. F. May, *Fuel*, 2019, **252**, 448–457.

Open Access Article. Published on 22 Junie 2020. Downloaded on 2026-02-11 12:42:38 nm..
This article is licensed under a Creative Commons Attribution-NonCommercial 3.0 Unported Licence.

703 E. D. Sloan and F. Fleyfel, *AIChE J.*, 1991, **37**, 1281–1292.
704 G.-J. Guo, Y.-G. Zhang, M. Li and C.-H. Wu, *J. Chem. Phys.*, 2008, **128**, 194504.
705 N. J. English, M. Lauricella and S. Meloni, *J. Chem. Phys.*, 2014, **140**, 204714.
706 G.-J. Guo and P. M. Rodger, *J. Phys. Chem. B*, 2013, **117**, 6498–6504.
707 S. Subramanian and E. D. Sloan Jr, *Fluid Phase Equilib.*, 1999, **158**, 813–820.
708 P. Buchanan, A. K. Soper, H. Thompson, R. E. Westacott, J. L. Creek, G. Hobson and C. A. Koh, *J. Chem. Phys.*, 2005, **123**, 164507.
709 H. Conrad, F. Lehmkühler, C. Sternemann, A. Sakko, D. Paschek, L. Simonelli, S. Huotari, O. Feroughi, M. Tolan and K. Hämäläinen, *Phys. Rev. Lett.*, 2009, **103**, 218301.
710 A. Vysniauskas and P. R. Bishnoi, *Chem. Eng. Sci.*, 1983, **38**, 1061–1072.
711 E. D. Sloan, S. Subramanian, P. N. Matthews, J. P. Lederhos and A. A. Khokhar, *Ind. Eng. Chem. Res.*, 1998, **37**, 3124–3132.
712 R. Ohmura, M. Ogawa, K. Yasuoka and Y. H. Mori, *J. Phys. Chem. B*, 2003, **107**, 5289–5293.
713 B. Sowa and N. Maeda, *J. Phys. Chem. A*, 2015, **119**, 10784–10790.
714 C. J. Benmore and A. K. Soper, *J. Chem. Phys.*, 1998, **108**, 6558–6560.
715 M. Chaouachi, A. Falenty, K. Sell, F. Enzmann, M. Kersten, D. Haberthür and W. F. Kuhs, *Geochem., Geophys., Geosyst.*, 2015, **16**, 1711–1722.
716 T. Uchida, K. Yamazaki and K. Gohara, *J. Phys. Chem. C*, 2016, **120**, 26620–26629.
717 S. A. Bagherzadeh, S. Alavi, J. Ripmeester and P. Englezos, *J. Chem. Phys.*, 2015, **142**, 214701.
718 M. Sugaya and Y. H. Mori, *Chem. Eng. Sci.*, 1996, **51**, 3505–3517.
719 T. Uchida, T. Ebinuma, J. Kawabata and H. Narita, *J. Cryst. Growth*, 1999, **204**, 348–356.
720 P. Servio and P. Englezos, *AIChE J.*, 2003, **49**, 269–276.
721 E. M. Freer, M. S. Selim and E. D. Sloan Jr, *Fluid Phase Equilib.*, 2001, **185**, 65–75.
722 T. Mochizuki and Y. H. Mori, *Chem. Eng. Sci.*, 2017, **171**, 61–75.
723 R. Ohmura, S. Kashiwazaki and Y. H. Mori, *J. Cryst. Growth*, 2000, **218**, 372–380.
724 R. Tanaka, R. Sakemoto and R. Ohmura, *Cryst. Growth Des.*, 2009, **9**, 2529–2536.
725 K. Saito, M. Kishimoto, R. Tanaka and R. Ohmura, *Cryst. Growth Des.*, 2010, **11**, 295–301.
726 S.-L. Li, C.-Y. Sun, B. Liu, Z.-Y. Li, G.-J. Chen and A. K. Sum, *Sci. Rep.*, 2014, **4**, 4129.
727 X. Y. Zeng, G. Wu, J. R. Zhong, D. Y. Chen, C. Y. Sun and G. J. Chen, *Cryst. Growth Des.*, 2019, **19**, 3158–3165.
728 S.-L. Li, Y.-F. Wang, C.-Y. Sun, G.-J. Chen, B. Liu, Z.-Y. Li and Q.-L. Ma, *Chem. Eng. Sci.*, 2015, **135**, 412–420.
729 I. L. Moudrakovski, A. A. Sanchez, C. I. Ratcliffe and J. A. Ripmeester, *J. Phys. Chem. B*, 2001, **105**, 12338–12347.
730 J. M. Schicks and J. A. Ripmeester, *Angew. Chem., Int. Ed.*, 2004, **43**, 3310–3313.
731 J. Zhu, S. Du, X. Yu, J. Zhang, H. Xu, S. C. Vogel, T. C. Germann, J. S. Francisco, F. Izumi and K. Momma, *Nat. Commun.*, 2014, **5**, 4128.
732 L. C. Jacobson, M. Matsumoto and V. Molinero, *J. Chem. Phys.*, 2011, **135**, 74501.
733 S. Liang and P. G. Kusalik, *J. Chem. Phys.*, 2015, **143**, DOI: 10.1063/1.4923465.
734 S. Takeya, T. Hondoh and T. Uchida, *Ann. N. Y. Acad. Sci.*, 2000, **912**, 973–982.
735 R. W. Henning, A. J. Schultz, V. Thieu and Y. Halpern, *J. Phys. Chem. A*, 2000, **104**, 5066–5071.
736 X. Wang, A. J. Schultz and Y. Halpern, *J. Phys. Chem. A*, 2002, **106**, 7304–7309.
737 W. F. Kuhs, D. K. Staykova and A. N. Salamatin, *J. Phys. Chem. B*, 2006, **110**, 13283–13295.
738 A. Falenty, A. N. Salamatin and W. F. Kuhs, *J. Phys. Chem. C*, 2013, **117**, 8443–8457.
739 A. N. Salamatin, A. Falenty, T. C. Hansen and W. F. Kuhs, *Energy Fuels*, 2015, **29**, 5681–5691.
740 V. A. Vlasov, *Theor. Found. Chem. Eng.*, 2012, **46**, 576–582.
741 V. S. Shagapov, A. S. Chiglintseva and G. R. Rafikova, *Theor. Found. Chem. Eng.*, 2018, **52**, 560–567.
742 W. Liu, Y. Li, L. Zhang, S. Shen, M. Yang, J. Zhao and Y. Song, *Theor. Found. Chem. Eng.*, 2019, **53**, 305–317.
743 M. T. Nguyen, J. Amtawong, K. Smoll, A. Chanez, M. Yamano, G.-B. H. Dinh, S. Sengupta, R. W. Martin and K. C. Janda, *J. Phys. Chem. C*, 2016, **120**, 8482–8489.
744 G.-J. Guo, Y.-G. Zhang, Y.-J. Zhao, K. Refson and G.-H. Shan, *J. Chem. Phys.*, 2004, **121**, 1542–1547.
745 R. Radhakrishnan and B. L. Trout, *J. Chem. Phys.*, 2002, **117**, 1786–1796.
746 L. C. Jacobson, W. Hujo and V. Molinero, *J. Am. Chem. Soc.*, 2010, **132**, 11806–11811.
747 G.-J. Guo, M. Li, Y.-G. Zhang and C.-H. Wu, *Phys. Chem. Chem. Phys.*, 2009, **11**, 10427–10437.
748 G.-J. Guo, Y.-G. Zhang and H. Liu, *J. Phys. Chem. C*, 2007, **111**, 2595–2606.
749 G.-J. Guo, Y.-G. Zhang, C.-J. Liu and K.-H. Li, *Phys. Chem. Chem. Phys.*, 2011, **13**, 12048–12057.
750 S. Sarupria and P. G. Debenedetti, *J. Phys. Chem. Lett.*, 2012, **3**, 2942–2947.
751 M. Lauricella, S. Meloni, N. J. English, B. Peters and G. Ciccotti, *J. Phys. Chem. C*, 2014, **118**, 22847–22857.
752 M. Lauricella, G. Ciccotti, N. J. English, B. Peters and S. Meloni, *J. Phys. Chem. C*, 2017, **121**, 24223–24234.
753 R. W. Hawtin, D. Quigley and P. M. Rodger, *Phys. Chem. Chem. Phys.*, 2008, **10**, 4853–4864.
754 L. C. Jacobson and V. Molinero, *J. Am. Chem. Soc.*, 2011, **133**, 6458–6463.
755 M. R. Walsh, G. T. Beckham, C. A. Koh, E. D. Sloan, D. T. Wu and A. K. Sum, *J. Phys. Chem. C*, 2011, **115**, 21241–21248.
756 J. A. Ripmeester and S. Alavi, *ChemPhysChem*, 2010, **11**, 978–980.

 This journal is © The Royal Society of Chemistry 2020

Open Access Article. Published on 22 Junie 2020. Downloaded on 2026-02-11 12:42:38 nm..
This article is licensed under a Creative Commons Attribution-NonCommercial 3.0 Unported Licence.

757 K. W. Hall, S. Carpendale and P. G. Kusalik, *Proc. Natl. Acad. Sci. U. S. A.*, 2016, **113**, 12041–12046.
758 K. W. Hall, Z. Zhang, C. J. Burnham, G.-J. Guo, S. Carpendale, N. J. English and P. G. Kusalik, *J. Phys. Chem. Lett.*, 2018, **9**, 6991–6998.
759 M. Lauricella, S. Meloni, S. Liang, N. J. English, P. G. Kusalik and G. Ciccotti, *J. Chem. Phys.*, 2015, **142**, 244503.
760 E. Małolepsza and T. Keyes, *J. Phys. Chem. B*, 2015, **119**, 15857–15865.
761 Y. Bi and T. Li, *J. Phys. Chem. B*, 2014, **118**, 13324–13332.
762 Y. Bi, A. Porras and T. Li, *J. Chem. Phys.*, 2016, **145**, 211909.
763 N. J. English and S. T. John, *Comput. Mater. Sci.*, 2017, **126**, 1–6.
764 Y. Bi, E. Xu, T. A. Strobel and T. Li, *Commun. Chem.*, 2018, **1**, 15.
765 Z. Futera, M. Celli, L. del Rosso, C. J. Burnham, L. Ulivi and N. J. English, *J. Phys. Chem. C*, 2017, **121**, 3690–3696.
766 R. Ohmura, W. Shimada, T. Uchida, Y. H. Mori, S. Takeya, J. Nagao, H. Minagawa, T. Ebinuma and H. Narita, *Philos. Mag.*, 2004, **84**, 1–16.
767 R. Ohmura, S. Matsuda, T. Uchida, T. Ebinuma and H. Narita, *Cryst. Growth Des.*, 2005, **5**, 953–957.
768 J. D. Lee, M. Song, R. Susilo and P. Englezos, *Cryst. Growth Des.*, 2006, **6**, 1428–1439.
769 R. Larsen, C. A. Knight and E. D. Sloan Jr, *Fluid Phase Equilib.*, 1998, **150**, 353–360.
770 P. Gayet, C. Dicharry, G. Marion, A. Graciaa, J. Lachaise and A. Nesterov, *Chem. Eng. Sci.*, 2005, **60**, 5751–5758.
771 M. T. Storr, P. C. Taylor, J.-P. Monfort and P. M. Rodger, *J. Am. Chem. Soc.*, 2004, **126**, 1569–1576.
772 B. J. Anderson, J. W. Tester, G. P. Borghi and B. L. Trout, *J. Am. Chem. Soc.*, 2005, **127**, 17852–17862.
773 B. Kvamme, T. Kuznetsova and K. Aasoldsen, *J. Mol. Graphics Modell.*, 2005, **23**, 524–536.
774 S. Y. Lee, H. C. Kim and J. D. Lee, *J. Cryst. Growth*, 2014, **402**, 249–259.
775 H. Hayama, M. Mitarai, H. Mori, J. Verrett, P. Servio and R. Ohmura, *Cryst. Growth Des.*, 2016, **16**, 6084–6088.
776 A. Kumar, G. Bhattacharjee, B. D. Kulkarni and R. Kumar, *Ind. Eng. Chem. Res.*, 2015, **54**, 12217–12232.
777 Y. He, M.-T. Sun, C. Chen, G.-D. Zhang, K. Chao, Y. Lin and F. Wang, *J. Mater. Chem. A*, 2019, **7**, 21634–21661.
778 A. Gupta, S. F. Dec, C. A. Koh and E. D. Sloan, *J. Phys. Chem. C*, 2007, **111**, 2341–2346.
779 S. F. Dec, K. E. Bowler, L. L. Stadterman, C. A. Koh and E. D. Sloan, *J. Phys. Chem. A*, 2007, **111**, 4297–4303.
780 M. Kida, Y. Jin, N. Takahashi, J. Nagao and H. Narita, *J. Phys. Chem. A*, 2010, **114**, 9456–9461.
781 S. F. Dec, *J. Phys. Chem. C*, 2012, **116**, 9660–9665.
782 J.-R. Zhong, Y.-F. Sun, W.-Z. Li, Y. Xie, G.-J. Chen, C.-Y. Sun, L.-Y. Yang, H.-B. Qin, W.-X. Pang and Q.-P. Li, *Appl. Energy*, 2019, **250**, 873–881.
783 N. J. English, J. K. Johnson and C. E. Taylor, *J. Chem. Phys.*, 2005, **123**, 244503.
784 N. J. English and E. T. Clarke, *J. Chem. Phys.*, 2013, **139**, 94701.
785 Z. Sun, H. Wang, J. Yao, Z. Sun, K. Bongole, X. Zhu, L. Liu and J. Wang, *J. Nat. Gas Sci. Eng.*, 2018, **55**, 235–242.
786 J. Kondori, S. Zendehboudi and L. James, *Fuel*, 2019, **249**, 264–276.
787 H. C. Kim, P. R. Bishnoi, R. A. Heidemann and S. S. H. Rizvi, *Chem. Eng. Sci.*, 1987, **42**, 1645–1653.
788 M. A. Clarke and P. R. Bishnoi, *Chem. Eng. Sci.*, 2001, **56**, 4715–4724.
789 T. Kawamura, K. Ohga, K. Higuchi, J. H. Yoon, Y. Yamamoto, T. Komai and H. Haneda, *Energy Fuels*, 2003, **17**, 614–618.
790 T. Kawamura, Y. Sakamoto, M. Ohtake, Y. Yamamoto, T. Komai, H. Haneda and J.-H. Yoon, *Ind. Eng. Chem. Res.*, 2006, **45**, 360–364.
791 S. Fan, Y. Zhang, G. Tian, D. Liang and D. Li, *Energy Fuels*, 2006, **20**, 324–326.
792 S. Yao, Y. Li, W. Wang, G. Song, Z. Shi, X. Wang and S. Liu, *Energy Fuels*, 2019, **33**(6), 5208–5215, DOI: 10.1021/acs.energyfuels.9b01003.
793 Z. Yin, Z. R. Chong, H. K. Tan and P. Linga, *J. Nat. Gas Sci. Eng.*, 2016, **35**, 1362–1387.
794 V. A. Istomin and V. S. Yakushev, Gas-Hydrates Self-Preservation Effect, in *Physics and Chemistry of Ice*, ed. N. Maeno and T. Hondoh, Hokkaido University Press, Sapporo, Japan, 1992, pp. 136–140.
795 S. Takeya, W. Shimada, Y. Kamata, T. Ebinuma, T. Uchida, J. Nagao and H. Narita, *J. Phys. Chem. A*, 2001, **105**, 9756–9759.
796 S. Takeya, T. Ebinuma, T. Uchida, J. Nagao and H. Narita, *J. Cryst. Growth*, 2002, **237**, 379–382.
797 V. R. Belosludov, O. S. Subbotin, D. S. Krupskii, T. Ikeshoji, R. V. Belosludov, Y. Kawazoe and J. Kudoh, *J. Phys.: Conf. Ser.*, 2006, **29**, 198.
798 D. Bai, D. Zhang, X. Zhang and G. Chen, *Sci. Rep.*, 2015, **5**, 14599.
799 V. A. Vlasov, *Int. J. Heat Mass Transfer*, 2016, **102**, 631–636.
800 L. A. Stern, S. Circone, S. H. Kirby and W. B. Durham, *J. Phys. Chem. B*, 2001, **105**, 1756–1762.
801 W. F. Kuhs, G. Genov, D. K. Staykova and T. Hansen, *Phys. Chem. Chem. Phys.*, 2004, **6**, 4917–4920.
802 K. Takeya, K. Nango, T. Sugahara, K. Ohgaki and A. Tani, *J. Phys. Chem. B*, 2005, **109**, 21086–21088.
803 W. Shimada, S. Takeya, Y. Kamata, T. Uchida, J. Nagao, T. Ebinuma and H. Narita, *J. Phys. Chem. B*, 2005, **109**, 5802–5807.
804 S. Takeya and J. A. Ripmeester, *ChemPhysChem*, 2010, **11**, 70–73.
805 V. P. Melnikov, A. N. Nesterov, A. M. Reshetnikov and V. A. Istomin, *Chem. Eng. Sci.*, 2011, **66**, 73–77.
806 M. Kida, M. Watanabe, Y. Jin and J. Nagao, *Jpn. J. Appl. Phys.*, 2015, **54**, 65502.
807 S. Y. Misyura, *Sci. Rep.*, 2016, **6**, 30324.
808 S. Takeya, A. Yoneyama, K. Ueda, K. Hyodo, T. Takeda, H. Mimachi, M. Takahashi, T. Iwasaki, K. Sano and H. Yamawaki, *J. Phys. Chem. C*, 2011, **115**, 16193–16199.
809 S. Takeya, A. Yoneyama, K. Ueda, H. Mimachi, M. Takahashi, K. Sano, K. Hyodo, T. Takeda and

Open Access Article. Published on 22 Junie 2020. Downloaded on 2026-02-11 12:42:38 nm..
This article is licensed under a Creative Commons Attribution-NonCommercial 3.0 Unported Licence.

Y. Gotoh, *J. Phys. Chem. C*, 2012, **116**(26), 13842–13848, DOI: 10.1021/jp302269v.
810 A. Falenty, W. F. Kuhs, M. Glockzin and G. Rehder, *Energy Fuels*, 2014, **28**(10), 6275–6283, DOI: 10.1021/ef501409g.
811 T. Takaoki, 4th International Conference on Natural Gas Hydrate, Japan, 2002, 2002.
812 G. Rehder, R. Eckl, M. Elfgen, A. Falenty, R. Hamann, N. Kähler, W. F. Kuhs, H. Osterkamp and C. Windmeier, *Energies*, 2012, **5**, 2499–2523.
813 H. J. Kang, Y. Yang, M. S. Ki, M. S. Shin, J. Choi, J. H. Cha and D. Lee, *Ocean Eng.*, 2016, **113**, 162–173, DOI: 10.1016/j.oceaneng.2015.12.052.
814 H. Mimachi, M. Takahashi, S. Takeya, Y. Gotoh, A. Yoneyama, K. Hyodo, T. Takeda and T. Murayama, *Energy Fuels*, 2015, **29**, 4827–4834.
815 G. Zhang and R. E. Rogers, *Chem. Eng. Sci.*, 2008, **63**, 2066–2074.
816 A. Hachikubo, S. Takeya, E. Chuvilin and V. Istomin, *Phys. Chem. Chem. Phys.*, 2011, **13**, 17449–17452, DOI: 10.1039/c1cp22353d.
817 A. S. Stoporev, A. Y. Manakov, L. K. Altunina, A. V. Bogoslovsky, L. A. Strelets and E. Y. Aladko, *Energy Fuels*, 2014, **28**(2), 794–802, DOI: 10.1021/ef401779d.
818 V. P. Mel'nikov, L. S. Podenko, A. N. Nesterov, A. O. Drachuk, N. S. Molokitina and A. M. Reshetnikov, *Dokl. Chem.*, 2016, **466**, 53–56, DOI: 10.1134/S0012500816020038.
819 H. Sato, H. Sakamoto, S. Ogino, H. Mimachi, T. Kinoshita, T. Iwasaki, K. Sano and K. Ohgaki, *Chem. Eng. Sci.*, 2013, **91**, 86–89, DOI: 10.1016/j.ces.2013.01.014.
820 S. Takeya, H. Mimachi and T. Murayama, *Appl. Energy*, 2018, **230**, 86–93, DOI: 10.1016/j.apenergy.2018.08.015.
821 P. S. R. Prasad and B. S. Kiran, *Sci. Rep.*, 2019, **9**, 5860.
822 S. Takeya and J. A. Ripmeester, *Angew. Chem., Int. Ed.*, 2008, **47**(7), 1276–1279, DOI: 10.1002/anie.200703718.
823 H. Ohno, H. Narita and J. Nagao, *J. Phys. Chem. Lett.*, 2011, **2**(3), 201–205, DOI: 10.1021/jz101595t.
824 J. A. Priest, E. V. L. Rees and C. R. I. Clayton, *J. Geophys. Res. Solid Earth*, 2009, **114**, B11205, DOI: 10.1029/2009JB006284.
825 B. Tohidi, R. Anderson, M. Ben Clennell, R. W. Burgass and A. B. Biderkab, *Geology*, 2001, **21**(9), 867–870, DOI: 10.1130/0091-7613(2001)029<0867:VOOGHF>2.0.CO;2.
826 D. Katsuki, R. Ohmura, T. Ebinuma and H. Narita, *Philos. Mag.*, 2006, **86**(12), 1753–1761, DOI: 10.1080/14786430500509062.
827 D. Katsuki, R. Ohmura, T. Ebinuma and H. Narita, *Philos. Mag.*, 2007, **87**(7), 1057–1069, DOI: 10.1080/14786430601021652.
828 D. Katsuki, R. Ohmura, T. Ebinuma and H. Narita, *J. Appl. Phys.*, 2008, **104**, 083514, DOI: 10.1063/1.3000622.
829 K. Nagashima, T. Suzuki, M. Nagamoto and T. Shimizu, *J. Phys. Chem. B*, 2008, **112**(32), 9876–9882, DOI: 10.1021/jp802487d.
830 M. Muraoka and K. Nagashima, *J. Phys. Chem. C*, 2012, **116**(44), 23342–23350, DOI: 10.1021/jp306224w.
831 M. Mork, G. Schei and R. Larsen, *Ann. N. Y. Acad. Sci.*, 2000, **912**(1), 897–905, DOI: 10.1111/j.1749-6632.2000.tb06843.x.
832 T. Uchida, S. Dallimore and J. Mikami, *Ann. N. Y. Acad. Sci.*, 2000, **912**(1), 1021–1033, DOI: 10.1111/j.1749-6632.2000.tb06857.x.
833 S. Jin, S. Takeya, J. Hayashi, J. Nagao, Y. Kamata, T. Ebinuma and H. Narita, *Jpn. J. Appl. Phys., Part 1*, 2004, **43**(8A), DOI: 10.1143/JJAP.43.5673.
834 S. Jin, J. Nagao, S. Takeya, Y. Jin, J. Hayashi, Y. Kamata, T. Ebinuma and H. Narita, *Jpn. J. Appl. Phys., Part 2*, 2006, **45**, 24–28, DOI: 10.1143/JJAP.45.L714.
835 S. A. Bagherzadeh, I. L. Moudrakovski, J. A. Ripmeester and P. Englezos, *Energy Fuels*, 2011, **25**(7), 3083–3092.
836 P. Kerkar, K. W. Jones, R. Kleinberg, W. B. Lindquist, S. Tomov, H. Feng and D. Mahajan, *Appl. Phys. Lett.*, 2009, **95**, 024102, DOI: 10.1063/1.3120544.
837 P. B. Kerkar, K. Horvat, K. W. Jones and D. Mahajan, *Geochem., Geophys., Geosyst.*, 2014, **15**, 4759–4768, DOI: 10.1002/2014GC005373.
838 L. Yang, A. Falenty, M. Chaouachi, D. Haberthür and W. F. Kuhs, *Geochem., Geophys., Geosyst.*, 2016, **17**(9), 3717–3732, DOI: 10.1002/2016GC006521.
839 L. Lei, Y. Seol, J. H. Choi and T. J. Kneafsey, *Mar. Pet. Geol.*, 2019, **104**, 451–467, DOI: 10.1016/j.marpetgeo.2019.04.004.
840 S. J. Cox, D. J. F. Taylor, T. G. A. Youngs, A. K. Soper, T. S. Totton, R. G. Chapman, M. Arjmandi, M. G. Hodges, N. T. Skipper and A. Michaelides, *J. Am. Chem. Soc.*, 2018, **140**, 3277–3284.
841 P. Y. Yu, W. Y. Sean, R. Y. Yeh, L. H. Chiang Hsieh, R. Q. Hsu and T. Sato, *Int. J. Heat Mass Transfer*, 2017, **113**, 176–183, DOI: 10.1016/j.ijheatmasstransfer.2017.05.053.
842 X. Wang, B. Dong, W. Li, M. Yu and Y. Song, *Int. J. Heat Mass Transfer*, 2018, **122**, 1182–1197.
843 X. Wang, B. Dong, C. Chen, W. Li and Y. Song, *Int. J. Heat Mass Transfer*, 2019, **144**, 118656.
844 A. Fukumoto, K. Kamada, T. Sato, H. Oyama, H. Torii, F. Kiyono, J. Nagao, N. Temma and H. Narita, *J. Nat. Gas Sci. Eng.*, 2018, **50**, 269–281, DOI: 10.1016/j.jngse.2017.12.016.
845 S. R. Gainey and M. E. Elwood Madden, *Icarus*, 2012, **218**(1), 513–524, DOI: 10.1016/j.icarus.2011.12.019.
846 D. Ambuehl and M. Elwood Madden, *Icarus*, 2014, **234**, 45–52, DOI: 10.1016/j.icarus.2014.01.037.
847 V. S. Yakushev and E. M. Chuvilin, *Cold Reg. Sci. Technol.*, 2000, **31**(3), 189–197, DOI: 10.1016/S0165-232X(00)00012-4.
848 E. Chuvilin, B. Bukhanov, D. Davletshina, S. Grebenkin and V. Istomin, *Geosciences*, 2018, **8**, 431.
849 V. D. Chari, D. V. Sharma, P. S. R. Prasad and S. R. Murthy, *J. Nat. Gas Sci. Eng.*, 2013, **11**, 7–11.
850 F. Farhang, A. V. Nguyen and K. B. Sewell, *Energy Fuels*, 2014, **28**, 7025–7037.
851 M. Cha, S. Baek, J. Morris and J. W. Lee, *Chem. – Asian J.*, 2014, **9**, 261–267.
852 S. Arjang, M. Manteghian and A. Mohammadi, *Chem. Eng. Res. Des.*, 2013, **91**, 1050–1054.

Open Access Article. Published on 22 Junie 2020. Downloaded on 2026-02-11 12:42:38 nm..
This article is licensed under a Creative Commons Attribution-NonCommercial 3.0 Unported Licence.

853 M. Aliabadi, A. Rasoolzadeh, F. Esmaeilzadeh and A. Alamdari, *J. Nat. Gas Sci. Eng.*, 2015, **27**, 1518–1522.
854 R. Wang, T. Liu, F. Ning, W. Ou, L. Zhang, Z. Wang, L. Peng, J. Sun, Z. Liu, T. Li, H. Sun and G. Jiang, *J. Energy Chem.*, 2019, **30**, 90–100.
855 J. Grdadolnik, F. Merzel and F. Avbelj, *Proc. Natl. Acad. Sci. U. S. A.*, 2017, **114**, 322–327.
856 D. Chandler, *Nature*, 2005, **437**(7059), 640–647.
857 W. Kauzmann, *Advances in protein chemistry*, Elsevier, 1959, vol. 14, pp. 1–63.
858 H. Lee, J. Lee, D. Y. Kim, J. Park, Y.-T. Seo, H. Zeng, I. L. Moudrakovski, C. I. Ratcliffe and J. A. Ripmeester, *Materials For Sustainable Energy: A Collection of Peer-Reviewed Research and Review Articles from Nature Publishing Group*, World Scientific, 2011, pp. 285–288.
859 L. J. Florusse, C. J. Peters, J. Schoonman, K. C. Hester, C. A. Koh, S. F. Dec, K. N. Marsh and E. D. Sloan, *Science*, 2004, **306**, 469–471.
860 B. Tohidi, A. Danesh, A. C. Todd, R. W. Burgass and K. K. Østergaard, *Fluid Phase Equilib.*, 1997, **138**, 241–250.
861 L. C. Ho, P. Babu, R. Kumar and P. Linga, *Energy*, 2013, **63**, 252–259.
862 X.-S. Li, Z.-M. Xia, Z.-Y. Chen and H.-J. Wu, *Energy Fuels*, 2011, **25**, 1302–1309.
863 N. H. Duc, F. Chauvy and J.-M. Herri, *Energy Convers. Manage.*, 2007, **48**, 1313–1322.
864 X.-S. Li, C.-G. Xu, Z.-Y. Chen and H.-J. Wu, *Energy*, 2010, **35**, 3902–3908.
865 S. M. Kim, J. D. Lee, H. J. Lee, E. K. Lee and Y. Kim, *Int. J. Hydrogen Energy*, 2011, **36**, 1115–1121.
866 M. Arjmandi, A. Chapoy and B. Tohidi, *J. Chem. Eng. Data*, 2007, **52**, 2153–2158.
867 M. Ricaurte, C. Dicharry, X. Renaud and J.-P. Torré, *Fuel*, 2014, **122**, 206–217.
868 J. Du, H. Li and L. Wang, *Adv. Powder Technol.*, 2014, **25**, 1227–1233.
869 M. Ricaurte, C. Dicharry, D. Broseta, X. Renaud and J.-P. Torré, *Ind. Eng. Chem. Res.*, 2012, **52**, 899–910.
870 C. F. da Silva Lirio, F. L. P. Pessoa and A. M. C. Uller, *Chem. Eng. Sci.*, 2013, **96**, 118–123.
871 K. Okutani, Y. Kuwabara and Y. H. Mori, *Chem. Eng. Sci.*, 2008, **63**, 183–194.
872 H. J. Lee, J. D. Lee, P. Linga, P. Englezos, Y. S. Kim, M. S. Lee and Y. Do Kim, *Energy*, 2010, **35**, 2729–2733.
873 J.-P. Torré, C. Dicharry, M. Ricaurte, D. Daniel-David and D. Broseta, *Energy Procedia*, 2011, **4**, 621–628.
874 H. Ganji, M. Manteghian, M. R. Omidkhah and H. R. Mofrad, *Fuel*, 2007, **86**, 434–441.
875 A. Kumar, T. Sakpal, P. Linga and R. Kumar, *Fuel*, 2013, **105**, 664–671.
876 J. Zhang, P. Yedlapalli and J. W. Lee, *Chem. Eng. Sci.*, 2009, **64**, 4732–4736.
877 H. Li, P. Stanwix, Z. Aman, M. Johns, E. May and L. Wang, *J. Phys. Chem. A*, 2016, **120**, 417–424.
878 N. N. Nguyen, A. V. Nguyen, K. M. Steel, L. X. Dang and M. Galib, *J. Phys. Chem. C*, 2017, **121**, 3830–3840.
879 S. Dong, M. Li and A. Firoozabadi, *Fuel*, 2017, **210**, 713–720.
880 S. Dong and A. Firoozabadi, *J. Chem. Thermodyn.*, 2018, **117**, 214–222.
881 F. Jiménez-Ángeles and A. Firoozabadi, *ACS Cent. Sci.*, 2018, **4**, 820–831.
882 N. N. Nguyen and A. V. Nguyen, *Fuel*, 2015, **156**, 87–95.
883 F. Farhang, A. V. Nguyen and M. A. Hampton, *Energy Fuels*, 2014, **28**, 1220–1229.
884 B. Sowa, X. H. Zhang, P. G. Hartley, D. E. Dunstan, K. A. Kozielski and N. Maeda, *Energy Fuels*, 2014, **28**, 6877–6888.
885 B. Lukanov and A. Firoozabadi, *Langmuir*, 2014, **30**, 6373–6383.
886 L. Piatkowski, Z. Zhang, E. H. G. Backus, H. J. Bakker and M. Bonn, *Nat. Commun.*, 2014, **5**, 4083.
887 P. Jungwirth and D. J. Tobias, *J. Phys. Chem. B*, 2002, **106**, 6361–6373.
888 S. Pal and F. Müller-Plathe, *J. Phys. Chem. B*, 2005, **109**, 6405–6415.
889 A. Kumar, S. S. Vedula, R. Kumar and P. Linga, *J. Chem. Thermodyn.*, 2018, **117**, 2–8.
890 A. Kumar, H. P. Veluswamy, R. Kumar and P. Linga, *Appl. Energy*, 2019, **235**, 21–30.
891 A. V. Palodkar and A. K. Jana, *Energy Fuels*, 2019, **33**, 1433–1443.
892 P. Thoutam, S. Rezaei Gomari, A. Chapoy, F. Ahmad and M. Islam, *ACS Omega*, 2019, **4**(19), 18210–18218.
893 G. C. Nihous, C. K. Kinoshita and S. M. Masutani, *Chem. Eng. Sci.*, 2009, **64**, 2767–2771.
894 F. E. Anderson and J. M. Prausnitz, *AIChE J.*, 1986, **32**, 1321–1333.
895 E. D. Sloan and C. A. Koh, *Clathrate hydrates of natural gases*, third edition, Chem. IndThen Boca Raton-Marcel Dekker Then CRC Press, York, 2008.
896 S. Bobev and K. T. Tait, *Am. Mineral.*, 2004, **89**, 1208–1214.
897 H. K. Abay and T. M. Svartaas, *Energy Fuels*, 2009, **24**, 752–757.
898 J. Amtawong, J. Guo, J. S. Hale, S. Sengupta, E. B. Fleischer, R. W. Martin and K. C. Janda, *J. Phys. Chem. Lett.*, 2016, **7**, 2346–2349.
899 P. Linga and M. A. Clarke, *Energy Fuels*, 2017, **31**, 1–13.
900 M. Yang, Y. Song, L. Jiang, W. Liu, B. Dou and W. Jing, *Appl. Energy*, 2014, **135**, 504–511.
901 A. Siangsai, P. Rangsunvigit, B. Kitiyanan, S. Kulprathipanja and P. Linga, *Chem. Eng. Sci.*, 2015, **126**, 383–389.
902 V. Govindaraj, D. Mech, G. Pandey, R. Nagarajan and J. S. Sangwai, *J. Nat. Gas Sci. Eng.*, 2015, **26**, 810–818.
903 Y. Zhang, X.-S. Li, Z.-Y. Chen, G. Li and Y. Wang, *J. Nat. Gas Sci. Eng.*, 2016, **35**, 1463–1471.
904 S. H. B. Yang, P. Babu, S. F. S. Chua and P. Linga, *Appl. Energy*, 2016, **162**, 1131–1140.
905 S. Wang, M. Yang, W. Liu, J. Zhao and Y. Song, *J. Pet. Sci. Eng.*, 2016, **145**, 565–572.
906 B.-H. Shi, L. Yang, S.-S. Fan and X. Lou, *Fuel*, 2017, **194**, 395–405.
907 J. Li, D. Liang, K. Guo, R. Wang and S. Fan, *Energy Convers. Manage.*, 2006, **47**, 201–210.

Open Access Article. Published on 22 Junie 2020. Downloaded on 2026-02-11 12:42:38 nm..
This article is licensed under a Creative Commons Attribution-NonCommercial 3.0 Unported Licence.

908 A. Mohammadi, M. Manteghian, A. Haghtalab, A. H. Mohammadi and M. Rahmati-Abkenar, *Chem. Eng. J.*, 2014, **237**, 387–395.
909 F. Wang, Y.-M. Song, G.-Q. Liu, G. Guo, S.-J. Luo and R.-B. Guo, *Appl. Energy*, 2018, **213**, 227–234.
910 H. Najibi, M. M. Shayegan and H. Heidary, *J. Nat. Gas Sci. Eng.*, 2015, **23**, 315–323.
911 H. Kakati, A. Mandal and S. Laik, *J. Ind. Eng. Chem.*, 2016, **35**, 357–368.
912 M. Mohammadi, A. Haghtalab and Z. Fakhroueian, *J. Chem. Thermodyn.*, 2016, **96**, 24–33.
913 A. Ghozatloo, N. M. Shariaty and M. Hassanisadi, *Iran. J. Chem. Eng.*, 2014, **11**, 67–73.
914 N.-J. Kim, S.-S. Park, H. T. Kim and W. Chun, *Int. Commun. Heat Mass Transfer*, 2011, **38**, 31–36.
915 J. Pasieka, S. Coulombe and P. Servio, *Chem. Eng. Sci.*, 2013, **104**, 998–1002.
916 Y.-M. Song, F. Wang, G. Guo, S.-J. Luo and R.-B. Guo, *Appl. Energy*, 2018, **224**, 175–183.
917 Y. Song, F. Wang, G. Liu, S. Luo and R. Guo, *Energy Fuels*, 2017, **31**, 1850–1857.
918 I. S. Gudmundsson, RF Pat.
919 D. Liang, S. He and D. Li, *Chin. Sci. Bull.*, 2009, **54**, 965–971.
920 C. Cheng, F. Wang, Y. Tian, X. Wu, J. Zheng, J. Zhang, L. Li, P. Yang and J. Zhao, *Renewable Sustainable Energy Rev.*, 2020, **117**, 109492.
921 S.-S. Park and N.-J. Kim, *J. Ind. Eng. Chem.*, 2013, **19**, 1668–1672.
922 H. J. Hong, C. H. Ko, M. H. Song, S. Lee and K. Seong, *J. Ind. Eng. Chem.*, 2016, **41**, 183–189.
923 Y. Kozo, F. Tetsuro, K. Takahiro and K. Yuichi, Production method for gas hydrates and device for producing same, *Pat.GB*, 2000, 2347938.
924 K. Carpenter and V. Bahadur, *J. Phys. Chem. Lett.*, 2016, **7**, 2465–2469.
925 H. Kumano, T. Hirata, K. Mitsuishi and K. Ueno, *Int. J. Refrig.*, 2012, **35**, 1266–1274.
926 A. A. Chernov, A. A. Pil'Nik, D. S. Elistratov, I. V. Mezentsev, A. V. Meleshkin, M. V. Bartashevich and M. G. Vlasenko, *Sci. Rep.*, 2017, **7**, 40809.
927 V. E. Dontsov, V. E. Nakoryakov and A. A. Chernov, *J. Appl. Mech. Tech. Phys.*, 2007, **48**, 346–360.
928 V. E. Dontsov, V. E. Nakoryakov and A. A. Chernov, Dokl. Ross. Akad. Nauk, 2006, vol. 411, pp. 190–193.
929 V. S. Shagapov, S. A. Lepikhin and I. A. Chiglintsev, *Thermophys. Aeromechanics*, 2010, **17**, 229–241.
930 V. E. Dontsov, A. A. Chernov and E. V. Dontsov, *Thermophys. Aeromechanics*, 2007, **14**, 21–35.
931 V. E. Dontsov and A. A. Chernov, *Int. J. Heat Mass Transfer*, 2009, **52**, 4919–4928.
932 V. E. Dontsov, V. E. Nakoryakov and A. A. Chernov, *J. Eng. Thermophys.*, 2009, **18**, 1–7.
933 Y. Zhang, L. Zhao, S. Deng, R. Zhao, X. Nie and Y. Liu, *J. Therm. Sci.*, 2019, **28**, 948–961.
934 A. A. Chernov and V. E. Dontsov, *Int. J. Heat Mass Transfer*, 2011, **54**, 4307–4316.
935 J. Park, K. Shin, J. Kim, H. Lee, Y. Seo, N. Maeda, W. Tian and C. D. Wood, *J. Phys. Chem. C*, 2015, **119**, 1690–1699.
936 S. Fan, L. Yang, Y. Wang, X. Lang, Y. Wen and X. Lou, *Chem. Eng. Sci.*, 2014, **106**, 53–59.
937 P. Linga, N. Daraboina, J. A. Ripmeester and P. Englezos, *Chem. Eng. Sci.*, 2012, **68**, 617–623.
938 D. J. Turner, K. T. Miller and E. D. Sloan, *Chem. Eng. Sci.*, 2009, **64**, 3996–4004.
939 X. Zhao, Z. Qiu and W. Huang, *J. Nat. Gas Sci. Eng.*, 2015, **22**, 270–278.
940 M. Mork, *Formation rate of natural gas hydrate-reactor experiments and models*, 2002.
941 P. Skovborg, H. J. Ng, P. Rasmussen and U. Mohn, *Chem. Eng. Sci.*, 1993, **48**, 445–453.
942 J. S. Parent and P. R. Bishnoi, *Chem. Eng. Commun.*, 1996, **144**, 51–64.
943 P. Englezos, N. Kalogerakis, P. D. Dholabhai and P. R. Bishnoi, *Chem. Eng. Sci.*, 1987, **42**, 2647–2658.
944 J. D. Lee and P. Englezos, *Chem. Eng. Sci.*, 2006, **61**, 1368–1376.
945 J. Yang and B. Tohidi, *Chem. Eng. Sci.*, 2011, **66**, 278–283.
946 M. F. Qureshi, M. Atilhan, T. Altamash, S. Aparicio, M. Aminnaji and B. Tohidi, *J. Nat. Gas Sci. Eng.*, 2017, **38**, 50–58.
947 S. Fujita, K. Watanabe and Y. H. Mori, *AIChE J.*, 2009, **55**, 1056–1064.
948 R. Ohmura, S. Kashiwazaki, S. Shiota, H. Tsuji and Y. H. Mori, *Energy Fuels*, 2002, **16**, 1141–1147.
949 M. Takahashi, T. Kawamura, Y. Yamamoto, H. Ohnari, S. Himuro and H. Shakutsui, *J. Phys. Chem. B*, 2003, **107**, 2171–2173.
950 B. P. Binks and R. Murakami, *Nat. Mater.*, 2006, **5**, 865.
951 W. Wang, C. L. Bray, D. J. Adams and A. I. Cooper, *J. Am. Chem. Soc.*, 2008, **130**, 11608–11609.
952 G. Hu, Y. Ye, C. Liu, Q. Meng, J. Zhang and S. Diao, *Fuel Process. Technol.*, 2011, **92**, 1617–1622.
953 Q. Zhang, C. Li, Q. Wu and B. Zhang, *RSC Adv.*, 2018, **8**, 27171–27180.
954 E. D. Sloan Jr, Method for Controlling Clathrate Hydrates in Fluid Systems, *US Pat.*, 5432292, 1995.
955 S. Mokhatab, R. J. Wilkens and K. J. Leontaritis, *Energy Sources, Part A*, 2007, **29**, 39–45.
956 C. Vörös, V. Füvesi and Á. Pintér, *Hung. J. Ind. Chem.*, 2013, **41**, 7–10.
957 M. Tariq, D. Rooney, E. Othman, S. Aparicio, M. Atilhan and M. Khraisheh, *Ind. Eng. Chem. Res.*, 2014, **53**, 17855–17868.
958 L. E. Zerpa, J.-L. Salager, C. A. Koh, E. D. Sloan and A. K. Sum, *Ind. Eng. Chem. Res.*, 2010, **50**, 188–197.
959 A. Qasim, M. S. Khan, B. Lal and A. M. Shariff, *J. Pet. Sci. Eng.*, 2019, 106418.
960 A. Striolo, *Mol. Phys.*, 2019, 1–13.
961 S. R. Davies, M. S. Selim, E. D. Sloan, P. Bollavaram and D. J. Peters, *AIChE J.*, 2006, **52**, 4016–4027.
962 J.-H. Cha, C. Ha, S.-P. Kang, J. W. Kang and K.-S. Kim, *Fluid Phase Equilib.*, 2016, **413**, 75–79.

Open Access Article. Published on 22 Junie 2020. Downloaded on 2026-02-11 12:42:38 nm..
This article is licensed under a Creative Commons Attribution-NonCommercial 3.0 Unported Licence.

963 M. Nepomiluev and V. Streletskaya, *SPE Russian Oil and Gas Exploration & Production Technical Conference and Exhibition*, Society of Petroleum Engineers, 2014.
964 E. M. Reyna and S. R. Stewart, *SPE/IADC drilling conference*, Society of Petroleum Engineers, 2001.
965 M. Aminnaji, B. Tohidi, R. Burgass and M. Atilhan, *J. Nat. Gas Sci. Eng.*, 2017, **45**, 840–847.
966 N. Daraboina, P. Linga, J. Ripmeester, V. K. Walker and P. Englezos, *Energy Fuels*, 2011, **25**, 4384–4391.
967 M. Cha, K. Shin, Y. Seo, J.-Y. Shin and S.-P. Kang, *J. Phys. Chem. A*, 2013, **117**, 13988–13995.
968 J. Kim, K. Shin, Y. Seo, S. J. Cho and J. D. Lee, *J. Phys. Chem. B*, 2014, **118**, 9065–9075.
969 M. A. Kelland, *Energy Fuels*, 2018, **32**, 12001–12012.
970 M. S. Kamal, I. A. Hussein, A. S. Sultan and N. von Solms, *Renewable Sustainable Energy Rev.*, 2016, **60**, 206–225.
971 M. A. Kelland, *Energy Fuels*, 2006, **20**, 825–847.
972 T. Yagasaki, M. Matsumoto and H. Tanaka, *Phys. Chem. Chem. Phys.*, 2015, **17**, 32347–32357.
973 X. Sun, G. Zhou, J. Zhu, H. Wu, G. Lu and D. Bai, *ChemPhysChem*, 2019, **20**, 2553–2565.
974 T. Y. Sylva, C. K. Kinoshita and S. M. Masutani, *Chem. Eng. Sci.*, 2016, **155**, 10–15.
975 Q. Lv, X. Zang, X. Li and G. Li, *Fluid Phase Equilib.*, 2018, **458**, 272–277.
976 D. Bai, Z. Wu, C. Lin and D. Zhou, *Fluid Phase Equilib.*, 2019, **487**, 76–82.
977 H. Piramoon, M. K. Moraveji, A. Parvareh and A. Azimi, *Pet. Sci. Technol.*, 2019, **37**, 1924–1930.
978 R. J. Kirkpatrick, *Am. Mineral. J. Earth Planet. Mater.*, 1975, **60**, 798–814.
979 T. Yagasaki, M. Matsumoto, Y. Andoh, S. Okazaki and H. Tanaka, *J. Phys. Chem. B*, 2014, **118**, 11797–11804.
980 K. S. Sujith and C. N. Ramachandran, *J. Phys. Chem. B*, 2017, **121**, 153–163.
981 H. Kim, H. P. Veluswamy, Y. Seo and P. Linga, *Cryst. Growth Des.*, 2018, **18**, 6984–6994.
982 A. Majumdar, E. Mahmoodaghdam and P. R. Bishnoi, *J. Chem. Eng. Data*, 2000, **45**, 20–22.
983 A. H. Mohammadi and D. Richon, *J. Chem. Thermodyn.*, 2012, **44**, 26–30.
984 H. Najibi, Z. Kamali and A. H. Mohammadi, *Fluid Phase Equilib.*, 2013, **342**, 71–74.
985 N. A. Sami, K. Das, J. S. Sangwai and N. Balasubramanian, *J. Chem. Thermodyn.*, 2013, **65**, 198–203.
986 H. Najibi, E. Amiri and A. H. Mohammadi, *Fluid Phase Equilib.*, 2014, **363**, 70–73.
987 M. Dastanian, A. A. Izadpanah and M. Mofarahi, *J. Chem. Eng. Data*, 2017, **62**, 1701–1707.
988 M. Dastanian, A. A. Izadpanah and M. Mofarahi, *J. Chem. Eng. Data*, 2018, **63**, 1675–1681.
989 K. N. Mahadev and P. R. Bishnoi, *Can. J. Chem. Eng.*, 1999, **77**, 718–722.
990 M. D. Jager, C. J. Peters and E. D. Sloan, *Fluid Phase Equilib.*, 2002, **193**, 17–28.
991 C. Eichholz, A. Majumdar, M. A. Clarke, L. R. Oellrich and P. R. Bishnoi, *J. Chem. Eng. Data*, 2004, **49**, 847–851.
992 R. Masoudi, B. Tohidi, A. Danesh, A. C. Todd, R. Anderson, R. W. Burgass and J. Yang, *Chem. Eng. Sci.*, 2005, **60**, 4213–4224.
993 A. H. Mohammadi and D. Richon, *J. Chem. Thermodyn.*, 2009, **41**, 1374–1377.
994 H. Najibi, A. Chapoy, H. Haghighi and B. Tohidi, *Fluid Phase Equilib.*, 2009, **275**, 127–131.
995 G.-H. Kwak, K.-H. Lee, S. Y. Hong, S. D. Seo, J. D. Lee, B. R. Lee and A. K. Sum, *J. Chem. Eng. Data*, 2018, **63**, 2179–2184.
996 R. Masoudi, B. Tohidi, R. Anderson, R. W. Burgass and J. Yang, *Fluid Phase Equilib.*, 2004, **219**, 157–163.
997 P. D. Dholabhai, J. S. Parent and P. R. Bishnoi, *Fluid Phase Equilib.*, 1997, **141**, 235–246.
998 Q. Nasir, K. K. Lau, B. Lal and K. M. Sabil, *J. Chem. Eng. Data*, 2014, **59**, 3920–3926.
999 Z.-G. Sun, S.-S. Fan, L. Shi, Y.-K. Guo and K.-H. Guo, *J. Chem. Eng. Data*, 2001, **46**, 927–929.
1000 A. P. Semenov, A. S. Stoporev, R. I. Mendgaziev, P. A. Gushchin, V. N. Khlebnikov, V. S. Yakushev, V. A. Istomin, D. V. Sergeeva and V. A. Vinokurov, *J. Chem. Thermodyn.*, 2019, **137**, 119–130.
1001 J.-W. Lee and S.-P. Kang, *Ind. Eng. Chem. Res.*, 2011, **50**, 8750–8755.
1002 Y. Seo, H. Kim and J. Park, *ASME 2016 35th International Conference on Ocean, Offshore and Arctic Engineering*, American Society of Mechanical Engineers Digital Collection, 2016.
1003 H. Kim, J. Park, Y. Seo and M. Ko, *Chem. Eng. Sci.*, 2017, **158**, 172–180.
1004 S. Xu, S. Fan, H. Yao, Y. Wang, X. Lang, P. Lv and S. Fang, *J. Chem. Thermodyn.*, 2017, **104**, 212–217.
1005 J.-H. Sa, G.-H. Kwak, B. R. Lee, D.-H. Park, K. Han and K.-H. Lee, *Sci. Rep.*, 2013, **3**, 2428.
1006 C. B. Bavoh, O. Nashed, M. S. Khan, B. Partoon, B. Lal and A. M. Sharif, *J. Chem. Thermodyn.*, 2018, **117**, 48–53.
1007 Y. Liu, B. Chen, Y. Chen, S. Zhang, W. Guo, Y. Cai, B. Tan and W. Wang, *Energy Technol.*, 2015, **3**, 815–819.
1008 H. P. Veluswamy, Q. W. Hong and P. Linga, *Cryst. Growth Des.*, 2016, **16**, 5932–5945.
1009 J.-H. Sa, B. R. Lee, D.-H. Park, K. Han, H. D. Chun and K.-H. Lee, *Environ. Sci. Technol.*, 2011, **45**, 5885–5891.
1010 H. Roosta, A. Dashti, S. H. Mazloumi and F. Varaminian, *J. Mol. Liq.*, 2016, **215**, 656–663.
1011 C. B. Bavoh, B. Partoon, B. Lal, G. Gonfa, S. F. Khor and A. M. Sharif, *Chem. Eng. Sci.*, 2017, **171**, 331–339.
1012 J.-H. Sa, G.-H. Kwak, K. Han, D. Ahn, S. J. Cho, J. D. Lee and K.-H. Lee, *Sci. Rep.*, 2016, **6**, 31582.
1013 J.-H. Sa, G.-H. Kwak, K. Han, D. Ahn and K.-H. Lee, *Sci. Rep.*, 2015, **5**, 11526.
1014 S. K. Nagappayya, R. M. Lucente-Schultz, V. M. Nace and V. M. Ho, *J. Chem. Eng. Data*, 2014, **60**, 351–355.
1015 K.-S. Kim, J. W. Kang and S.-P. Kang, *Chem. Commun.*, 2011, **47**, 6341–6343.
1016 A. Perrin, O. M. Musa and J. W. Steed, *Chem. Soc. Rev.*, 2013, **42**, 1996–2015.

Open Access Article. Published on 22 Junie 2020. Downloaded on 2026-02-11 12:42:38 nm..
This article is licensed under a Creative Commons Attribution-NonCommercial 3.0 Unported Licence.

1017 M. A. Kelland, *Energy Fuels*, 2017, **31**, 5046–5054.
1018 E. Luna-Ortiz, M. Healey, R. Anderson and E. Sørhaug, *Energy Fuels*, 2014, **28**, 2902–2913.
1019 O. Nashed, K. M. Sabil, L. Ismail, A. Japper-Jaafar and B. Lal, *J. Chem. Thermodyn.*, 2018, **117**, 147–154.
1020 C. Magnusson, E. Abrahamsen, M. A. Kelland, A. Cely, K. Kinnari, X. Li and K. M. Askvik, *Energy Fuels*, 2018, **32**, 5772–5778.
1021 M. Muraoka, N. Susuki and Y. Yamamoto, *RSC Adv.*, 2016, **6**, 63880–63885.
1022 P. C. Chua and M. A. Kelland, *Energy Fuels*, 2012, **26**, 4481–4485.
1023 L. Cheng, K. Liao, Z. Li, J. Cui, B. Liu, F. Li, G. Chen and C. Sun, *Chem. Eng. Sci.*, 2019, **207**, 305–316, DOI: 10.1016/j.ces.2019.06.032.
1024 E. D. Sloan Jr, *Method for Controlling Clathrate Hydrates in Fluid Systems*, *US Pat.*, 5880319, 1999.
1025 F. T. Reyes and M. A. Kelland, *Energy Fuels*, 2013, **27**, 3730–3735.
1026 H.-B. Qin, Z.-Y. Zhang, C.-Y. Sun, G.-J. Chen, Q.-L. Ma and Z.-F. Ning, *J. Chem. Eng. Data*, 2017, **62**, 2770–2775.
1027 Q. Zhang, X. Shen, X. Zhou and D. Liang, *Energy Fuels*, 2016, **31**, 839–846.
1028 J. Xu, L. Li, J. Liu, X. Wang, Y. Yan and J. Zhang, *Phys. Chem. Chem. Phys.*, 2018, **20**, 8326–8332.
1029 J. Park, S. S. Lee, H. Kim, S.-H. Kim and Y. Seo, *Energy Fuels*, 2018, **32**, 9001–9009.
1030 A. Perrin, M. J. Goodwin, O. M. Musa, D. J. Berry, P. Corner, K. Edkins, D. S. Yufit and J. W. Steed, *Cryst. Growth Des.*, 2017, **17**, 3236–3249.
1031 T. Yagasaki, M. Matsumoto and H. Tanaka, *J. Am. Chem. Soc.*, 2015, **137**, 12079–12085.
1032 Q. Wang, C. Wang, S. Ma, P. Lu and J. Dong, *ACS Sustainable Chem. Eng.*, 2018, **6**, 13532–13542.
1033 P. C. Chua, M. A. Kelland, T. Hirano and H. Yamamoto, *Energy Fuels*, 2012, **26**, 4961–4967.
1034 P. C. Chua, M. A. Kelland, K. Ishitake, K. Satoh, M. Kamigaito and Y. Okamoto, *Energy Fuels*, 2012, **26**, 3577–3585.
1035 L. S. Ree, E. Opsahl and M. A. Kelland, *Energy Fuels*, 2010, **24**(4), 2554–2562.
1036 H. Roosta, A. Dashti, S. H. Mazloumi and F. Varaminian, *J. Mol. Liq.*, 2018, **253**, 259–269.
1037 M. A. Kelland, T. M. Svartaas, J. Øvsthus and T. Namba, *Ann. N. Y. Acad. Sci.*, 2000, **912**, 281–293.
1038 L. Del Villano, M. A. Kelland, G. M. Miyake and E. Y.-X. Chen, *Energy Fuels*, 2010, **24**, 2554–2562.
1039 H. Ajiro, Y. Takemoto, M. Akashi, P. C. Chua and M. A. Kelland, *Energy Fuels*, 2010, **24**, 6400–6410.
1040 A. A. Bertolazzo, P. M. Naullage, B. Peters and V. Molinero, *J. Phys. Chem. Lett.*, 2018, **9**, 3224–3231.
1041 B. Widom, P. Bhimalapuram and K. Koga, *Phys. Chem. Chem. Phys.*, 2003, **5**, 3085–3093.
1042 M. A. Kelland, *Production chemicals for the oil and gas industry*, CRC Press, 2014.
1043 C. D. Magnusson and M. A. Kelland, *Energy Fuels*, 2015, **29**, 6347–6354.
1044 J. Wang, R. Wang, R.-H. Yoon and Y. Seol, *J. Chem. Eng. Data*, 2014, **60**, 383–388.
1045 M. A. Kelland, *Production Chemicals for the Oil and Gas Industry*, 2010, vol. 72.
1046 L. Wan, D.-Q. Liang, Q. Ding and G. Hou, *Fuel*, 2019, **239**, 173–179.
1047 A. M. P. S. G. da Silva, S. I. C. Lopes, P. Brogueira, T. J. V. Prazeres, M. Beija and J. M. G. Martinho, *J. Colloid Interface Sci.*, 2008, **327**, 129–137.
1048 I. Idziak, D. Avoce, D. Lessard, D. Gravel and X. X. Zhu, *Macromolecules*, 1999, **32**, 1260–1263.
1049 E. G. Dirdal and M. A. Kelland, *Energy Fuels*, 2019, **33**, 7127–7137.
1050 L. H. S. Ree and M. A. Kelland, *Energy Fuels*, 2018, **32**, 10639–10648.
1051 Q. Zhang, I. M. Heyns, R. Pfukwa, B. Klumperman and M. A. Kelland, *Energy Fuels*, 2018, **32**, 12337–12344.
1052 M. S. Khan, B. Lal, A. M. Shariff and H. Mukhtar, *J. Mol. Liq.*, 2019, **274**, 33–44.
1053 C. Xiao, N. Wibisono and H. Adidharma, *Chem. Eng. Sci.*, 2010, **65**, 3080–3087.
1054 C. Xiao and H. Adidharma, *Chem. Eng. Sci.*, 2009, **64**, 1522–1527.
1055 K. Kim and S.-P. Kang, *Proceedings of the 7th International Conference on Gas Hydrates (ICGH 2011)*, 2011, pp. 17–21.
1056 T. Kitajima, N. Ohtsubo, S. Hashimoto, T. Makino, D. Kodama and K. Ohgaki, *Am. Chem. Sci. J.*, 2012, **2**, 100–110.
1057 L. K. Chun and A. Jaafar, *Asian J. Sci. Res.*, 2013, **6**, 374–380.
1058 R. K. McMullan, T. C. Mak and G. A. Jeffrey, *J. Chem. Phys.*, 1966, **44**, 2338–2345.
1059 Q. Chen, Y. Yu, P. Zeng, W. Yang, Q. Liang, X. Peng, Y. Liu and Y. Hu, *J. Nat. Gas Chem.*, 2008, **17**, 264–267.
1060 X.-S. Li, Y.-J. Liu, Z.-Y. Zeng, Z.-Y. Chen, G. Li and H.-J. Wu, *J. Chem. Eng. Data*, 2010, **56**, 119–123.
1061 K. Tumba, P. Reddy, P. Naidoo, D. Ramjugernath, A. Eslamimanesh, A. H. Mohammadi and D. Richon, *J. Chem. Eng. Data*, 2011, **56**, 3620–3629.
1062 H. Zeng, L. D. Wilson, V. K. Walker and J. A. Ripmeester, *J. Am. Chem. Soc.*, 2006, **128**, 2844–2850.
1063 X. Guo, W. Zhao, X. Pang, X. Liao, X. Hu and J. Wu, *Food Hydrocolloids*, 2014, **35**, 217–225.
1064 D. Le Corre, J. Bras and A. Dufresne, *Biomacromolecules*, 2010, **11**, 1139–1153.
1065 M. R. Talaghat, *J. Nat. Gas Sci. Eng.*, 2014, **18**, 7–12.
1066 L. Wan, N. Zhang and D.-Q. Liang, *J. Mol. Liq.*, 2019, **292**, 111435.
1067 S. Yaqub and L. K. Keong, *J. Ind. Eng. Chem.*, 2019, **79**, 131–145.
1068 S. Yaqub, A. bin Mohd Shariff and N. B. Mellon, *J. Nat. Gas Sci. Eng.*, 2019, **65**, 68–81.
1069 Y. Xu, M. Yang and X. Yang, *J. Nat. Gas Chem.*, 2010, **19**, 431–435.
1070 S. Yaqub, B. Lal, B. Partoon and N. B. Mellon, *Fluid Phase Equilib.*, 2018, **477**, 40–57.

 This journal is © The Royal Society of Chemistry 2020

Open Access Article. Published on 22 Junie 2020. Downloaded on 2026-02-11 12:42:38 nm..
This article is licensed under a Creative Commons Attribution-NonCommercial 3.0 Unported Licence.

1071 V. Srivastava, D. S. Chauhan, P. G. Joshi, V. Maruthapandian, A. A. Sorour and M. A. Quraishi, *ChemistrySelect*, 2018, **3**, 1990–1998.
1072 P. L. Davies, J. Baardsnes, M. J. Kuiper and V. K. Walker, *Philos. Trans. R. Soc., B*, 2002, **357**, 927–935.
1073 S. Xu, S. Fan, S. Fang, X. Lang, Y. Wang and J. Chen, *Sci. Rep.*, 2016, **6**, 23220.
1074 A. Farhadian, M. A. Varfolomeev, A. Kudbanov and S. R. Gallyamov, *Chem. Eng. Sci.*, 2019, **206**, 507–517.
1075 A. Farkhadian, M. A. Varfolomeev, Y. F. Zaripova and V. V. Yarkovoi, *Chem. Technol. Fuels Oils*, 2019, **55**, 159–164.
1076 A. Farhadian, A. Kudbanov, M. A. Varfolomeev and D. Dalmazzone, *Sci. Rep.*, 2019, **9**, 1–10.
1077 X. Zhou, Y. Li, C. Fang, S. Li, Y. Cheng, W. Lei and X. Meng, *J. Mater. Sci. Technol.*, 2015, **31**, 708–722.
1078 J. Hu, K. Peng, J. Guo, D. Shan, G. B. Kim, Q. Li, E. Gerhard, L. Zhu, W. Tu and W. Lv, *ACS Appl. Mater. Interfaces*, 2016, **8**, 17499–17510.
1079 H. K. Shendi, I. Omrani, A. Ahmadi, A. Farhadian, N. Babanejad and M. R. Nabid, *Prog. Org. Coat.*, 2017, **105**, 303–309.
1080 Q. Sheng, K. C. da Silveira, W. Tian, C. Fong, N. Maeda, R. Gubner and C. D. Wood, *Energy Fuels*, 2017, **31**, 6724–6731.
1081 J. Park, H. Kim, Q. Sheng, C. D. Wood and Y. Seo, *Energy Fuels*, 2017, **31**, 9363–9373.
1082 Z. M. Aman, K. Olcott, K. Pfeiffer, E. D. Sloan, A. K. Sum and C. A. Koh, *Langmuir*, 2013, **29**, 2676–2682.
1083 C. Liu, M. Li, C. Liu, K. Geng and Y. Li, *Energy Fuels*, 2016, **30**, 6240–6248.
1084 E. P. Brown, S. Hu, J. Wells, X. Wang and C. A. Koh, *Energy Fuels*, 2018, **32**, 6619–6626.
1085 T. Bui, A. Phan, D. Monteiro, Q. Lan, M. Ceglio, E. Acosta, P. Krishnamurthy and A. Striolo, *Langmuir*, 2017, **33**, 2263–2274.
1086 Z. Huo, E. Freer, M. Lamar, B. Sannigrahi, D. M. Knauss and E. D. Sloan Jr, *Chem. Eng. Sci.*, 2001, **56**, 4979–4991.
1087 A. Phan, T. Bui, E. Acosta, P. Krishnamurthy and A. Striolo, *Phys. Chem. Chem. Phys.*, 2016, **18**, 24859–24871.
1088 M. A. Kelland, T. M. Svartaas, J. Øvsthus, T. Tomita and K. Mizuta, *Chem. Eng. Sci.*, 2006, **61**, 4290–4298.
1089 M. R. Anklam, J. D. York, L. Helmerich and A. Firoozabadi, *AIChE J.*, 2008, **54**, 565–574.
1090 E. P. Brown and C. A. Koh, *Energy Fuels*, 2016, **30**, 8065–8071.
1091 L. M. Frostman, *SPE Annual Technical Conference and Exhibition*, Society of Petroleum Engineers, 2000.
1092 P. C. Chua and M. A. Kelland, *Energy Fuels*, 2018, **32**, 1674–1684.
1093 T. Bui, F. Sicard, D. Monteiro, Q. Lan, M. Ceglio, C. Burress and A. Striolo, *J. Phys. Chem. Lett.*, 2018, **9**, 3491–3496.
1094 Y. Tokiwa, H. Sakamoto, T. Takiue, M. Aratono and H. Matsubara, *J. Phys. Chem. B*, 2015, **119**, 6235–6241.
1095 Q. Lei and C. D. Bain, *Phys. Rev. Lett.*, 2004, **92**, 176103.
1096 R. B. Asserson, A. C. Hoffmann, S. Høiland and K. M. Asvik, *J. Pet. Sci. Eng.*, 2009, **68**, 209–217.
1097 Z. M. Aman, L. E. Dieker, G. Aspenes, A. K. Sum, E. D. Sloan and C. A. Koh, *Energy Fuels*, 2010, **24**, 5441–5445.
1098 J. D. York and A. Firoozabadi, *J. Phys. Chem. B*, 2008, **112**, 10455–10465.
1099 J. D. York and A. Firoozabadi, *Energy Fuels*, 2009, **23**, 2937–2946.
1100 S. Gao, *Energy Fuels*, 2009, **23**, 2118–2121.
1101 Z. M. Aman, A. Haber, N. N. A. Ling, A. Thornton, M. L. Johns and E. F. May, *Energy Fuels*, 2015, **29**, 7948–7955.
1102 C. Liu, M. Li, V. K. Srivastava and C. A. Koh, *Energy Fuels*, 2016, **30**, 2555–2562.
1103 H. Mehrabian, M. A. Bellucci, M. R. Walsh and B. L. Trout, *J. Phys. Chem. C*, 2018, **122**, 12839–12849.
1104 A. Striolo, A. Phan and M. R. Walsh, *Curr. Opin. Chem. Eng.*, 2019, **25**, 57–66.
1105 J. S. Gudmundsson, Method for Production of Gas Hydrates for Transportation and Storage, *US Pat.*, 5536893, 1996.
1106 Y. Katoh, K. Horiguchi, T. Iwasaki and S. Nagamori, Process for Producing Gas Hydrate Pellet, *US Pat.*, 7999141, 2011.
1107 K. Park, S. Y. Hong, J. W. Lee, K. C. Kang, Y. C. Lee, M.-G. Ha and J. D. Lee, *Desalination*, 2011, **274**, 91–96.
1108 P. Babu, R. Kumar and P. Linga, *Chem. Eng. Sci.*, 2014, **117**, 342–351.
1109 X. J. Shi and P. Zhang, *Int. J. Refrig.*, 2014, **42**, 77–89.
1110 A. Eslamimanesh, A. H. Mohammadi, D. Richon, P. Naidoo and D. Ramjugernath, *J. Chem. Thermodyn.*, 2012, **46**, 62–71.
1111 P. Pirzadeh and P. G. Kusalik, *J. Am. Chem. Soc.*, 2013, **135**, 7278–7287.
1112 B. C. Knott, V. Molinero, M. F. Doherty and B. Peters, *J. Am. Chem. Soc.*, 2012, **134**, 19544–19547.
1113 J. Zhang, R. W. Hawtin, Y. Yang, E. Nakagava, M. Rivero, S. K. Choi and P. M. Rodger, *J. Phys. Chem. B*, 2008, **112**, 10608–10618.
1114 F. Jiménez-Ángeles and A. Firoozabadi, *J. Phys. Chem. C*, 2015, **119**, 8798–8804.
1115 S. V. Joshi, G. A. Grasso, P. G. Lafond, I. Rao, E. Webb, L. E. Zerpa, E. D. Sloan, C. A. Koh and A. K. Sum, *Chem. Eng. Sci.*, 2013, **97**, 198–209.
1116 G. Song, Y. Li, W. Wang, K. Jiang, X. Ye and P. Zhao, *Chem. Eng. Sci.*, 2017, **158**, 480–489.
1117 C. Ruan, L. Ding, B. Shi, Q. Huang and J. Gong, *RSC Adv.*, 2017, **7**, 48127–48135.
1118 J. W. Nicholas, C. A. Koh, E. D. Sloan, L. Nuebling, H. He and B. Horn, *AIChE J.*, 2009, **55**, 1882–1888.
1119 J. Chen, K.-L. Yan, G.-J. Chen, C.-Y. Sun, B. Liu, N. Ren, D.-J. Shen, M. Niu, Y.-N. Lv and N. Li, *Chem. Eng. Sci.*, 2015, **122**, 284–290.
1120 X. F. Lv, B. H. Shi, Y. Wang, Y. X. Tang, L. Y. Wang and J. Gong, *Oil Gas Sci. Technol.*, 2015, **70**, 1111–1124.
1121 I. Rao, C. A. Koh, E. D. Sloan and A. K. Sum, *Ind. Eng. Chem. Res.*, 2013, **52**, 6262–6269.
1122 L. Jensen, K. Thomsen and N. von Solms, *Chem. Eng. Sci.*, 2008, **63**, 3069–3080.

Open Access Article. Published on 22 Junie 2020. Downloaded on 2026-02-11 12:42:38 nm..
This article is licensed under a Creative Commons Attribution-NonCommercial 3.0 Unported Licence.

1123 X. Li, C. Chen, Y. Chen, Y. Li and H. Li, *Energy Fuels*, 2015, **29**, 2277–2288.
1124 S. Douïeb, S. Archambault, L. Fradette, F. Bertrand and B. Haut, *Can. J. Chem. Eng.*, 2017, **95**, 187–198.
1125 M. Aminnaji, B. Tohidi, R. Burgass and M. Atilhan, *J. Nat. Gas Sci. Eng.*, 2017, **40**, 17–23.
1126 A. Lone and M. A. Kelland, *Energy Fuels*, 2013, **27**, 2536–2547.
1127 N. Maeda, M. A. Kelland and C. D. Wood, *Chem. Eng. Sci.*, 2018, **183**, 30–36.
1128 Q. Guo and G. W. Small, *Appl. Spectrosc.*, 2013, **67**, 913–923.
1129 A. Ouyang and J. Liu, *Meas. Sci. Technol.*, 2013, **24**, 25502.
1130 A. A. Gowen, F. Marini, Y. Tsuchisaka, S. De Luca, M. Bevilacqua, C. O'Donnell, G. Downey and R. Tsenkova, *Talanta*, 2015, **131**, 609–618.
1131 R. Anderson, F. Tohidi, H. Mozaffar and B. Tohidi, *J. Pet. Sci. Eng.*, 2016, **145**, 520–526.
1132 M. K. Gibbons and B. Örmeci, *J. Water Supply Res. Technol.*, 2013, **62**, 205–213.
1133 R. K. Haghi, J. Yang and B. Tohidi, *Ind. Eng. Chem. Res.*, 2018, **57**, 11728–11737.
1134 J.-H. Sa, A. Melchuna, X. Zhang, R. Morales, A. Cameirao, J.-M. Herri and A. K. Sum, *Ind. Eng. Chem. Res.*, 2019, **58**, 8544–8552.
1135 H. Mozaffar, R. Anderson and B. Tohidi, *Energy Fuels*, 2016, **30**, 10055–10063.
1136 B. Tohidi, R. Anderson, H. Mozaffar and F. Tohidi, *Energy Fuels*, 2015, **29**, 8254–8260.
1137 A. Ding, L. Yang, S. Fan and X. Lou, *Chem. Eng. Sci.*, 2013, **96**, 124–130.
1138 F. Su, C. L. Bray, B. Tan and A. I. Cooper, *Adv. Mater.*, 2008, **20**, 2663–2666.
1139 B. Tohidi, R. Anderson, A. Chapoy, J. Yang and R. W. Burgass, *Energy Fuels*, 2012, **26**, 4053–4058.
1140 J. Yang, A. Chapoy, S. Mazloum and B. Tohidi, *SPE Prod. Oper.*, 2012, **27**, 376–381.
1141 B. Tohidi, A. Chapoy, J. Yang, F. Ahmadloo, I. Valko and Z. M. Zain, *Offshore Technology Conference*, Offshore Technology Conference, 2008.
1142 M. Akhfash, Z. M. Aman, J. Du, P. F. Pickering, M. L. Johns, C. A. Koh and E. F. May, *Energy Fuels*, 2017, **31**, 4875–4885.
1143 J. A. Boxall, C. A. Koh, E. D. Sloan, A. K. Sum and D. T. Wu, *Langmuir*, 2011, **28**, 104–110.
1144 J. A. Boxall, C. A. Koh, E. D. Sloan, A. K. Sum and D. T. Wu, *Ind. Eng. Chem. Res.*, 2009, **49**, 1412–1418.
1145 D. J. Turner, K. T. Miller and E. D. Sloan, *Chem. Eng. Sci.*, 2009, **64**, 5066–5072.
1146 J. Chen, Y.-F. Wang, C.-Y. Sun, F.-G. Li, N. Ren, M.-L. Jia, K.-L. Yan, Y.-N. Lv, B. Liu and G.-J. Chen, *Energy Fuels*, 2014, **29**, 122–129.
1147 A. Cameirão, H. Le Ba, M. Darbouret, J.-M. Herri, J.-L. Peytavy and P. Glénat, *J. Cryst. Growth*, 2012, **342**, 65–71.
1148 M. A. Clarke and P. R. Bishnoi, *Chem. Eng. Sci.*, 2005, **60**, 695–709.
1149 K. AlHarooni, A. Barifcani, D. Pack, R. Gubner and V. Ghodkay, *J. Pet. Sci. Eng.*, 2015, **135**, 608–617.
1150 T. M. Latta, M. E. Seiersten and S. A. Bufton, *Offshore Technology Conference*, Offshore Technology Conference, 2013.
1151 K. Alef, C. Smith, S. Iglauer, R. Gubner and A. Barifcani, *Fuel*, 2018, **222**, 638–647.
1152 A. Hussain, S. Gharfeh and S. S. Adham, *SPE International Production and Operations Conference & Exhibition*, Society of Petroleum Engineers, 2012.
1153 S. Xu, S. Fan, Y. Wang and X. Lang, *Chem. Eng. Sci.*, 2017, **171**, 293–302.
1154 J. W. Bartels, R. A. Jones and R. M. Lucente-Schultz, Removal of Hydrate Inhibitors from Waste Streams, *US Pat.*, 15/423,797, 2017.
1155 J. Minier-Matar, S. Gharfeh, A. Hussain and S. Adham, Separation of Kinetic Hydrate Inhibitors from an Aqueous Solution, *US Pat.*, 10131551, 2016.
1156 Z. R. Chong, S. H. B. Yang, P. Babu, P. Linga and X. Sen Li, *Appl. Energy*, 2016, **162**, 1633–1652.
1157 K. A. Kvenvolden and T. D. Lorenson, *Geophysical Monograph Series*, 2000, vol. 124, pp. 3–18.
1158 K. A. Kvenvolden and M. A. McMenamin, *Geolocial Surv. Circ.*, 1980, **825**, 1–11.
1159 J. H. Hand, D. L. Katz and V. K. Verma, *Natural Gases in Marine Sediments*, Springer US, MA, 1974, pp. 179–194.
1160 R. Boswell and T. S. Collett, *Energy Environ. Sci.*, 2011, **4**, 1206–1215.
1161 X. Sen Li, C. G. Xu, Y. Zhang, X. K. Ruan, G. Li and Y. Wang, *Appl. Energy*, 2016, **172**, 286–322.
1162 L. G. Tang, R. Xiao, G. Li, Z. P. Feng, X. Sen Li and S. S. Fan, *Guocheng Gongcheng Xuebao*, 2006, **6**, 548–553.
1163 G. Li, X. Sen Li and Y. Wang, *Energy Procedia*, 2014, **61**, 803–807.
1164 D. L. Li, D. Q. Liang, S. S. Fan, X. Sen Li, L. G. Tang and N. S. Huang, *Energy Convers. Manage.*, 2008, **49**, 2207–2213.
1165 C. Cranganu, *J. Pet. Sci. Eng.*, 2009, **65**, 76–80.
1166 J. M. Schicks, E. Spangenberg, R. Giese, M. MLuzi-Helbin, M. Priegnitz and B. Beeskow-Strauch, *Energies*, 2013, **6**, 3002–3016.
1167 Y. Song, Y. Kuang, Z. Fan, Y. Zhao and J. Zhao, *Int. J. Heat Mass Transfer*, 2018, **121**, 207–214.
1168 Z. Yin, G. Moridis, Z. R. Chong, H. K. Tan and P. Linga, *Ind. Eng. Chem. Res.*, 2018, **57**, 5776–5791.
1169 M. Terzariol, G. Goldsztein and J. C. Santamarina, *Energy*, 2017, **141**, 1622–1628.
1170 Ş. Merey and S. N. Longinos, *J. Nat. Gas Sci. Eng.*, 2018, **52**, 248–266.
1171 Z. Yin, G. Moridis, Z. R. Chong, H. K. Tan and P. Linga, *Appl. Energy*, 2018, **230**, 444–459.
1172 K. Yamamoto, Y. Terao, T. Fujii, T. Ikawa, M. Seki, M. Matsuzawa and T. Kanno, *Proceedings of the Annual Offshore Technology Conference*, Offshore Technology Conference, 2014, vol. 3, pp. 1802–1812.
1173 Z. R. Chong, Z. Yin and P. Linga, *Energy Procedia*, 2017, **105**, 4963–4969.

Open Access Article. Published on 22 Junie 2020. Downloaded on 2026-02-11 12:42:38 nm..
This article is licensed under a Creative Commons Attribution-NonCommercial 3.0 Unported Licence.

1174 R. Sun, Z. Fan, M. Yang, W. Pang, Y. Li and Y. Song, *J. Nat. Gas Sci. Eng.*, 2019, **65**, 125–134.
1175 S. Circone, L. A. Stern, S. H. Kirby, J. C. Pinkston and W. B. Durham, *Ann. N. Y. Acad. Sci.*, 2006, **912**, 544–555.
1176 M. Yang, Y. Gao, H. Zhou, B. Chen and Y. Li, *Int. J. Energy Res.*, 2019, **43**(10), 5493–5505, DOI: 10.1002/er.4669.
1177 Y. Gao, M. Yang, J. Nan Zheng and B. Chen, *Fuel*, 2018, **232**, 99–107.
1178 K. U. Heeschen, S. Abendroth, M. Priegnitz, E. Spangenberg, J. Thaler and J. M. Schicks, *Energy Fuels*, 2016, **30**, 6210–6219.
1179 Y. Wang, J. C. Feng, X. Sen Li, L. Zhan and X. Y. Li, *Energy*, 2018, **160**, 835–844.
1180 T. Lv, X. Li, Z. Chen, D. Sun, Y. Zhang, K. Yan and J. Cai, *Energy Technol.*, 2018, **6**, 2501–2511.
1181 Z. R. Chong, J. W. R. Moh, Z. Yin, J. Zhao and P. Linga, *Appl. Energy*, 2018, **229**, 637–647.
1182 Z. R. Chong, J. Zhao, J. H. R. Chan, Z. Yin and P. Linga, *Appl. Energy*, 2018, **214**, 117–130.
1183 H. Shin and J. C. Santamarina, *Acta Geotech.*, 2017, **12**, 883–895.
1184 B. R. C. Malagar, K. P. Lijith and D. N. Singh, *J. Nat. Gas Sci. Eng.*, 2019, 168–184.
1185 L. Yang, Y. Liu, H. Zhang, B. Xiao, X. Guo, R. Wei, L. Xu, L. Sun, B. Yu, S. Leng and Y. Li, *Chin. J. Chem. Eng.*, 2019, **27**(9), 2133–2147, DOI: 10.1016/j.cjche.2019.02.028.
1186 Z. R. Chong, S. H. B. Yang, P. Babu, P. Linga, X.-S. Sen Li, Z. R. Chong, P. Babu and X.-S. Sen-Li, *Appl. Energy*, 2015, **162**, 1633–1652.
1187 Z. Yin and P. Linga, *Chin. J. Chem. Eng.*, 2019, **27**(9), 2026–2036, DOI: 10.1016/j.cjche.2019.01.005.
1188 K. Yamamoto, T. Kanno, X. X. Wang, M. Tamaki, T. Fujii, S. S. Chee, X. W. Wang, V. Pimenov and V. Shako, *RSC Adv.*, 2017, **7**, 5554–5577.
1189 Y. Bai and Q. Li, *Sci. China: Technol. Sci.*, 2010, **53**, 2469–2476.
1190 V. C. Nair, S. K. Prasad, R. Kumar and J. S. Sangwai, *Appl. Energy*, 2018, **225**, 755–768.
1191 Y. Wang, X. Sen Li, G. Li, N. S. Huang and J. C. Feng, *Fuel*, 2014, **117**, 688–696.
1192 J. H. Sira, S. L. Patil and V. A. Kamath, in *Proceedings - SPE Annual Technical Conference and Exhibition*, Society of Petroleum Engineers, 1990, vol. Pi, pp. 977–984.
1193 G. Li, D. Wu, X. Li, Y. Zhang, Q. Lv and Y. Wang, *Energy Fuels*, 2017, **31**, 5411–5418.
1194 V. Chandrasekharan Nair, D. Mech, P. Gupta and J. S. Sangwai, *Energy Fuels*, 2018, **32**, 6657–6668.
1195 S. Merey, R. I. Al-Raoush, J. Jung and K. A. Alshibli, *J. Pet. Sci. Eng.*, 2018, **171**, 48–62.
1196 A. V. Palodkar and A. K. Jana, *Sci. Rep.*, 2018, **8**, 16563.
1197 J. L. Panter, A. L. Ballard, A. K. Sum, E. D. Sloan and C. A. Koh, *Energy Fuels*, 2011, **25**, 2572–2578.
1198 A. Okwananke, J. Yang, B. Tohidi, E. Chuvilin, V. Istomin, B. Bukhanov and A. Cheremisin, *J. Chem. Thermodyn.*, 2018, **117**, 138–146.
1199 L. Zhang, Y. Kuang, X. Zhang, Y. Song, Y. Liu and J. Zhao, *Ind. Eng. Chem. Res.*, 2017, **56**, 7585–7592.
1200 K. Rose, R. Boswell and T. Collett, *Mar. Pet. Geol.*, 2011, **28**, 311–331.
1201 J. Ye, X. Qin, H. Qiu, N. Wu, H. Lu, W. Xie, J. Lu, C. Lu, Z. Kuang, Q. Liang, H. Lu, B. Kou and J. Wei, *China Geol.*, 2018, **1**, 1–5.
1202 R. Boswell, D. Schoderbek, T. S. Collett, S. Ohtsuki, M. White and B. J. Anderson, *Energy Fuels*, 2017, **31**, 140–153.
1203 S. H. Hancock, T. S. Collett, S. R. Dallimore, T. Satoh, T. Inoue, E. Huenges, J. Henninges and B. Weatherill, *Geol. Surv. Can., Bull.*, 2005, **585**, 1–15.
1204 C. Ruppel, MITEI Nat. gas Report, Suppl. Pap. Methane Hydrates 4, 2011, 4, 1–25.
1205 K. A. Kvenvolden, *Global Biogeochem. Cycles*, 1988, **2**, 221–229.
1206 K. A. Kvenvolden, *Rev. Geophys.*, 1993, **31**, 173–187.
1207 G. J. F. MacDonald, *Clim. Change*, 1990, **16**, 247.
1208 J. Bohannon, *Science*, 2008, **319**(5871), 1753.
1209 V. Krey, J. G. Canadell, N. Nakicenovic, Y. Abe, H. Andruleit, D. Archer, A. Grubler, N. T. M. Hamilton, A. Johnson, V. Kostov, J.-F. Lamarque, N. Langhorne, E. G. Nisbet, B. O'Neill, K. Riahi, M. Riedel, W. Wang and V. Yakushev, *Environ. Res. Lett.*, 2009, **4**, 34007.
1210 A. Mascarelli, A sleeping giant?, *Nat. Clim. Change*, 2009, 46–49.
1211 G. Whiteman, C. Hope and P. Wadhams, *Nature*, 2013, **499**, 401–403.
1212 J. P. Kennett and L. D. Stott, *Nature*, 1991, **353**, 225–229.
1213 G. R. Dickens, J. R. O'Neil, D. K. Rea and R. M. Owen, *Paleoceanography*, 1995, **10**, 965–971.
1214 G. R. Dickens, M. M. Castillo and J. C. G. Walker, *Geology*, 1997, **25**, 259–262.
1215 J. P. Kennett, K. G. Cannariato, I. L. Hendy and R. J. Behl, *Science*, 2000, **288**, 128–133.
1216 J. P. Kennett, K. G. Cannariato, I. L. Hendy and R. J. Behl, *Methane hydrates in Quaternary climate change: The clathrate gun hypothesis*, American Geophysical Union, Washington, D.C., 2002.
1217 K. G. Cannariato and L. D. Stott, *Geochem., Geophys., Geosyst.*, 2004, **5**(5), DOI: 10.1029/2003GC000600.
1218 P. Serov, S. Vadakkepuliyambatta, J. Mienert, H. Patton, A. Portnov, A. Silyakova, G. Panieri, M. L. Carroll, J. Carroll and K. Andreassen, *Proc. Natl. Acad. Sci. U. S. A.*, 2017, 201619288.
1219 R. E. Fisher, S. Sriskantharajah, D. Lowry, M. Lanoisellé, C. M. R. Fowler, R. H. James, O. Hermansen, C. Lund Myhre, A. Stohl, J. Greinert, P. B. R. Nisbet-Jones, J. Mienert and E. G. Nisbet, *Geophys. Res. Lett.*, 2011, **38**, L21803, DOI: 10.1029/2011GL049319.
1220 C. A. Graves, L. Steinle, G. Rehder, H. Niemann, D. P. Connelly, D. Lowry, R. E. Fisher, A. W. Stott, H. Sahling and R. H. James, *J. Geophys. Res.: Oceans*, 2015, **120**, 6185–6201.
1221 J. W. Pohlman, J. Greinert, C. Ruppel, A. Silyakova, L. Vielstädte, M. Casso, J. Mienert and S. Bünz, *Proc. Natl. Acad. Sci. U. S. A.*, 2017, **114**, 5355–5360.

Open Access Article. Published on 22 Junie 2020. Downloaded on 2026-02-11 12:42:38 nm..
This article is licensed under a Creative Commons Attribution-NonCommercial 3.0 Unported Licence.

1222 K. J. Sparrow, J. D. Kessler, J. R. Southon, F. Garcia-Tigreros, K. M. Schreiner, C. D. Ruppel, J. B. Miller, S. J. Lehman and X. Xu, *Sci. Adv.*, 2018, **4**, eaao4842.
1223 B. F. Thornton, M. C. Geibel, P. M. Crill, C. Humborg and C.-M. Mörth, *Geophys. Res. Lett.*, 2016, **43**, 5869–5877.
1224 N. Shakhova, I. Semiletov, I. Leifer, V. Sergienko, A. Salyuk, D. Kosmach, D. Chernykh, C. Stubbs, D. Nicolsky and V. Tumskoy, *Nat. Geosci.*, 2014, **7**, 64.
1225 T. F. Stocker, D. Qin, G. K. Plattner, M. M. B. Tignor, S. K. Allen, J. Boschung, A. Nauels, Y. Xia, V. Bex and P. M. Midgley, *Climate change 2013 the physical science basis: Working Group I contribution to the fifth assessment report of the intergovernmental panel on climate change*, Cambridge University Press, 2013, vol. 9781107057.
1226 R. H. James, P. Bousquet, I. Bussmann, M. Haeckel, R. Kipfer, I. Leifer, H. Niemann, I. Ostrovsky, J. Piskozub, G. Rehder, T. Treude, L. Vielstädte and J. Greinert, *Limnol. Oceanogr.*, 2016, **61**, S283–S299.
1227 C. D. Ruppel, *Nat. Educ. Knowl.*, 2011, **3**, 29.
1228 A. E. Taylor, S. R. Dallimore, P. R. Hill, D. R. Issler, S. Blasco and F. Wright, *J. Geophys. Res.: Earth Surf.*, 2013, **118**, 2365–2379.
1229 W. S. Reeburgh, *Chem. Rev.*, 2007, **107**, 486–513.
1230 K. Knittel and A. Boetius, *Annu. Rev. Microbiol.*, 2009, **63**, 311–334.
1231 D. F. McGinnis, J. Greinert, Y. Artemov, S. E. Beaubien and A. Wuest, *J. Geophys. Res.*, 2006, **111**, C09007.
1232 G. Rehder, P. W. Brewer, E. T. Peltzer and G. Friederich, *Geophys. Res. Lett.*, 2002, **29**, 21–24.
1233 G. Rehder, I. Leifer, P. G. Brewer, G. Friederich and E. T. Peltzer, *Mar. Chem.*, 2009, **114**, 19–30.
1234 B. Wang, S. A. Socolofsky, J. A. Breier and J. S. Seewald, *J. Geophys. Res.: Oceans*, 2016, **121**, 2203–2230.
1235 B. B. Ward, K. A. Kilpatrick, P. C. Novelli and M. I. Scranton, *Nature*, 1987, **327**, 226–229.
1236 S. Mau, D. L. Valentine, J. F. Clark, J. Reed, R. Camilli and L. Washburn, *Geophys. Res. Lett.*, 2007, **34**(22), L22603, DOI: 10.1029/2007GL031344.
1237 F. Garcia-Tigreros and J. D. Kessler, *J. Geophys. Res.: Biogeosci.*, 2018, **123**, 2135–2144.
1238 R. J. Davies, J. Yang, A. Li, S. Mathias and R. Hobbs, *Earth Planet. Sci. Lett.*, 2015, **423**, 202–209.
1239 A. R. Gorman and K. Senger, *J. Geophys. Res.: Solid Earth*, 2010, **115**, B07105, DOI: 10.1029/2009JB006680.
1240 B. J. Phrampus and M. J. Hornbach, *Nature*, 2012, **490**, 527–530.
1241 B. J. Phrampus, M. J. Hornbach, C. D. Ruppel and P. E. Hart, *J. Geophys. Res.: Solid Earth*, 2014, **119**, 8594–8609.
1242 S. L. Hautala, E. A. Solomon, H. P. Johnson, R. N. Harris and U. K. Miller, *Geophys. Res. Lett.*, 2014, **41**, 8486–8494.
1243 H. P. Johnson, U. K. Miller, M. S. Salmi and E. A. Solomon, *Geochem., Geophys., Geosyst.*, 2015, **16**, 3825–3839.
1244 I. R. MacDonald, N. L. Guinasso, R. Sassen, J. M. Brooks, L. Lee and K. T. Scott, *Geology*, 1994, **22**, 699–702.
1245 G. K. Westbrook, K. E. Thatcher, E. J. Rohling, A. M. Piotrowski, H. Pälike, A. H. Osborne, E. G. Nisbet, T. A. Minshull, M. Lanoisellé, R. H. James, V. Hühnerbach, D. Green, R. E. Fisher, A. J. Crocker, A. Chabert, C. Bolton, A. Beszczynska-Möller, C. Berndt and A. Aquilina, *Geophys. Res. Lett.*, 2009, **36**, L15608.
1246 A. Skarke, C. Ruppel, M. Kodis, D. Brothers and E. Lobecker, *Nat. Geosci.*, 2014, **7**, 657.
1247 C. Berndt, T. Feseker, T. Treude, S. Krastel, V. Liebetrau, H. Niemann, V. J. Bertics, I. Dumke, K. Dünnbier, B. Ferré, C. Graves, F. Gross, K. Hissmann, V. Hühnerbach, S. Krause, K. Lieser, J. Schauer and L. Steinle, *Science*, 2014, **343**, 284–287.
1248 L. L. Brothers, P. E. Hart and C. D. Ruppel, *Geophys. Res. Lett.*, 2012, **39**, L15501, DOI: 10.1029/2012GL052222.
1249 L. L. Brothers, B. M. Herman, P. E. Hart and C. D. Ruppel, *Geochem., Geophys., Geosyst.*, 2016, **17**(11), 4354–4365, DOI: 10.1002/2016GC006584.
1250 P. P. Overduin, T. Schneider von Deimling, F. Miesner, M. N. Grigoriev, C. Ruppel, A. Vasiliev, H. Lantuit, B. Juhls and S. Westermann, *J. Geophys. Res.: Oceans*, 2019, **124**, 3490–3507.
1251 V. Rachold, D. Y. Bolshiyanov, M. N. Grigoriev, H.-W. Hubberten, R. Junker, V. V. Kunitsky, F. Merker, P. P. Overduin and W. Schneider, *EOS, Trans. Am. Geophys. Union*, 2007, **88**, 149.
1252 P. Rekant, H. A. Bauch, T. Schwenk, A. Portnov, E. Gusev, V. Spiess, G. Cherkashov and H. Kassens, *Arktos*, 2015, **1**, 11.
1253 P. Serov, A. Portnov, J. Mienert, P. Semenov and P. Ilatovskaya, *J. Geophys. Res.: Earth Surf.*, 2015, **120**, 1515–1529.
1254 A. Portnov, A. J. Smith, J. Mienert, G. Cherkashov, P. Rekant, P. Semenov, P. Serov and B. Vanshtein, *Geophys. Res. Lett.*, 2013, **40**, 3962–3967.
1255 C. D. Ruppel, B. M. Herman, L. L. Brothers and P. E. Hart, *Geochem., Geophys., Geosyst.*, 2016, **17**, 4333–4353.
1256 K. Andreassen, A. Hubbard, M. Winsborrow, H. Patton, S. Vadakkepuliyambatta, A. Plaza-Faverola, E. Gudlaugsson, P. Serov, A. Deryabin and R. Mattingsdal, *Science*, 2017, **356**, 948–953.
1257 A. Portnov, S. Vadakkepuliyambatta, J. Mienert and A. Hubbard, *Nat. Commun.*, 2016, **7**, 10314, DOI: 10.1038/ncomms10314.
1258 P. Serov, S. Vadakkepuliyambatta, J. Mienert, H. Patton, A. Portnov, A. Silyakova, G. Panieri, M. L. Carroll, J. L. Carroll, K. Andreassen and A. Hubbard, *Proc. Natl. Acad. Sci. U. S. A.*, 2017, **114**, 6215–6220.
1259 M. Waage, A. Portnov, P. Serov, S. Bünz, K. A. Waghorn, S. Vadakkepuliyambatta, J. Mienert and K. Andreassen, *Geochem., Geophys., Geosyst.*, 2019, **20**, 630–650.
1260 J. L. Wadham, S. Arndt, S. Tulaczyk, M. Stibal, M. Tranter, J. Telling, G. P. Lis, E. Lawson, A. Ridgwell, A. Dubnick, M. J. Sharp, A. M. Anesio and C. E. H. Butler, *Nature*, 2012, **488**, 633–637.
1261 G. Lamarche-Gagnon, J. L. Wadham, B. S. Lollar, S. Arndt, P. Fietzek, A. D. Beaton, A. J. Tedstone, J. Telling, E. A. Bagshaw and J. R. Hawkings, *Nature*, 2019, **565**, 73.
1262 R. John Parkes, B. A. Cragg and P. Wellsbury, *Hydrogeol. J.*, 2000, **8**, 11–28.

Open Access Article. Published on 22 Junie 2020. Downloaded on 2026-02-11 12:42:38 nm..
This article is licensed under a Creative Commons Attribution-NonCommercial 3.0 Unported Licence.

1263 B. D. Lanoil, R. Sassen, M. T. La Duc, S. T. Sweet and K. H. Nealson, *Appl. Environ. Microbiol.*, 2001, **67**, 5143–5153.
1264 H. J. Mills, R. J. Martinez, S. Story and P. A. Sobecky, *Appl. Environ. Microbiol.*, 2005, **71**, 3235–3247.
1265 J. R. Marchesi, A. J. Weightman, B. A. Cragg, R. John Parkes and J. C. Fry, *FEMS Microbiol. Ecol.*, 2001, **34**, 221–228.
1266 F. Inagaki, T. Nunoura, S. Nakagawa, A. Teske, M. Lever, A. Lauer, M. Suzuki, K. Takai, M. Delwiche, F. S. Colwell, K. H. Nealson, K. Horikoshi, S. D'Hondt and B. B. Jørgensen, *Proc. Natl. Acad. Sci. U. S. A.*, 2006, **103**, 2815–2820.
1267 R. J. Parkes, G. Sellek, G. Webster, D. Martin, E. Anders, A. J. Weightman and H. Sass, *Environ. Microbiol.*, 2009, **11**, 3140–3153.
1268 L. J. Hamdan, M. Sikaroodi and P. M. Gillevet, *Geomicrobiol. J.*, 2012, **29**, 340–351.
1269 B. R. Briggs, F. Inagaki, Y. Morono, T. Futagami, C. Huguet, A. Rosell-Mele, T. D. Lorenson and F. S. Colwell, *FEMS Microbiol. Ecol.*, 2012, **81**, 88–98.
1270 J. C. Fry, G. Webster, B. A. Cragg, A. J. Weightman and R. J. Parkes, *FEMS Microbiol. Ecol.*, 2006, **58**, 86–98.
1271 J.-W. Lee, K. K. Kwon, A. Azizi, H.-M. Oh, W. Kim, J.-J. Bahk, D.-H. Lee and J.-H. Lee, *Mar. Pet. Geol.*, 2013, **47**, 136–146.
1272 L. Jiao, X. Su, Y. Wang, H. Jiang, Y. Zhang and F. Chen, *Geosci. Front.*, 2015, **6**, 627–633.
1273 H. Lei, Y. Yang, S. Kandasamy and C. Shi, *Acta Geol. Sin. Ed.*, 2018, **92**, 333–341.
1274 H. Cui, X. Su, F. Chen, M. Holland, S. Yang, J. Liang, P. Su, H. Dong and W. Hou, *Mar. Environ. Res.*, 2019, **144**, 230–239.
1275 M. D. Max, *Natural gas hydrate in oceanic and permafrost environments*, Springer Science & Business Media, 2003, vol. 5.
1276 R. K. Thauer, A. K. Kaster, H. Seedorf, W. Buckel and R. Hedderich, *Nat. Rev. Microbiol.*, 2008, **6**, 579–591.
1277 K. U. Hinrichs, J. M. Hayes, W. Bach, A. J. Spivackl, L. R. Hmelo, N. G. Holm, C. G. Johnson and S. P. Sylva, *Proc. Natl. Acad. Sci. U. S. A.*, 2006, **103**, 14684–14689.
1278 R. Conrad, *Environ. Microbiol. Rep.*, 2009, **1**, 285–292.
1279 K. Knittel, G. Wegener and A. Boetius, *Microbial Communities Utilizing Hydrocarbons and Lipids: Members, Metagenomics and Ecophysiology*, 2019, pp. 1–21.
1280 P. J. Talling, M. L. Clare, M. Urlaub, E. Pope, J. E. Hunt and S. F. L. Watt, *Oceanography*, 2014, **27**, 32–45.
1281 M. J. Hornbach, L. L. Lavier and C. D. Ruppel, *Geochem., Geophys., Geosyst.*, 2007, **8**(12), DOI: 10.1029/2007GC001722.
1282 J. C. Hill, D. S. Brothers, M. J. Hornbach, D. E. Sawyer, D. J. Shillington and A. Bécel, *Geol. Soc. London, Spec. Publ.*, 2019, **477**, 169–181.
1283 D. E. Smith, S. Harrison and J. T. Jordan, *Quat. Sci. Rev.*, 2013, **82**, 93–103.
1284 E. L. Soutter, I. A. Kane and M. Huuse, *Geology*, 2018, **46**, 511–514.
1285 B. Dugan and P. B. Flemings, *Science*, 2000, **289**, 288–291.
1286 R. E. Kayen and H. J. Lee, *Mar. Geotechnol.*, 1991, **10**, 125–141.
1287 J. Mienert, J. Posewang and M. Baumann, *Geol. Soc. London, Spec. Publ.*, 1998, **137**, 275–291.
1288 J. J. Mountjoy, I. Pecher, S. Henrys, G. Crutchley, P. M. Barnes and A. Plaza-Faverola, *Geochem., Geophys., Geosyst.*, 2014, **15**, 4137–4156.
1289 S. Yelisetti, G. D. Spence and M. Riedel, *Geophys. J. Int.*, 2014, **199**, 441–458.
1290 D. E. Sawyer, R. A. Mason, A. E. Cook and A. Portnov, *Sci. Rep.*, 2019, **9**, 128.
1291 X. Wu, Q. Liang, Y. Ma, Y. Shi, Z. Xia, L. Liu and M. Haeckel, *Energies*, 2018, 11.
1292 S. Bünz, J. Mienert, M. Vanneste and K. Andreassen, *Geophysics*, 2005, **70**, B19–B34.
1293 J. Mienert, M. Vanneste, S. Bünz, K. Andreassen, H. Haflidason and H. P. Sejrup, *Mar. Pet. Geol.*, 2005, **22**, 233–244.
1294 H. Haflidason, R. Lien, H. Sejrup, C. Forsberg and P. Bryn, *Mar. Pet. Geol.*, 2005, **22**, 123–136.
1295 M. Hovland, J. V. Gardner and A. G. Judd, *Geofluids*, 2002, **2**, 127–136.
1296 N. Sultan, G. Bohrmann, L. Ruffine, T. Pape, V. Riboulot, J.-L. Colliat, A. De Prunelé, B. Dennielou, S. Garziglia, T. Himmler, T. Marsset, C. A. Peters, A. Rabiu and J. Wei, *J. Geophys. Res. Solid Earth*, 2014, **119**, 2679–2694.
1297 W. J. Winters, I. A. Pecher, W. F. Waite and D. H. Mason, *Am. Mineral.*, 2004, **89**, 1221–1227.
1298 T. S. Yun, C. J. Santamarina and C. Ruppel, *J. Geophys. Res. Solid Earth*, 2007, **12**, B04106, DOI: 10.1029/2006JB004484.
1299 H. Daigle and B. Dugan, *J. Geophys. Res. Solid Earth*, 2010, **115**, B11103.
1300 J. Elger, C. Berndt, L. Rüpke, S. Krastel, F. Gross and W. H. Geissler, *Nat. Commun.*, 2018, **9**, 715.
1301 W. Xu and L. N. Germanovich, *J. Geophys. Res. Solid Earth*, 2006, **111**, B01104, DOI: 10.1029/2004JB003600.
1302 J. L. H. Grozic, *Submarine mass movements and their consequences*, Springer, 2010, pp. 11–30.
1303 J. L. H. Grozic and H. Ghiassian, in Proc., 63rd Canadian Geotechnical Conf, 2010, pp. 459–466.
1304 J. S. Booth, D. W. O'leary, P. Popenoe, W. W. Danforth and W. C. Schwab, in *Submarine Landslides Selected Studies in the US Exclusive Economic Zone*, ed. W. C. Schwab, H. J. Lee and D. C. Twichell, 1993, pp. 14–22.
1305 P. Popenoe, E. A. Schmuck, W. P. Dillon, W. C. Schwab, H. J. Lee and D. C. Twichell, *Submarine Landslides Selected Studies in the US Exclusive Economic Zone*, 1993, pp. 40–53.
1306 M. F. Nixon and J. L. H. Grozic, *Can. Geotech. J.*, 2007, **44**, 314–325.
1307 T.-H. Kwon and G.-C. Cho, *Energies*, 2012, 5.
1308 J. P. Kennett, K. G. Cannariato, I. L. Hendy and R. J. Behl, *Methane hydrates in quaternary climate change: the clathrate gun hypothesis*, 2003, vol. 54, pp. 1–9.
1309 A. Dawson, S. Bondevik and J. T. Teller, *The Holocene*, 2011, **21**, 1167–1171.
1310 M. Maslin, M. Owen, S. Day and D. Long, *Geology*, 2004, **32**, 53–56.

Open Access Article. Published on 22 Junie 2020. Downloaded on 2026-02-11 12:42:38 nm..
This article is licensed under a Creative Commons Attribution-NonCommercial 3.0 Unported Licence.

1311 K. Andreassen, A. Hubbard, M. Winsborrow, H. Patton, S. Vadakkepuliyambatta, A. Plaza-Faverola, E. Gudlaugsson, P. Serov, A. Deryabin, R. Mattingsdal, J. Mienert and S. Bünz, *Science*, 2017, **356**, 948–953.
1312 M. Hovland and H. Svensen, *Mar. Geol.*, 2006, **228**, 15–23.
1313 R. Freij-Ayoub, C. Tan, B. Clennell, B. Tohidi and J. Yang, *J. Pet. Sci. Eng.*, 2007, **57**, 209–220.
1314 M. Hovland and O. T. Gudmestad, *Nat. Gas Hydrates Occur. Distrib. Detect.*, 2001, 307–315.
1315 C. Hadley, D. Peters, A. Vaughan and D. Bean, in *International Petroleum Technology Conference*, International Petroleum Technology Conference, 2008.
1316 T. Kvalstad, K. Yamamoto, S. Noguchi, S. Uchida and K. Soga, *Effect of gas hydrate production on seabed stability in the Eastern Nankai Trough area*, 2011.
1317 H. Zhang, X. Luo, J. Bi, G. He and Z. Guo, *Mar. Georesour. Geotechnol.*, 2019, **37**, 467–476.
1318 J. I. Lunine and D. J. Stevenson, *Astrophys. J. Suppl. Ser.*, 1985, **58**, 493.
1319 J. S. Kargel and J. I. Lunine, Clathrate Hydrates on Earth and in the Solar System, in *Solar System Ices*, ed. B. Schmitt, C. De Bergh and M. Festou, Springer Netherlands, Dordrecht, 1998, pp. 97–117.
1320 O. Mousis, J. I. Lunine, C. Thomas, M. Pasek, U. Marbœuf, Y. Alibert, V. Ballenegger, D. Cordier, Y. Ellinger, F. Pauzat and S. Picaud, *Astrophys. J.*, 2009, **691**, 1780–1786.
1321 O. Mousis, E. Chassefière, N. G. Holm, A. Bouquet, J. H. Waite, W. D. Geppert, S. Picaud, Y. Aikawa, M. Ali-Dib, J. L. Charlou and P. Rousselot, *Astrobiology*, 2015, **15**, 308–326.
1322 R. W. Carlson, M. S. Anderson, R. Mehlman and R. E. Johnson, *Icarus*, 2005, **177**, 461–471.
1323 S. H. Royle, W. Montgomery, S. P. Kounaves and M. A. Sephton, *J. Geophys. Res.: Planets*, 2017, **122**, 2793–2802.
1324 S. L. Miller, *Proc. Natl. Acad. Sci. U. S. A.*, 1961, **47**, 1798–1808.
1325 I.-M. Chou, A. Sharma, R. C. Burruss, R. J. Hemley, A. F. Goncharov, L. A. Stern and S. H. Kirby, *J. Phys. Chem. A*, 2001, **105**, 4664–4668.
1326 M. Choukroun, S. W. Kieffer, X. Lu and G. Tobie, Clathrate Hydrates: Implications for Exchange Processes in the Outer Solar System, in *The Science of Solar System Ices*, ed. M. S. Gudipati and J. Castillo-Rogez, Astrophysics and Space Science Library, Springer New York, New York, NY, 2013, pp. 409–454.
1327 A. Dobrovolskis and A. P. Ingersoll, *Icarus*, 1975, **26**, 353–357.
1328 S. L. Miller and W. D. Smythe, *Science*, 1970, **170**, 531–533.
1329 O. Mousis, E. Chassefière, J. Lasue, V. Chevrier, M. E. Elwood Madden, A. Lakhlifi, J. I. Lunine, F. Montmessin, S. Picaud, F. Schmidt and T. D. Swindle, *Space Sci. Rev.*, 2013, **174**, 213–250.
1330 R. E. Pellenbarg, M. D. Max and S. M. Clifford, *J. Geophys. Res.: Planets*, 2003, **108**(E4), 8042, DOI: 10.1029/2002JE001901.
1331 A. G. Davies, C. Sotin, M. Choukroun, D. L. Matson and T. V. Johnson, *Icarus*, 2016, **274**, 23–32.
1332 J. P. Osegovic and M. D. Max, *J. Geophys. Res.: Planets*, 2005, **110**, E08004, DOI: 10.1029/2005JE002435.
1333 R. R. Fu, A. I. Ermakov, S. Marchi, J. C. Castillo-Rogez, C. A. Raymond, B. H. Hager, M. T. Zuber, S. D. King, M. T. Bland, M. Cristina De Sanctis, F. Preusker, R. S. Park and C. T. Russell, *Earth Planet. Sci. Lett.*, 2017, **476**, 153–164.
1334 S. Kamata, F. Nimmo, Y. Sekine, K. Kuramoto, N. Noguchi, J. Kimura and A. Tani, *Nat. Geosci.*, 2019, **12**, 407–410.
1335 K. Shin, R. Kumar, K. A. Udachin, S. Alavi and J. A. Ripmeester, *Proc. Natl. Acad. Sci. U. S. A.*, 2012, **109**, 14785–14790.
1336 U. Marboeuf, O. Mousis, J.-M. Petit, B. Schmitt, A. L. Cochran and H. A. Weaver, *Astron. Astrophys.*, 2010, **525**, DOI: 10.1051/0004-6361/201015438.
1337 A. Luspay-Kuti, O. Mousis, M. Hässig, S. A. Fuselier, J. I. Lunine, B. Marty, K. E. Mandt, P. Wurz and M. Rubin, *Sci. Adv.*, 2016, **2**, e1501781.
1338 J. Ghosh, R. R. J. Methikkalam, R. G. Bhuin, G. Ragupathy, N. Choudhary, R. Kumar and T. Pradeep, *Proc. Natl. Acad. Sci. U. S. A.*, 2019, **116**, 1526–1531.
1339 M. Choukroun, T. H. Vu and E. C. Fayolle, *Proc. Natl. Acad. Sci. U. S. A.*, 2019, **116**, 14407–14408.
1340 G. J. Flynn, F. Horz, S. Bajt and S. R. Sutton, *Lunar and Planetary Science Conference*, 1996, vol. 27.
1341 M. Fries, A. Christou, D. Archer, P. Conrad, W. Cooke, J. Eigenbrode, I. L. ten Kate, M. Matney, P. Niles, M. Sykes, A. Steele and A. Treiman, *Geochemical Perspect. Lett.*, 2016, **2**, 10–23.
1342 M. J. Russell, A. E. Murray and K. P. Hand, *Astrobiology*, 2017, **17**, 1265–1273.
1343 K. P. Hand, C. F. Chyba, J. C. Priscu, R. W. Carlson and K. H. Nealson, *Europa*, 2009, 589–629.
1344 IPCC, IPCC report Global Warming of 1.5 C: Summary for Policymakers, 2018.
1345 J. Rogelj, A. Popp, K. V. Calvin, G. Luderer, J. Emmerling, D. Gernaat, S. Fujimori, J. Strefler, T. Hasegawa, G. Marangoni, V. Krey, E. Kriegler, K. Riahi, D. P. Van Vuuren, J. Doelman, L. Drouet, J. Edmonds, O. Fricko, M. Harmsen, P. Havlík, F. Humpenöder, E. Stehfest and M. Tavoni, *Nat. Clim. Change*, 2018, **8**, 325–332.
1346 D. Y. C. Leung, G. Caramanna and M. M. Maroto-Valer, *Renewable Sustainable Energy Rev.*, 2014, **39**, 426–443.
1347 S. Budinis, S. Krevor, N. Mac Dowell, N. Brandon and A. Hawkes, *Energy Strateg. Rev.*, 2018, **22**, 61–81.
1348 P. Babu, P. Linga, R. Kumar and P. Englezos, *Energy*, 2015, **85**, 261–279.
1349 E. D. Sloan Jr. and C. A. Koh, *Clathrate Hydrates of Natural Gases*, CRC Press, 3rd edn, 2007.
1350 B. Chazallon and C. Pirim, *Chem. Eng. J.*, 2018, **342**, 171–183.
1351 A. Hassanpouryouzband, J. Yang, B. Tohidi, E. Chuvilin, V. Istomin and B. Bukhanov, *ACS Sustainable Chem. Eng.*, 2019, **7**, 5338–5345.
1352 A. Hassanpouryouzband, J. Yang, B. Tohidi, E. Chuvilin, V. Istomin, B. Bukhanov and A. Cheremisin, *ACS Sustainable Chem. Eng.*, 2018, **6**, 5732–5736.

 This journal is © The Royal Society of Chemistry 2020

Open Access Article. Published on 22 Junie 2020. Downloaded on 2026-02-11 12:42:38 nm..
This article is licensed under a Creative Commons Attribution-NonCommercial 3.0 Unported Licence.

1353 S. Adisasmito, R. J. Frank and E. D. Sloan, *J. Chem. Eng. Data*, 1991, **36**, 68–71.
1354 H. Oyama, W. Shimada, T. Ebinuma, Y. Kamata, S. Takeya, T. Uchida, J. Nagao and H. Narita, *Fluid Phase Equilib.*, 2005, **234**, 131–135.
1355 N. Mayoufi, D. Dalmazzone, A. Delahaye, P. Clain, L. Fournaison and W. Fürst, *J. Chem. Eng. Data*, 2011, **56**, 2987–2993.
1356 Y. Zhang, S. M. Sheng, X. D. Shen, X. B. Zhou, W. Z. Wu, X. P. Wu and D. Q. Liang, *J. Chem. Eng. Data*, 2017, **62**, 2461–2465.
1357 J. N. Zheng and M. Yang, *J. Chem. Eng. Data*, 2019, **64**, 372–379.
1358 R. Mcmullan and G. A. Jeffrey, *J. Chem. Phys.*, 1959, **31**, 1231–1234.
1359 H. Dashti, L. Zhehao Yew and X. Lou, *J. Nat. Gas Sci. Eng.*, 2015, **23**, 195–207.
1360 Z. W. Ma, P. Zhang, H. S. Bao and S. Deng, *Renewable Sustainable Energy Rev.*, 2016, **53**, 1273–1302.
1361 R. Kumar, P. Englezos, I. Moudrakovski and J. A. Ripmeester, *AIChE J.*, 2009, **55**, 1548–1594.
1362 S. Kim, S. D. Choi and Y. Seo, *Energy*, 2017, **118**, 950–956.
1363 Z. Xia, Z. Li, X. Li, Z. Chen, G. Li and Y. Wang, *Energy Procedia*, 2019, **158**, 5850–5855.
1364 S. Muromachi, S. Takeya, Y. Yamamoto and R. Ohmura, *CrystEngComm*, 2014, **16**, 2056–2060.
1365 T. Kobori, S. Muromachi, T. Yamasaki, S. Takeya, Y. Yamamoto, S. Alavi and R. Ohmura, *Cryst. Growth Des.*, 2015, **15**, 3862–3867.
1366 W. Shimada, M. Shiro, H. Kondo, S. Takeya, H. Oyama, T. Ebinuma and H. Marita, *Acta Crystallogr., Sect. C: Cryst. Struct. Commun.*, 2005, **61**, 65–66.
1367 H. Hashimoto, T. Yamaguchi, H. Ozeki and S. Muromachi, *Sci. Rep.*, 2017, **7**, 17216.
1368 P. Linga, R. Kumar and P. Englezos, *Chem. Eng. Sci.*, 2007, **62**, 4268–4276.
1369 H. P. Veluswamy, K. P. Premasinghe and P. Linga, *Energy Procedia*, 2017, **105**, 5048–5054.
1370 J. Lim, W. Choi, J. Mok and Y. Seo, *Chem. Eng. J.*, 2019, **369**, 686–693.
1371 C. T. Rodriguez, Q. Du Le, C. Focsa, C. Pirim and B. Chazallon, *Chem. Eng. J.*, 2020, **382**, 122867.
1372 U. Karaaslan and M. Parlaktuna, *Energy Fuels*, 2000, **14**, 1103–1107.
1373 H. P. Veluswamy, P. Y. Lee, K. Premasinghe and P. Linga, *Ind. Eng. Chem. Res.*, 2017, **56**, 6145–6154.
1374 J. Zheng, K. Bhatnagar, M. Khurana, P. Zhang, B. Y. Zhang and P. Linga, *Appl. Energy*, 2018, **217**, 377–389.
1375 C. Lo, J. S. ZHang, P. Somasundaran, S. Lu, A. Couzis and J. W. Lee, *Langmuir*, 2008, **24**, 12723–12726.
1376 C. Lo, J. Zhang, P. Somasundaran and J. W. Lee, *J. Phys. Chem. Lett.*, 2010, **1**, 2676–2679.
1377 L. Zhang, Y. Kuang, S. Dai, J. Wang, J. Zhao and Y. Song, *Chem. Eng. J.*, 2020, **379**, 122357.
1378 P. Di Profio, V. Canale, N. D'Alessandro, R. Germani, A. Di Crescenzo and A. Fontana, *ACS Sustainable Chem. Eng.*, 2017, **5**, 1990–1997.
1379 J. Yi, D. L. Zhong, J. Yan and Y. Y. Lu, *Energy*, 2019, **171**, 61–68.
1380 M. Ricaurte, C. Dicharry, D. Broseta, X. Renaud and J. P. Torré, *Ind. Eng. Chem. Res.*, 2013, **52**, 899–910.
1381 T. J. Kneafsey, L. Tomutsa, G. J. Moridis, Y. Seol, B. M. Freifeld, C. E. Taylor and A. Gupta, *J. Pet. Sci. Eng.*, 2007, **56**, 108–126.
1382 A. Adeyemo, R. Kumar, P. Linga, J. Ripmeester and P. Englezos, *Int. J. Greenhouse Gas Control*, 2010, **4**, 478–485.
1383 Y. T. Seo, I. L. Moudrakovski, J. A. Ripmeester, J. W. Lee and H. Lee, *Environ. Sci. Technol.*, 2005, **39**, 2315–2319.
1384 A. Nambiar, P. Babu and P. Linga, *Can. J. Chem.*, 2015, **93**, 808–814.
1385 I. Kim, M. Nole, S. Jang, S. Ko, H. Daigle, G. A. Pope and C. Huh, *RSC Adv.*, 2017, **7**, 9545–9550.
1386 S. Said, V. Govindaraj, J. M. Herri, Y. Ouabbas, M. Khodja, M. Belloum, J. S. Sangwai and R. Nagarajan, *J. Nat. Gas Sci. Eng.*, 2016, **32**, 95–108.
1387 R. Coupan, F. Plantier, J. P. Torré, C. Dicharry, P. Sénéchal, F. Guerton, P. Moonen, A. Khoukh, S. A. Kessas and M. Hemati, *Chem. Eng. J.*, 2017, **325**, 35–48.
1388 P. S. R. Prasad, Y. Sowjanya and V. Dhanunjana Chari, *J. Phys. Chem. C*, 2014, **118**, 7759–7764.
1389 L. Yang, S. Fan, Y. Wang, X. Lang and D. Xie, *Ind. Eng. Chem. Res.*, 2011, **50**, 11563–11569.
1390 F. Su, C. L. Bray, B. O. Carter, G. Overend, C. Cropper, J. A. Iggo, Y. Z. Khimyak, A. M. Fogg and A. I. Cooper, *Adv. Mater.*, 2009, **21**, 2382–2386.
1391 B. O. Carter, W. Wang, D. J. Adams and A. I. Cooper, *Langmuir*, 2010, **26**, 3186–3193.
1392 W. Zhao, J. Bai, J. S. Francisco and X. C. Zeng, *J. Phys. Chem. C*, 2018, **122**, 7951–7958.
1393 Z. Y. Li, Z. M. Xia, X. Sen Li, Z. Y. Chen, J. Cai, G. Li and T. Lv, *Energy Fuels*, 2018, **32**, 2064–2072.
1394 Y. He and F. Wang, *J. Mater. Chem. A*, 2018, **6**, 22619–22625.
1395 R. T. J. Porter, M. Fairweather, M. Pourkashanian and R. M. Woolley, *Int. J. Greenhouse Gas Control*, 2015, **36**, 161–174.
1396 A. Chapoy, R. Burgass, B. Tohidi and I. Alsiyabi, *J. Chem. Eng. Data*, 2015, **60**, 447–463.
1397 M. Nohra, T. K. Woo, S. Alavi and J. A. Ripmeester, *J. Chem. Thermodyn.*, 2012, **44**, 5–12.
1398 B. Kvamme, E. Iden, J. Tveit, V. Veland, M. Zarifi and K. Qorbani, *J. Chem. Eng. Data*, 2017, **62**, 1645–1658.
1399 N. Daraboina, J. Ripmeester and P. Englezos, *Int. J. Greenhouse Gas Control*, 2013, **15**, 97–103.
1400 C. Y. Sun, G. J. Chen, W. Lin and T. M. Guo, *J. Chem. Eng. Data*, 2003, **48**, 600–602.
1401 Z. T. Ward, C. E. Deering, R. A. Marriott, A. K. Sum, E. D. Sloan and C. A. Koh, *J. Chem. Eng. Data*, 2015, **60**, 403–408.
1402 B. Beeskow-Strauch, J. M. Schicks, E. Spangenberg and J. Erzinger, *Chem. – Eur. J.*, 2011, **17**, 4376–4384.
1403 A. Chapoy, M. Nazeri, M. Kapateh, R. Burgass, C. Coquelet and B. Tohidi, *Int. J. Greenhouse Gas Control*, 2013, **19**, 92–100.

Open Access Article. Published on 22 Junie 2020. Downloaded on 2026-02-11 12:42:38 nm..
This article is licensed under a Creative Commons Attribution-NonCommercial 3.0 Unported Licence.

1404 X. Zang and D. Liang, *J. Chem. Eng. Data*, 2018, **63**, 197–201.
1405 B. Kvamme, T. Kuznetsova, B. Jensen, S. Stensholt, J. Bauman, S. Sjøblom and K. Nes Lervik, *Phys. Chem. Chem. Phys.*, 2014, **16**, 8623–8638.
1406 F. Lang and P. Servio, *J. Chem. Eng. Data*, 2014, **59**, 2547–2550.
1407 A. Hassanpouryouzband, M. V. Farahani, J. Yang, B. Tohidi, E. Chuvilin, V. Istomin and B. Bukhanov, *Ind. Eng. Chem. Res.*, 2019, **58**, 3377–3394.
1408 A. Burnol, I. Thinon, L. Ruffine and J. M. Herri, *Int. J. Greenhouse Gas Control*, 2015, **35**, 96–109.
1409 F. M. Orr, *JPT, J. Pet. Technol.*, 2004, **56**, 90–97.
1410 F. M. Orr Jr., *Science*, 2009, **325**, 1656–1658.
1411 D. P. Schrag, *Science*, 2009, **325**, 1658–1659.
1412 Y. Teng and D. Zhang, *Sci. Adv.*, 2018, **4**, eaao6588.
1413 H. Koide, M. Takahashi, Y. Shindo, Y. Tazaki, M. Iijima, K. Ito, N. Kimura and K. Omata, *Energy*, 1997, **22**, 279–283.
1414 B. A. Remepel and A. W. Buffett, *J. Geophys. Res.*, 1997, **102**, 10151–10164.
1415 S. Almenningen, J. Gauteplass, L. P. Hauge, T. Barth, M. A. Fernø and G. Ersland, *J. Pet. Sci. Eng.*, 2019, **177**, 880–888.
1416 J. Gauteplass, S. Almenningen, G. Ersland and T. Barth, *Int. J. Greenhouse Gas Control*, 2018, **78**, 21–26.
1417 X. H. Ta, T. S. Yun, B. Muhunthan and T.-H. Kwon, *Geochem., Geophys., Geosyst.*, 2015, **16**, 912–924.
1418 J. W. Jung and J. C. Santamarina, *Geochem., Geophys., Geosyst.*, 2011, **12**, 1–9.
1419 K. Miyazaki, Y. Oikawa, H. Haneda and T. Yamaguchi, *Int. J. Offshore Polar Eng.*, 2016, **26**, 315–320.
1420 M. Uddin, D. Coombe and F. Wright, *J. Energy Resour. Technol.*, 2008, **130**, 032502.
1421 O. Y. Zatsepina and M. Pooladi-Darvish, *SPE Reserv. Eval. Eng.*, 2012, **15**, 98–108.
1422 O. Y. Zatsepina and B. A. Buffett, *Fluid Phase Equilib.*, 2002, **200**, 263–275.
1423 D. Y. Koh, H. Kang, D. O. Kim, J. Park, M. Cha and H. Lee, *ChemSusChem*, 2012, **5**, 1443–1448.
1424 P. Mekala, M. Busch, D. Mech, R. S. Patel and J. S. Sangwai, *J. Pet. Sci. Eng.*, 2014, **122**, 1–9.
1425 K. Lee, S. H. Lee and W. Lee, *Int. J. Greenhouse Gas Control*, 2013, **14**, 15–24.
1426 Z. He, P. Linga and J. Jiang, *Phys. Chem. Chem. Phys.*, 2017, **19**, 15657–15661.
1427 C. Holzammer, J. M. Schicks, S. Will and A. S. Braeuer, *J. Phys. Chem. B*, 2017, **121**, 8330–8337.
1428 D. Sun and P. Englezos, *J. Nat. Gas Sci. Eng.*, 2016, **35**, 1416–1425.
1429 M. Massah, D. Sun, H. Sharifi and P. Englezos, *J. Chem. Thermodyn.*, 2018, **117**, 106–112.
1430 D. Sun and P. Englezos, *Int. J. Greenhouse Gas Control*, 2014, **25**, 1–8.
1431 D. Sun and P. Englezos, *Can. J. Chem. Eng.*, 2017, **95**, 69–76.
1432 K. Ohgaki, K. Takano, H. Sangawa, T. Matsubara and S. Nakano, *J. Chem. Eng. Jpn.*, 1996, **29**, 478–483.
1433 Y. T. Seo and H. Lee, *J. Phys. Chem. B*, 2001, **105**, 10084–10090.
1434 E. M. Yezdimer, P. T. Cummings and A. A. Chialvo, *J. Phys. Chem. A*, 2002, **106**, 7982–7987.
1435 T. Uchida, I. Y. Ikeda, S. Takeya, Y. Kamata, R. Ohmura, J. Nagao, O. Y. Zatsepina and B. A. Buffett, *ChemPhysChem*, 2005, **6**, 646–654.
1436 G. Ersland, J. Husebø, A. Graue, B. A. Baldwin, J. Howard and J. Stevens, *Chem. Eng. J.*, 2010, **158**, 25–31.
1437 A. Graue, B. Kvamme, B. Baldwin, J. Stevens, J. J. Howard, E. Aspenes, G. Ersland, J. Husebo and D. Zornes, *SPE J.*, 2008, **13**, 146–152.
1438 M. Ota, Y. Abe, M. Watanabe, R. L. Smith and H. Inomata, *Fluid Phase Equilib.*, 2005, **228–229**, 553–559.
1439 S. Lee, S. Park, Y. Lee and Y. Seo, *Chem. Eng. J.*, 2013, **225**, 636–640.
1440 Q. Yuan, C. Y. Sun, B. Liu, X. Wang, Z. W. Ma, Q. L. Ma, L. Y. Yang, G. J. Chen, Q. P. Li, S. Li and K. Zhang, *Energy Convers. Manage.*, 2013, **67**, 257–264.
1441 M. Ota, T. Saito, T. Aida, M. Watanabe, Y. Sato, R. L. Smith and H. Inomata, *AIChE J.*, 2007, **53**, 2715–2721.
1442 M. Ota, K. Morohashi, Y. Abe, M. Watanabe, R. Lee Smith and H. Inomata, *Energy Convers. Manage.*, 2005, **46**, 1680–1691.
1443 Y. Qi, M. Ota and H. Zhang, *Energy Convers. Manage.*, 2011, **52**, 2682–2687.
1444 N. I. Papadimitriou, I. N. Tsimpanogiannis, I. G. Economou and A. K. Stubos, *Phys. Chem. Chem. Phys.*, 2018, **20**, 28026–28038.
1445 K. Shin, Y. Park, M. Cha, K. P. Park, D. G. Huh, J. Lee, S. J. Kim and H. Lee, *Energy Fuels*, 2008, **22**, 3160–3163.
1446 Y. Lee, W. Choi, K. Shin and Y. Seo, *Energy Convers. Manage.*, 2017, **150**, 356–364.
1447 Y. Lee, Y. Ju Seo, T. Ahn, J. Lee, J. Y. Lee, S. J. Kim and Y. Seo, *Chem. Eng. J.*, 2017, **308**, 50–58.
1448 J. M. Schicks, M. Luzi and B. Beeskow-Strauch, *J. Phys. Chem. A*, 2011, **115**, 13324–13331.
1449 J. Yang, A. Chapoy, B. Tohidi, P. S. Jadhawar and J. Lee, *OTC*, 2008.
1450 J. H. Yoon, T. Kawamura, Y. Yamamoto and T. Komai, *J. Phys. Chem. A*, 2004, **108**, 5057–5059.
1451 J. W. Jung and J. C. Santamarina, *Geochem., Geophys., Geosyst.*, 2010, **11**, 1–8.
1452 L. Zhang, L. Yang, J. Wang, J. Zhao, H. Dong, M. Yang, Y. Liu and Y. Song, *Chem. Eng. J.*, 2017, **308**, 40–49.
1453 P. L. Stanwix, N. M. Rathnayake, F. P. P. De Obanos, M. L. Johns, Z. M. Aman and E. F. May, *Energy Environ. Sci.*, 2018, **11**, 1828–1840.
1454 A. M. Gambelli and F. Rossi, *Energy*, 2019, **172**, 423–434.
1455 H. Kang, D. Y. Koh and H. Lee, *Sci. Rep.*, 2014, **4**, 1–8.
1456 D. Lim, H. Ro, Y. Seo, Y. Ju Seo, J. Y. Lee, S. J. Kim, J. Lee and H. Lee, *J. Chem. Thermodyn.*, 2017, **106**, 16–21.
1457 S. S. Tupsakhare and M. J. Castaldi, *Appl. Energy*, 2019, **236**, 825–836.
1458 D. R. Bhawangirkar and J. S. Sangwai, *Ind. Eng. Chem. Res.*, 2019, **58**, 14462–14475.

 This journal is © The Royal Society of Chemistry 2020

Open Access Article. Published on 22 Junie 2020. Downloaded on 2026-02-11 12:42:38 nm..
This article is licensed under a Creative Commons Attribution-NonCommercial 3.0 Unported Licence.

1459 D. Schoderbek and K. L. Martin, J. Howard, S. Silpngarmlert and K. Hester, in *Society of Petroleum Engineers - Arctic Technology Conference 2012*, Offshore Technology Conference, 2012, vol. 1, pp. 155–171.
1460 J. Yang, A. Okwananke, B. Tohidi, E. Chuvilin, K. Maerle, V. Istomin, B. Bukhanov and A. Cheremisin, *Energy Convers. Manage.*, 2017, **136**, 431–438.
1461 A. Hassanpouryouzband, J. Yang, B. Tohidi, E. Chuvilin, V. Istomin, B. Bukhanov and A. Cheremisin, *Environ. Sci. Technol.*, 2018, **52**, 4324–4330.
1462 D. Sun, J. Ripmeester and P. Englezos, *J. Chem. Eng. Data*, 2016, **61**, 4061–4067.
1463 J. M. Schicks, B. Strauch, K. U. Heeschen, E. Spangenberg and M. Luzi-Helbing, *J. Geophys. Res. Solid Earth*, 2018, **123**, 3608–3620.
1464 D. Bai, X. Zhang, G. Chen and W. Wang, *Energy Environ. Sci.*, 2012, **5**, 7033–7041.
1465 Y. T. Tung, L. J. Chen, Y. P. Chen and S. T. Lin, *J. Phys. Chem. B*, 2011, **115**, 15295–15302.
1466 G. Wu, L. Tian, D. Chen, M. Niu and H. Ji, *J. Phys. Chem. C*, 2019, **123**, 13401–13409.
1467 S. Lee, Y. Lee, J. Lee, H. Lee and Y. Seo, *Environ. Sci. Technol.*, 2013, **47**, 13184–13190.
1468 A. N. Salamatin, A. Falenty and W. F. Kuhs, *J. Phys. Chem. C*, 2017, **121**, 17603–17616.
1469 T. Yasunami, K. Sasaki and Y. Sugai, *J. Can. Pet. Technol.*, 2010, **49**, 44–50.
1470 J. A. Jimenez and R. J. Chalaturnyk, *Proc. SPE/ISRM Rock Mech. Pet. Eng. Conf.*, 2002, 340–352.
1471 K. Edlmann, S. Haszeldine and C. I. McDermott, *Environ. Earth Sci.*, 2013, **70**, 3393–3409.
1472 H. Koide, M. Takahashi, H. Tsukamoto and Y. Shindo, *Energy Convers. Manage.*, 1995, **36**, 505–508.
1473 C. A. Rochelle, A. P. Camps, D. Long, A. Milodowski, K. Bateman, D. Gunn, P. Jackson, M. A. Lovell and J. Rees, *Geol. Soc. Spec. Publ.*, 2009, **319**, 171–183.
1474 J. S. Levine, J. M. Matter, D. Goldberg, A. Cook and K. S. Lackner, *Geophys. Res. Lett.*, 2007, **34**, 1–5.
1475 J. K. Eccles and L. Pratson, *Geophys. Res. Lett.*, 2012, **39**, 1–7.
1476 B. Tohidi, J. Yang, M. Salehabadi, R. Anderson and A. Chapoy, *Environ. Sci. Technol.*, 2010, **44**, 1509–1514, DOI: 10.1021/es902450j.
1477 E. M. Myshakin, W. A. Saidi, V. N. Romanov, R. T. Cygan and K. D. Jordan, *J. Phys. Chem. C*, 2013, **117**, 11028–11039.
1478 J. Gauteplass, S. Almenningen, G. Ersland, T. Barth, J. Yang and A. Chapoy, *Chem. Eng. J.*, 2020, **381**, 122646.
1479 J. S. Gudmundsson, F. Hveding and A. Berrehaug, *Proc. Int. Offshore Polar Eng. Conf.*, 1995, 282–288.
1480 V. Andersson and J. Ó. N. S. Gudmundsson, *Ann. N. Y. Acad. Sci.*, 2000, **912**, 322–329.
1481 R. Larsen, A. Lund, V. Andersson and K. W. Hjarbo, *Proc. - SPE Annu. Tech. Conf. Exhib.*, 2001, 1905–1909.
1482 R. Azarinezhad, A. Chapoy, R. Anderson and B. Tohidi, *SPE Proj. Facil. Constr.*, 2010, **5**, 58–64.
1483 S. Matsuo, H. Umeda, S. Takeya and T. Fujita, *Energies*, 2017, **10**, 1–13.
1484 B. Prah and R. Yun, *Appl. Therm. Eng.*, 2018, **128**, 653–661.
1485 H. P. Veluswamy, A. Kumar, Y. Seo, J. D. Lee and P. Linga, *Appl. Energy*, 2018, **216**, 262–285.
1486 C. Han, U. Zahid, J. An, K. Kim and C. Kim, *Curr. Opin. Chem. Eng.*, 2015, **10**, 42–48.
1487 S. P. Kang and H. Lee, *Environ. Sci. Technol.*, 2000, **34**, 4397–4400.
1488 G. Deppe, A. Lee, O. Han, B. Nguyen-Phuoc and D. Spencer, 3rd Annu. Conf. Carbon Sequestration, Washint. DC, 2004.
1489 C.-G. Xu, Y.-S. Yu, W.-J. Xie, Z.-M. Xia, Z.-Y. Chen and X.-S. Li, *Appl. Energy*, 2019, **255**, 113791.
1490 Y. Liu, S. Deng, R. Zhao, J. He and L. Zhao, *Renewable Sustainable Energy Rev.*, 2017, **77**, 652–669.
1491 M. Bai, Z. Zhang and X. Fu, *Renewable Sustainable Energy Rev.*, 2016, **59**, 920–926.
1492 V. Vilarrasa and J. Rutqvist, *Earth-Sci. Rev.*, 2017, **165**, 245–256.
1493 R. Shukla, P. Ranjith, A. Haque and X. Choi, *Fuel*, 2010, **89**, 2651–2664.
1494 Z. Yang, J. Zhang, M. C. W. Kintner-Meyer, X. Lu, D. Choi, J. P. Lemmon and J. Liu, *Chem. Rev.*, 2011, **111**, 3577–3613.
1495 R. Moliner, M. J. Lázaro and I. Suelves, *Int. J. Hydrogen Energy*, 2016, **41**, 19500–19508.
1496 D. Parra, L. Valverde, F. J. Pino and M. K. Patel, *Renewable Sustainable Energy Rev.*, 2019, **101**, 279–294.
1497 P. Di Profio, S. Arca, F. Rossi and M. Filipponi, *Int. J. Hydrogen Energy*, 2009, **34**, 9173–9180.
1498 P. Jena, *J. Phys. Chem. Lett.*, 2011, **2**, 206–211.
1499 F. Nadeem, S. M. S. Hussain, P. K. Tiwari, A. K. Goswami and T. S. Ustun, *IEEE Access*, 2019, **7**, 4555–4585.
1500 R. Tarkowski, *Renewable Sustainable Energy Rev.*, 2019, **105**, 86–94.
1501 J. Andersson and S. Grönkvist, *Int. J. Hydrogen Energy*, 2019, **44**, 11901–11919.
1502 K. Sordakis, C. Tang, L. K. Vogt, H. Junge, P. J. Dyson, M. Beller and G. Laurenczy, *Chem. Rev.*, 2018, **118**, 372–433.
1503 L. J. Murray, M. Dincă and J. R. Long, *Chem. Soc. Rev.*, 2009, **38**, 1294–1314.
1504 V. V. Struzhkin, B. Militzer, W. L. Mao, H. K. Mao and R. J. Hemley, *Chem. Rev.*, 2007, **107**, 4133–4151.
1505 H. P. Veluswamy, R. Kumar and P. Linga, *Appl. Energy*, 2014, **122**, 112–132.
1506 S. Alavi and J. A. Ripmeester, *Mol. Simul.*, 2017, **43**, 808–820.
1507 T. A. Strobel, C. A. Koh and E. D. Sloan, *Fluid Phase Equilib.*, 2007, **261**, 382–389.
1508 T. A. Strobel, K. C. Hester, C. A. Koh, A. K. Sum and E. D. Sloan, *Chem. Phys. Lett.*, 2009, **478**, 97–109.
1509 K. A. Udachin, J. Ltpkowski and M. Tkacz, *Supramol. Chem.*, 1994, **3**, 181–183.
1510 W. L. Mao, H. Kwang Mao, A. F. Goncharov, V. V. Struzhkin, Q. Guo, J. Hu, J. Hu, R. J. Hemley, M. Somayazulu and Y. Zhao, *Science*, 2002, **297**, 2247–2249.
1511 V. V. Struzhkin, B. Militzer, W. L. Mao, H. K. Mao and R. J. Hemley, *Chem. Rev.*, 2007, **107**, 4133–4151.

Open Access Article. Published on 22 Junie 2020. Downloaded on 2026-02-11 12:42:38 nm..
This article is licensed under a Creative Commons Attribution-NonCommercial 3.0 Unported Licence.

1512 K. A. Lokshin and Y. Zhao, *Appl. Phys. Lett.*, 2006, **88**, 131909.
1513 H. Lee, J. W. Lee, D. Y. Kim, J. Park, Y. T. Seo, H. Zeng, I. L. Moudrakovski, C. I. Ratcliffe and J. A. Ripmeester, *Mater. Sustainable Energy Appl.*, 2010, **434**, 285–288.
1514 R. Anderson, A. Chapoy and B. Tohidi, *Langmuir*, 2007, **23**, 3440–3444.
1515 T. A. Strobel, C. J. Taylor, K. C. Hester, S. F. Dec, C. A. Koh, K. T. Miller and E. D. Sloan, *J. Phys. Chem. B*, 2006, **110**, 17121–17125.
1516 D. Y. Kim, J. Park, J. W. Lee, J. A. Ripmeester and H. Lee, *J. Am. Chem. Soc.*, 2006, **128**, 15360–15361.
1517 D. Y. Koh, H. Kang and H. Lee, *Chem. Commun.*, 2013, **49**, 6782–6784.
1518 J. Liu, J. Hou, J. Xu, H. Liu, G. Chen and J. Zhang, *Int. J. Hydrogen Energy*, 2017, **42**, 17136–17143.
1519 J. Cai, R. Yan, C. G. Xu, Z. Y. Chen and X. Sen Li, *Energy Procedia*, 2019, **158**, 5149–5155.
1520 S. P. Kaur and C. N. Ramachandran, *Int. J. Hydrogen Energy*, 2018, **43**, 19559–19566.
1521 H. P. Veluswamy, T. Yang and P. Linga, *Cryst. Growth Des.*, 2014, **14**, 1950–1960.
1522 J. Cai, Y. Q. Tao, N. von Solms, C. G. Xu, Z. Y. Chen and X. Sen Li, *Appl. Energy*, 2019, **243**, 1–9.
1523 D. Jianwei, L. Deqing, L. Dongliang and L. Xinjun, *Ind. Eng. Chem. Res.*, 2010, **49**, 11797–11800.
1524 T. A. Strobel, K. C. Hester, E. D. Sloan and C. A. Koh, *J. Am. Chem. Soc.*, 2007, **129**, 9544–9545.
1525 T. Tsuda, K. Ogata, S. Hashimoto, T. Sugahara, M. Moritoki and K. Ohgaki, *Chem. Eng. Sci.*, 2009, **64**, 4150–4154.
1526 T. A. Strobel, C. A. Koh and E. D. Sloan, *J. Phys. Chem. B*, 2008, **112**, 1885–1887.
1527 K. C. Hester, T. A. Strobel, E. D. Sloan, C. A. Koh, A. Huq and A. J. Schultz, *J. Phys. Chem. B*, 2006, **110**, 14024–14027.
1528 R. Kumar, D. D. Klug, C. I. Ratcliffe, C. A. Tulk and J. A. Ripmeester, *Angew. Chem., Int. Ed.*, 2013, **52**, 1531–1534.
1529 R. G. Grim, P. B. Kerkar, E. D. Sloan, C. A. Koh and A. K. Sum, *J. Chem. Phys.*, 2012, **136**, 234504.
1530 Y. Matsumoto, R. G. Grim, N. M. Khan, T. Sugahara, K. Ohgaki, E. D. Sloan, C. A. Koh and A. K. Sum, *J. Phys. Chem. C*, 2014, **118**, 3581–3589.
1531 R. V. Belosludov, R. K. Zhdanov, O. S. Subbotin, H. Mizuseki, Y. Kawazoe and V. R. Belosludov, *J. Renewable Sustainable Energy*, 2014, **6**, 53132.
1532 M. N. Khan, L. J. Rovetto, C. J. Peters, E. D. Sloan, A. K. Sum and C. A. Koh, *J. Chem. Eng. Data*, 2015, **60**, 418–423.
1533 Z. Zhang, P. G. Kusalik and G. J. Guo, *J. Phys. Chem. C*, 2018, **122**, 7771–7778.
1534 H. P. Veluswamy, J. C. Yew and P. Linga, *J. Chem. Eng. Data*, 2015, **60**, 228–237.
1535 H. P. Veluswamy, J. Y. Chen and P. Linga, *Chem. Eng. Sci.*, 2015, **126**, 488–499.
1536 S. Alavi and J. A. Ripmeester, *Angew. Chem., Int. Ed.*, 2007, **46**, 6102–6105.
1537 D. P. Luis, I. E. Romero-Ramirez, A. González-Calderón and J. López-Lemus, *J. Chem. Phys.*, 2018, **148**, 114503.
1538 Q. Lu, X. He, W. Hu, X. Chen and J. Liu, *J. Phys. Chem. C*, 2019, **123**, 12052–12061.
1539 A. Celzard and V. Fierro, *Energy Fuels*, 2005, **19573–583**.
1540 V. Rozyyev, D. Thirion, R. Ullah, J. Lee, M. Jung, H. Oh, M. Atilhan and C. T. Yavuz, *Nat. Energy*, 2019, **4**, 604–611.
1541 D. Lozano-Castelló, J. Alcañiz-Monge, M. A. De La Casa-Lillo, D. Cazorla-Amorós and A. Linares-Solano, *Fuel*, 2002, **81**, 1777–1803.
1542 J. A. Mason, M. Veenstra and J. R. Long, *Chem. Sci.*, 2014, **5**, 32–51.
1543 J. Silvestre-Albero, *Green Energy and Technology*, Springer, 2019, pp. 383–403.
1544 K. Kim, H. Kang and Y. Kim, *Energies*, 2015, **8**, 3142–3164.
1545 W. Wang, C. Ma, P. Lin, L. Sun and A. I. Cooper, *Energy Environ. Sci.*, 2013, **6**, 105–107.
1546 J. G. Speight, *Natural Gas: A Basic Handbook*, Gulf Professional Publishing, 2007.
1547 I. N. Tsimpanogiannis, J. Costandy, P. Kastanidis, S. El Meragawi, V. K. Michalis, N. I. Papadimitriou, S. N. Karozis, N. I. Diamantonis, O. A. Moultos, G. E. Romanos, A. K. Stubos and I. G. Economou, *Mol. Phys.*, 2018, **116**, 2041–2060.
1548 B. Miller and E. R. Strong, *Am. Gas Assoc. Mon.*, 1946, **28**, 63–67.
1549 S. Song, B. Shi, W. Yu, L. Ding, Y. Chen, Y. Yu, C. Ruan, Y. Liu, W. Wang and J. Gong, *Chem. Eng. J.*, 2019, **361**, 1264–1284.
1550 S. Ma, J. Nan Zheng, M. Tian, D. Tang and M. Yang, *Fuel*, 2020, **261**, 116364.
1551 A. Gupta, J. Lachance, E. D. Sloan and C. A. Koh, *Chem. Eng. Sci.*, 2008, **63**, 5848–5853.
1552 G. McLaurin, K. Shin, S. Alavi and J. A. Ripmeester, *Angew. Chem., Int. Ed.*, 2014, **53**, 10429–10433.
1553 Y.-A. Chen, L.-K. Chu, C.-K. Chu, R. Ohmura and L.-J. Chen, *Sci. Rep.*, 2019, **9**, 1–11.
1554 G. Pandey, H. P. Veluswamy, J. Sangwai and P. Linga, *Energy Fuels*, 2019, **33**, 4865–4876.
1555 A. Kumar, H. P. Veluswamy, P. Linga and R. Kumar, *Fuel*, 2019, **236**, 1505–1511.
1556 M. Khurana, H. P. Veluswamy, N. Daraboina and P. Linga, *Chem. Eng. J.*, 2019, **370**, 760–771.
1557 W. Wang, B. O. Carter, C. L. Bray, A. Steiner, J. Bacsa, J. T. A. Jones, C. Cropper, Y. Z. Khimyak, D. J. Adams and A. I. Cooper, *Chem. Mater.*, 2009, **21**, 3810–3815.
1558 L. Li, S. Wang and W. Wang, *IOP Conference Series: Materials Science and Engineering*, IOP Publishing, 2018, vol. 301, p. 12033.
1559 L. Yang, X. Lan, D. Liu, G. Cui, B. Dou and J. Wang, *Chem. Eng. J.*, 2019, **374**, 802–810.
1560 E. Chaturvedi, N. Prasad and A. Mandal, *J. Nat. Gas Sci. Eng.*, 2018, **56**, 246–257.
1561 Q. Sun, B. Chen, Y. Li, Z. Xu, X. Guo, X. Li, W. Lan and L. Yang, *Fluid Phase Equilib.*, 2018, **475**, 95–99.
1562 Y. M. Song, F. Wang, S. J. Luo, R. B. Guo and D. Xu, *Fuel*, 2019, **243**, 185–191.
1563 J. Chen, T. Wang, Z. Zeng, J. H. Jiang, B. Deng, C. Z. Chen, J. Y. Li, C. H. Li, L. M. Tao, X. Li and S. X. Xiao, *Chem. Eng. J.*, 2019, **363**, 349–355.

 This journal is © The Royal Society of Chemistry 2020

Open Access Article. Published on 22 Junie 2020. Downloaded on 2026-02-11 12:42:38 nm..
This article is licensed under a Creative Commons Attribution-NonCommercial 3.0 Unported Licence.

1564 A. Farhadian, M. A. Varfolomeev, Z. Abdelhay, D. Emelianov, A. Delaunay and D. Dalmazzone, *Ind. Eng. Chem. Res.*, 2019, **58**, 7752–7760.
1565 Z. Zhang, P. G. Kusalik and G.-J. Guo, *J. Phys. Chem. C*, 2019, **123**, 20579–20586.
1566 F. Filarsky, C. Schmuck and H. J. Schultz, *Ind. Eng. Chem. Res.*, 2019, **58**, 16687–16695.
1567 J. D. Lee, J. W. Lee, K. N. Park and J. H. Kim, Double helix type gas hydrate reactor, *US Pat.*, 8,936,759.20, 2015.
1568 J. Javanmardi, K. Nasrifar, S. H. Najibi and M. Moshfeghian, *Appl. Therm. Eng.*, 2005, **25**, 1708–1723.
1569 M. J. Molina and F. S. Rowland, *Nature*, 1974, **249**, 810–812.
1570 P. S. Bailey, CHAPTER XI – The Practical Side, in *Ozonation in Organic Chemistry*, ed. P. S. Bailey, Academic Press, 1982, pp. 355–370.
1571 M. Sillanpää, M. C. Ncibi and A. Matilainen, *J. Environ. Manage.*, 2018, **208**, 56–76.
1572 F. Zhang, B. Hong, W. Zhao, Y. Yang, J. Bao, C. Gao and S. Sun, *Chem. Commun.*, 2019, **55**, 3757–3760.
1573 S. Öztekin, *Emerging Postharvest Treatment of Fruits and Vegetables*, Apple Academic Press, 2018, pp. 213–276.
1574 R. Pandiselvam, S. Subhashini, E. P. Banuu Priya, A. Kothakota, S. V. Ramesh and S. Shahir, *Ozone Sci. Eng.*, 2019, **41**, 17–34.
1575 N. F. Gray, *Microbiology of Waterborne Diseases*, Elsevier, 2014, pp. 617–630.
1576 G. McTurk and J. G. Waller, *Nature*, 1964, **202**, 1107.
1577 T. A. Vysokikh, T. V. Yagodovskaya, S. V. Savilov and V. V. Lunin, *Russ. J. Phys. Chem. A*, 2008, **82**, 686–689.
1578 S. Muromachi, K. A. Udachin, S. Alavi, R. Ohmura and J. A. Ripmeester, *Chem. Commun.*, 2016, **52**, 5621–5624.
1579 T. Nakajima, S. Akatsu, R. Ohmura, S. Takeya and Y. H. Mori, *Angew. Chem., Int. Ed.*, 2011, **50**, 10340–10343.
1580 S. Muromachi, T. Nakajima, R. Ohmura and Y. H. Mori, *Fluid Phase Equilib.*, 2011, **305**, 145–151.
1581 S. Muromachi, H. D. Nagashima, J.-M. Herri and R. Ohmura, *J. Chem. Thermodyn.*, 2013, **64**, 193–197.
1582 S. Muromachi, R. Ohmura and Y. H. Mori, *J. Chem. Thermodyn.*, 2012, **49**, 1–6.
1583 K. Shishido, S. Muromachi and R. Ohmura, *World Acad. Sci. Eng. Technol. Int. J. Chem. Mol. Nucl. Mater. Metall. Eng.*, 2013, **7**, 111–115.
1584 O. S. Subbotin, T. P. Adamova, R. V. Belosludov, H. Mizuseki, Y. Kawazoe and V. R. Belosludov, *J. Struct. Chem.*, 2012, **53**, 627–633.
1585 Y. Yu Bozhko, K. V. Gets, R. K. Zhdanov and O. S. Subbotin, *J. Phys.: Conf. Ser.*, 2018, **1128**, 12084.
1586 K. Shishido, S. Muromachi, R. Nakamura, S. Takeya and R. Ohmura, *New J. Chem.*, 2014, **38**, 3160–3165.
1587 T. Nakajima, T. Kudo, R. Ohmura, S. Takeya and Y. H. Mori, *PLoS One*, 2012, **7**, e48563.
1588 O. S. Subbotin, Y. Y. Bozhko, R. K. Zhdanov, K. V. Gets, V. R. Belosludov, R. V. Belosludov and Y. Kawazoe, *Phys. Chem. Chem. Phys.*, 2018, **20**, 12637–12641.
1589 K. Watanabe, H. D. Nagashima, R. Nakamura and R. Ohmura, *ACS Sustainable Chem. Eng.*, 2018, **6**, 11624–11632.
1590 G. J. M. Velders, A. R. Ravishankara, M. K. Miller, M. J. Molina, J. Alcamo, J. S. Daniel, D. W. Fahey, S. A. Montzka and S. Reimann, *Science*, 2012, **335**, 922–923.
1591 N. Abas, A. R. Kalair, N. Khan, A. Haider, Z. Saleem and M. S. Saleem, *Renewable Sustainable Energy Rev.*, 2018, **90**, 557–569.
1592 P. A. Domanski, M. O. McLinden, A. F. Kazakov, J. S. Brown, R. Brignoli, J. Heo, J. Wojtusiak and I. I. R. G. 13th, Review of Refrigerants Evolution, *Lorentzen Conference of Natural Refrigerants*, 2018.
1593 A. Kasaeian, S. M. Hosseini, M. Sheikhpour, O. Mahian, W. M. Yan and S. Wongwises, *Renewable Sustainable Energy Rev.*, 2018, **96**, 91–99.
1594 G. Li, Y. Hwang, R. Radermacher and H. H. Chun, *Energy*, 2013, **51**, 1–17.
1595 G. Li, Y. Hwang, R. Radermacher and H. H. Chun, *Energy*, 2013, **51**, 1–17.
1596 T. Ogawa, T. Ito, K. Watanabe, K. Ichi Tahara, R. Hiraoka, J. Ichi Ochiai, R. Ohmura and Y. H. Mori, *Appl. Therm. Eng.*, 2006, **26**, 2157–2167.
1597 X. Wang, M. Dennis and L. Hou, *Renewable Sustainable Energy Rev.*, 2014, **36**, 34–51.
1598 A. Delahaye, L. Fournaison and D. Dalmazzone, *Gas Hydrates 2 Geosci. Issues Potential Ind. Appl*, 2018, 315–358.
1599 H. Hashemi, S. Babaee, A. H. Mohammadi, P. Naidoo and D. Ramjugernath, *Int. J. Refrig.*, 2019, **98**, 410–427.
1600 P. Zhang and Z. W. Ma, *Renewable Sustainable Energy Rev.*, 2012, **16**, 5021–5058.
1601 Y. Bi, T. Guo, T. Zhu, S. Fan, D. Liang and L. Zhang, *Appl. Energy*, 2004, **78**, 111–121.
1602 Y. Xie, G. Li, D. Liu, N. Liu, Y. Qi, D. Liang, K. Guo and S. Fan, *Appl. Energy*, 2010, **87**, 3340–3346.
1603 J. Chen, Z. Qiu and Y. Zheng, *Int. Conf. Power Eng. 2013, ICOPE 2013*, 2013, **65**, 120–132.
1604 N. Xie, C. Tan, S. Yang and Z. Liu, *ACS Sustainable Chem. Eng.*, 2019, **7**, 1502–1511.
1605 R. Matsuura, K. Watanabe, Y. Yamauchi, H. Sato and R. Ohmura, *Renew. Energy Power Qual. J.*, 2019, **17**, 118–122.
1606 Z. Youssef, L. Fournaison, A. Delahaye and M. Pons, *Int. J. Refrig.*, 2019, **98**, 202–210.
1607 Q. Sun and Y. T. Kang, *Renewable Sustainable Energy Rev.*, 2016, **62**, 478–494.
1608 A. Eslamimanesh, A. H. Mohammadi and D. Richon, *Chem. Eng. Sci.*, 2011, **66**, 5439–5445.
1609 H. Hashemi, S. Babaee, P. Naidoo, A. H. Mohammadi and D. Ramjugernath, *J. Chem. Eng. Data*, 2014, **59**, 3907–3911.
1610 H. Hashemi, S. Babaee, A. H. Mohammadi, P. Naidoo and D. Ramjugernath, *J. Chem. Thermodyn.*, 2015, **82**, 47–52.
1611 F. Nikbakht, A. A. Izadpanah, F. Varaminian and A. H. Mohammadi, *Int. J. Refrig.*, 2012, **35**, 1914–1920.
1612 M. Karamoddin and F. Varaminian, *J. Chem. Thermodyn.*, 2013, **65**, 213–219.
1613 P. T. Ngema, P. Naidoo, A. H. Mohammadi, D. Richon and D. Ramjugernath, *J. Chem. Eng. Data*, 2016, **61**, 827–836.
1614 P. T. Ngema, P. Naidoo, A. H. Mohammadi and D. Ramjugernath, *J. Chem. Eng. Data*, 2019, **136**, 59–76.

Open Access Article. Published on 22 Junie 2020. Downloaded on 2026-02-11 12:42:38 nm..
This article is licensed under a Creative Commons Attribution-NonCommercial 3.0 Unported Licence.

1615 S. Zafar, I. Dincer and M. Gadalla, *International Communications in Heat and Mass Transfer*, Springer, 2017, vol. 89, pp. 165–175.
1616 S. Zafar, I. Dincer and M. Gadalla, *Green Energy and Technology*, Springer, 2018, pp. 1165–1175.
1617 M. A. M. Hassan, H. M. Abdel-Hameed and O. E. Mahmoud, *J. Energy Resour. Technol.*, 2019, **141**, 42003.
1618 X. Wang and M. Dennis, *Appl. Energy*, 2016, **167**, 59–69.
1619 Q. Sun, S. Kim and Y. T. Kang, *Appl. Energy*, 2017, **190**, 249–256.
1620 S. Kim, S. H. Lee and Y. T. Kang, *Energy*, 2017, **120**, 362–373.
1621 K. Nemoto, T. Ikeda, H. Mori, S. Alavi, S. Takeya and R. Ohmura, *New J. Chem.*, 2019, **43**, 13068–13074.
1622 H. Lee, C. Park, E. Lee, J. D. Lee and Y. Kim, *J. Chem. Eng. Data*, 2017, **62**, 4395–4400.
1623 S. Jerbi, A. Delahaye, L. Fournaison and P. Haberschill, *Int. J. Refrig.*, 2010, **33**, 1625–1631.
1624 Y. S. Choi and S. Nešić, *Int. J. Greenhouse Gas Control*, 2011, **5**, 788–797.
1625 Y. Bi, T. Guo, L. Zhang, L. Chen and F. Sun, *Appl. Energy*, 2010, **87**, 1149–1157.
1626 Y. Bi, X. Liu and M. Jiang, *Energy*, 2014, **73**, 908–915.
1627 C. J. Vörösmarty, A. Y. Hoekstra, S. E. Bunn, D. Conway and J. Gupta, *Science*, 2015, **349**, 478–479.
1628 C. J. Vörösmarty, P. B. McIntyre, M. O. Gessner, D. Dudgeon, A. Prusevich, P. Green, S. Glidden, S. E. Bunn, C. A. Sullivan and C. R. Liermann, *Nature*, 2010, **467**, 555.
1629 M. Rodell, J. S. Famiglietti, D. N. Wiese, J. T. Reager, H. K. Beaudoing, F. W. Landerer and M.-H. Lo, *Nature*, 2018, **557**(7707), 651–659.
1630 A. D. Khawaji, I. K. Kutubkhanah and J.-M. Wie, *Desalination*, 2008, **221**, 47–69.
1631 M. Kummu, J. H. A. Guillaume, H. De Moel, S. Eisner, M. Flörke, M. Porkka, S. Siebert, T. I. E. Veldkamp and P. J. Ward, *Sci. Rep.*, 2016, **6**, 38495.
1632 M. A. Shannon, P. W. Bohn, M. Elimelech, J. G. Georgiadis, B. J. Marinas and A. M. Mayes, *Nanoscience And Technology: A Collection of Reviews from Nature Journals*, World Scientific, 2010, pp. 337–346.
1633 A. Subramani and J. G. Jacangelo, *Water Res.*, 2015, **75**, 164–187.
1634 N. Ghaffour, T. M. Missimer and G. L. Amy, *Desalination*, 2013, **309**, 197–207.
1635 N. Ghaffour, J. Bundschuh, H. Mahmoudi and M. F. A. Goosen, *Desalination*, 2015, **356**, 94–114.
1636 J. Zheng, F. Cheng, Y. Li, X. Lü and M. Yang, *Chin. J. Chem. Eng.*, 2019, **27**, 2037–2043.
1637 M. Elimelech and W. A. Phillip, *Science*, 2011, **333**, 712–717.
1638 P. Babu, A. Nambiar, T. He, I. A. Karimi, J. D. Lee, P. Englezos and P. Linga, *ACS Sustainable Chem. Eng.*, 2018, **6**, 8093–8107.
1639 Y.-N. Lv, S.-S. Wang, C.-Y. Sun, J. Gong and G.-J. Chen, *Desalination*, 2017, **413**, 217–222.
1640 C. Xu, X. Li, K. Yan, X. Ruan, Z. Chen and Z. Xia, *Chin. J. Chem. Eng.*, 2019, **27**, 1998–2013.
1641 P. Sahu, S. Krishnaswamy, K. Ponnani and N. K. Pande, *Desalination*, 2018, **436**, 144–151.
1642 W. G. Knox, M. Hess, G. E. Jones and H. B. Smith, *Chem. Eng. Prog.*, 1961, **57**, 66–71.
1643 Y. T. Ngan and P. Englezos, *Ind. Eng. Chem. Res.*, 1996, **35**, 1894–1900.
1644 M. Nakajima, R. Ohmura and Y. H. Mori, *Ind. Eng. Chem. Res.*, 2008, **47**, 8933–8939.
1645 D. Corak, T. Barth, S. Høiland, T. Skodvin, R. Larsen and T. Skjetne, *Desalination*, 2011, **278**, 268–274.
1646 L. Cai, B. A. Pethica, P. G. Debenedetti and S. Sundaresan, *Chem. Eng. Sci.*, 2014, **119**, 147–157.
1647 L. Cai, B. A. Pethica, P. G. Debenedetti and S. Sundaresan, *Chem. Eng. Sci.*, 2016, **141**, 125–132.
1648 H. Xu, M. N. Khan, C. J. Peters, E. D. Sloan and C. A. Koh, *J. Chem. Eng. Data*, 2018, **63**, 1081–1087.
1649 S. Ho-Van, B. Bouillot, J. Douzet, S. M. Babakhani and J. M. Herri, *J. Environ. Chem. Eng.*, 2019, **7**, 103359.
1650 K. C. Kang, P. Linga, K. Park, S.-J. Choi and J. D. Lee, *Desalination*, 2014, **353**, 84–90.
1651 M. Yang, Y. Song, L. Jiang, Y. Liu and Y. Li, *Ind. Eng. Chem. Res.*, 2014, **53**, 10753–10761.
1652 R. A. McCormack and G. A. Niblock, *Investigation of high freezing temperature, zero ozone, and zero global warming potential, clathrate formers for desalination*, US Department of the Interior, Bureau of Reclamation, Technical Service, 2000.
1653 B. A. Simmons, R. W. Bradshaw, D. E. Dedrick, R. T. Cygan, J. A. Greathouse and E. H. Majzoub, *Desalination utilizing clathrate hydrates (LDRD final report)*, Sandia National Laboratories, 2008.
1654 M. Karamoddin and F. Varaminian, *Desalin. Water Treat.*, 2014, **52**, 2450–2456.
1655 P. T. Ngema, C. Petticrew, P. Naidoo, A. H. Mohammadi and D. Ramjugernath, *J. Chem. Eng. Data*, 2014, **59**, 466–475.
1656 Y. Seo, D. Moon, C. Lee, J.-W. Park, B.-S. Kim, G.-W. Lee, P. Dotel, J.-W. Lee, M. Cha and J.-H. Yoon, *Environ. Sci. Technol.*, 2015, **49**, 6045–6050.
1657 L. J. Wang, X. M. Zhang, H. H. Li, L. Shao, D. Zhang and L. Jiao, *Adv. Mater. Res.*, 2013, **616–618**, 1202–1207.
1658 D. Lee, Y. Lee, S. Lee and Y. Seo, *Korean J. Chem. Eng.*, 2016, **33**, 1425–1430.
1659 M. N. Khan, *Phase Equilibria Modeling of Inhibited Gas Hydrate Systems Including Salts: Applications in Flow Assurance, Seawater Desalination and Gas Separation*, Colorado School of Mines, Arthur Lakes Library, 2016.
1660 Y. Zhang, S.-M. Sheng, X.-D. Shen, X.-B. Zhou, W.-Z. Wu, X.-P. Wu and D.-Q. Liang, *J. Chem. Eng. Data*, 2017, **62**, 2461–2465.
1661 S. Ho-Van, B. Bouillot, J. Douzet, S. M. Babakhani and J.-M. Herri, *Ind. Eng. Chem. Res.*, 2018, **57**, 14774–14783.
1662 S. Maghsoodloo Babakhani, S. Ho-Van, B. Bouillot, J. Douzet and J.-M. Herri, *Chem. Eng. Sci.*, 2020, **214**, 115442.

 This journal is © The Royal Society of Chemistry 2020

Open Access Article. Published on 22 Junie 2020. Downloaded on 2026-02-11 12:42:38 nm..
This article is licensed under a Creative Commons Attribution-NonCommercial 3.0 Unported Licence.

1663 J.-H. Cha and Y. Seol, *ACS Sustainable Chem. Eng.*, 2013, **1**, 1218–1224.
1664 Q. Lv, L. Li, X. Li and Z. Chen, *Energy Fuels*, 2015, **29**, 6104–6110.
1665 Q. Lv, X. Li and G. Li, *Energy Procedia*, 2019, **158**, 5144–5148.
1666 W. Choi, Y. Lee, J. Mok, S. Lee, J. D. Lee and Y. Seo, *Chem. Eng. J.*, 2019, **358**, 598–605.
1667 S. D. Seo, S. Y. Hong, A. K. Sum, K.-H. Lee, J. D. Lee and B. R. Lee, *Chem. Eng. J.*, 2019, **370**, 980–987.
1668 A. Nambiar, P. Babu and P. Linga, *ChemEngineering*, 2019, **3**, 31.
1669 M. N. Khan, C. J. Peters and C. A. Koh, *Desalination*, 2019, **468**, 114049.
1670 S. Han, J.-Y. Shin, Y.-W. Rhee and S.-P. Kang, *Desalination*, 2014, **354**, 17–22.
1671 M. Karamoddin and F. Varaminian, *J. Mol. Liq.*, 2016, **223**, 1021–1031.
1672 S. Han, Y.-W. Rhee and S.-P. Kang, *Desalination*, 2017, **404**, 132–137.
1673 H. Fakharian, H. Ganji and A. Naderifar, *J. Environ. Chem. Eng.*, 2017, **5**, 4269–4273.
1674 H. Fakharian, H. Ganji and A. Naderifar, *J. Taiwan Inst. Chem. Eng.*, 2017, **72**, 157–162.
1675 K. C. Kang, S. Y. Hong, S. J. Cho, D. H. Kim and J. D. Lee, *J. Nanosci. Nanotechnol.*, 2017, **17**, 4059–4062.
1676 H. Lee, J. D. Lee and Y. Kim, *Ind. Eng. Chem. Res.*, 2018, **57**, 12980–12986.
1677 H. Fakharian, H. Ganji, A. Naderifar, H. R. Mofrad and M. Kakavand, *J. Water Reuse Desalin.*, 2019, **9**, 396–404.
1678 J. Javanmardi and M. Moshfeghian, *Appl. Therm. Eng.*, 2003, **23**, 845–857.
1679 Y. Ghalavand, M. S. Hatamipour and A. Rahimi, *Desalin. Water Treat.*, 2015, **54**, 1526–1541.
1680 S.-H. Yun and D.-S. Woo, *J. Korean Soc. Water Wastewater*, 2019, **33**, 281–289.
1681 H. Lee, H. Ryu, J.-H. Lim, J.-O. Kim, J. Dong Lee and S. Kim, *Desalin. Water Treat.*, 2016, **57**, 9009–9017.
1682 T. He, S. K. Nair, P. Babu, P. Linga and I. A. Karimi, *Appl. Energy*, 2018, **222**, 13–24.
1683 Z. R. Chong, T. He, P. Babu, J. Zheng and P. Linga, *Desalination*, 2019, **463**, 69–80.
1684 T. He, Z. R. Chong, J. Zheng, Y. Ju and P. Linga, *Energy*, 2019, **170**, 557–568.
1685 J. Zheng and M. Yang, *Desalination*, 2020, **478**, 114284.
1686 M. Sarshar and A. H. Sharafi, *Desalin. Water Treat.*, 2011, **28**, 59–64.
1687 M. Yang, J. Zheng, W. Liu, Y. Liu and Y. Song, *Energy*, 2015, **93**, 1971–1979.
1688 J. Zheng, M. Yang, Y. Liu, D. Wang and Y. Song, *J. Chem. Thermodyn.*, 2017, **104**, 9–15.
1689 J. Lee, K.-S. Kim and Y. Seo, *Chem. Eng. J.*, 2019, **375**, 121974.
1690 S. Hong, S. Moon, Y. Lee, S. Lee and Y. Park, *Chem. Eng. J.*, 2019, **363**, 99–106.
1691 D. Saha, H. A. Grappe, A. Chakraborty and G. Orkoulas, *Chem. Rev.*, 2016, **116**, 11436–11499.
1692 N. W. Ockwig and T. M. Nenoff, *Chem. Rev.*, 2007, **107**, 4078–4110.
1693 L. C. Tome and I. M. Marrucho, *Chem. Soc. Rev.*, 2016, **45**, 2785–2824.
1694 S. Basu, A. L. Khan, A. Cano-Odena, C. Liu and I. F. J. Vankelecom, *Chem. Soc. Rev.*, 2010, **39**, 750–768.
1695 J.-R. Li, R. J. Kuppler and H.-C. Zhou, *Chem. Soc. Rev.*, 2009, **38**, 1477–1504.
1696 T. W. Jagger, A. E. Van Brunt and N. P. Van Brunt, Pressure Swing Adsorption Gas Separation Method and Apparatus, *US Pat.*, 6641644, 2003.
1697 A. S. Holmes and J. M. Ryan, Cryogenic distillative separation of acid gases from methane, *US Pat.*, 4318723, 1982.
1698 J. Yao and H. Wang, *Chem. Soc. Rev.*, 2014, **43**, 4470–4493.
1699 C.-G. Xu and X.-S. Li, *RSC Adv.*, 2014, **4**, 18301–18316.
1700 Y. Wang, X. Lang and S. Fan, *J. Energy Chem.*, 2013, **22**, 39–47.
1701 A. Li, J. Wang and B. Bao, *Greenhouse Gases: Sci. Technol.*, 2019, **9**, 175–193.
1702 P. Kastanidis, I. N. Tsimpanogiannis, G. E. Romanos, A. K. Stubos and I. G. Economou, *J. Chem. Eng. Data.*, 2019, **64**(12), 4991–5016, DOI: 10.1021/acs.jced.9b00630.
1703 D.-L. Zhong, J.-L. Wang, Y.-Y. Lu, Z. Li and J. Yan, *Energy*, 2016, **102**, 621–629.
1704 P. Linga, R. Kumar and P. Englezos, *Chem. Eng. Sci.*, 2007, **62**, 4268–4276.
1705 Z. Xia, X. Li, Z. Chen, G. Li, J. Cai, Y. Wang, K. Yan and C. Xu, *Appl. Energy*, 2017, **207**, 584–593.
1706 J. Zhao, Y. Zhao and W. Liang, *Energy Technol.*, 2016, **4**, 864–869.
1707 E. K. Lee, J. D. Lee, H. J. Lee, B. R. Lee, Y. S. Lee, S. M. Kim, H. O. Park, Y. S. Kim, Y.-D. Park and Y. Do Kim, *Environ. Sci. Technol.*, 2009, **43**, 7723–7727.
1708 I. Cha, S. Lee, J. D. Lee, G. Lee and Y. Seo, *Environ. Sci. Technol.*, 2010, **44**, 6117–6122.
1709 C. K. Ahn, G.-H. Kim, J. E. Lee, K. S. Kim and K. Kim, *Sep. Purif. Technol.*, 2019, **217**, 221–228.
1710 G. Ko and Y. Seo, *Environ. Sci. Technol.*, 2019, **53**, 12945–12952.
1711 Y.-H. Ahn, D. Lim, J. Min, J. Kim, B. Lee, J. W. Lee and K. Shin, *Chem. Eng. J.*, 2019, **359**, 1629–1634.
1712 E. Kim, G. Ko and Y. Seo, *ACS Sustainable Chem. Eng.*, 2017, **5**, 5485–5492.
1713 H. Tajima, T. Nagata, Y. Abe, A. Yamasaki, F. Kiyono and K. Yamagiwa, *Ind. Eng. Chem. Res.*, 2010, **49**, 2525–2532.
1714 E. Kim, W. Choi and Y. Seo, *Fluid Phase Equilib.*, 2018, **471**, 55–60.
1715 J. Wang, W. Han, S. Wang, H. Tang, W. Liu, Y. Li, C. Lu, J. Zhang, E. M. Kennedy and X. Li, *Catal. Sci. Technol.*, 2019, **9**, 1338–1348.
1716 P. Warrier, M. Naveed Khan, M. A. Carreon, C. J. Peters and C. A. Koh, *J. Renewable Sustainable Energy*, 2018, **10**, 34701.
1717 R. Kumar, P. Linga, J. A. Ripmeester and P. Englezos, *J. Environ. Eng.*, 2009, **135**, 411–417.